Dinuclear Metal Catalysts for the Synthesis of Oxygenated Polymers

Prabhjot Kaur Saini

A thesis submitted in partial fulfilment of the requirements for the degree of Doctor of Philosophy in Chemistry

Department of Chemistry
Imperial College London
November 2014

For my Nearest and Dearest Family and Friends

Declaration

This work described in this thesis was conducted in the Department of Chemistry, Imperial College London, between October 2011 and October 2014 and is the work of the author unless otherwise stated.

Acknowledgements

When I started this journey, three years ago, I was frequently told that doing a Ph.D. is character building. Now reaching the end and reminiscing over the past, I completely agree with this sentiment. I have realised that I have changed drastically during my Ph.D., in all respects, physically, mentally and emotionally. The last few years have been a roller-coaster, with a fair few highs and lows, but I wouldn't change it. This experience has not only moulded me into a better scientist, but also a better person.

During my journey I have been guided and supported by many people who have all had an impact, whether small or large, and I am very grateful to all. In particular, I would like to thank my supervisor Professor Charlotte Williams. I have learnt a tremendous amount from her and I couldn't have asked for a more caring and helpful supervisor. Charlotte has played a key role in my development over the past three years and I can't thank her enough.

Many people in the Chemistry Department of Imperial College London have helped make this thesis possible and I want to express my gratitude to all. Especially to Peter Haycock and Richard Sheppard for conducting several NMR experiments for me and listening to my woes; Dr. Andrew White for attempting to solve X-ray crystal structures for me, which unfortunately have not been shown here and Dr. John Barton and Lisa Haigh for their mass spectrometry service. Additionally, I would like to acknowledge Stephen Boyer, from London Metropolitan University, for elemental analysis.

I also want to show my gratitude to all the members of the Williams group, past and present, for all the fun times in the lab, but more importantly for all the socialising outside of the lab. They have kept me sane, or at least what can pass as sane, over the past three years. They are what I like to call 'my Chemistry family.'

The post-doctoral researchers in the group and at Econic technologies have all been invaluable to me. Thank you: Dr. Charles Romain, Dr. Jenni Garden, Dr. Clare Bakewell, Dr. Valentin Poirier, Dr. Andres Garcia-Trenco, Dr. Seb Pike, Dr. Anish Cyriac, Dr. Mike Kember, Dr. Colin Keyworth, Dr. Andy Chapman, Dr. Anthony Chartoire and Dr. Emma Hollis.

The current Ph.D. students have all created a cheerful environment to work in. A special thank you goes to Matt Allinson who has been by my side throughout and has become one of my closest friends. I am also indebted to Yoni Weiner who always makes me laugh. Additionally, thanks to: Shyeni Paul, Dom Myers, Jameel Marafie, Gemma Trott, Alice Leung, Ni Yi, Yunqing Zhu, Rachel Brooks and Arnaud Thevenon.

Past members have also been pivotal during my Ph.D. and I am appreciative to: Dr. Neil Brown, Dr. Jon Harris, Dr. John Shaw, Dr. Stuart Oram, Dr. Allan Petersen, Pippa Chalk and Chloe Lianos.

Furthermore, other friends outside the group, old and new, have all made this experience easier and worthwhile. I am thankful to: Jess Shaw, Nafeezah Padamsey, Sandra Tenggren, Jeeves Dattani, Adam Clancy, Kate Morgan, Phil Raymond, Owen Davies, Heather Au, Hannah Leese, Hui Huang Tay, Cynthia Hu, Dave Anthony and Hin Chun Yau.

Finally, I would like to thank my whole family, in particular my parents and my brother. I love them dearly and they have been my inspiration. For those who have not been mentioned by name, you are not appreciated any less, I am very grateful to you as well and I hold a special place for you all in my heart. Thank you for your support.

Abstract

This thesis describes the synthesis of heterodinuclear and homodinuclear catalysts and the in depth investigations carried out when using these catalysts for the ring opening copolymerisation of epoxide/CO_2 or epoxide/anhydride to generate polycarbonates or polyesters, respectively.

Chapter 2 reports the kinetic and mechanistic studies carried out for cyclohexene oxide/CO_2 copolymerisation reactions. Several di-magnesium catalysts bearing a symmetrical N_4O_2 macrocyclic ligand and different co-ligands (acetate, trifluoroacetate, benzoate, aryl oxide and bromide) were explored. These investigations revealed that both metal centres of the catalyst are involved in the copolymerisation reaction and that the rate determining step is likely to be the carbonate attack on the metal bound epoxide. CO_2 insertion is relatively fast. Additionally, there seems to be a co-ligand effect on the rate of copolymerisation, with an optimum activity observed with the acetate co-ligand. These findings support the hypothesis that one co-ligand remains bound to the catalyst during copolymerisation reactions.

Chapter 3 describes the synthesis of a Zn-Mg heterodinuclear catalyst, albeit as a mixture with di-zinc and di-magnesium catalysts. However, this mixed catalyst system has an improved activity in cyclohexene oxide or propylene oxide/CO_2 copolymerisation reactions, compared to the di-zinc and di-magnesium counterparts alone or in combination. This suggests that the heterodinuclear catalyst promotes the enhanced activity observed with the mixed catalyst system. Furthermore, this mixed catalyst system has enabled the selective formation of α,ω-di-hydroxyl end-capped polycarbonate chains, which can be used in polyurethane synthesis. Additionally, two asymmetrical di-zinc complexes and an asymmetrical Zn-Mg complex have been synthesised and fully characterised.

Chapter 4 shows that the di-magnesium and di-zinc catalysts previously reported by our group, for epoxide/CO_2 copolymerisations, are also active in cyclohexene oxide/phthalic anhydride copolymerisation reactions. The di-magnesium catalyst is four times faster than the di-zinc derivative. These homodinuclear catalysts were used in terpolymerisation reactions of epoxide/anhydride/CO_2, to form block copoly(ester-carbonates), which have significantly higher T_g values (> 90 °C) compared to polyester and polycarbonate chains (< 85 °C).

List of Publications

Publications in Peer-Reviewed Journals

1. *Dinuclear metal catalysts: improved performance of heterodinuclear mixed catalysts for CO_2-epoxide copolymerisation*
   P. K. Saini, C. Romain and C. K. Williams, *Chem. Commun.,* 2014, **50**, 4164-4167.

2. *Di-magnesium and zinc catalysts for the copolymerisation of phthalic anhydride and cyclohexene oxide*
   P. K. Saini, C. Romain, Y. Zhu and C. K. Williams, *Polym. Chem.,* 2014, **5**, 6068-6075.

3. *Kinetic and mechanistic investigations of di-magnesium catalysts in CHO/CO_2 copolymerisation reactions*
   P. K. Saini, A. Chapman and C. K. Williams, *Manuscript in Preparation.*

4. *Ring-opening copolymerisation (ROCOP): synthesis and properties of aliphatic polyesters and polycarbonate*
   S. Paul, Y. Zhu, C. Romain, R. Brooks, P. K. Saini and C. K. Williams, *Chem. Commun., Manuscript Accepted.*

Additional Publications

1. *Dinuclear metal complex-mediated formation of CO_2-based polycarbonates*
   C. Romain, A. Thevenon, P. K. Saini and C. K. Williams, *Topics in Organometallic Chemistry: Carbon Dioxide and Organometallics*, 2014, *In Publication.*

2. *Improved heterodinuclear mixed catalysts for CO_2/epoxide copolymerisation*
   P. K. Saini, C. Romain and C. K. Williams, Patent Application No: 1402109.1.

List of Abbreviations

Ar	Aryl
ATR-IR	Attenuated Total Reflectance Infrared
BDI	β-diiminate
CCS	Carbon Capture Storage
CHD	Cyclohexane-1,2-diol
CHC	Cyclohexene Carbonate
CHO	Cyclohexene Oxide
CPA	Cyclopentane-1,2-dicarboxylic Acid Anhydride
CPO	Cyclopentene Oxide
CPrA	Cyclopropane-1,2-dicarboxylic Acid Anhydride
DCM	Dichloromethane
DFT	Density Functional Theory
DGA	Diglycolic Anhydride
DMAP	4-Dimethylaminopyridine
DMC	Double Metal Cyanide
DMSO	Dimethyl Sulfoxide
DSC	Differential Scanning Calorimetry
EO	Ethylene Oxide
ESI	Electrospray Ionisation
EtOH	Ethanol
GPE	Glycidyl Phenyl Ether
^{i}Pr	*Iso*-propyl
IR	Infrared
L	Ligand
LO	Limonene Oxide
M	Lewis Acidic Metal Centre
MA	Maleic Anhydride
MALDI	Matrix Assisted Laser Desorption Ionisation
Me	Methyl
MeIm	1-Methylimidazole
MeOH	Methanol
M_n	Number Average Molecular Weight

MS	Mass Spectrometry
NMR	Nuclear Magnetic Resonance
Nu	Nucleophile
OEP	2,3,7,8,12,13,17,18-octaethylporphyrin
PA	Phthalic Anhydride
PC	Propylene Carbonate
PCHC	Poly(cyclohexene) Carbonate
PDI	Polydispersity Index
PE	Poly(1,2-cyclohexylene-1,2-phthalate)
PO	Propylene Oxide
PPC	Poly(propylene) Carbonate
PPN^+	Bis(triphenylphosphene)iminium
Py	Pyridyl
ROCOP	Ring Opening Copolymerisation
ROP	Ring Opening Polymerisation
rpm	Revolutions Per Minute
SA	Succinic Anhydride
SEC	Size Exclusion Chromatography
SO	Styrene Oxide
^{t}Bu	*Tert*-butyl
TCE	1,12,2-Tetrachloroethane
T_d	Decomposition Temperature
TFA	Trifluoroacetic Acid
TFPP	5,10,15,20-Tetrakis(pentafluorophenyl)porphyrin
T_g	Glass Transition Temperature
TGA	Thermogravimetric Analysis
THF	Tetrahydrofuran
tmtaa	Tetramethyltetraazaannulene
ToF	Time of Flight
TOF	Turnover Frequency
TON	Turnover Number
TPP	5,10,15,20-Tetraphenylporphyrin
X	Co-ligand

List of Figures, Schemes and Tables

Chapter 1

Figure 1.1: Synthesis of polycarbonates *via* bisphenol A and phosgene, using a base catalyst.

Figure 1.2: Illustrates the ROCOP of epoxides and CO_2 for polycarbonate production.

Figure 1.3: Conventional and alternative synthesis to polyurethanes.

Figure 1.4: Proposed mechanism for the copolymerisation of epoxide and CO_2.

Figure 1.5: Proposed bimetallic mechanism adopted by heterogeneous zinc dicarboxylate catalysts.

Figure 1.6: Al(TPP)X complex synthesis by Takeda and Inoue.

Figure 1.7: Zinc phenoxide and benzoate complexes produced by Darensbourg and others.

Figure 1.8: TFPP and OEP metal complexes synthesised by Chisholm and co-workers.

Figure 1.9: Zinc β-diiminate complex and proposed bimetallic transition state.

Figure 1.10: Zinc anildo-amidinate complexes by Lee and co-workers.

Figure 1.11: Trost's phenolate complex by Xiao *et al.*

Figure 1.12: Bimetallic macrocyclic ligands synthesised by Williams and co-workers.

Figure 1.13: Multidentate complexes synthesised by Lin and others.

Figure 1.14: Dimeric zinc complexes produced by Nozaki and co-workers.

Figure 1.15: Rare earth metal dimeric complexes synthesised by Hou and co-workers.

Figure 1.16: Sugimoto's dimeric β-diketiminate aluminium complexes.

Figure 1.17: Dimeric iron corrole complex by Nozaki.

Figure 1.18: Mono-, di- and tri-meric copper complexes by Lin and co-workers.

Figure 1.19: Tethered zinc BDI complexes.

Figure 1.20: Tethered zinc complexes reported by Rieger and co-workers.

Figure 1.21: Tethered cobalt porphyrin complexes by Rieger and others.

Figure 1.22: Generic structure of metal salen complexes.

Figure 1.23: Proposed initiation pathways for metal salen complexes.

Figure 1.24: Illustrates one or two copolymer chains growing per salen complex.

Figure 1.25: Cr(tmtaa) and Cr(stmtaa) complexes.

Figure 1.26: Bifunctional cobalt salen catalyst with piperdinium arm synthesised by Nozaki and co-workers.

Figure 1.27: Single component salen complex by Lee and others.

Figure 1.28: Cobaltate salen complex structure and two of the possible configurations that an octahedral salen complex can adopt.

Figure 1.29: Single component salen complexes by Lu, with ammonium salts or Lewis base attached to the ligand motif.

Figure 1.30: Bimetallic cobalt salen complexes by Nozaki and co-workers.

Figure 1.31: Bimetallic Cr(III)salphen complex reported by Rieger and co-workers.

Figure 1.32: Bimetallic cobalt salen complex by Lu.

Figure 1.33: Bimetallic cobalt salen complex with a rigid linker, reported by Lu.

Figure 1.34: Proposed catalyst targets for this thesis.

Chapter 2

Figure 2.1: Other analogues of the catalyst synthesised by Williams and co-workers.

Figure 2.2: One mechanistic hypothesis.

Figure 2.3: Proposed dinuclear and mononuclear mechanisms for epoxide/CO_2 copolymerisation reactions.

Figure 2.4: Di-cobalt analogues synthesised by Williams and co-workers and the crystal structure showing the 'bowl' shape conformation of the macrocyclic ligand.

Figure 2.5: Illustrates two common macrocyclic ligand conformations.

Figure 2.6: Illustrates the predicted $\Delta\Delta G$ for different catalyst conformations with one or two chain growth sites.

Figure 2.7: Proposed mechanism for bimetallic catalysts.

Figure 2.8: Catalyst structures recorded by IR spectroscopy.

Figure 2.9: Illustrates chain transfer reactions in CHO/CO_2 copolymerisation reactions with cyclohexane-1,2-diol (CHD).

Figure 2.10: *Trans*- and *cis*-cyclic carbonate by-product formation from metal bound copolymer chains.

Figure 2.11: Generic reaction co-ordinate *vs.* energy profile for PCHC and CHC formation.

Figure 2.12: Typical ATIR-IR spectra recorded during the course of CHO/CO_2 copolymerisation reactions.

Figure 2.13: Change in absorbance *vs.* time plot of vibrational mode 1239-1176 cm^{-1} for a CHO/CO_2 copolymerisation reaction.

Figure 2.14: Change in absorbance *vs.* time plot for three vibrational modes.
Figure 2.15: Initial rate *vs.* [catalyst **1a**] plot.
Figure 2.16: Initial rate *vs.* [catalyst **2**] plot.
Figure 2.17: ln[CHO] *vs.* time plot for **1a**.
Figure 2.18: ln[CHO] *vs.* time plot produced by Williams and co-workers for **2**.
Figure 2.19: Initial rate *vs*. charged CO_2 pressure plot for catalyst **1a**.
Figure 2.20: Initial rate *vs*. CO_2 pressure plot for catalyst **2** produced by Williams and co-workers.
Figure 2.21: Proposed mechanism for catalyst **1a**.
Figure 2.22: Structures of the seven di-magnesium catalyst derivatives investigated.
Figure 2.23: Proposed initiation process for di-magnesium catalysts **1c** and **1e**.
Figure 2.24: Initial rate *vs.* [catalyst **1c**] plot.
Figure 2.25: Initial rate *vs.* [catalyst **1d**] plot.
Figure 2.26: Graph of initial rate *vs.* different magnesium catalyst derivatives.
Scheme 2.1: CHO/CO_2 copolymerisation reactions using catalyst **1a** or **2**.
Scheme 2.2: Synthesis route for **1a** or **2**.

Chapter 3

Figure 3.1: Examples of different types of bimetallic complexes for epoxide/CO_2 ROCOP.
Figure 3.2: Structure of turbo-Hauser base [$(THF)_2Li(\mu\text{-}Cl)_2Mg(THF)(TMP)$].
Figure 3.3: Ti and Zr monometallic and heterodinuclear catalysts synthesised by Marks and co-workers.
Figure 3.4: Proposed mechanism for bimetallic catalysts synthesised by Williams and co-workers.
Figure 3.5: Heterodinuclear asymmetrical complexes synthesised by Bosnich and co-workers.
Figure 3.6: ^{1}H NMR spectrum of the half macrocycle in $CDCl_3$.
Figure 3.7: ^{1}H NMR spectrum of the complex **3** in $CDCl_3$.
Figure 3.8: ^{1}H NMR spectrum of heterodinuclear complex **4** in CD_3OD.
Figure 3.9: Other proposed structure for heterodinuclear complex **4**.
Figure 3.10: Illustrates complex **5** (tetra-imine complex).
Figure 3.11: Part of the MALDI-ToF mass spectrum for catalyst system **7**.

Figure 3.12: MALDI-ToF spectrum of 50:50 mixture of **1a** and **2**.

Figure 3.13: ^{1}H NMR spectrum of crude CHO/CO_2 copolymerisation reaction mixture used to calculate the catalyst's TON and TOF.

Figure 3.14: *Trans*- and *cis*-cyclic carbonate by-product formation from metal bound copolymer chains.

Figure 3.15: SEC trace of polycarbonate formed using catalyst system **7**.

Figure 3.16: MALDI-ToF mass spectrum of the poly(cyclohexene carbonate) produced by using catalyst system **7**.

Figure 3.17: Illustrates chain transfer reactions in CHO/CO_2 copolymerisation reactions with cyclohexane-1,2-diol (CHD).

Figure 3.18: Cobalt salen and di-magnesium Trost phenolate catalysts.

Figure 3.19: MALDI-ToF spectrum of the poly(cyclohexene carbonate) produced by using catalyst system **7,** with 16 equivalents of water.

Figure 3.20: ^{1}H NMR Spectrum of asymmetric macrocyclic pro-ligand **1** in $CDCl_3$.

Figure 3.21: Lithium-zincate synthesised and used to make a Li-Zn heterodinuclear complex.

Scheme 3.1: Synthetic routes attempted to produce heterodinuclear catalysts.

Scheme 3.2: Illustrates the unsuccessful attempt to react a BOC protected diamine with 3-bromo-5-*t*-butylsalicylaldehyde.

Scheme 3.3: Illustrates the attempts to protect the aldehyde moiety of 3-bromo-5-*t*-butylsalicylaldehyde.

Scheme 3.4: Synthesis route for heterodinuclear complexes adopted by Bosnich and co-workers.

Scheme 3.5: Modified synthesis route for heterodinuclear complexes.

Scheme 3.6: Illustrates the synthesis of a zinc salen complex.

Scheme 3.7: Illustrates the synthesis of catalyst system **7**.

Scheme 3.8: Illustrates the synthesis of asymmetric complexes.

Table 3.1: Illustrating the catalytic activity, productivity, selectivity and M_n data for copolymerisation reactions using catalysts **1a**, **2** and **7**.

Table 3.2: CHO/CO_2 copolymerisation reactions with **7** at different temperatures.

Table 3.3: CHO/CO_2 copolymerisation reactions with **7** at CO_2 pressures.

Table 3.4: Optimised CHO/CO_2 copolymerisation reactions with **7** and comparison with literature catalysts.

Table 3.5: CHO/CO_2 copolymerisation data for catalyst system **7** with 16 eq. of H_2O.

Table 3.6: PO/CO_2 copolymerisation reactions with catalyst system **7**.

Chapter 4

Figure 4.1: Aluminium tetraphenylporphyrin complex.

Figure 4.2: Zinc BDI complex by Coates and co-workers.

Figure 4.3: Proposed mechanism for epoxide/anhydride copolymerisation.

Figure 4.4: Cr, Mn and Co salphen and tetraphenylporphyrin (TPP) complexes.

Figure 4.5: *N,N'*-bis(3,5-di-*tert*-butylsalicylidine)-1,2-cyclohexanediaminochromium(III) chloride complex.

Figure 4.6: (a) ^{1}H NMR spectrum of polyester (PE) (without any ether linkages) in DMSO-d_6; (b) ^{1}H NMR spectrum of polyether in DMSO-d_6; (c) ^{1}H NMR spectrum of a mixture of PE and polyether in DMSO-d_6.

Figure 4.7: SEC trace for PE sample produced using **2**.

Figure 4.8: MALDI-ToF mass spectrum of the polyester sample formed by complex **1a**.

Figure 4.9: Illustrates chain transfer reactions in CHO/PA copolymerisation reactions with cyclohexane-1,2-diol (CHD).

Figure 4.10: ^{1}H NMR spectrum of polyester (PE) in DMSO-d_6.

Figure 4.11: PA conversion *vs*. time plot for catalysts **1a** and **2**.

Figure 4.12: Evolution of M_n against PA conversion for ROCOP of CHO/PA initiated by catalyst **1a** (a) and **2** (b).

Figure 4.13: Graphs illustrating the change in intensity *vs.* time for various signals in the IR spectra recorded for the ROCOP of CHO/PA using **1a** (a) and **2** (b).

Figure 4.14: Proposed mechanism for CHO/PA copolymerisation reactions using **1a** and **2**, which indicates that the rate determining step is the ring opening of CHO.

Figure 4.15: Shows changes in the intensity of the ATR-FTIR resonances observed during the terpolymerisation of CHO, PA and CO_2 using catalyst **1a** (a) and **2** (b).

Figure 4.16: ^{1}H NMR spectra for terpolymerisation of CHO/PA/CO_2 using **1a** after 1 h and 10 h.

Figure 4.17: Proposed pathways for the ROCOP of CHO/CO_2 and CHO/PA.

Figure 4.18: SEC trace for PE and PE-PCHC block copolymer formation using **2**.

Figure 4.19: DOSY spectrum of block copolymer and a mixture of PE and PCHC in $CDCl_3$.

Figure 4.20: Photograph of thin films produced from PE, PCHC and block copolymer samples, overlaying a quote, which demonstrates their transparency.

Figure 4.21: Bimetallic catalysts based on Trost's phenolate ligands by Xiao *et al.*

Scheme 4.1: Illustrates the ROCOP of epoxides/anhydrides.

Scheme 4.2: Illustrates ROCOP of cyclohexene oxide (CHO) and phthalic anhydride (PA), initiated by complexes **1a** or **2**.

Scheme 4.3: The terpolymerisation of CHO, PA and CO_2 to produce a copoly(ester-carbonate) (PE-PCHC), using catalyst **1a** and **2**.

Table 4.1: Data for the ROCOP of CHO/PA initiated by catalysts **1a** or **2** in neat conditions.

Table 4.2: Data for the ROCOP of CHO/PA initiated by catalysts **1a** or **2** in toluene solutions.

Table 4.3: Thermal properties of selected polymers obtained from catalysts **1a** and **2**.

Table of Contents

Declaration iii

Acknowledgements iv

Abstract vi

List of Publications vii

List of Abbreviations viii

List of Figures, Schemes and Tables x

Chapter 1: Introduction 1

1.1 Fossil Fuel Feedstocks 2

1.2 Working towards a Solution 2

1.3 Using CO_2 as a Feedstock 3

1.4 Polymer Industry 4

1.5 Catalyst Development for Epoxide/CO_2 ROCOP 6

1.6 Early Catalyst Developments and Heterogeneous Catalysts 7

1.7 Homogeneous Catalysts 9

1.7.1 Early Developments 9

1.7.2 Porphyrin Based Catalysts 11

1.7.3 β-Diiminate Catalysts 12

1.7.4 Bimetallic Catalysts 13

1.7.5 Salen Based Catalysts 21

1.8 Outlook 32

1.9 Aims and Objectives 33

1.10 References 35

Chapter 2: Kinetic and Mechanistic Investigations of Homodinuclear Magnesium Catalysts for Cyclohexene Oxide/CO_2 Ring Opening Copolymerisation Reactions 42

2.1 Kinetic and Mechanistic Hypothesis: Introduction 43

2.1.1 General Introduction 43

2.1.2 Rate Law for the Di-zinc Catalyst (2) 45

2.1.3 Support for Dinuclear Mechanism – Di-cobalt (II) Catalysts 47
2.1.4 Catalyst Conformations 49
2.1.5 Computational Studies 50
2.1.6 Solid State and *In Situ* IR Spectroscopy Studies 52
2.1.7 Immortal Copolymerisation Reactions 53
2.1.8 Side Reactions During Copolymerisation Reactions 54
2.1.9 Background and Aims 56
2.2 Kinetic Methods to Determine Reaction Order 57
2.2.1 Isolation and Initial Rates Method 57
2.2.2 Isolation and Integrated Rate Law Method 58
2.3 Kinetic and Mechanistic Investigations of $LMg_2(OAc)_2$ Catalyst (1a) 59
2.3.1 Reaction Order in [Catalyst 1a] 59
2.3.2 Reaction Order in [CHO] 64
2.3.3 Reaction Order in CO_2 Pressure 66
2.4 Copolymerisation Mechanism 68
2.5 Kinetic Investigations for Other Di-magnesium Complexes 70
2.6 Different Co-Ligands 75
2.7 Conclusions and Future Work 78
2.8 References 81
Chapter 3: Synthesis of Heterodinuclear Complexes for Epoxide/CO_2 Ring Opening Copolymerisation Reactions 83
3.1 Introduction 84
3.1.1 Heterodinuclear Catalysts for Epoxide/CO_2 Copolymerisation Reactions 84
3.1.2 Other Heterodinuclear Complexes 86
3.1.3 Background and Aims 88
3.2 Synthesising Heterodinuclear Complexes *via* Stepwise Route 90
3.2.1 Synthesis of Monometallic Complexes 90

3.2.2 Synthesis of Monometallic Complex 3 & Heterodinuclear Complex 4 93
3.3 *In Situ* Route to Heterodinuclear Mixed Catalyst System 101
3.4 CHO/CO_2 Ring Opening Copolymerisation Results Using 7 104
3.4.1 Comparative Studies 104
3.4.2 Polymer Characteristics 106
3.4.3 Optimisation Study 110
3.4.4 Polyol Selectivity 112
3.5 PO/CO_2 Ring Opening Copolymerisation Results Using 7 114
3.6 Synthesis of Asymmetric Macrocycles and Complexes 115
3.7 Conclusions 118
3.8 Future Work 121
3.9 References 123
Chapter 4: Homodinuclear Metal Catalysts for Epoxide/Anhydride Ring Opening Copolymerisation Reactions 127
4.1 Introduction 128
4.1.1 General Introduction 128
4.1.2 Catalysts for Epoxide/Anhydride Ring Opening Copolymerisation Reactions 129
4.1.3 Proposed Mechanism 131
4.1.4 Terpolymerisation Reactions of Epoxide/Anhydride/CO_2 132
4.1.5 Chapter Aims 134
4.2 ROCOP of CHO/PA in Neat Conditions 135
4.2.1 Rate: Point Kinetics 135
4.2.2 Polymer Characterisation 137
4.2.3 Molecular Weight (M_n) 138
4.2.4 MALDI-ToF Mass Spectrometry 140
4.3 ROCOP of CHO/PA in Toluene Solutions 141
4.4 Copolymerisation Kinetic Study 143

4.4.1 Aliquoting Reactions 143
4.4.2 Monitoring by ATR-IR Spectroscopy 146
4.5 Terpolymerisations 149
4.5.1 Results 149
4.6 Discussion 154
4.7 Characterisation of Block Copolymer 155
4.7.1 Molecular Weight (M_n) 155
4.7.2 NMR Spectroscopy 156
4.8 Thermal and Optical Analysis of Polymers 158
4.9 Catalyst Sensitivity to Acid Impurities 160
4.10 Conclusions 160
4.11 Future Work 162
4.12 References 164
Chapter 5: Conclusion 166
5.1 Outlook 167
5.2 Future Directions for the Field 169
Chapter 6: Experimental 171
6.1 General Procedures 172
6.1.1 Materials and Methods 172
6.1.2 Measurements 172
6.2 Synthesis of Pro-Ligands 173
6.3 Synthesis of Metal Complexes 183
6.4 Epoxide/CO_2 Copolymerisation Reactions 192
6.4.1 Low Pressure CHO/CO_2 Copolymerisation Reactions 192
6.4.2 High Pressure CHO/CO_2 Copolymerisation Reactions 193
6.4.3 High Pressure PO/CO_2 Copolymerisation Reactions 193
6.5 Phthalic Anhydride/CHO Copolymerisation Reactions 194

6.5.1 Copolymerisation Reactions in Toluene Solutions 194
6.5.2 Copolymerisation Reactions in Neat Conditions 194
6.6 Phthalic Anhydride/CHO/CO_2 Terpolymerisation Reactions 194
6.6.1 General Procedure 194
6.7 Monitoring Reactions with *In Situ* ATR-IR Spectroscopy 195
6.7.1 Initial Rates for CHO/CO_2 Copolymerisation Reactions 195
6.7.2 Phthalic Anhydride/CHO/CO_2 Terpolymerisation Reactions 195
6.8 Purification of Polymers 195
6.8.1 General Procedure 195
6.9 References 196
Appendices 197
Appendix A – Raw Data Plots for Chapter 2 198
Appendix B – Spectra for Chapter 3 209
Appendix C – Spectra for Chapter 4 218

Chapter 1

Introduction

"I am the master of my fate,
I am the captain of my soul"
Invictus by William Ernest Henley

1.1 Fossil Fuel Feedstocks

Fossil fuels (crude oil, coal and natural gas) have been used on a large scale since the industrial revolution in the 18th century.[1] Fossil fuels are not only used as an energy source, they are also very useful in the production of fine chemicals.[2] However, there is a limited supply of fossil fuels, as they were produced from the anaerobic decomposition of dead buried organisms, which took millions of years to achieve.[3] There are concerns about the fate of society when these resources run out, as society has been accustomed to a certain way of life. It has been estimated that crude oil and natural gas reverses may be depleted in the next 100 years.[3]

The depletion of these fossil fuel feedstocks is not the only concern; the use of these carbon-rich compounds has led to an increase in CO_2 emissions into the atmosphere. CO_2 is believed to be one of the major reasons for climate change.[2] It is considered as a greenhouse gas and thus its accumulation in the atmosphere is believed to slowly cause the temperature of the Earth to rise.[2,4-6] This in turn is thought to cause extreme weather conditions and rising sea levels, such as, the heavy storms that occurred in Britain, in January 2014.[2,7]

In 2014, the projected amount of CO_2 emitted worldwide is expected to reach 40 Gt, which suggests an increase of 2.5 % from the global CO_2 emissions recorded for 2013.[8] It has been calculated that two thirds of the total quota of the world's CO_2 emissions, in order to achieve only a 2 °C increase in temperature of the Earth's surface, has already been exhausted.[8] At the current rate of increase in global CO_2 emissions annually, it is expected that the CO_2 emissions quota will be reached in 30 years. Therefore, a reduction in global CO_2 emissions is necessary in order to limit the global average temperature rise by 2 °C.[6,8]

1.2 Working towards a Solution

Academia and industry have been investigating several different technologies in order to attempt to solve the two major concerns outlined in Section 1.1. Currently, in order to stop the usage of finite fossil fuel resources for energy and fuel, renewable sources of energy, such as, solar, wind and hydrothermal are being investigated.[2] Additionally, research into making chemicals from renewable feedstocks, such as, biomass and CO_2 are also being developed. Furthermore, the development of carbon capture storage (CCS) technologies is being carried out in order to reduce global CO_2 emissions.[2]

These different technologies cannot singlehandedly solve the concerns of fossil fuel depletion and increasing global CO_2 emissions, but instead a blend of all these technologies need to be implemented simultaneously.[2,9] For instance, CCS has the potential to reduce CO_2 emissions, but the reduction in using fossil fuels as energy sources and substituting them with renewable resources will also reduce CO_2 emissions and compliment CCS. Furthermore, CCS is an expensive process, but by using CO_2 as a renewable feedstock for chemical synthesis will add value to CCS and thus help with development and cost.[2]

1.3 Using CO_2 as a Feedstock

Carbon dioxide is a waste product of many industrial processes and as there is currently little economic incentive to capture it, it is being emitted into the atmosphere.[1,2,4,9] This is one of the major causes of global warming (Section 1.1). However, since CO_2 is emitted by many industrial processes, it is relatively abundant and thus thought to be a renewable feedstock. Coupled with its low toxicity, CO_2 has the potential to be a highly desirable feedstock for the production of fine chemicals.[2,4,5] This will in turn reduce the use of fossil fuels for chemical production. It should be noted that that CO_2 consumption *via* chemical synthesis (≈ 100 Mt per year) is not a means to reducing CO_2 levels in the atmosphere, but by adding value to CCS, will encourage the use of this technology (CCS) and thus lower the amount of emitted CO_2.[2,5,6]

However, using CO_2 as a feedstock is difficult because CO_2 is the highest oxidised form of carbon and is thermodynamically stable.[5,10,11] In order for CO_2 to be used in the synthesis of important chemicals, it needs to be reduced. The process of reduction is energy intensive and physical methods, such as, high temperatures and pressures, or the addition of highly reactive reagents, are expensive and inefficient.[10,11] A more attractive method for utilising CO_2 as a chemical feedstock is by using catalysts that can lower the energy barriers for incorporating CO_2 in chemical reactions. Such catalysts will allow accessing CO_2 as a feedstock at lower physical energy inputs, which are more manageable and less costly.[5,10]

The use of CO_2 has been very successful in nature, in particular in photosynthesis, which is carried out by many plants and other primary producing organisms. This process converts two hundred billion tonnes of CO_2 per year to carbohydrates (food for organisms).[5] Synthetically converting CO_2 is difficult (*vide supra*), but there are already a few industrial

synthetic processes which use CO_2. These include the synthesis of urea, inorganic and organic carbonates, salicylic acid, methanol and polycarbonates.[12]

1.4 Polymer Industry

One of the largest sectors of the chemical industry is the polymer industry. It is a growth industry and currently 288 Mt of polymer is produced worldwide annually.[5,13,14-16] The most commonly synthesised polymers are polyethylene, polypropylene, polyethylene terephthalate and polystyrene.[14,16] Approximately, 8 % of the world's oil and gas supply annually is used in polymer synthesis.[5,17] Therefore, investigations into using renewable feedstocks for polymer synthesis have been carried out for many years.

Polycarbonates are also synthesised within the polymer industry because they are a vital commodity. They are used in many applications, such as, clothing, adhesives, packaging and construction.[5] Approximately, 5 Mt of polycarbonates are synthesised by industry per year.[13,14] The conventional route to producing polycarbonates involves copolymerising bisphenol A and phosgene using a base catalyst (NaOH). An alternative route has been sought because bisphenol A and phosgene are highly toxic and petrochemically derived and thus this process is not safe or sustainable (Figure 1.1).[5]

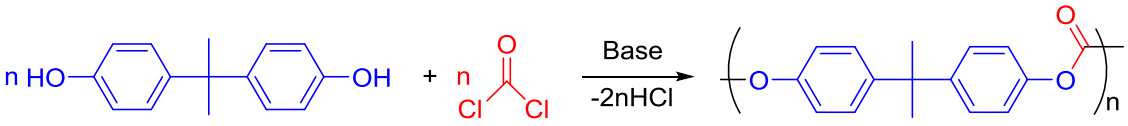

Figure 1.1: Synthesis of polycarbonates *via* bisphenol A and phosgene, using a base catalyst.

An alternative process involving the ring opening copolymerisation (ROCOP) of epoxides and CO_2 has been investigated.[18] This process is seen as a desirable alternative because it uses CO_2 as a feedstock and thus has improved sustainability compared to the conventional route (Figure 1.2). This is because approximately 20-40 % of the polycarbonate produced is derived from CO_2, depending on the epoxide monomer used.[19,20] However, it must be noted that polycarbonates produced by this copolymerisation reaction have different thermal, chemical and mechanical properties compared to bisphenol A derived polycarbonates. There is potential for synthesising 100 % renewably derived polycarbonates by the

copolymerisation of epoxide and CO_2. This can be achieved by using renewable epoxides, such as, limonene oxide and α-pinene oxide.[5,21,22,23]

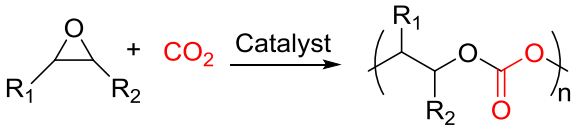

Figure 1.2: Illustrates the ROCOP of epoxides and CO_2 for polycarbonate production.

Conventionally, high number average molecular weight (M_n) polycarbonate chains are required for the applications discussed previously. However, low M_n polycarbonates are also useful as they can be used in the synthesis of higher polymers, such as, polyurethanes.[19,24-27] Polyurethanes are also a highly desirable commodity (roughly 20 Mt are produced globally each year) because they are used to make furniture, foams, adhesives and insulation.[13,14] Currently, polyurethanes are synthesised in industry by reacting polyols with diisocyanates. The polyols used are commonly polyether or polyester based. Both are derived from petrochemicals, for example, polyether polyols are synthesised by the homopolymerisation of epoxides.[28] However, substituting these polyols with polycarbonate polyols, derived from the copolymerisation of epoxide and CO_2, will improve the sustainability of polyurethane synthesis (Figure 1.3).[19]

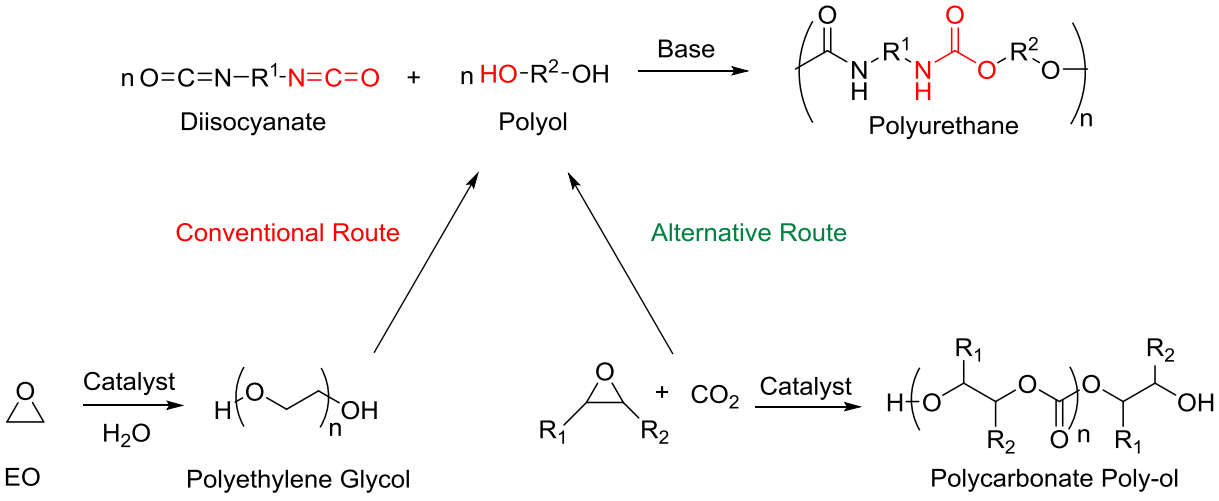

Figure 1.3: Conventional and alternative synthesis to polyurethanes.

The copolymerisation reaction between epoxides and CO_2 to form polycarbonates requires a high energy input in order to overcome the high stability of CO_2 (Section 1.3), which is not

cost or energy efficient. Therefore a catalyst is required to lower the activation energy barrier of this process and promote the reaction.

1.5 Catalyst Development for Epoxide/CO_2 ROCOP

Research into developing catalysts for the ring opening copolymerisation (ROCOP) of epoxides and CO_2 has been occurring since the late 1960s.[18] The catalysts generally consist of a Lewis acidic metal halide, carboxylate, alkoxide or aryloxide surrounded by an ancillary ligand (L). The mechanism for this copolymerisation is believed to involve coordination-insertion processes (Figure 1.4).[5]

The epoxide monomer coordinates to the metal centre and undergoes ring opening by nucleophilic attack by the halide/carboxylate/alkoxide/aryloxide co-ligand (X – in Figure 1.4). However, if the co-ligand (X) is an alkoxide and aryloxide group, CO_2 insertion occurs first before epoxide ring opening occurs.[29] The formation of the metal alkoxide species (from ring opening) then undergoes CO_2 insertion to form a metal carbonate species. The latter process is highly dependent on the metal used. The metal carbonate species produced then further nucleophilically attacks another metal bound epoxide monomer, to regenerate a metal alkoxide species. The cycling between metal alkoxide and metal carbonate species produces a polycarbonate chain, with 100 % carbonate linkages.[5]

However, there are two side reactions which can occur during these copolymerisation reactions. The sequential enchainment of epoxide monomers can occur, which leads to the formation of ether linkages within the growing polycarbonate chain, which can affect the thermal and mechanical properties of the polycarbonate produced. Moreover, the propagating polycarbonate chain can undergo backbiting reactions to form a five-membered cyclic carbonate by-product. This by-product is thermodynamically more stable than the copolymer product and hence forms more readily at higher temperatures.[5]

Furthermore, the ROCOP of epoxides and CO_2 have been shown by many research groups to undergo chain transfer reactions with alcohols or water (present as contaminants in these copolymerisation reactions). These chain transfer reactions produce a hydroxyl terminated copolymer chain and a metal alkoxide or hydroxide species, which can initiate copolymerisation.[5] Due to these chain transfer reactions, the M_n of the copolymer chains

produced are lower than expected, but it has been seen that the polydispersity indices (PDIs) remain narrow (*vide infra*). Therefore, ROCOP of epoxides and CO_2 are 'immortal polymerisations,' where the rate of chain transfer is more rapid than chain propagation.[30]

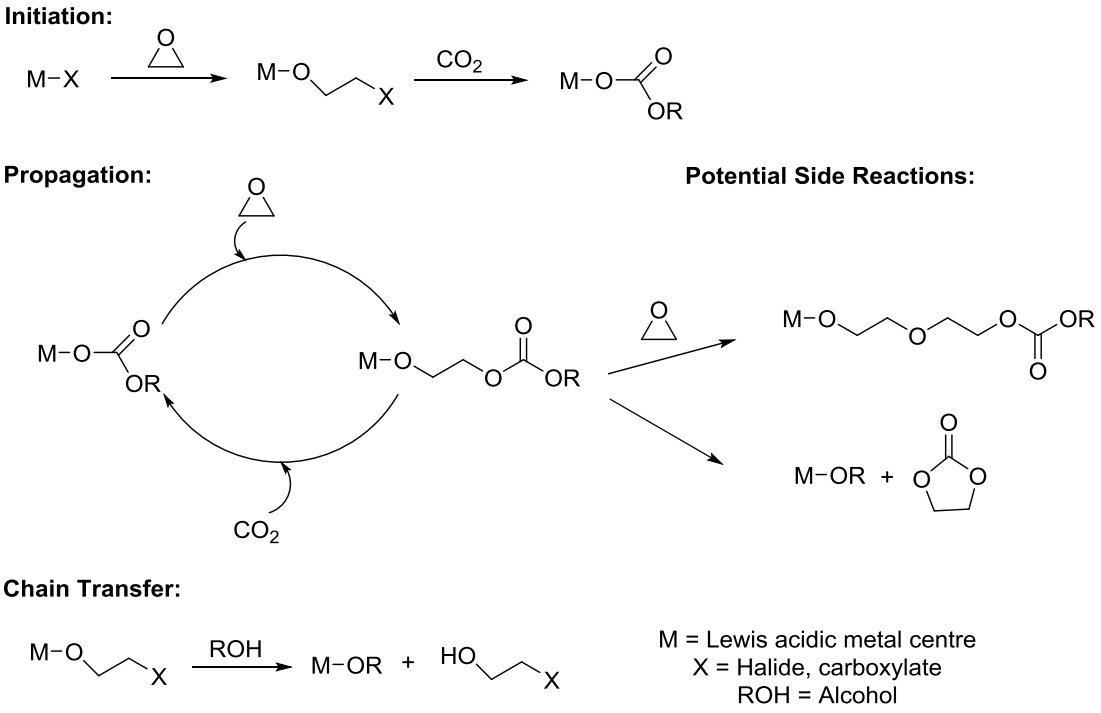

Figure 1.4: Proposed mechanism for the copolymerisation of epoxide and CO_2.

The productivity and activity of the catalysts are measured by TON (turnover number), which is the number of mols of monomer consumed per mol of catalyst used and TOF (turnover frequency), which is the TON/h, respectively. Productivity of the catalyst can also be calculated by the grams of copolymer formed per gram of catalyst used.[5]

1.6 Early Catalyst Developments and Heterogeneous Catalysts

The ROCOP of epoxides and CO_2 was discovered by Inoue and co-workers in 1969. The first catalyst system consisted of a mixture of $ZnEt_2$ and H_2O. It was used in propylene oxide (PO) and CO_2 copolymerisation reactions at 80 °C and 50-60 bar CO_2 pressure. The activity of the system was very low (TOF = 0.12 h^{-1}).[18]

This prompted investigations into using different mixtures of dialkyl zinc reagents (ZnR_2) with either alcohols, water or amines for poly(propylene carbonate) (PPC) formation.[31,32,33]

The use of monohydric sources (alcohol or secondary amines) were observed to have lower or no activity compared to multi-hydric sources (H_2O).[34] Heterogeneous mixtures of carboxylic acids and $Zn(OH)_2$ also showed promising activities for epoxide/CO_2 copolymerisations.[33]

The results recorded for zinc carboxylates, led to the discovery of a heterogeneous catalyst: zinc glutarate $[Zn(O_2C(CH_2)_3CO_2)]_n$. This catalyst was produced by reacting zinc oxide and glutaric acid and several modified procedures have been reported.[35,36] The catalyst can be crystalline or amorphous, but the crystalline derivatives have shown higher activity (≈ 300 g PPC/g Zn).[37] X-ray diffraction has shown that the zinc atoms adopt a tetrahedral configuration and are coordinated by four oxygen atoms of different glutarate molecules.[38]

Another heterogeneous catalyst system has also been developed, which involves double metal cyanides (DMCs). DMCs have a generic structure of $Zn_3[M(CN)_6]_2$, where M = Fe(III) or Co(III).[39] These catalysts have shown activity in epoxide/CO_2 copolymerisation reactions, but produce copolymers with a high content of ether linkages (Chapter 3 for more detail).

The heterogeneous nature of these catalysts has made establishing a mechanism very difficult.[36,38] Rieger and co-workers have reported that the surface areas, particle sizes and morphologies were very similar for four zinc dicarboxylate catalysts.[40] The catalysts with a high proportion of Zn-Zn surface couples with a separation of 4.6-4.8 Å had the highest activity. An ideal Zn-Zn distance of 4.3-5.0 Å was calculated and it is believed that such separations may lead to a reduction in activation energy and an increase in copolymerisation selectivity. The experimental and theoretical investigations therefore suggest that heterogeneous zinc dicarboxylate catalysts adopt a bimetallic mechanism (Figure 1.5).[40]

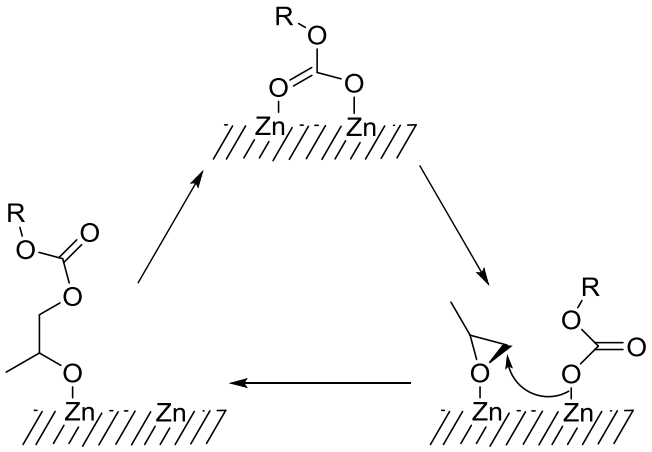

Figure 1.5: Proposed bimetallic mechanism adopted by heterogeneous zinc dicarboxylate catalysts.

1.7 Homogeneous Catalysts

1.7.1 Early Developments

Section 1.6 has shown that heterogeneous catalysts have low activities and low selectivities in the ROCOP of epoxides and CO_2 and cannot be easily characterised. The latter therefore makes it difficult to define the active site and thus it is also difficult to improve catalyst activity. Therefore, investigations in the field of ROCOP of epoxides and CO_2 have become more focussed on homogeneous catalysts. Initially, monometallic catalysts were targeted.

In 1978, Takeda and Inoue discovered the first homogeneous catalyst for PO or cyclohexene oxide (CHO) and CO_2 copolymerisation reactions. The aluminium 5,10,15,20-tetraphenylporphyrin (TPP) catalyst was used in conjunction with a co-catalyst ($EtPh_3PBr$) and produced low M_n copolymers (3500-6000 g/mol) with narrow PDIs (< 1.10). However, it took 13 days for the copolymerisation reactions to reach full conversion (Figure 1.6).[41]

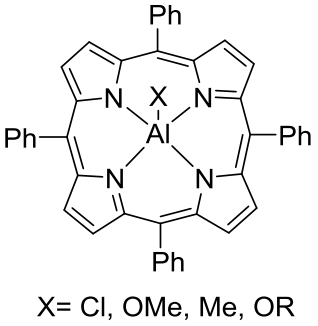

Figure 1.6: Al(TPP)X complex synthesis by Takeda and Inoue.[41]

The next breakthrough in homogenous catalysis came in 1995 by Darensbourg and co-workers.[42] They discovered the first discrete zinc complex that catalysed the copolymerisation of epoxides and CO_2. These zinc bisphenoxide complexes were very active, but unfortunately produced copolymers with varying chain lengths (PDI > 2). In addition, these catalysts could be used in epoxide homopolymerisation reactions and thus the copolymer products formed contained a fairly high number of ether linkages.[42-44]

Structure activity relationships revealed that *ortho*-substituents on the phenoxide did not affect the activity significantly and electron-donating substituents at the *para*- position on the phenoxide increased activity.[44] Darensbourg and others then prepared a zinc benzoate complex (TOF of 7.7 h^{-1}) for CHO/CO_2 copolymerisations (Figure 1.7).[45] It was also found that some of these zinc catalysts adopt di- or multi-metallic structures and thus these homogeneous catalysts were the first to indicate that epoxide/CO_2 copolymerisations may adopt a bimetallic pathway.

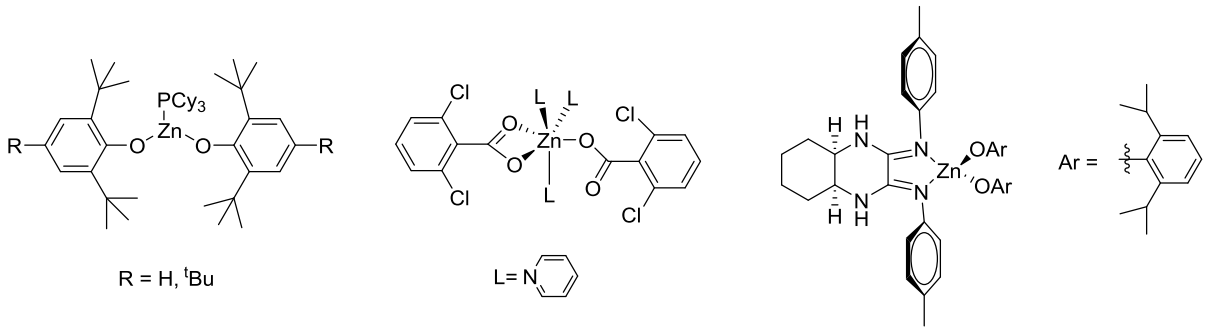

Figure 1.7: Zinc phenoxide or benzoate complexes produced by Darensbourg and others.[42-44]

Several homogeneous catalysts for the copolymerisation of epoxides and CO_2 have been developed over the past 45 years. Some of the most common and active catalysts are based on only a handful of ligand motifs. These include porphyrins and corroles,[46,47,48,49-51] salens,[23,52] β-diiminates[29,53,54-56] and phenoxy-amine macrocyclic ligands.[57,58,59,60] The catalysts can be further characterised as either bifunctional, bimetallic or binary catalyst systems.

1.7.2 Porphyrin Based Catalysts

After the initial discovery by Inoue of Al(TPP)X complexes (Figure 1.6), other derivatives of this catalyst were synthesised. Manganese and cobalt analogues showed reasonable activity in CHO/CO_2 copolymerisation reactions (TOF = 16 h^{-1}). The activity with CHO was slightly higher than for PO and these complexes were the first catalysts reported to be active at low CO_2 pressures (TOF = 3 h^{-1}, at 1 atm of CO_2 pressure).[49] Additionally, the cobalt derivative of this complex was slightly more active, the highest activity recorded was 21 h^{-1}.[61]

Chisholm and others have also synthesised aluminium, chromium and cobalt complexes based on three different porphyrin ligands, for PO/CO_2 copolymerisation reactions. It was found that the most active chromium and cobalt analogues were based on the TPP ligand (Figure 1.6) and the most active aluminium catalyst consisted of the 5,10,15,20-tetrakis(pentafluorophenyl)porphyrin (TFPP) ligand (Figure 1.8).[47,62] Catalysts based on the 2,3,7,8,12,13,17,18-octaethylporphyrin (OEP) ligand motif had the lowest activities, regardless of the metal centres used (Figure 1.8). The order of reactivity for the metals investigated was found to be Cr > Co ≈ Al. This was attributed to the difference in the electronic properties of the metal centres.[47,62]

Furthermore, it was found that these catalysts require co-catalysts in order to be active (binary catalysts systems). No co-catalysts added to the copolymerisation reaction resulted in either inactivity or the formation of ether enriched copolymers.[47,62] The co-catalyst is believed to bind *trans* to the co-ligand, which causes the metal-co-ligand bond to lengthen and nucleophilically attack the epoxide monomer to form a metal alkoxide species. The addition of more than one equivalent of co-catalyst enhanced cyclic carbonate by-product formation, which is thought to be because the copolymer readily dissociates from the metal with more equivalents of co-catalysts present and thus undergoes backbiting.[47,62]

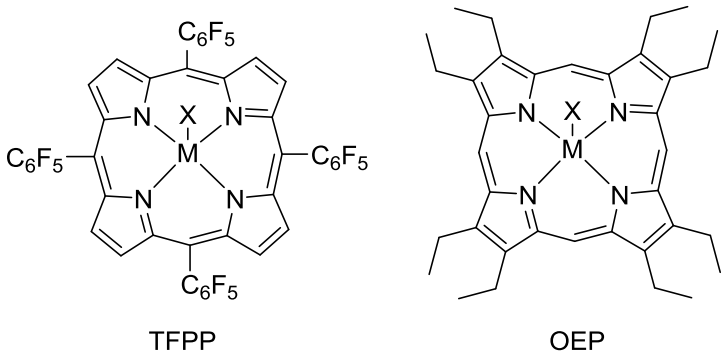

Figure 1.8: TFPP and OEP metal complexes synthesised by Chisholm and co-workers.[47,62]

1.7.3 β-Diiminate Catalysts

Coates and others discovered a class of zinc catalysts which had high activities and selectivities for PO or CHO/CO_2 copolymerisation reactions.[63] The copolymerisation reaction conditions used for the β-diiminate (BDI) zinc catalysts (Figure 1.9) were 25 °C or 50 °C for PO and CHO, respectively and 7 atm of CO_2 pressure. The highest activity reported was 2290 h^{-1} (CHO/CO_2 copolymerisation reactions with a methoxy co-ligand) and the copolymers produced consisted of > 99 % carbonate linkages.[54,63,64]

The catalysts were investigated thoroughly and structure activity relationships showed that the substituents on the phenyl rings in the BDI ligand (R_1 and R_3 – Figure 1.9) and the initiating group (X) affected the activity of the catalyst significantly. It was found that changing the R_1 and R_3 groups affected the dimeric nature of the β-diiminate catalysts (Figure 1.9). If the groups were sterically bulky, the catalysts were monomeric in nature and therefore showed low activity.[29,54,63,64] When the R_1 and R_3 groups were sterically unencumbered, the catalysts formed tightly bound dimers, which also had low activity. However, the highest activity was observed with catalysts with R_1 and R_3 groups that had intermediate steric bulk, which promoted the formation of loosely held dimers (Figure 1.9).[29,54,63,64]

The most active catalysts had Et groups in the R_1 and R_3 positions and hydrogen atoms in the R_4 position. Electron withdrawing substituents on the backbone of the BDI ligand (e.g. R_2 = CN) and alkoxide initiating groups (X) also improved the activity of the catalyst.[29,54,63]

From these structure activity relationships and kinetic and mechanistic studies, it was hypothesised that a bimetallic pathway was adopted by these zinc BDI catalysts during copolymerisation reactions. It was suggested that the one metal coordinates the epoxide and the other metal feeds the co-ligand or growing copolymer chain to nucleophilically attack the epoxide for ring opening and thus alkoxide formation (Figure 1.9).[29,54,63]

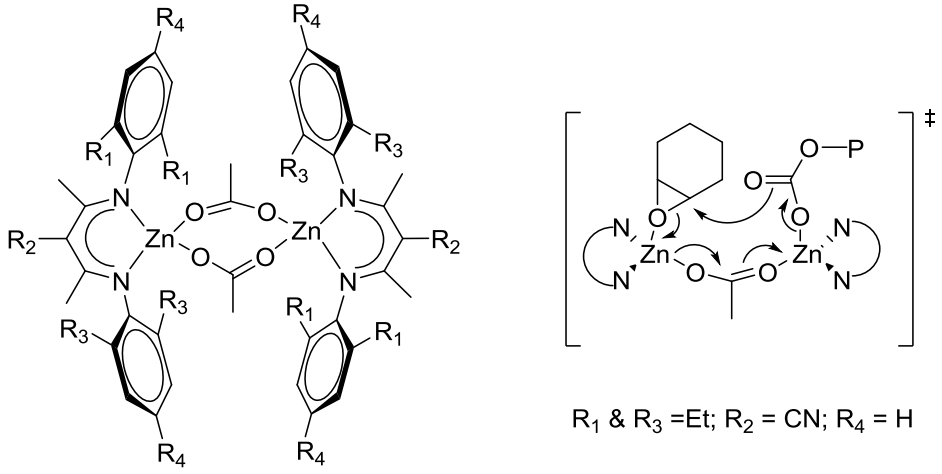

Figure 1.9: Zinc β-diiminate complex and proposed bimetallic transition state.[29,54,63]

1.7.4 Bimetallic Catalysts

The findings by Coates and co-workers led to a surge into the development of discrete bimetallic catalysts for epoxide/CO_2 copolymerisation reactions.[28] Three main classes of bimetallic complexes have been developed: bimetallic complexes containging a single binucleating ligand, monometallic complexes that form dimeric and multimeric structures and monometallic complexes covalently tethered together *via* the ligand motif.

a) Single Ligand Bimetallic Catalysts

The first bimetallic catalysts were reported by Lee and co-workers. The complexes contained an anilido-aldimine ligand bound to two zinc metal centres (Figure 1.10).[65,66] These catalysts were very active (TON = 2980) in CHO/CO_2 copolymerisation reactions. The copolymer samples contained a high proportion of carbonate linkages (85-96 %) and had high M_n values (90-280 kg/mol), with slightly broad PDIs (1.30-1.70). Structure-activity studies were also carried out and showed that the bulky groups on the terminal aryl rings (R') and electron withdrawing groups (fluorine) on the anildo-amidinate moieties increased the activity (R'').[65]

Adding bulky substituents on the phenyl rings linking the ligand backbone (R) reduced the activity of the catalyst (Figure 1.10).[65,66]

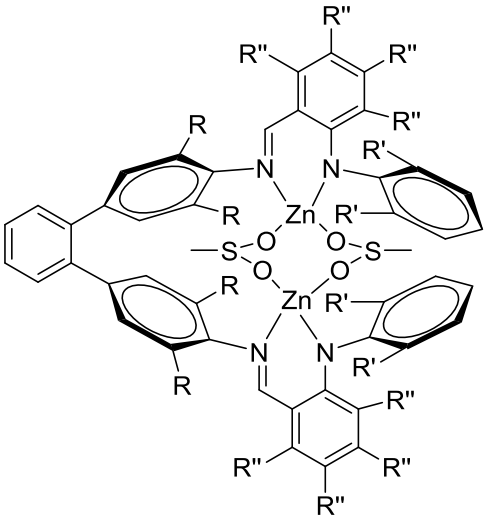

R = Me; R' = ^{i}Pr; R" = H

Figure 1.10: Zinc anildo-amidinate complexes by Lee and co-workers.[65,66]

Other bimetallic catalysts were reported by Ding *et al.*, which included di-zinc and di-magnesium complexes surround by a Trost's phenolate ligand (Figure 1.11).[67] The zinc analogue was active in CHO/CO_2 copolymerisation reactions (TOF = 142 h^{-1} at 20 atm of CO_2 pressure and 80 °C). Additionally, this catalyst worked at 1 atm of CO_2 pressure (TOF = 3 h^{-1}). However, the catalyst required high loadings (5 mol %) compared to the zinc anilido-aldimine catalysts (0.006 mol %).[65,66,68] The magnesium derivative was less active at lower catalyst loadings, but more active at 1 atm CO_2 pressure, as the same TOF value (3 h^{-1}) was recorded at a lower temperature (60 °C) compared to the zinc analogue.[67,68]

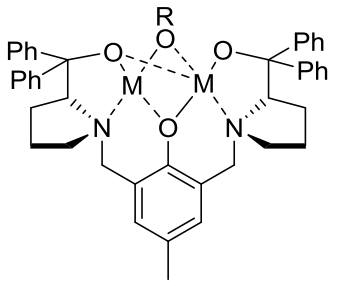

M = Zn, Mg; R = Et, Bu

Figure 1.11: Trost's phenolate complex by Xiao *et al.*[67,68]

Our group (Williams and co-workers) have also reported a class of bimetallic catalysts for poly(cyclohexene carbonate) (PCHC) production. These catalysts consist of two metal centres coordinated to a macrocyclic N_4O_2 ligand (Figure 1.12). Many derivatives of this catalyst have been synthesised, including the first iron catalyst for such copolymerisation reactions.[58,59,69] In depth kinetic and mechanistic studies have also been carried out on these catalysts and have revealed that both metals are involved in the reaction mechanism.[59,60] These catalysts are quite remarkable as they show some of the highest activities (TOF = 6-172 h^{-1}) at low pressures of CO_2 (1 bar).[58,69] It has been suggested that these high activities are attributed to the macrocyclic ligand and bimetallic nature of the catalysts.[5] These catalysts are discussed in more detail in Chapter 2, Section 2.1.

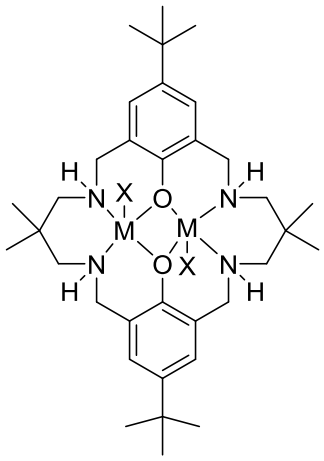

M = Mg, Zn, Co; X = OAc
M = Fe; X= Cl

Figure 1.12: Bimetallic macrocyclic ligands synthesised by Williams and co-workers.[58,59,69]

Lin and co-workers have also reported bis(benzotriazole iminophenol) bimetallic zinc(II), nickel(II) and cobalt(II) catalysts for CHO/CO_2 copolymerisation reactions.[70] The di-zinc catalyst produced a substantial quantity of cyclic carbonate (66 % *vs* copolymer), the di-nickel and di-cobalt catalysts (Figure 1.13) showed good copolymer selectivity (94 or > 99 %, respectively). The copolymer produced had a high carbonate linkage content (> 99 %). Optimal conditions were 120 °C, 21 bar of CO_2 pressure and 0.0625 mol % catalyst loading. The TOF values recorded were 40 and 53 h^{-1}, for the di-nickel and di-cobalt catalysts, respectively.[70,71]

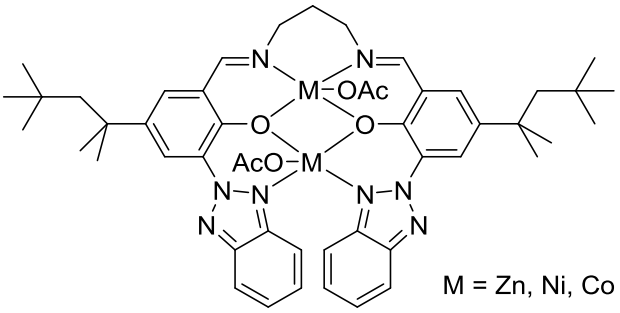

Figure 1.13: Multidentate complexes synthesised by Lin and others.[70,71]

All these discoveries suggest that a bimetallic mechanism is adopted during epoxide/CO_2 copolymerisation reactions and thus having two metal centres in close proximity to one and other improves the activity of the catalyst. Additionally, the choice of metal and substituents on the ligand backbones are important, as the electronic properties at the metal centre affect the ability for the epoxide to bind and the metal co-ligand or metal carbonate bonds to nucleophilically attack the epoxide for ring opening.

b) Dimeric and Multimeric Catalyst Structures

Another class of bimetallic catalysts (dimeric complexes) have also been reported for epoxide/CO_2 copolymerisation reactions. These structures are usually based on Schiff base ligands or multi- *N,O* donor ligands. The dimers can form *via* oxo bridges, which can be between the ligand motifs or between the co-ligands (alkoxides or carboxylates).

Nozaki and others have discovered chiral dimeric zinc complexes (Figure 1.14) for the copolymerisation of CHO/CO_2.[72] The catalyst produced (*R,R*)-PCHC with an *ee* of ≈ 80 %. The proposed mechanism involves a bimetallic pathway, but it is unclear if the dimer remains under polymerisation conditions or monomeric structures work cooperatively.[72]

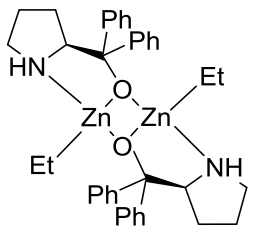

Figure 1.14: Dimeric zinc complexes produced by Nozaki and co-workers.[72]

Hou and co-workers have synthesised a series of dimeric rare earth metal catalysts for CHO/CO_2 copolymerisation reactions.[73] They found that half-sandwich bis(alkyl) lutetium complexes undergo CO_2 insertion to form dimeric compounds, which initiate CHO/CO_2 copolymerisation reactions. The most active of the series (Figure 1.15) produced PCHC (M_n = 23000 g/mol, PDI = 4.0) with 92 % carbonate linkages, at 12 atm of CO_2 pressure and 70 ºC.[73]

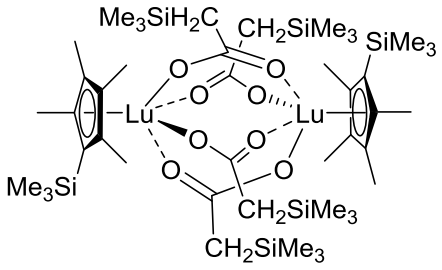

Figure 1.15: Rare earth metal dimeric complexes synthesised by Hou and co-workers.[73]

Additionally, Sugimoto found that dimeric β-diketiminate and Schiff-base aluminium complexes (Figure 1.16) were active in CHO/CO_2 copolymerisation reactions in the presence of Et_4NOAc.[74] Good selectivity (carbonate linkages > 98 %), reasonable activity (TOF < 13 h^{-1}) and low enantioselectivity (*ee* ≈ 25 % for (*R,R*)-PCHC) was observed. The *ee* increased to ≈ 62 % by the use of different Lewis bases (bis-*N*-MeIm or bis-*N*-MeBzIm). The importance of the co-catalysts suggests that a bi-component mechanism may be occurring, which has also been seen with porphyrin based catalysts (Section 1.7.1 and 1.7.2).[74]

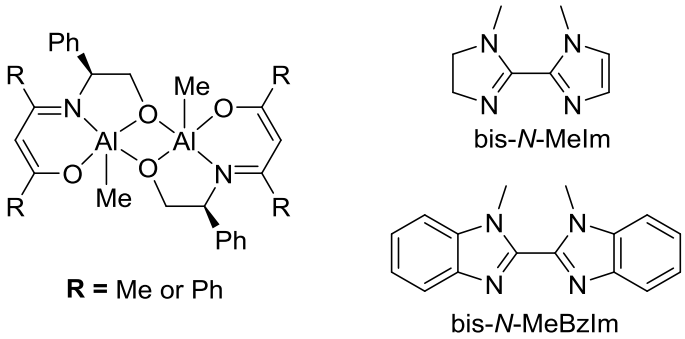

Figure 1.16: Sugimoto's dimeric β-diketiminate aluminium complexes.[74]

Furthermore, Nozaki in 2013, reported a dimeric iron-corrole complex (Figure 1.17), for CHO, PO or glycidyl phenyl ether (GPE) and CO_2 copolymerisation reactions.[50] This dimeric catalyst required a co-catalyst (for example, PPNCl) and showed good activity (PO, TOF >

1000 h^{-1}). However, the copolymers produced had a high content of ether linkages, up to 71 % and 78 % for PO and GPE, respectively. The manganese derivatives of these catalysts were also active in PO/CO_2 copolymerisation reactions, but they were less active than their iron counterparts. However, the carbonate content in the PPC formed was higher for the manganese derivatives.[50,51]

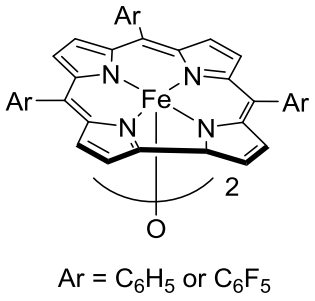

Figure 1.17: Dimeric iron corrole complex by Nozaki.[50,51]

Finally, Lin and co-workers have investigated dimeric copper complexes for CHO/CO_2 copolymerisation reactions (Figure 1.18).[71] The dimeric complexes had higher activities than the mono- and tri-metallic analogues (TOF up to 18 h^{-1}). The optimal conditions were 120 ºC, a CO_2 pressure of 21 bar and catalyst loading of 0.2 mol %. The dimeric species also showed good copolymer selectivity (> 71%) and produced low M_n copolymers (3000 < M_n < 7000 g/mol).[71]

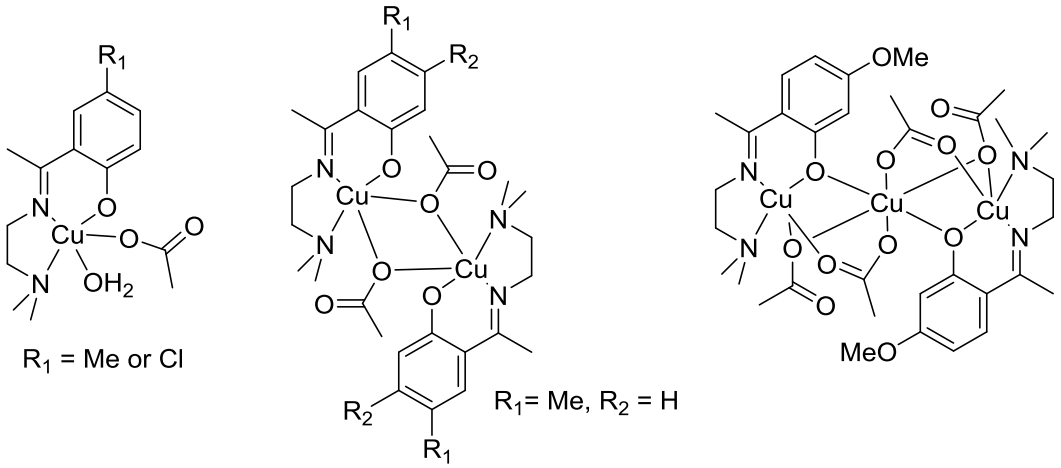

Figure 1.18: Mono-, di- and tri-meric copper complexes by Lin and co-workers.[71]

c) Tethered Monometallic Catalysts

From the high activities reported for single ligand bimetallic catalysts, some research groups have synthesised bimetallic complexes by tethering successful 'monometallic' catalysts. It is thought that this may improve the activity of the catalysts even more.[46,47,62] The conventional route to obtain these tethered catalysts is to covalently link two identical ligand motifs together and then coordinate the ligands to metal centres to form homo-bimetallic catalysts.

The high activity of the zinc BDI catalysts and the mechanistic studies carried out by Coates and others (Section 1.7.3), led to the natural progression of tethering the zinc BDIs. Pilz *et al.* have synthesised such a complex, in which the zinc metal centres are in parallel to one and other (Figure 1.19, left).[75] The zinc-zinc distance was observed to be 4.92 Å, but unfortunately the hypothesis did not hold, as the activity of this bimetallic complex (TOF = 9 h^{-1}) was lower than the conventional zinc BDI catalyst. This lower activity is potentially due to steric effects.[75]

However, by bridging two BDI ligands *via para*- and *meta*-substituted phenyl groups produced tethered zinc BDI complexes, which had good activity for PCHC formation (Figure 1.19, right).[56] Harder and co-workers reported a Zn-Zn distance of 3.79 Å and a TOF of 262 h^{-1}, at 10 atm of CO_2 pressure and 60 °C. The copolymer produced consisted of > 99 % carbonate linkages and had high M_n (45–100 kg/mol).[56]

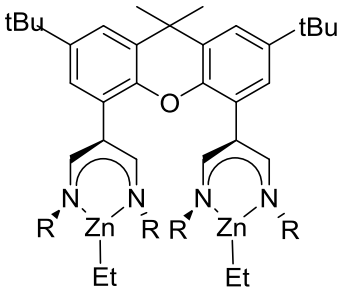

R= 2,3-dimethylphenyl

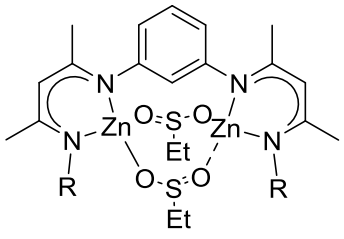

R = 2,5-^{i}Pr-C_6H_5

Figure 1.19: Tethered zinc BDI complexes.[56,75]

Rieger and co-workers have also worked extensively on tethering known mono-metallic complexes. One report also showed zinc BDI species linked through the phenyl rings.[55] Two derivatives were synthesised, but the analogue with the more rigid linker had a low activity in

CHO/CO_2 copolymerisation reactions (Figure 1.20, right). The more flexible catalyst showed the highest activity (9130 h^{-1}) at 40 bar CO_2 pressure and 100 °C (Figure 1.20, left).[55]

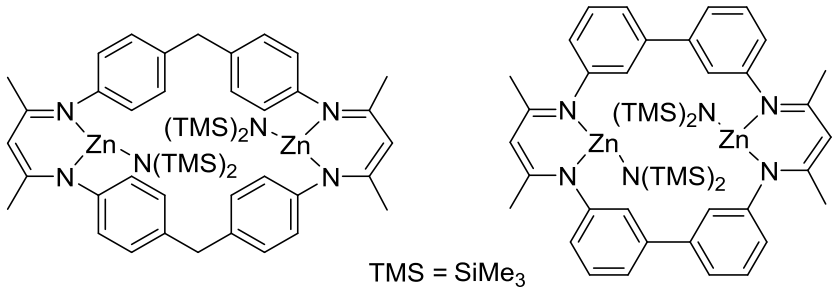

Figure 1.20: Tethered zinc complexes reported by Rieger and co-workers.[55]

Kinetic and DFT studies carried out with the more active analogue (Figure 1.20, left) suggested that the rate-determining step changes with CO_2 pressure. Under 25 bar CO_2 pressure, it was shown that the rate of copolymerisation is first order dependent on CO_2 pressure and zero order dependent on epoxide concentration.[55] Therefore, it was proposed that CO_2 insertion is the rate limiting step. However, above 25 bar CO_2 pressure, the rate determining step seemed to be the ring opening of the epoxide and CO_2 insertion was non-rate determining.[55]

Moreover, Rieger and others have also tethered porphyrin ligands to make bis-porphyrin complexes (Figure 1.21). The bimetallic cobalt complexes showed lower productivities compared to their monometallic counterparts (TON = 300 – 696 depending on linker *vs* 983).[76] Furthermore, it was essential to use co-catalysts with these complexes. A possible explanation for this lower activity could be catalyst deactivation. It was observed that the reduction of cobalt (III) to cobalt (II) was faster in the bimetallic complexes compared to the monometallic counterparts.[76]

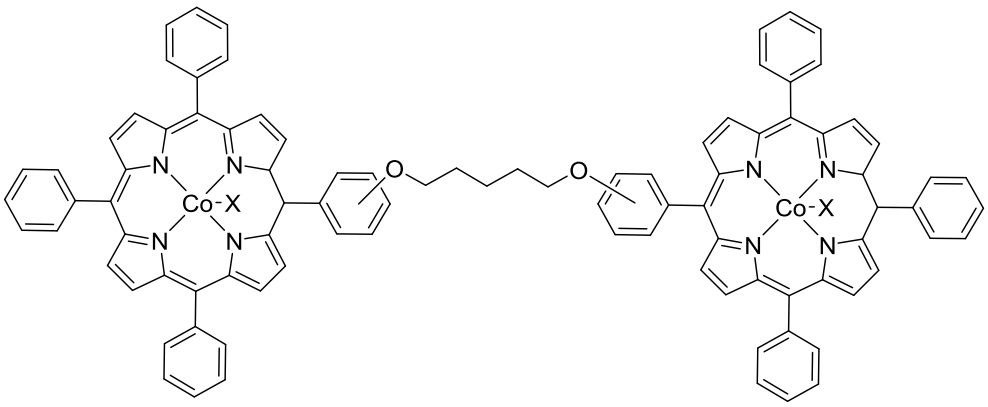

Figure 1.21: Tethered cobalt porphyrin complexes by Rieger and others.[76]

1.7.5 Salen Based Catalysts

Another major class of monometallic catalysts for epoxide/CO_2 copolymerisation reactions are the metal salen complexes (Figure 1.22). These have been extensively researched over the past 15 years and thus many structure activity relationships have been reported. From all of these modifications and in depth investigations, the metal salen complexes are some of the most active, if not the most active, catalysts for epoxide/CO_2 copolymerisation reactions.

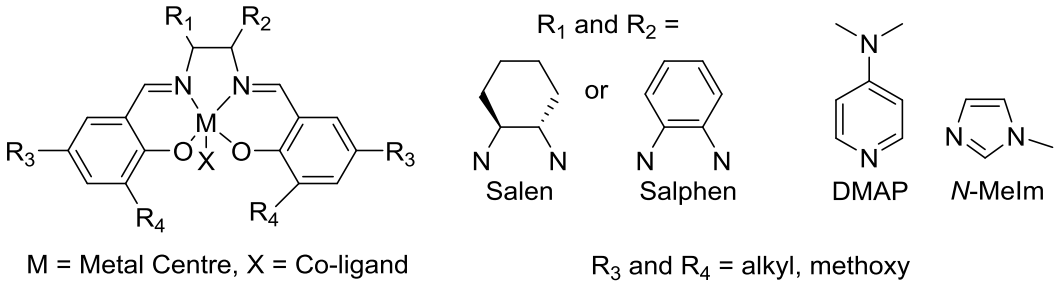

Figure 1.22: Generic structure of metal salen complexes.

a) Binary Systems

The initial detailed report for the use of metal salen complexes for epoxide/CO_2 copolymerisation reactions came from Darensbourg. A Cr(III) salen complex (R_3 and R_4 = ^{t}Bu, X = Cl) with a Lewis base co-catalyst (*N*-MeIm or DMAP) showed good activity in CHO/CO_2 copolymerisation reactions (TOF = 32 h^{-1}, 80 ºC, 58.5 bar of CO_2 pressure).[77] There have been a vast quantity of modifications to this Cr(III) salen complex and these have been recently reviewed extensively, but some of the key modifications have been discussed below.[23,52,78]

The first modifications of these catalysts were carried out by Rieger and co-workers. A Cr(III) salphen complex (R_3 and R_4 = ^{t}Bu, X = Cl) with DMAP, as the co-catalyst, worked well for PPC formation.[79] Coates and others have also modified the Cr(III) salen catalyst established by Darensbourg. Coates and co-workers replaced the Cr(III) metal centre with Co(III).[27,80] The cobalt derivative was also active for PO/CO_2 copolymerisation reactions (TOF up to 81 h^{-1}).[27,80] The PPC chains produced also contained a high content of carbonate linkages (> 95 %). However, unlike their chromium counterparts, these analogues did not require any co-catalysts.[80] Additionally, these cobalt complexes worked at room temperature and under 55 bar CO_2 pressure.[27,80]

However, it was also reported that by increasing the temperature (40 °C) or decreasing the pressure (40 bar) reduced activity of the cobalt salen complexes (TOF < 20 h^{-1}). Lu *et al.* therefore added ammonium salts ($n$$Bu_4NX$, X = Cl, Br, I, OAc) in conjunction with the Co(III) salen catalyst in PO/CO_2 copolymerisation reactions and found that this improved the activity (TOF > 160 h^{-1}), at lower pressures of CO_2 (20 bar).[81] Other metals have also been explored, such as, aluminium and gallium, but these analogues have shown lower activity, if any, compared to the chromium and cobalt derivatives.[82]

Many other salen ligand modifications have also been carried out, by either modifying the substituents on the phenyl rings, changing the imine backbone or reducing the imine moieties to amines. The replacement of the conventional ^{t}Bu groups in the R_3 and R_4 positions with Me and OMe groups has been carried out. Generally, changing more than two ^{t}Bu groups with other substituents reduced the solubility of the complex and hence activity.[83] By replacing the ^{t}Bu groups with Me did not affect activity significantly, but a slight lower activity was observed. The use of OMe groups improved the activity of the complexes and this is thought to be due to electronic effects. The OMe groups are believed to reduce the electrophilicity of the metal centre of the complex and hence make the metal-X or metal-carbonate bonds more nucleophilic and therefore attack of the epoxide, for ring opening, is thought to be more likely.[83]

Changing the co-ligand groups also affected the activity of salen complexes. Azide groups showed a better activity compared to halide groups. This is believed to be because the azide co-ligands more rapidly initiate epoxide ring opening.[83]

Moreover, as described earlier, co-catalysts are required to be used in conjunction with these salen complexes. Many different co-catalysts have been screened and it has been established that the use of one equivalent of co-catalyst is optimum. Using more than one equivalent of co-catalyst can deactivate the catalyst as its coordination sphere becomes saturated and therefore the epoxide monomer is unable to bind to the metal centre.[84,85] This saturation is more prominent if *N*-heterocyclic amines are used as co-catalysts. Adding more than one equivalent of co-catalyst also enhances the displacement of the growing copolymer chain and thus backbiting reactions within the free copolymer chain occur, which leads to an increase in cyclic carbonate by-product formation.[23,77,83,85]

The co-catalysts investigated with salen complexes are all Lewis basic species and can be ionic compounds derived from bis(triphenylphosphine)iminium (PPN^+) and tetraalkylammonium salts, or neutral, such as, *N*-heterocyclic amines and phosphines. The ionic co-catalysts were generally more effective than the neutral co-catalysts because they have reduced initiation periods. When salen complexes were used without co-catalysts, activity within these copolymerisation reactions was still observed (*vide supra*), but the reactions had large initiation periods.[23,77,86]

Anions derived from PPN^+ salts compared to n-Bu_4N^+ salts were more effective co-catalysts. The reason for this is that PPN^+ salts are more easily isolated and purified as they are highly hydrophobic. Azide anions were the more reactive followed by Cl > Br > I, which is due to the fact that azides are better nucleophiles.[23,77,86,87]

b) Kinetic and Mechanistic Studies

Coates and Darensbourg have observed separately that metal salen catalysts operate a monometallic propagation mechanism.[27,77] However, Nozaki and co-workers have looked at a Co(salen)Cl/PPNCl system and the order in catalyst concentration was recorded to be 1.57, which suggests that complex propagation pathways occur.[88] Fractional orders in catalyst concentration have also been observed by Rieger and others when investigating chromium salen complexes without the use of co-catalysts.[89]

Several mechanisms have been proposed for the initiation pathway of metal salen/co-catalyst systems. One involves a bimetallic pathway (two metal salen complexes) and the other two proposed mechanisms involve only one metal salen complex (Figure 1.23).[26,76,85,90] The monometallic pathways adopted have been shown to be dependent on the type of co-catalyst used.[5,90]

The co-catalyst has been shown to bind *trans* to the X initiating group on the metal centre of the salen complex, if ionic in nature. This leads to the formation of an anionic octahedral intermediate. Upon addition of epoxide the formation of a neutral complex [salenCr(X)(epoxide)] occurs, but the reaction is in equilibrium and heavily favours the anionic intermediate [salenCr$(X)_2$].[5,90] However, by ATR-IR spectroscopy it has been seen that the metal bound epoxide undergoes ring opening by the displaced anion. It is difficult to

know if the co-catalyst or X initiating group is displaced because MALDI-ToF spectra have shown both the initiating group and the co-catalyst as copolymer end groups. This therefore suggests that two chains may grow from the salen complex (Figure 1.23).[5,90]

For neutral co-catalysts, it is believed a neutral octahedral intermediate is formed and that the co-catalyst binds *trans* to the X initiating group and causes the M-X bond to weaken. This therefore promotes the X initiating group to ring open an epoxide molecule.[5,90] However, another hypothesis is that, like for ionic co-catalysts, when epoxides are present, the co-catalyst is displaced by an epoxide monomer, but this also weakens the M-X bond and thus the X initiating group can still ring open an approaching epoxide monomer. However additionally, the bound epoxide can be ring opened by the displaced co-catalyst. In this latter mechanism two chains may propagate from the salen complex (Figure 1.23).[5,90]

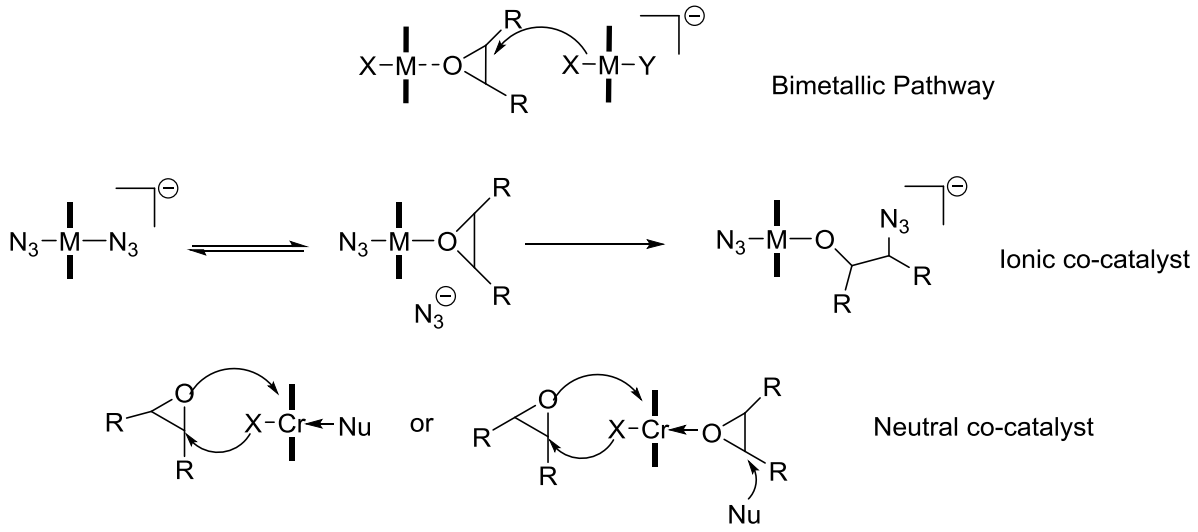

Figure 1.23: Proposed initiation pathways for metal salen complexes.[5,90]

The complex nature of these initiation steps has led to the proposal that complex propagation pathways may also be adopted. The nuclearity of the propagating species and the charge of the complex are still unknown. Moreover, it is uncertain about how many polycarbonate chains grow per salen catalyst. Lower than expected M_n values are recorded when using metal salen complexes. Initially, it was thought that these lower M_n values were due to two polycarbonate chains growing per catalyst. However, the recorded values were even lower

than the expected values calculated for two growing chains per catalyst, thus suggesting that chain transfer reactions were occurring in these copolymerisation reactions (Figure 1.4 and 1.24).[23]

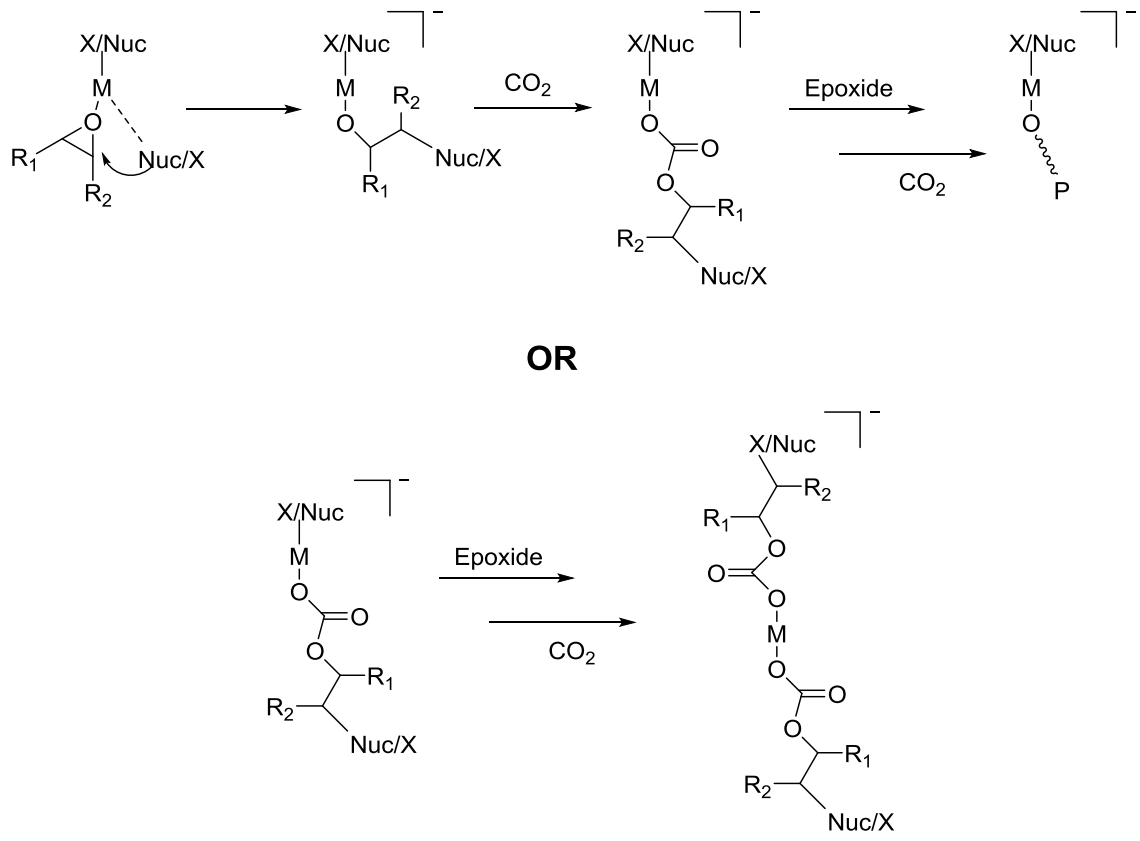

Figure 1.24: Illustrates one or two copolymer chains growing per salen complex.

Darensbourg and co-workers tried to shed light onto whether one or two chains grow per salen catalyst by assuming that a chromium tetramethyltetraazaannulene complex (Cr(tmtaa)) copolymerises epoxide and CO_2 in the same manner as salen complexes (chain propagation in the axial position of the complex). Darensbourg recorded the catalytic activities of both a Cr(tmtaa) complex and a Cr(stmtaa) complex (Figure 1.25).[91] The Cr(stmtaa) complex contained a sterically encumbering strap moiety, which runs beneath the ligand and thus prevents chain growth occurring from one of the axial positions in the complex. Therefore, it was believed that if the Cr(tmtaa) grows two chains per catalysts (in both axial positions), then the activity of this catalyst would be higher than for the Cr(stmtaa) catalyst.[91]

It was found that both complexes copolymerised CHO and CO_2 with similar activities and thus it was suggested that only one chain grows per catalyst. A tentative comparison to metal salen and phorphyrin catalysts was carried out and thus led to the suggestion that one chain may also grow per salen catalysts.[91]

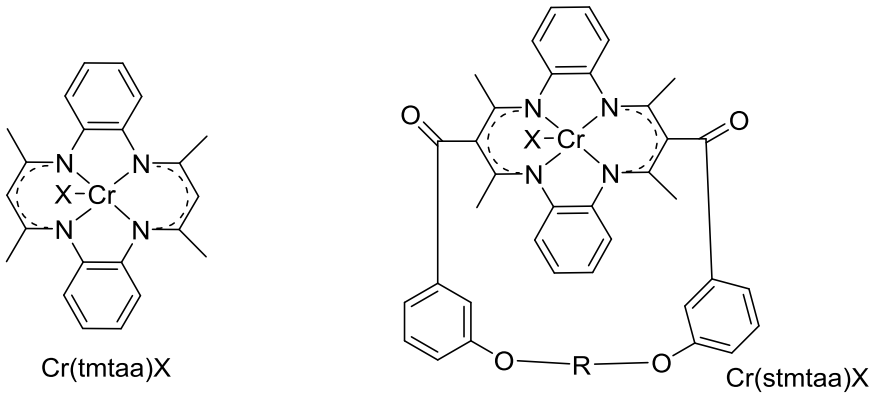

Figure 1.25: Cr(tmtaa) and Cr(stmtaa) complexes.[91]

c) Bifunctional Systems

From early studies (*vide supra*) it has been seen that metal salen complexes require a co-catalyst in order to function in epoxide/CO_2 copolymerisation reactions. These binary systems are highly active, but a considerable amount of research into developing optimised bifunctional catalyst systems has also been carried out. This involves a co-catalyst being covalently tethered to the ligand motif of the metal salen complex. Some of these bifunctional catalyst systems show the best catalytic activities in epoxide/CO_2 copolymerisation reactions.

In 2006, Nozaki investigated a novel two component salen ligand based catalyst.[92] This cobalt(III) salen complex with a piperidinium group tethered to the ligand motif required no addition of an exogenous co-catalyst (Figure 1.26). The complex had high copolymer selectivity (>99%) and activity (TOF = 250 h^{-1}) in PO/CO_2 copolymerisation reactions at 14 bar CO_2 pressure and 25 ºC. It was also suggested that the piperidinium group quelled backbiting reactions and thus minimal cyclic carbonate by-product was observed. Therefore, higher temperatures could be used whilst still maintaining high copolymer selectivity (≈ 90 %) and thus higher activities were recorded (TOF = 680 h^{-1}). [92]

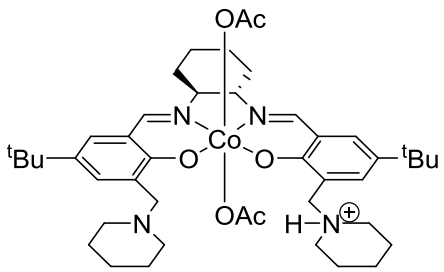

Figure 1.26: Bifunctional cobalt salen catalyst with piperdinium arm synthesised by Nozaki and co-workers. [92]

In 2007, Lee and others synthesised a cobalt(III) metal salen complex with two ammonium arms on the ligand motif and used it in PPC formation.[26] This complex had a high activity (TOF = 3500 h^{-1}), at 90 ºC, which also showed good copolymer selectivity (≈ 90 %). These complexes showed higher activities and selectivities compared to their binary counterparts.[26]

Lee has also reported a cobalt(III) metal salen complex tethered to four ammonium groups for PO/CO_2 copolymerisation reactions (Figure 1.27). This complex is even more active and produced PPC, at 70 ºC, with high copolymer selectivity (>99 %).[25,93] The activities reported were > 20 000 h^{-1}. This complex also maintained such high activities and selectivities at extremely low catalyst loadings (1:150 000, catalyst:PO), which allowed high M_n polycarbonate chains to be accessed (285 000 g/mol).[24,92]

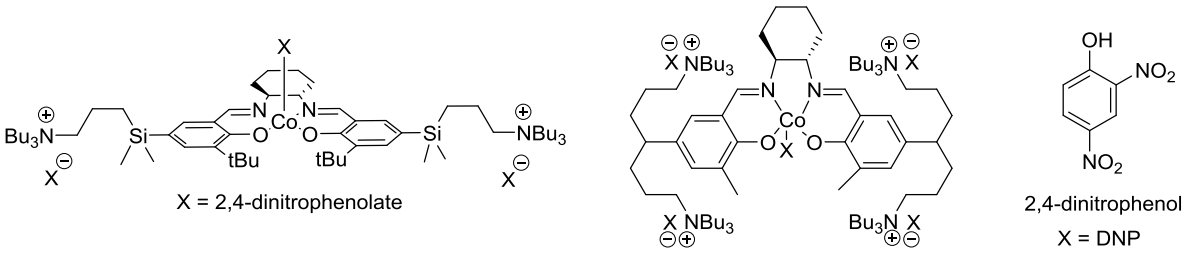

Figure 1.27: Single component salen complex by Lee and others. [24,92]

Moreover, this catalyst can easily be removed from the copolymer sample produced as the quaternary ammonium cations can tether to silica when a solution of the polymer is poured through a silica pad. Once recovered the catalyst can be re-used with minimal loss of catalytic activity.[93] Kinetic and mechanistic investigations have also revealed that these bifunctional complexes adopt cobaltate intermediates and unique coordination geometries (cis-β), which may be important for good activity (Figure 1.28).[94,25,95] Furthermore, these catalysts have

been used to form telechelic PPC, which have been used to synthesise higher polymers (polyurethanes).[96,97]

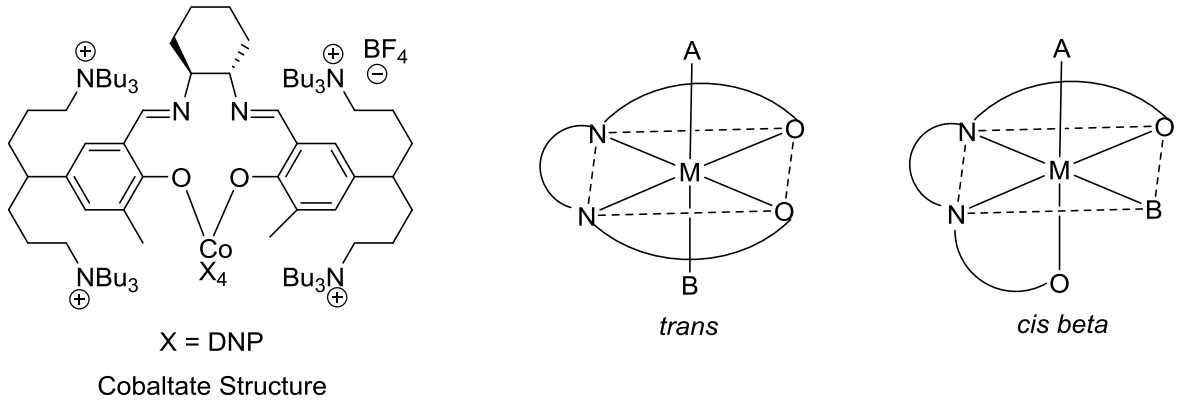

Figure 1.28: Cobaltate salen complex structure and two of the possible configurations that an octahedral salen complex can adopt.[25,95]

Lu and co-workers have also reported cobalt(III) metal salen complexes with ammonium salts or neutral Lewis bases covalently bonded to the salen ligand architecture (Figure 1.29).[98] Similar high activities were observed for these bifunctional complexes in both PO and CHO/CO_2 copolymerisation reactions compared to their binary analogues.[99]

It was proposed that these high activities occurred because the tethered ammonium salts keep any dissociated polycarbonate chains in 'close proximity' to the metal centre. The enhanced selectivities were also attributed to the likelihood that there is a higher activation barrier to forming cyclic by-products in these bifunctional catalyst systems compared to their binary counterparts.[99]

In addition, these catalysts also managed to produce isotactic poly(chloropropylene carbonate).[100] This prompted Darensbourg to use these catalysts with various other epoxides, such as, cyclopentene oxide and indene oxide; which have been shown to be difficult to copolymerise. These bifunctional catalysts have shown promise to being able to copolymerise unique epoxides, which are renewably derived.[101] Poly(cyclopentene carbonate) is particularly interesting because it undergoes depolymerisation readily to regenerate its constituent epoxide and CO_2 monomers, which is unusual as most polycarbonates depolymerise to cyclic carbonates.[102]

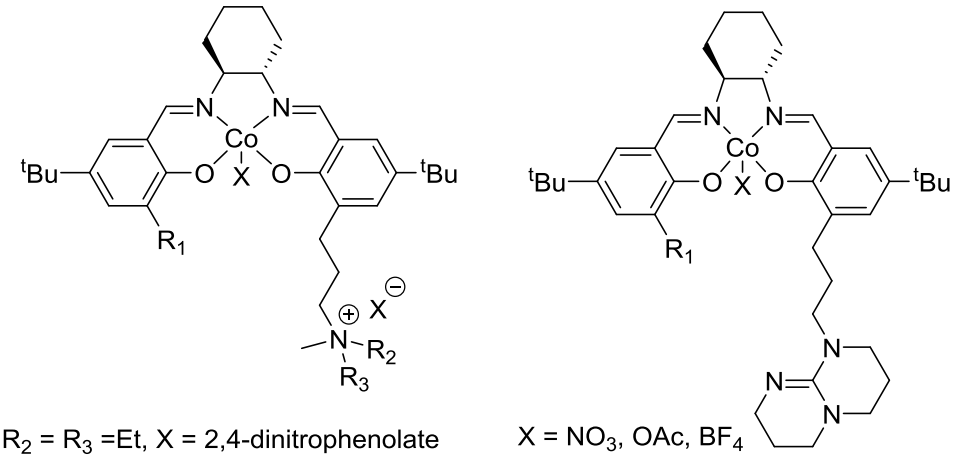

Figure 1.29: Single component salen complexes by Lu, with ammonium salts or Lewis base attached to the ligand motif.

Finally, the salen complexes tethered to neutral Lewis bases (TBD – triazabicyclodecene).[78,98] were not only highly active (TOF up to 10,000 h^{-1}) and selective towards copolymer formation (> 97%) at high temperatures (up to 100 ºC) in CHO/CO_2 and PO/CO_2 copolymerisations reactions,[99,103] but they also worked for styrene oxide (SO)/CO_2 copolymerisation reactions (Figure 1.29).[104] Additionally, the catalyst can copolymerise epichlorohydrin and CO_2 and the copolymer formed has high carbonate content (> 99 %). Lowering the reaction temperature, from 25 ºC to 0 ºC, increased copolymer selectivity (> 99 % *vs* cyclic carbonate), but comparatively the binary cobalt salen/PPNX systems only showed a maximum of 66 % copolymer selectivity at even low temperatures.[105]

d) Bimetallic Systems

From the reports in literature (*vide supra*), metal salen complexes and bimetallic complexes have good activities and selectivities for epoxide/CO_2 copolymerisation reactions and therefore the natural progression for the field of salen complexes was to investigate bimetallic salen based complexes.

In 2010, Nozaki investigated several bimetallic cobalt(III) salen complexes in PO/CO_2 copolymerisation reactions. These bimetallic complexes were formed by tethering two salen based ligands together (Figure 1.30). It was found that without a co-catalyst, the copolymerisation occurs by a bimetallic process.[106] The bimetallic catalysts showed higher

activities compared to their monometallic counterparts and could operate at lower catalyst loadings more effectively, in some cases five times faster at a 1:3000, catalyst:PO loading.[106]

Moreover, the length of the linker between the two salen complexes significantly affected activity and selectivity. The optimum spacer was when n = 4 (TOF = 180 h^{-1} at PO/Co = 3000). This highlights that a bimetallic mechanism is in play. The presence of ionic co-catalysts (ammonium salts) prompted the copolymerisation to occur *via* more complex or monometallic mechanisms.[106]

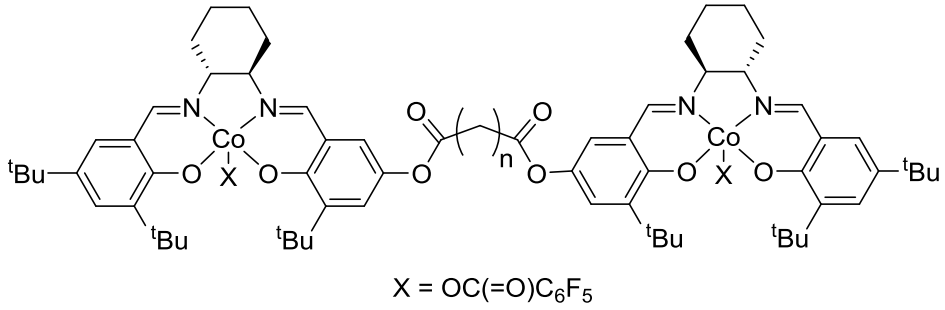

Figure 1.30: Bimetallic cobalt salen complexes by Nozaki and co-workers.[106]

Rieger and others have also reported bimetallic chromium salphen complexes for PO/CO_2 copolymerisation reactions (Figure 1.31).[89] Similar to Nozaki's findings, the presence of no co-catalyst, the bimetallic complex has a higher activity compared to its monometallic analogue (TOF = 82 h^{-1} and 7 h^{-1}, respectively at 1:20000, catalyst:PO loadings). However, at higher catalyst loadings (PO/Cr = 2000) the activities were very similar (TOF = 67 h^{-1} for bimetallic complex and 49 h^{-1} for monometallic complex). Again the mechanism occurs *via* a bimetallic pathway, but upon addition of co-catalysts the bimetallic catalysts revert to a bi-component monometallic mechanism.[89]

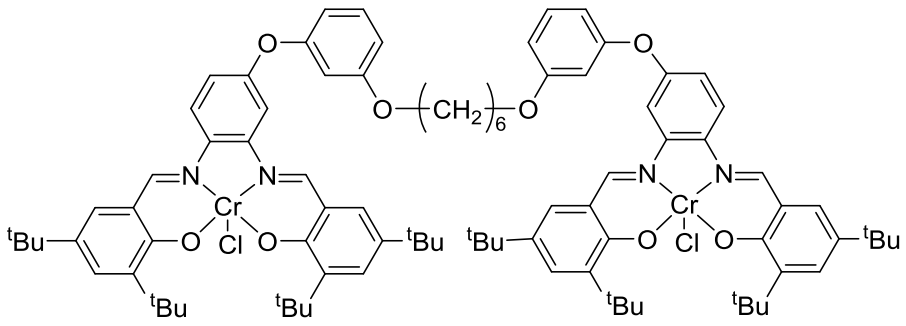

Figure 1.31: Bimetallic Cr(III)salphen complex reported by Rieger and co-workers.[89]

Finally, Lu and co-workers in 2013, used dinuclear cobalt(III) complexes for CHO or cyclopentene oxide (CPO) and CO_2 copolymerisation reactions (Figure 1.32).[107] CPO/CO_2 copolymerisations at 25 ºC and 20 bar CO_2 pressure with PPNX (X = 2,4-dinitrophenoxide) as a co-catalyst were carried out and high enantioselectivities (*ee* > 99 %) were obtained alongside high activities (TOF ≈ 200 h^{-1}). These complexes also worked at low pressures (1 atm) and still maintained reasonable activities (TOF = 40 h^{-1}) and good enantioselectivities (*ee* = 96 %). With no co-catalyst present the bimetallic catalysts showed low activities and enantioselectivities for both CHO/CO_2 or CPO/CO_2 copolymerisation reactions.[107]

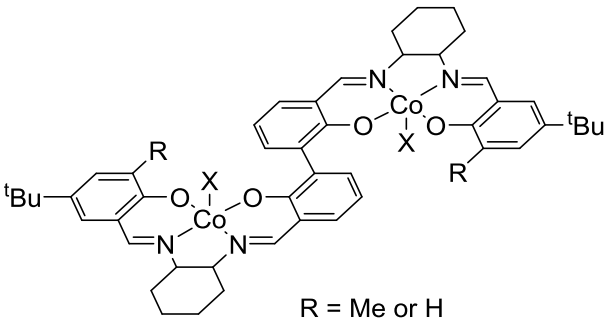

Figure 1.32: Bimetallic cobalt salen complex by Lu.[107]

Moreover, similar to Nozaki's findings, the spacer linking the two monometallic salen complexes not only affects activity and copolymer selectivity, but also enantioselectivity. The catalyst in Figure 1.33 showed a reduction in *ee* (< 33 %) in CPO/CO_2 copolymerisation reactions. This suggests that the linker is not only very important in governing the metal-metal distance and thus activity, but also the geometry of the complex, which affects *ee*.[107]

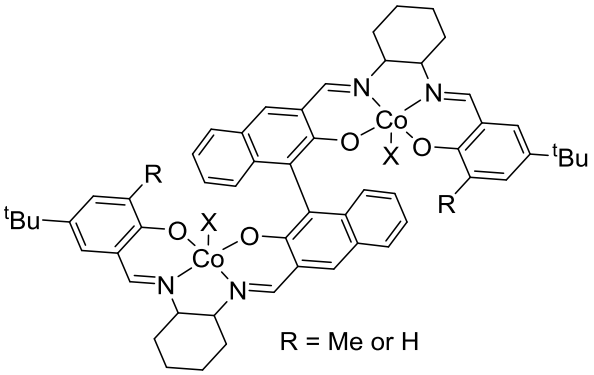

Figure 1.33: Bimetallic cobalt salen complex with a rigid linker, reported by Lu.[107]

1.8 Outlook

As seen in Sections 1.5-1.7, many catalysts for epoxide/CO_2 copolymerisation reactions have been developed over the past 45 years. The activities of these catalysts are very varied, but the most active catalysts to date are the bifunctional salen complexes, which have a TOF of approximately 26 000 h^{-1}.[24,92] However, much more work is needed to be carried in this field before the implementation of this process within industry can occur.

There are still several problems that need to be tackled. Firstly, further catalyst development needs to be carried out in order to produce a third generation of catalysts, which have even higher activities. The TOF values need to exceed 10 000 h^{-1} in order to produce society's current demand of polycarbonates.

Moreover, the catalysts developed so far only work with a narrow range of epoxides, for example, PO and CHO. Even though their respective polycarbonates have desirable thermal and chemical properties (T_g for PCHC is 112 °C and for PPC is 45 °C)[5] a wider variety of polycarbonates, with different backbones and thus different properties need to be produced in order to be useful for industry. Therefore, the next generation of catalysts not only need to be highly active, but also robust and tolerant for a wide variety of monomers.

Additionally, research into using epoxides from renewable resources, such as, limonene oxide and α-pinene oxide needs to be carried out more extensively. This has already been attempted by Coates and a few others. Coates was the first to use limonene oxide from citrus peel to produce polycarbonate, but unfortunately the TOF values obtained with the zinc β-diiminates (33 h^{-1}) were fairly low.[21] If this is achieved more successfully, with new catalysts, the polycarbonates produced will be 100 % renewably derived.

Investigations into producing catalysts that can produce regioregular and enantiomerically enriched polycarbonates have already been carried out and this has been discussed briefly in Section 1.7 and extensively reported in several reviews.[5] However, further research into producing isotactic and regioregular copolymers needs to occur. These polymers also have desirable properties and morphologies that can be utilised by industry, for example, higher crystallinity.

Finally, the catalysts for the ROCOP of epoxide and CO_2 should also be investigated in other ring opening copolymerisation reactions. If successful, there is a potential to produce terpolymers, which may also have differing properties that could be useful in the polymer industry. Moreover, these block copolymers will be partially renewably derived, if not completely, and thus more desirable than current polymer products, which are petrochemically derived.

1.9 Aims and Objectives

The aims and objectives of this thesis are three-fold:

1. To gain in depth understanding of the kinetics and the mechanism employed by known homodinuclear catalysts, previously reported in our group, for CHO/CO_2 copolymerisation reactions.[58,59,69] In particular, to understand the role of each metal centre and the co-ligands and how varying the metal centres affects the rate of copolymerisation.
2. To modify these homodinuclear catalysts in order to improve the TOF values recorded for such catalyst systems. This will enable these catalysts to compete with the 'work-horses' of this field (bifunctional metal salen complexes). Additionally, this will also help with the end goal, which is to industrially produce polycarbonates from renewable feedstocks. The modifications considered by this thesis are to synthesise heterodinuclear catalysts and asymmetrical homodinuclear catalysts (Figure 1.34).
3. Use previously reported homodinuclear catalysts and potentially new analogues (Aim 2) in epoxide/anhydride copolymerisation reactions to yield polyesters, another useful commodity to society. Additionally, the use of one catalyst for two different ring opening copolymerisation reactions (epoxide/CO_2 and epoxide/anhydride) could lead to the potential to form block copolymers, which may have varying thermal and chemical properties that may be of interest to the polymer industry.

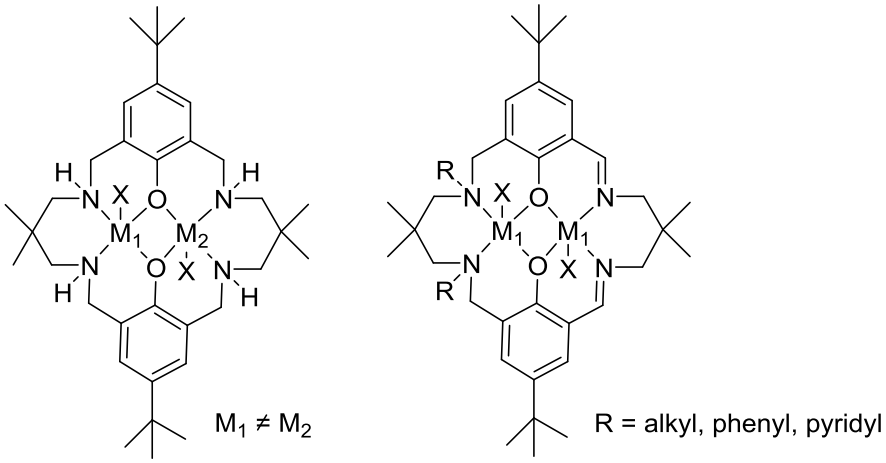

Figure 1.34: Proposed catalyst targets for this thesis. Where M = Lewis acidic metal and X = co-ligand (usually OAc).

1.10 References

1. P. R. Odell *Why Carbon Fuels Will Dominate The 21st Century's Global Energy Economy*; Multi-Science Publishing: Essex, U.K., 2004.

2. M. Aresta *Carbon Dioxide as Chemical Feedstck*; Wiley-VCH: Germany, 2010.

3. S. Shafiee and E. Topal, *Energy Policy,* 2009, ***37***, 181-189.

4. D. J. Darensbourg, *Inorg. Chem.,* 2010, ***49***, 10765-10780.

5. M. R. Kember, A. Buchard and C. K. Williams, *Chem. Commun.,* 2011, ***47***, 141-163.

6. P. Markewitz, W. Kuckshinrichs, W. Leitner, J. Linssen, P. Zapp, R. Bongartz, A. Schreiber and T. E. Muller, *Energy Environ. Sci.,* 2012, ***5***, 7281-7305.

7. http://www.globalcarbonproject.org/carbonbudget/14/hl-compact.htm, 15th October 2014.

8. P. Friedlingstein, R. M. Andrew, J. Rogelj, G. P. Peters, J. G. Canadell, R. Knutti, G. Luderer, M. R. Raupach, M. Schaeffer, D. P. van Vuuren and C. Le Quere, *Nature Geosci.,* 2014, *7*, 709-715.

9. R. Hill, P. O'Keefe and C. Snape *The Future of Energy Use*; Earthscan Publications Ltd: London, U.K., 1995.

10. H. Arakawa, M. Aresta, J. N. Armor, M. A. Barteau, E. J. Beckman, A. T. Bell, J. E. Bercaw, C. Creutz, E. Dinjus, D. A. Dixon, K. Domen, D. L. DuBois, J. Eckert, E. Fujita, D. H. Gibson, W. A. Goddard, D. W. Goodman, J. Keller, G. J. Kubas, H. H. Kung, J. E. Lyons, L. E. Manzer, T. J. Marks, K. Morokuma, K. M. Nicholas, R. Periana, L. Que, J. Rostrup-Nielson, W. M. H. Sachtler, L. D. Schmidt, A. Sen, G. A. Somorjai, P. C. Stair, B. R. Stults and W. Tumas, *Chem. Rev.,* 2001, ***101***, 953-996.

11. M. Aresta and A. Dibenedetto, *Dalton Trans.,* 2007, 2975-2992; T. Sakakura, J.-C. Choi and H. Yasuda, *Chem. Rev.,* 2007, ***107***, 2365-2387.

12. T. Sakakura and K. Kohno, *Chem. Commun.,* 2009, 1312-1330; B. Schäffner, F. Schäffner, S. P. Verevkin and A. Börner, *Chem. Rev.,* 2010, ***110***, 4554-4581.

13. https://www.polymersolutions.com/psi-newsletter-archive/january-2014/, 15th October 2014; http://www.basf.com/group/corporate/en_GB/function/conversions:/publish/content/investorrelations/calendar/images/120905/BASF_Investor_Day_Automotive_Polyurethanes.pdf, 15th October 2014.

14. http://www.plasticseurope.org/documents/document/20131014095824final_plastics_the_facts_2013_published_october2013.pdf, 15th October 2014.

15. M. Okada, *Prog. Polym. Sci.,* 2002, ***27***, 87-133.

16. http://www.petrochemconclave.com/presentation/2013/Mr.SMoolji.pdf, 24th October 2014.

17. http://www.bpf.co.uk/Press/Oil_Consumption.aspx, 24th October 2014.

18. S. Inoue, H. Koinuma and T. Tsuruta, *J. Poly. Sci., Part B: Polym. Lett.,* 1969, ***7***, 287-292.

19. N. von der Assen and A. Bardow, *Green Chem.,* 2014, ***16***, 3272-3280.

20. N. von der Assen, P. Voll, M. Peters and A. Bardow, *Chem. Soc. Rev.,* 2014, ***43***, 7982-7994.

21. C. M. Byrne, S. D. Allen, E. B. Lobkovsky and G. W. Coates, *J. Am. Chem. Soc.,* 2004, ***126***, 11404-11405.

22. W. Kuran, *Prog. Polym. Sci.,* 1998, ***23***, 919-992; G. W. Coates and D. R. Moore, *Angew. Chem. Int. Ed.,* 2004, ***43***, 6618-6639; D. J. Darensbourg and M. W. Holtcamp, *Coord. Chem. Rev.,* 1996, ***153***, 155-174; H. Sugimoto and S. Inoue, *J. Polym. Sci. A Polym. Chem.,* 2004, ***42***, 5561-5573.

23. D. J. Darensbourg, *Chem. Rev.,* 2007, ***107***, 2388-2410.

24. K. Nakano, M. Nakamura and K. Nozaki, *Macromolecules,* 2009, ***42***, 6972-6980.

25. S. J. Na, S. S, A. Cyriac, B. E. Kim, J. Yoo, Y. K. Kang, S. J. Han, C. Lee and B. Y. Lee, *Inorg. Chem.,* 2009, ***48***, 10455-10465.

26. E. K. Noh, S. J. Na, S. S, S.-W. Kim and B. Y. Lee, *J. Am. Chem. Soc.,* 2007, ***129***, 8082-8083.

27. C. T. Cohen, T. Chu and G. W. Coates, *J. Am. Chem. Soc.,* 2005, ***127***, 10869-10878.

28. M. Ionescu *Chemistry and Technology of Polyols for Polyurethanes*; Smithers Rapra Technology, 2005.

29. D. R. Moore, M. Cheng, E. B. Lobkovsky and G. W. Coates, *J. Am. Chem. Soc.,* 2003, ***125***, 11911-11924.

30. S. Inoue, *J. Polym. Sci. A Polym. Chem.,* 2000, ***38***, 2861-2871.

31. M. Kobayashi, Y.-L. Tang, T. Tsuruta and S. Inoue, *Macromol. Chem. Phys.,* 1973, ***169***, 69-81.

32. S. Inoue, H. Koinuma, Y. Yokoo and T. Tsuruta, *Macromol. Chem. Phys.,* 1971, ***143***, 97-104; T. Hirano, S. Inoue and T. Tsuruta, *Macromol. Chem. Phys.,* 1975, ***176***, 1913-1917; T. Hirano, S. Inoue and T. Tsuruta, *Macromol. Chem. Phys.,* 1976, ***177***, 3237-3243; Y. Hasebe and T. Tsuruta, *Macromol. Chem. Phys.,* 1987, ***188***, 1403-1414; Y. Hasebe and T. Tsuruta, *Macromol. Chem. Phys.,* 1988, ***189***, 1915-1926; N. Yoshino, C. Suzuki, H. Kobayashi and T.

Tsuruta, *Macromol. Chem. Phys.,* 1988, ***189***, 1903-1913; M. Ishimori, T. Hagiwara, T. Tsuruta, Y. Kai, N. Yasuoka and N. Kasai, *Bull. Chem. Soc. Jpn.,* 1976, ***49***, 1165-1166.

33. M. Kobayashi, S. Inoue and T. Tsuruta, *J. Polym. Sci. A Polym. Chem.,* 1973, ***11***, 2383-2385.

34. W. Kuran, S. Pasynkiewicz, J. Skupińska and A. Rokicki, *Macromol. Chem. Phys.,* 1976, ***177***, 11-20.

35. R. Eberhardt, M. Allmendinger, M. Zintl, C. Troll, G. A. Luinstra and B. Rieger, *Macromol. Chem. Phys.,* 2004, ***205***, 42-47; S. J. Wang, L. C. Du, X. S. Zhao, Y. Z. Meng and S. C. Tjong, *J. Appl. Polym. Sci.,* 2002, ***85***, 2327-2334; Y. Z. Meng, L. C. Du, S. C. Tiong, Q. Zhu and A. S. Hay, *J. Polym. Sci. A Polym. Chem.,* 2002, ***40***, 3579-3591.

36. J. S. Kim, M. Ree, S. W. Lee, W. Oh, S. Baek, B. Lee, T. J. Shin, K. J. Kim, B. Kim and J. Lüning, *J. Catal.,* 2003, ***218***, 386-395.

37. M. Ree, J. Y. Bae, J. H. Jung and T. J. Shin, *J. Polym. Sci. A Polym. Chem.,* 1999, ***37***, 1863-1876.

38. M. Ree, Y. Hwang, J.-S. Kim, H. Kim, G. Kim and H. Kim, *Catal. Today,* 2006, ***115***, 134-145.

39. S. Chen, G.-R. Qi, Z.-J. Hua and H.-Q. Yan, *J. Polym. Chem., Part A: Polym. Chem.,* 2004, ***42***, 5284-5291; I. Kim, M. J. Yi, S. H. Byun, D. W. Park, B. U. Kim and C. S. Ha, *Macromolecular Symp.,* 2005, ***224***, 181-192.

40. S. Klaus, M. W. Lehenmeier, E. Herdtweck, P. Deglmann, A. K. Ott and B. Rieger, *J. Am. Chem. Soc.,* 2011, ***133***, 13151-13161.

41. N. Takeda and S. Inoue, *Macromol. Chem. Phys.,* 1978, ***179***, 1377-1381.

42. D. J. Darensbourg and M. W. Holtcamp, *Macromolecules,* 1995, ***28***, 7577-7579.

43. D. J. Darensbourg, M. W. Holtcamp, G. E. Struck, M. S. Zimmer, S. A. Niezgoda, P. Rainey, J. B. Robertson, J. D. Draper and J. H. Reibenspies, *J. Am. Chem. Soc.,* 1998, ***121***, 107-116.

44. D. J. Darensbourg, J. R. Wildeson, J. C. Yarbrough and J. H. Reibenspies, *J. Am. Chem. Soc.,* 2000, ***122***, 12487-12496.

45. D. J. Darensbourg, J. R. Wildeson and J. C. Yarbrough, *Inorg. Chem.,* 2002, ***41***, 973-980.

46. M. H. Chisholm and Z. Zhou, *J. Am. Chem. Soc.,* 2004, ***126***, 11030-11039; N. D. Harrold, Y. Li and M. H. Chisholm, *Macromolecules,* 2013, ***46***, 692-698.

47. C. Chatterjee and M. H. Chisholm, *Inorg. Chem.,* 2011, ***50***, 4481-4492; C. Chatterjee and M. H. Chisholm, *Inorg. Chem.,* 2012, ***51***, 12041-12052; C. Chatterjee, M. H. Chisholm, A. El-Khaldy, R. D. McIntosh, J. T. Miller and T. Wu, *Inorg. Chem.,* 2013, ***52***, 4547-4553.

48. K. Nakano, K. Kobayashi, T. Ohkawara, H. Imoto and K. Nozaki, *J. Am. Chem. Soc.,* 2013, ***135***, 8456-8459; S. Mang, A. I. Cooper, M. E. Colclough, N. Chauhan and A. B. Holmes, *Macromolecules,* 1999, ***33***, 303-308; T. Aida, M. Ishikawa and S. Inoue, *Macromolecules,* 1986, ***19***, 8-13.

49. H. Sugimoto, H. Ohshima and S. Inoue, *J. Polym. Sci. A Polym. Chem.,* 2003, ***41***, 3549-3555.

50. K. Nakano, K. Kobayashi, T. Ohkawara, H. Imoto and K. Nozaki, *J. Am. Chem. Soc.,* 2013, ***135***, 8456-8459.

51. C. Robert, T. Ohkawara and K. Nozaki, *Chem. Eur. J.,* 2014, ***20***, 4789-4795.

52. D. J. Darensbourg In *Advances in Inorganic Chemistry*; Michele, A., Rudi van, E., Eds.; Academic Press, 2014; Vol. Volume 66, pp 1-23; D. J. Darensbourg, R. M. Mackiewicz, A. L. Phelps and D. R. Billodeaux, *Acc. Chem. Res.,* 2004, ***37***, 836-844.

53. W. C. Ellis, Y. Jung, M. Mulzer, R. Di Girolamo, E. B. Lobkovsky and G. W. Coates, *Chem. Sci.,* 2014, ***5***, 4004-4011; N. M. Rajendran, A. Haleel and N. D. Reddy, *Organometallics,* 2013, ***33***, 217-224; M. F. Pilz, C. Limberg, B. B. Lazarov, K. C. Hultzsch and B. Ziemer, *Organometallics,* 2007, ***26***, 3668-3676.

54. M. Cheng, D. R. Moore, J. J. Reczek, B. M. Chamberlain, E. B. Lobkovsky and G. W. Coates, *J. Am. Chem. Soc.,* 2001, ***123***, 8738-8749.

55. M. W. Lehenmeier, S. Kissling, P. T. Altenbuchner, C. Bruckmeier, P. Deglmann, A.-K. Brym and B. Rieger, *Angew. Chem. Int. Ed.,* 2013, ***52***, 9821-9826.

56. D. F. J. Piesik, S. Range and S. Harder, *Organometallics,* 2008, ***27***, 6178-6187.

57. P. K. Saini, C. Romain and C. K. Williams, *Chem. Commun.,* 2014, ***50***, 4164-4167.

58. M. R. Kember and C. K. Williams, *J. Am. Chem. Soc.,* 2012, ***134***, 15676-15679; M. R. Kember, A. J. P. White and C. K. Williams, *Macromolecules,* 2010, ***43***, 2291-2298; M. R. Kember, A. J. P. White and C. K. Williams, *Inorg. Chem.,* 2009, ***48***, 9535-9542; M. R. Kember, P. D. Knight, P. T. R. Reung and C. K. Williams, *Angew. Chem. Int. Ed.,* 2009, ***48***, 931-933.

59. M. R. Kember, F. Jutz, A. Buchard, A. J. P. White and C. K. Williams, *Chem. Sci.,* 2012, ***3***, 1245-1255.

60. A. Buchard, F. Jutz, M. R. Kember, A. J. P. White, H. S. Rzepa and C. K. Williams, *Macromolecules,* 2012, ***45***, 6781-6795; F. Jutz, A. Buchard, M. R. Kember, S. B. Fredriksen and C. K. Williams, *J. Am. Chem. Soc.,* 2011, ***133***, 17395-17405.

61. H. Sugimoto and K. Kuroda, *Macromolecules,* 2007, ***41***, 312-317.

62. A. Bernard, C. Chatterjee and M. H. Chisholm, *Polym. J.,* 2013, ***54***, 2639-2646.

63. M. Cheng, E. B. Lobkovsky and G. W. Coates, *J. Am. Chem. Soc.,* 1998, ***120***, 11018-11019.

64. D. R. Moore, M. Cheng, E. B. Lobkovsky and G. W. Coates, *Angew. Chem. Int. Ed.,* 2002, ***41***, 2599-2602.

65. T. Bok, H. Yun and B. Y. Lee, *Inorg. Chem.,* 2006, ***45***, 4228-4237.

66. B. Y. Lee, H. Y. Kwon, S. Y. Lee, S. J. Na, S.-i. Han, H. Yun, H. Lee and Y.-W. Park, *J. Am. Chem. Soc.,* 2005, ***127***, 3031-3037.

67. Y. Xiao, Z. Wang and K. Ding, *Macromolecules,* 2005, ***39***, 128-137.

68. Y. L. Xiao, Z. Wang and K. L. Ding, *Chem. Eur. J.,* 2005, ***11***, 3668-3678.

69. A. Buchard, M. R. Kember, K. G. Sandeman and C. K. Williams, *Chem. Commun.,* 2011, ***47***, 212-214.

70. C.-H. Li, H.-J. Chuang, C.-Y. Li, B.-T. Ko and C.-H. Lin, *Polym. Chem.,* 2014, ***5***, 4875-4878.

71. C.-Y. Tsai, B.-H. Huang, M.-W. Hsiao, C.-C. Lin and B.-T. Ko, *Inorg. Chem.,* 2014, ***53***, 5109-5116.

72. K. Nakano, T. Hiyama and K. Nozaki, *Chem. Commun.,* 2005, 1871-1873; K. Nakano, K. Nozaki and T. Hiyama, *J. Am. Chem. Soc.,* 2003, ***125***, 5501-5510.

73. D. Cui, M. Nishiura and Z. Hou, *Macromolecules,* 2005, ***38***, 4089-4095; D. Cui, M. Nishiura, O. Tardif and Z. Hou, *Organometallics,* 2008, ***27***, 2428-2435.

74. K. Nishioka, H. Goto and H. Sugimoto, *Macromolecules,* 2012, ***45***, 8172-8192.

75. M. F. Pilz, C. Limberg, B. B. Lazarov, K. C. Hultzsch and B. Ziemer, *Organometallics,* 2007, ***26***, 3668-3676.

76. C. E. Anderson, S. I. Vagin, M. Hammann, L. Zimmermann and B. Rieger, *ChemCatChem,* 2013, ***5***, 3269-3280.

77. D. J. Darensbourg and J. C. Yarbrough, *J. Am. Chem. Soc.,* 2002, ***124***, 6335-6342.

78. X.-B. Lu and D. J. Darensbourg, *Chem. Soc. Rev.,* 2012, ***41***, 1462-1484; X.-B. Lu, W.-M. Ren and G.-P. Wu, *Acc. Chem. Res.,* 2012, ***45***, 1721-1735.

79. R. Eberhardt, M. Allmendinger and B. Rieger, *Macromol. Rapid Commun.,* 2003, ***24***, 194-196.

80. Z. Qin, C. M. Thomas, S. Lee and G. W. Coates, *Angew. Chem. Int. Ed.,* 2003, ***42***, 5484-5487.

81. X.-B. Lu and Y. Wang, *Angew. Chem. Int. Ed.,* 2004, ***43***, 3574-3577.

82. D. A. Atwood, J. A. Jegier and D. Rutherford, *J. Am. Chem. Soc.,* 1995, ***117***, 6779-6780; X.-B. Lu, Y.-J. Zhang, K. Jin, L.-M. Luo and H. Wang, *J. Catal.,* 2004, ***227***, 537-541; D. J. Darensbourg and D. R. Billodeaux, *Comptes Rendus Chimie,* 2004, ***7***, 755-761.

83. D. J. Darensbourg, R. M. Mackiewicz, J. L. Rodgers and A. L. Phelps, *Inorg. Chem.,* 2004, ***43***, 1831-1833.

84. R. L. Paddock and S. T. Nguyen, *J. Am. Chem. Soc.,* 2001, ***123***, 11498-11499.

85. D. J. Darensbourg, P. Bottarelli and J. R. Andreatta, *Macromolecules,* 2007, ***40***, 7727-7729.

86. D. J. Darensbourg, Mackiewicz and J. L. Rodgers, *J. Am. Chem. Soc.,* 2005, ***127***, 17565-17565.

87. D. J. Darensbourg, M. J. Adams, J. C. Yarbrough and A. L. Phelps, *Inorg. Chem.,* 2003, ***42***, 7809-7818; D. J. Darensbourg, M. J. Adams and J. C. Yarbrough, *Inorg. Chem.,* 2001, ***40***, 6543-6544.

88. T. Ohkawara, K. Suzuki, K. Nakano, S. Mori and K. Nozaki, *J. Am. Chem. Soc.,* 2014, ***136***, 10728-10735.

89. S. I. Vagin, R. Reichardt, S. Klaus and B. Rieger, *J. Am. Chem. Soc.,* 2010, ***132***, 14367-14369.

90. D. J. Darensbourg and A. I. Moncada, *Inorg. Chem.,* 2008, ***47***, 10000-10008.

91. D. J. Darensbourg and S. B. Fitch, *Inorg. Chem.,* 2009, ***48***, 8668-8677.

92. K. Nakano, T. Kamada and K. Nozaki, *Angew. Chem. Int. Ed.,* 2006, ***45***, 7274-7277.

93. S. S, J. K. Min, J. E. Seong, S. J. Na and B. Y. Lee, *Angew. Chem. Int. Ed.,* 2008, ***47***, 7306-7309.

94. J. Yoo, S. J. Na, H. C. Park, A. Cyriac and B. Y. Lee, *Dalton Trans.,* 2010, ***39***, 2622-2630.

95. A. Cyriac, J. Y. Jeon, J. K. Varghese, J. H. Park, S. Y. Choi, Y. K. Chung and B. Y. Lee, *Dalton Trans.,* 2012, ***41***, 1444-1447.

96. J. E. Seong, S. J. Na, A. Cyriac, B.-W. Kim and B. Y. Lee, *Macromolecules,* 2009, ***43***, 903-908; A. Cyriac, S. H. Lee and B. Y. Lee, *Polym. Chem.,* 2011, ***2***, 950-956; A. Cyriac, S. H. Lee, J. K. Varghese, J. H. Park, J. Y. Jeon, S. J. Kim and B. Y. Lee, *Green Chem.,* 2011, ***13***, 3469-3475.

97. A. Cyriac, S. H. Lee, J. K. Varghese, E. S. Park, J. H. Park and B. Y. Lee, *Macromolecules,* 2010, ***43***, 7398-7401; S. H. Lee, A. Cyriac, J. Y. Jeon and B. Y. Lee, *Polym. Chem.,* 2012, ***3***, 1215-1220.

98. W.-M. Ren, Z.-W. Liu, Y.-Q. Wen, R. Zhang and X.-B. Lu, *J. Am. Chem. Soc.,* 2009, ***131***, 11509-11518.

99. W.-M. Ren, X. Zhang, Y. Liu, J.-F. Li, H. Wang and X.-B. Lu, *Macromolecules,* 2010, ***43***, 1396-1402.

100. G.-P. Wu, P.-X. Xu, X.-B. Lu, Y.-P. Zu, S.-H. Wei, W.-M. Ren and D. J. Darensbourg, *Macromolecules,* 2013, ***46***, 2128-2133.

101. D. J. Darensbourg, W.-C. Chung and S. J. Wilson, *ACS Catal.,* 2013, ***3***, 3050-3057; D. J. Darensbourg and S. J. Wilson, *Macromolecules,* 2013, ***46***, 5929-5934.

102. D. J. Darensbourg, S.-H. Wei, A. D. Yeung and W. C. Ellis, *Macromolecules,* 2013, ***46***, 5850-5855.

103. W.-M. Ren, Y. Liu, G.-P. Wu, J. Liu and X.-B. Lu, *J. Polym. Sci. A Polym. Chem.,* 2011, ***49***, 4894-4901.

104. G.-P. Wu, S.-H. Wei, X.-B. Lu, W.-M. Ren and D. J. Darensbourg, *Macromolecules,* 2010, ***43***, 9202-9204.

105. G.-P. Wu, S.-H. Wei, W.-M. Ren, X.-B. Lu, T.-Q. Xu and D. J. Darensbourg, *J. Am. Chem. Soc.,* 2011, ***133***, 15191-15199.

106. K. Nakano, S. Hashimoto and K. Nozaki, *Chem. Sci.,* 2010, 369-373.

107. Y. Liu, W.-M. Ren, J. Liu and X.-B. Lu, *Angew. Chem. Int. Ed.,* 2013, ***52***, 11594-11598.

Chapter 2

Kinetic and Mechanistic Investigations of Homodinuclear Magnesium Catalysts for Cyclohexene Oxide/CO_2 Ring Opening Copolymerisation Reactions

"Some are born great, some achieve greatness and some have greatness thrust upon them"

Twelfth Night by William Shakespeare

2.1 Kinetic and Mechanistic Hypothesis: Introduction

2.1.1 General Introduction

Previously our group (Williams and co-workers) have synthesised several homodinuclear catalysts based on a N_4O_2 macrocyclic ligand.[1-5] The metals explored have been cobalt, iron, magnesium and zinc with an observed order of activity of Co > Mg > Zn > Fe at 80 °C, 1 bar CO_2 pressure and 1:1000 catalyst:epoxide loading. The turnover frequency (TOF) values obtained for these catalysts in cyclohexene oxide (CHO)/CO_2 ring opening copolymerisation (ROCOP) reactions varied between 6 h^{-1} and 172 h^{-1} (Scheme 2.1).[1-6]

This variation in TOF values suggests that the nature of the metal centres influences the activity. It is envisaged that an ideal catalyst will contain electrophilic metal centres, to which the epoxide monomer can readily bind, facilitating initiation and hence chain propagation. Furthermore, the electrophilicity of the metal centres also governs the nucleophilicity (lability) of the metal-co-ligand or metal-carbonate bonds required for initiation and chain propagation, respectively. In this case, highly electrophilic metal centres will stabilise the metal carboxylate/carbonate bonds and thus reduce the lability of these bonds for epoxide ring opening. Therefore, a delicate balance of the electronic nature of the metal centre selected is required. So far, from the range of metals tested by our group, cobalt is the most effective catalyst.[7,8]

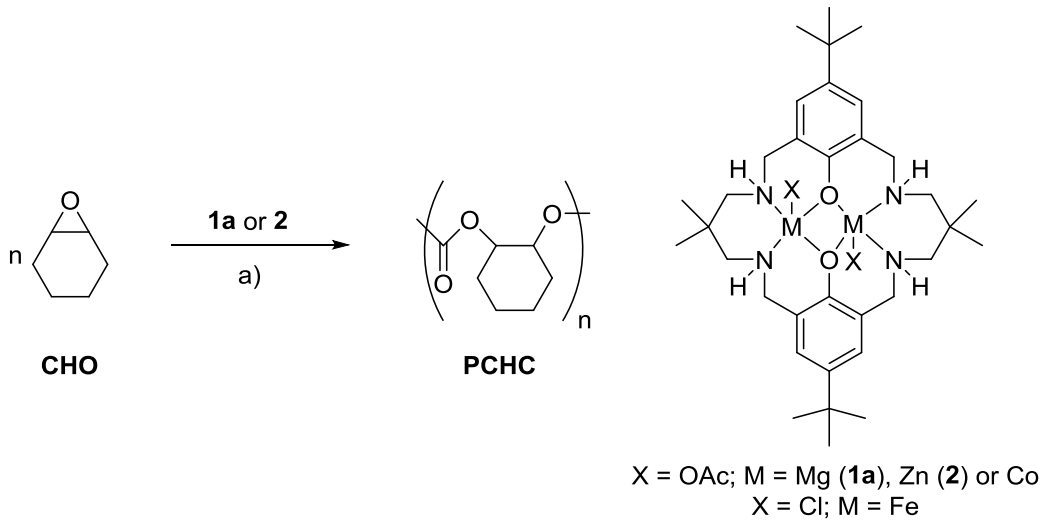

Scheme 2.1: CHO/CO_2 copolymerisation reactions using catalyst **1a** or **2**; a) 80 °C, 1 bar CO_2 pressure, 6 h.

More specifically, the di-magnesium analogue (**1a**) was found to have a TOF of 35 h^{-1} at 80 °C, 1:1000 catalyst:CHO loading and 1 bar CO_2 pressure, which is double the activity of the di-zinc derivative (TOF = 18 h^{-1}).[3,4] However, at 100 °C the TOF of the di-magnesium catalyst (**1a**) soars to 152 h^{-1} compared to the di-zinc catalyst (**2**), which has a TOF of 25 h^{-1}. Thus the magnesium analogue (**1a**) is six times faster than the zinc derivative (**2**) at 100 °C.[3,4]

Other analogues of this homodinuclear catalyst have also been targeted by the Williams group. Initially, di-zinc analogues surrounded by modified macrocyclic ligands or different co-ligands were synthesised. The functional groups in the *para* position of the phenoxide moiety were changed from *t*-butyl to methyl or methoxy (Figure 2.1).[5] It was observed that changing the group to methyl did not affect the activity of the di-zinc catalyst because the electron donating capabilities of *t*-butyl (TOF = 9 h^{-1}) and methyl (TOF = 8.3 h^{-1}) are very similar.[5] However, when changing the functional group to methoxy, the activity of the di-zinc catalyst reduced slightly (TOF = 6 h^{-1}). This is attributed to the fact that methoxy groups are more electron donating compared to alkyl groups and thus lower the electrophilicity of the zinc metal centres and hence their ability to bind efficiently to the epoxide.[5] Changing the co-ligand from acetate to trifluoroacetate did not affect the TOF values recorded.[9]

Moreover, trimetallic derivatives of the homodinuclear zinc and cobalt catalysts were synthesised by adding three equivalents of either zinc or cobalt precursors to the macrocyclic ligand (Figure 2.1).[5,6] These analogues showed lower activities compared to their dinuclear counterparts and it is believed that the third Zn or Co metal centre hinders the ability of CHO and CO_2 to bind to the catalyst. Additionally, it is thought that the external Zn or Co metal centre has a lower activity for copolymerising epoxide/CO_2.[5,6]

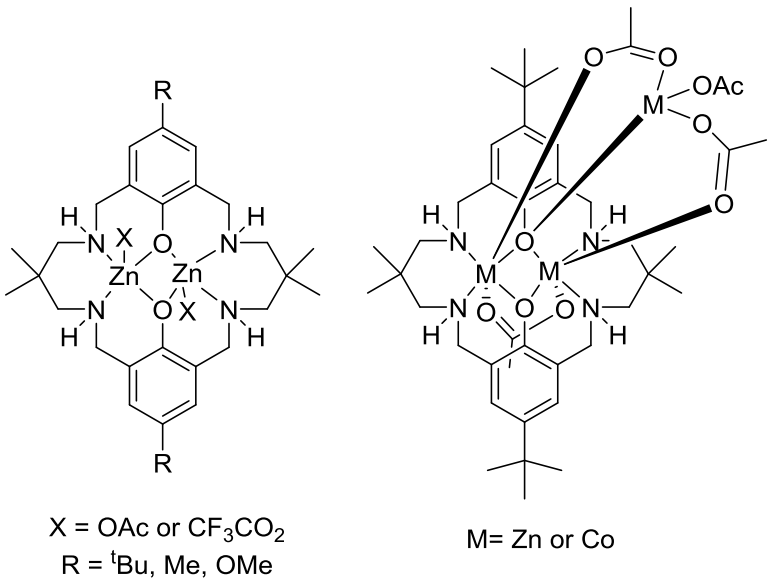

Figure 2.1: Other catalyst analogues of the catalyst synthesised by Williams and co-workers.

Many experimental, spectroscopic and computational studies have been carried out on the catalysts synthesised by our group (Section 2.1.2-2.1.8). In particular, the di-zinc and di-cobalt derivatives have been thoroughly investigated, previously in our group, in order to determine the possible mechanism adopted by these catalysts in CHO/CO_2 copolymerisation reactions.[2,10,11]

2.1.2 Rate Law for the Di-zinc Catalyst (2)

The rate law for CHO/CO_2 copolymerisation reactions with catalyst **2** (di-zinc catalyst) was found to be:

$$\text{Rate} = k_p[\text{CHO}][\text{catalyst}] \qquad (1)$$

This rate law suggests that the rate determining step of the copolymerisation reaction is likely to be the ring opening of the epoxide and not CO_2 insertion.[11]

The reaction order in the concentration of catalyst **2** (di-zinc analogue) was determined by using *in situ* attenuated total reflectance infrared (ATR-IR) spectroscopy. The first order dependence on the concentration of catalyst **2** indicates that aggregation does not occur and that the dinuclear complex structure is likely retained. Furthermore, it also implies that both metal centres of the homodinuclear catalyst are involved in the copolymerisation reaction mechanism. Therefore, it was initially proposed that the chain 'swaps' its coordination site to

each metal centre with every repeat unit (epoxide ring opening and CO_2 insertion – Figure 2.2).[2,11]

The reaction order in epoxide monomer (cyclohexene oxide – CHO) concentration was recorded by an integrated rate law method and again showed a first order dependence. This was curious as there are two metal sites from which copolymer chains can grow from and thus a second order dependence was anticipated. In order to rationalise this first order dependence, it was hypothesised that only one copolymer chain grows per catalyst molecule and therefore only one of the acetate co-ligand groups initiates copolymerisation. The other acetate is proposed to remain bridging between the zinc centres, in order to maintain an octahedral coordination sphere and neutral charge balance, during the copolymerisation reaction.[11]

Investigating the effect of CO_2 pressure (1-40 bar) showed that the initial rates of the CHO/CO_2 copolymerisation reactions, using catalyst **2**, were roughly the same. Therefore, this indicates that the rate of copolymerisation is zero order dependent on the pressure of CO_2 (1-40 bar), which suggests that CO_2 insertion is non-rate determining.[11]

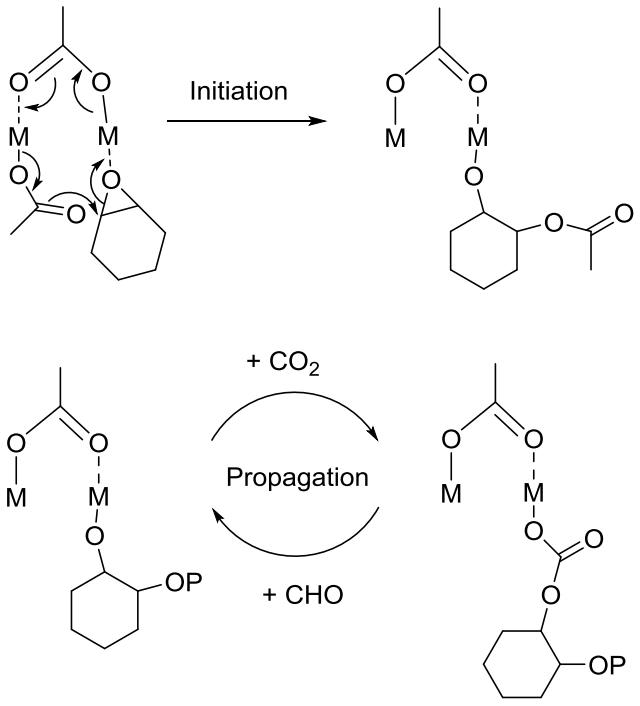

Figure 2.2: One mechanistic hypothesis. Macrocyclic ligand omitted for clarity.

2.1.3 Support for Dinuclear Mechanism – Di-cobalt (II) Catalysts

In order to further study the mechanism for these homodinuclear catalysts, various propagating structures, which have all been reported in literature, were considered: A – dinuclear mechanism,[7,12,13,14] B – intermolecular binuclear mechanism[14,15] or C and D – mononuclear co-catalyst mechanisms[16] (Figure 2.3) and several di-cobalt(II) catalyst compounds were synthesised and investigated.[2,17-20]

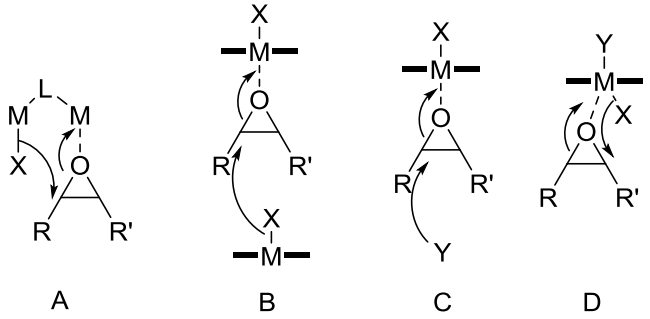

Figure 2.3: Proposed dinuclear and mononuclear mechanisms for epoxide/CO_2 copolymerisation reactions. M = metal, L = ligand, X = co-ligand or initiator, Y = co-catalyst.

The di-cobalt(II) catalysts were coordinated by the macrocyclic ligand, two chloride co-ligands and a neutral co-catalyst (Figure 2.4).[17,21] The crystal structures of these di-cobalt(II) catalyst analogues all showed that the ligand adopts a conformation which places all the N-H substituents on the same face (concave) of the molecule (Figure 2.4). In this conformation, the ligand is 'bowl-shaped' and therefore there are two different faces to the molecule.[2] Additionally, the chloride co-ligand adopts a bridging position between the two metal centres on the concave face of the catalyst structure. Due to the small nature of the chloride bridging co-ligand, the two axial coordination sites on the convex side of the complex are pushed further apart and thus the other chloride co-ligand does not bridge between the two metal centres on the convex face of the complex (Figure 2.4). Therefore, one axial position is occupied by a chloride co-ligand and the other vacant axial site is occupied by a nucleophile (MeIm or DMAP, which are known co-catalysts for salen complexes).[2]

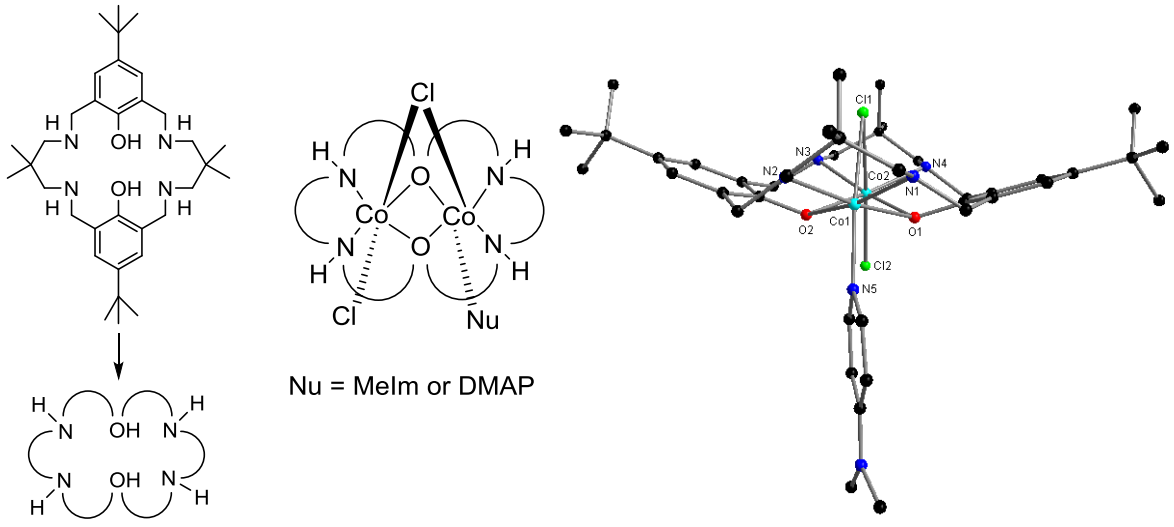

Figure 2.4: Di-cobalt analogues synthesised by Williams and co-workers and the crystal structure showing the 'bowl-shape' conformation of the macrocyclic ligand.[2]

These di-cobalt(II) derivatives were used in CHO/CO_2 copolymerisation reactions and all complexes showed good activity, but the TOF values obtained (20 and 104 h^{-1}, DMAP and MeIm, respectively), are lower than the TOF value obtained for the di-cobalt catalyst with acetate as the co-ligand (Scheme 2.1 – 159 h^{-1}).[2,6] Moreover, the poly(cyclohexene) carbonate (PCHC) samples obtained from these copolymerisation reactions showed a bimodal M_n (number average molecular weight) distribution. From MALDI-ToF mass spectrometry one copolymer chain series was found to be Cl end-capped and the other series was shown to be hydroxyl end-capped. However, no chains were end-capped with either of the nucleophilic co-catalysts, which suggests that the co-catalyst did not initiate the copolymerisation.[2]

The reduced activity was explained by the fact that the nucleophilic co-catalysts need to dissociate from the cobalt metal centres in order to create a vacant coordination site for the epoxide to bind to. The DMAP co-catalyst binds very strongly with the cobalt metal centres and this is reflected in the low activity observed (TOF = 20 h^{-1}), which indicates that the dissociation of DMAP is very slow, thus inhibiting CHO binding.[2] This significant reduction in activity also suggests that both chloride co-ligands do not initiate the copolymerisation reaction and thus the bridging chloride co-ligand on the sterically hindered concave face does not take part in the copolymerisation reaction. Additionally, this observation infers that both metals are involved in the copolymerisation reaction.[2] Overall, these findings support an intramolecular dinuclear mechanism during CHO/CO_2 copolymerisation reactions (A – Figure 2.3).[2]

Furthermore, the reaction order in epoxide and catalyst was investigated with these di-cobalt(II) derivatives and the study also revealed that the rate of copolymerisation is first order dependent on CHO and catalyst concentration, indicating that one copolymer chain grows per catalyst and that both metals are involved in the mechanism (Section 2.12).

Additionally, it was also seen that the rate of propagation is the same for both these di-cobalt analogues, which was expected as they both have Cl bridging co-ligands. Therefore, the difference in TOF values observed (20 h^{-1} *vs.* 104 h^{-1}) must be due to a difference in initiation periods because TOF is a point kinetic measurement and combines initiation and propagation.[2] From the TOF values, the DMAP analogue clearly has a longer initiation period (takes longer to dissociate) compared to the MeIm derivative.

2.1.4 Catalyst Conformations

Many attempts to crystallise all the derivatives of this dinuclear catalyst have been carried out, by our group, and some have been successful (Section 2.1.3).[2] All of the crystal structures showed that the co-ligands bridge between the two metal centres. Moreover, the macrocyclic ligand seems to adopt a common 'bowl-shape' conformation (Figure 2.4 and 2.5).[2,5,6,10] In only one case was a different 'S-shape' conformation observed (trimetallic cobalt complex – Figure 2.1 and 2.5).[2,5,6,10] In the 'bowl-shape' conformation, the N-H substituents are all on the concave side of the molecule. The implications of this are that the two bridging (μ) and chelating (κ^2 O, O') carboxylate co-ligands are in different environments when the 'bowl-shape' configuration is adopted.[2] However, it must be noted that the solution conformation of these catalysts is still not known.

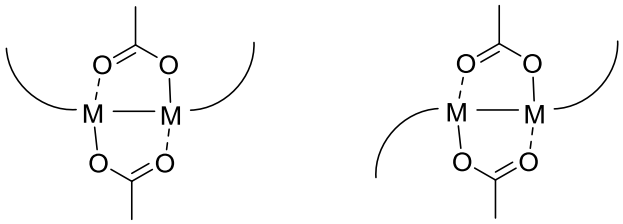

Bowl-shape S-shape

Figure 2.5: Illustrates two common macrocyclic ligand conformations.

2.1.5 Computational Studies

Computational studies have also been carried out to shed light on the mechanism of these dinuclear catalysts in CHO/CO_2 copolymerisation reactions (using DFT and the basis set 6-31G(d)). The investigation showed that the 'bowl-shape' and 'S-shape' conformations of the di-zinc catalyst (**2**) are isoenergetic and thus equally likely to occur.[10]

However, in order to determine which conformation is thermodynamically favoured during the copolymerisation reaction, the energy of both conformations with 2 equivalents of CHO and CO_2 was also computationally calculated. The results revealed that the favoured catalyst structure, albeit with only a slight energy difference, is where the ligand is in a 'bowl-shape' conformation. Moreover, it has been found that it is more favourable for only one copolymer chain to grow per catalyst structure and therefore, one acetate co-ligand remains bridging between the two zinc metal centres. According to the proposed mechanism, the bridging acetate group is on the concave face of the catalyst structure and propagation occurs from the convex face of the catalyst (Figure 2.6).[10]

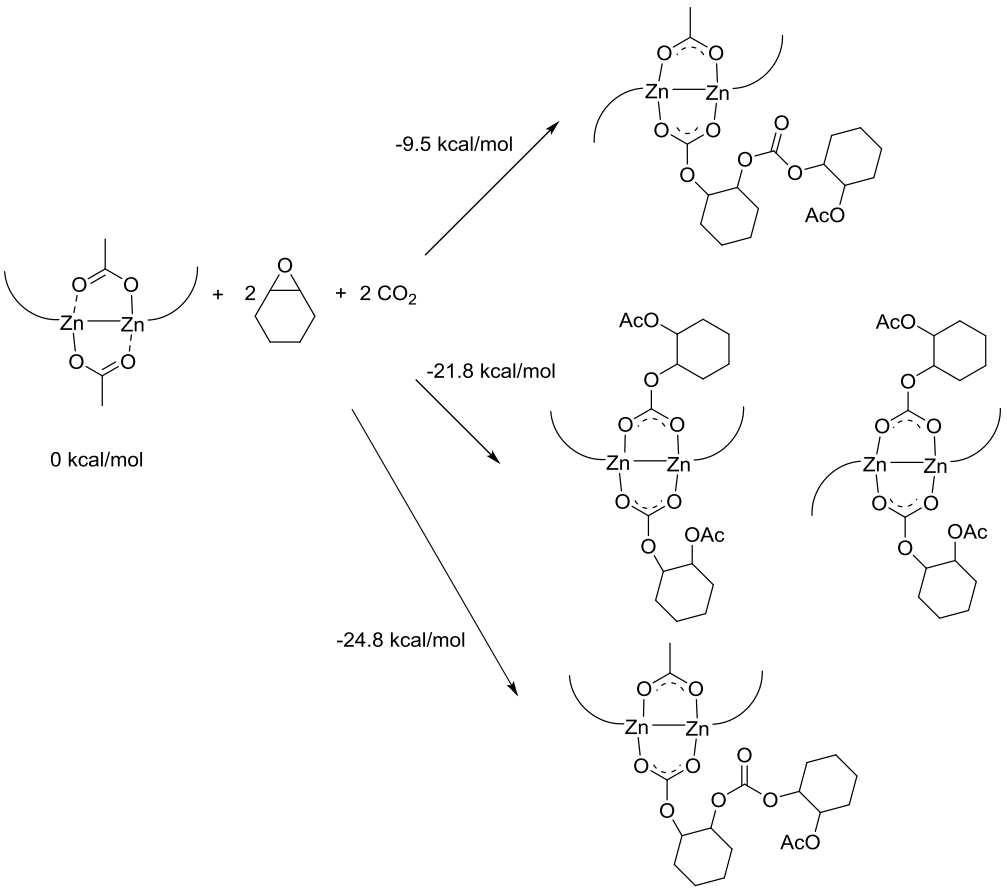

Figure 2.6: Illustrates the predicted ΔΔG for different catalyst conformations with one or two copolymer chain growth sites.[10]

From this result, the potential energy surface for CHO/CO_2 copolymerisation reactions using catalyst **2** was calculated, using the 'bowl-shape' catalyst conformation with only one site for copolymer chain growth as the starting point. These calculations indicated that the alternating incorporation of epoxide and CO_2 within the growing copolymer is favoured over side reactions. This is because sequential epoxide addition to form ether linkages has a high activation energy barrier and sequential CO_2 insertion is thermodynamically unfavourable and reversible.[10]

The potential energy surface calculations also indicated that CO_2 insertion does not affect the rate of copolymerisation because the activation energy barrier for this process is low. The highest activation barrier within the copolymerisation process was found to be due to the ring opening of CHO by a zinc-carbonate species.[10]

From all these observations, a potential mechanism for CHO/CO_2 copolymerisation reactions, using **2**, was hypothesised. The key features of the mechanism are that both zinc metal centres are involved in the copolymerisation reaction and that one acetate group remains bound to the concave face of the catalyst structure. The latter allows an octahedral coordination sphere and a neutral charge balance to be maintained. The growing copolymer chain grows on the convex face of the catalyst structure and the chain 'shuttles' between the two metal centres twice per catalytic cycle (Figure 2.7).[10]

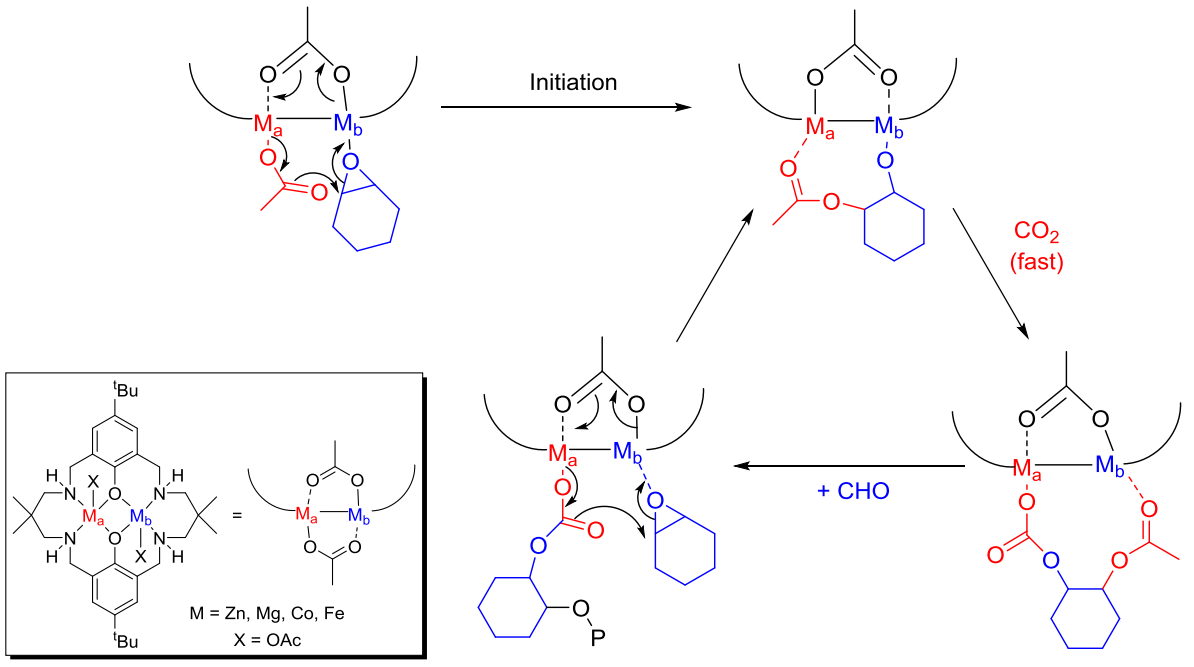

Figure 2.7: Proposed mechanism for bimetallic catalysts.[10]

2.1.6 Solid State and *In Situ* IR Spectroscopy Studies

The computationally derived energy profile for CHO/CO_2 copolymerisation reactions and the experimentally derived kinetic and structure activity studies using the di-zinc and di-cobalt complexes, have suggested that one co-ligand remains bridging on the concave face of the catalyst structure during copolymerisation reactions and therefore does not initiate copolymerisation. In order to prove that this occurs, spectroscopic and theoretical studies using the di-zinc catalyst have been carried out by our group.[10]

In this investigation the solid state IR spectrum of catalyst **2** (di-zinc catalyst) was recorded. Two *in situ* IR spectra, using ATR-IR, of catalyst **2** were also recorded. One recorded catalyst **2** dissolved in TCE and heated for 15 minutes at 80 °C and the other involved catalyst **2** being dissolved in neat CHO, heated for 2 h at 80 °C and then stirred for 14 h under 1 bar of CO_2 pressure.[10]

The solid state IR spectrum of catalyst **2** showed two carboxylate resonances at 1591 and 1615 cm^{-1}, which indicates that the two bridging acetate co-ligands are in slightly different environments due to the 'bowl-shape' conformation of the ligand (structure E – Figure 2.8). The *in situ* IR spectrum of catalyst **2** in TCE showed that the carboxylate resonance shifted to 1601 cm^{-1}, due to solvent effects. A minor signal at 1737 cm^{-1} was also recorded, which is attributed to the breaking of the bridging coordination mode (κ^2) of the acetate group bound on the convex face of the catalyst structure, leading to the formation of a terminal acetate (κ^1) coordination (structure F – Figure 2.8). The second *in situ* IR spectrum showed a resonance for the κ^2 acetate group at 1741 cm^{-1}, a resonance for the zinc-bound κ^1 carbonate group at 1804 cm^{-1} and another resonance at 1825 cm^{-1} that represents the cyclohexene bound acetate group (structure G – Figure 2.8). From these three spectra, it was deduced that one acetate group remains in the bridging coordination mode during the copolymerisation reaction. The calculated IR spectra (*via* computational methods) confirmed these findings. The calculated resonance values sometimes did not correlate exactly with experimental data, but the number and relative frequencies of the calculated signals matched closely to what was observed and proved to be useful.[10]

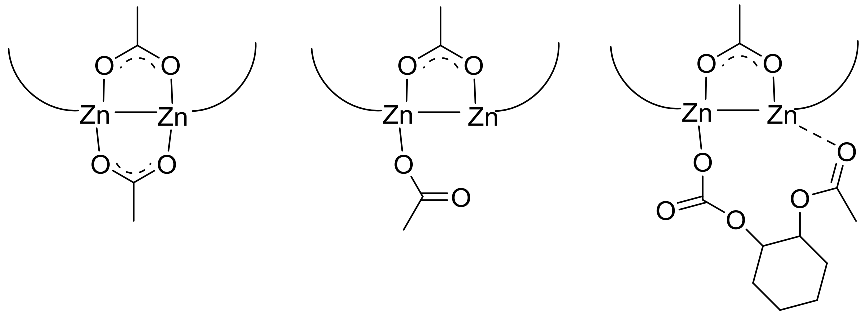

Figure 2.8: Catalyst structures recorded by solid state and *in situ* IR spectroscopy.

2.1.7 Immortal Copolymerisation Reactions

Conventionally in a controlled copolymerisation, the M_n of the copolymer formed can be used to determine the number of initiating groups within the catalyst structure.[22] This is not possible for epoxide/CO_2 copolymerisation reactions because it is an immortal copolymerisation and hence the investigations described in Section 2.1.6 had to be carried out by our group.[23,24]

In immortal copolymerisations, chain transfer agents are present within the copolymerisation reaction, usually trace amounts of water, even though the epoxide is distilled before use and the CO_2 is passed through a column of drierite.[23,24] Chain transfer reactions have been observed throughout the field and cause the M_n of the copolymer formed to be lower than expected.[14,25] Therefore, the M_n values cannot be used to determine the number of initiating groups in the catalyst structure.[10]

The MALDI-ToF mass spectra of the PCHC samples produced using any of the homodinuclear catalysts with acetate co-ligands show a bimodal M_n distribution. One copolymer series is acetate end-capped, which is expected to form due to initiation by one of the acetate co-ligands. The other copolymer series, which is usually double the M_n of the acetate end-capped chains, is hydroxyl end-capped. The latter series arises due to chain transfer reactions occurring with cyclohexane-1,2-diol (CHD), which forms by the reaction of CHO with water. This series is double the M_n of the acetate end-capped copolymers because the CHD initiated copolymer can grow from both hydroxyl groups to form a telechelic copolymer (Figure 2.9).[10,11]

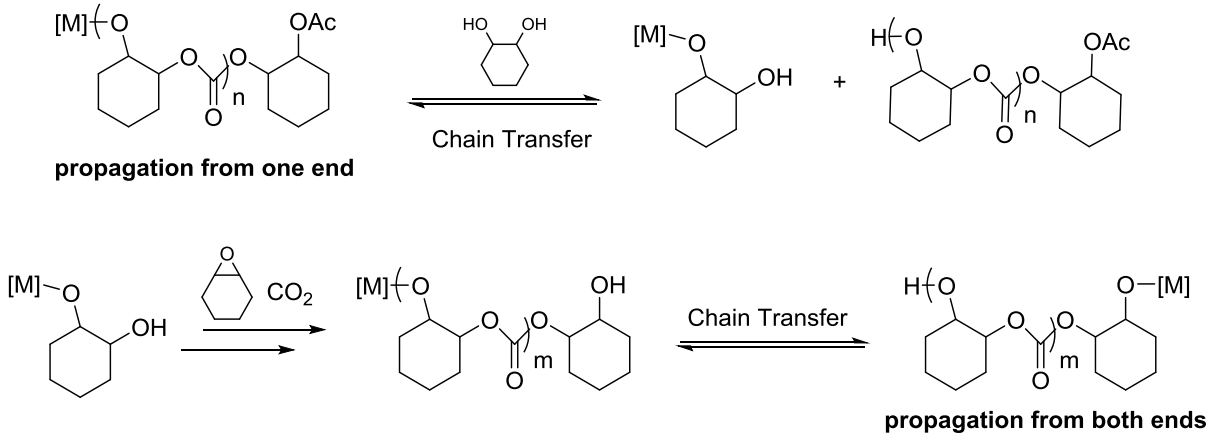

Figure 2.9: Illustrates chain transfer reactions in CHO/CO_2 copolymerisation reactions with cyclohexane-1,2-diol (CHD).

Immortal copolymerisation reactions produce lower than expected M_n copolymer chains. The M_n values can be predicted form the ratio of catalyst and chain transfer agent. Additionally, the polydisperity indices of the copolymer samples produced are narrow (PDI < 1.5), which arises because the rate of chain transfer occurs more rapidly compared to the rate of propagation.[23]

2.1.8 Side Reactions During Copolymerisation Reactions

Briefly mentioned in Section 2.1.5, side reactions during CHO/CO_2 copolymerisation reactions can occur. These side reactions can lead to the formation of ether linkages or cyclic carbonate as a by-product.[8] Ether linkages occur due to the sequential ring opening of epoxide monomers and no incorporation of CO_2. This affects the thermal, chemical and mechanical properties of the copolymer formed (reduces the T_g – glass transition temperature).[26] However, from computational and experimental results ether formation is negligible with these homodinuclear catalysts (< 1 %).[2-4]

Additionally, cyclic carbonate by-products can form by backbiting reactions within the growing copolymer chain.[8] This can occur when the copolymer is bound to the metal or dissociated from the metal centre (Figure 2.10).[27] Commonly, the *trans*-cyclic carbonate product is observed with these homodinuclear catalysts, which is due to backbiting within the copolymer chain from a metal alkoxide species.[1,3,8,20] *Cis*-cyclic carbonate forms when backbiting of the metal carbonate species occurs (Figure 2.10).[1,27]

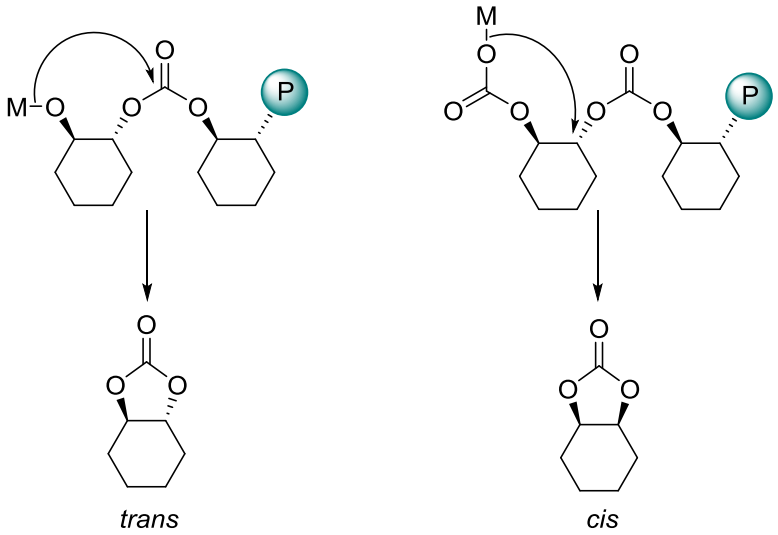

Figure 2.10: *Trans*- and *cis*-cyclic carbonate by-product formation from metal bound copolymer chains.

The cyclic carbonate by-product is the thermodynamic product within the copolymerisation reaction and increases in production at elevated temperatures (Figure 2.11).[11] The activation energy barrier of converting copolymer to cyclic carbonate when using the di-zinc catalyst (**2**) was calculated to be 137.5 kJmol^{-1}, which is comparable to cyclohexene carbonate (CHC) formation using chromium salen catalysts (133.0 kJmol^{-1}).[11,19] The activation energy barrier of PCHC formation is 96.8 kJmol^{-1}, for catalyst **2**, which is in good agreement with the computationally calculated value.[10,11] However, this value is approximately double the activation energy barrier for PCHC formation with chromium salen catalysts (46.9 kJmol^{-1}).[19] This explains the need to use high temperatures with the di-zinc catalyst (**2**) (> 60 °C) compared to the chromium salen complexes (25-50 °C) in CHO/CO_2 copolymerisation reactions.[11,19]

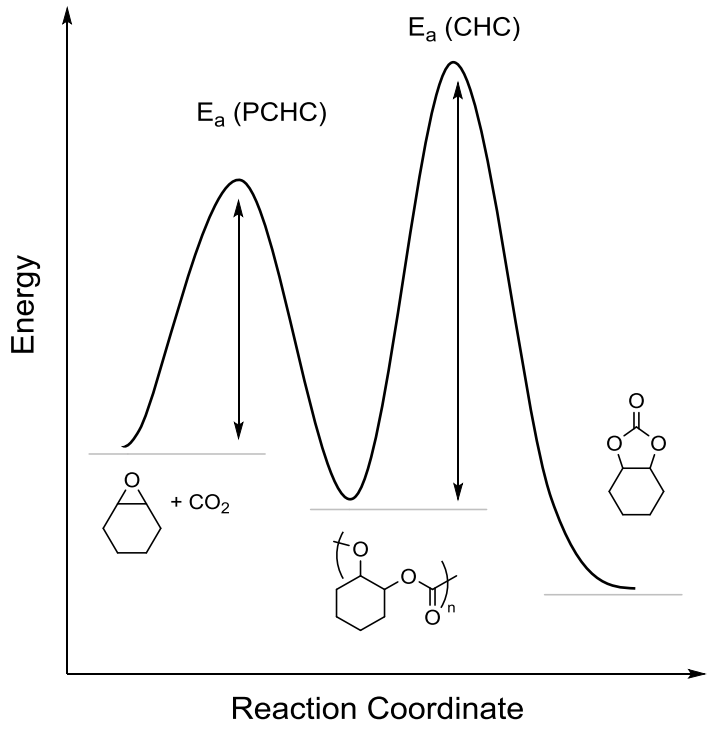

Figure 2.11: Generic reaction co-ordinate *vs.* energy profile for PCHC and CHC formation.

When increasing the temperature of the copolymerisation reaction from 80 °C to 100 °C, the di-zinc catalyst (**2**) produces more cyclic carbonate (6 % CHC compared to < 1 %), but the di-magnesium catalyst (**1a**) still maintains high selectivity towards copolymer formation (> 99 %), which suggests the activation energy barrier for the formation of CHC with the di-magnesium catalyst (**1a**) must be higher than the di-zinc catalyst (**2**).[3,4]

2.1.9 Background and Aims

As mentioned in Section 2.1.1, the di-magnesium catalyst (**1a**) is twice as active as the di-zinc catalyst (**2**) at 80 °C and 1 bar CO_2 pressure, but this result needs to be interpreted with some caution.[3,4] Comparing TOF values in order to understand catalytic activity and rate is not always accurate because TOF values are point kinetic measurements and combine initiation and propagation rates. As previously observed in our group, initiation can vary within complexes and affect the TOF value, even though the complexes may have the same rate of propagation (Section 2.1.3).[2]

Therefore, kinetic and mechanistic investigations need to be carried out with the di-magnesium catalyst in CHO/CO_2 copolymerisation reactions in order to find out the initial

rate of propagation for **1a**. These values can then be compared with the initial rate of propagation for **2** and hence a more accurate comparison of catalytic activity can be carried out. These studies will also help verify if the di-magnesium catalyst (**1a**) undergoes the same proposed mechanism as the di-zinc catalyst (**2**).

This chapter describes the kinetic investigations carried out using the di-magnesium catalyst (**1a**) in CHO/CO_2 copolymerisation reactions. Moreover, the effect of varying co-ligands within the di-magnesium catalyst (**1a**) on the initial rate of propagation in CHO/CO_2 copolymerisation reactions is also outlined. The latter investigation was conducted in order to probe any co-ligand influence on the rate of propagation and to further support the underpinning hypothesis, reported by our group, that one co-ligand may remain bound to the catalyst during copolymer propagation.

2.2 Kinetic Methods to Determine Reaction Order

Two different methods have been employed in order to determine the reaction order in catalyst **1a** and CHO concentration and CO_2 pressure.

2.2.1 Isolation and Initial Rates Method

Initially, it was assumed that the rate law for CHO/CO_2 copolymerisation reactions using **1a** was as follows:

$$\text{Rate} = k_p[\text{CHO}]^x[\text{catalyst}]^y p\text{CO}_2{}^z \qquad (2)$$

Therefore, the reaction order in each component (epoxide, catalyst and CO_2) needed to be determined. To determine the reaction order in [catalyst] and $p$$CO_2$, an isolation method was adopted. In most cases, this is where all components of the reaction but one, are in sufficient excess so that the concentration is assumed to be large and constant during the reaction process. From this, a pseudo order rate law is produced.[28]

The pseudo order rate law, when catalyst concentration is isolated, is as follows:

$$\text{Rate} = k_{obs}[\text{catalyst}]^y \qquad (3)$$

where:

$$k_{obs} = k_p[\text{CHO}]^x p\text{CO}_2{}^z \qquad (4)$$

Once a pseudo order rate law is obtained, the reaction order of the isolated component, in this case [catalyst **1a**] can be determined *via* an initial rates method. The initial rate of the copolymerisation reaction can then be recorded for many different catalyst concentrations. If the plot of initial rate *vs.* [catalyst] is linear then the rate of propagation is first order dependent on the concentration of catalyst.[28]

2.2.2 Isolation and Integrated Rate Law Method

The integrated rate law method can also be used to determine reaction orders and was used to determine the reaction order in [CHO]. Firstly, as in the initial rates method, all components in the proposed rate law (equation 2) need to be used in excess except one, in this case [CHO]. This produces the following pseudo order rate law:[28]

$$\text{Rate} = k_{obs}[\text{CHO}]^{x} \qquad (5)$$

where:

$$k_{obs} = k_{p}[\text{catalyst}]^{y} p\text{CO}_2{}^{z} \qquad (6)$$

Considering the rate of copolymerisation can be calculated by monitoring the change in concentration of CHO with respect to time, the following equation is obtained if there is a first order dependence in [CHO]:

$$\frac{d[CHO]}{dt} = -k[CHO] \qquad (7)$$

After integration, the following equation is obtained:

$$\ln\left(\frac{[CHO]}{[CHO]_0}\right) = -kt \qquad (8)$$

Therefore, by monitoring the change in concentration of CHO with respect to time over a copolymerisation reaction that has surpassed several half-lives, the plot of ln[CHO] *vs.* time can be obtained. If there is a linear correlation between these two parameters, the rate of copolymerisation is first order with respect to [CHO].[28]

2.3 Kinetic and Mechanistic Investigations of $LMg_2(OAc)_2$ Catalyst (1a)

2.3.1 Reaction Order in [Catalyst 1a]

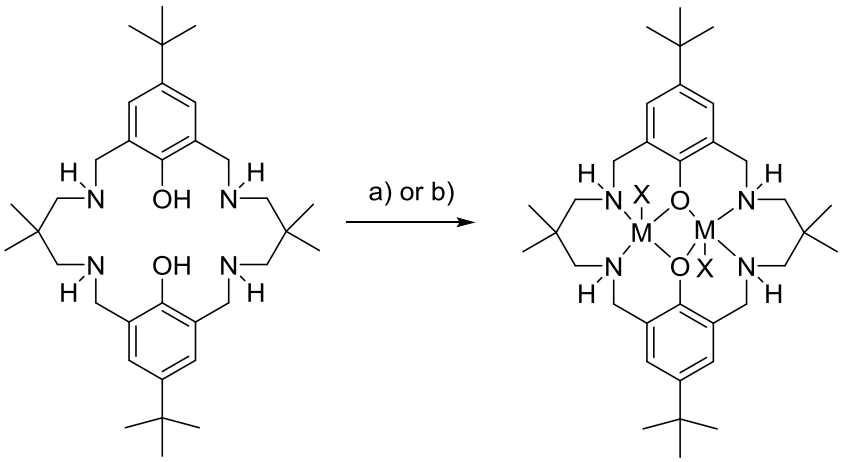

Scheme 2.2: Synthesis route for **1a** or **2**. Reaction conditions: a) 2 eq. $Mg(OAc)_2$, MeOH, 25 °C, 16 h; b) i) 3 eq. KH, dry THF, 25 °C, 2 h; ii) 2 eq. $Zn(OAc)_2$, 25 °C, 16 h.

Catalysts **1a** and **2** were synthesised according to slightly modified literature procedures (Scheme 2.2). The reaction order in [catalyst **1a**] was determined by using the initial rates method (Section 2.2.1). The catalyst concentrations studied were 4.2, 8.3, 12.5 and 16.6 mM, with an initial CHO concentration of 8.24 M in DEC at 80 °C and 1 bar CO_2 pressure. These copolymerisation reactions were monitored by *in situ* ATR-IR spectroscopy. This technique is non-invasive and therefore catalyst deactivation by water and air contamination was minimised. This catalyst deactivation can be problematic and can occur when applying alternative aliquoting methods.

The full IR spectrum (2700-600 cm^{-1}) of the reaction mixture was recorded every 30 seconds during each copolymerisation reaction at different catalyst concentrations (Figure 2.12). The change in absorbance for selected vibrational modes of the PCHC product was analysed. The three vibrational modes monitored were the C=O stretching mode (1787-1731 cm^{-1}), the C-O stretching mode in O-C=O at 1014 cm^{-1} and the C-O-C asymmetric mode (1239-1176 cm^{-1}). The latter vibrational mode usually has an absorption intensity of roughly double the other two vibrational modes. This higher intensity is due to the fact that there are two C-O-C

linkages per repeat unit within the copolymer chain (compared to only one C=O forming per repeat unit).[11]

All three vibrational mode signals increased in absorbance over the course of the copolymerisation reactions because all three signals represent the copolymer forming. The assumption that the increase in intensity of the copolymer signals is proportional to the decrease in CHO concentration (consumption of CHO) has been made.

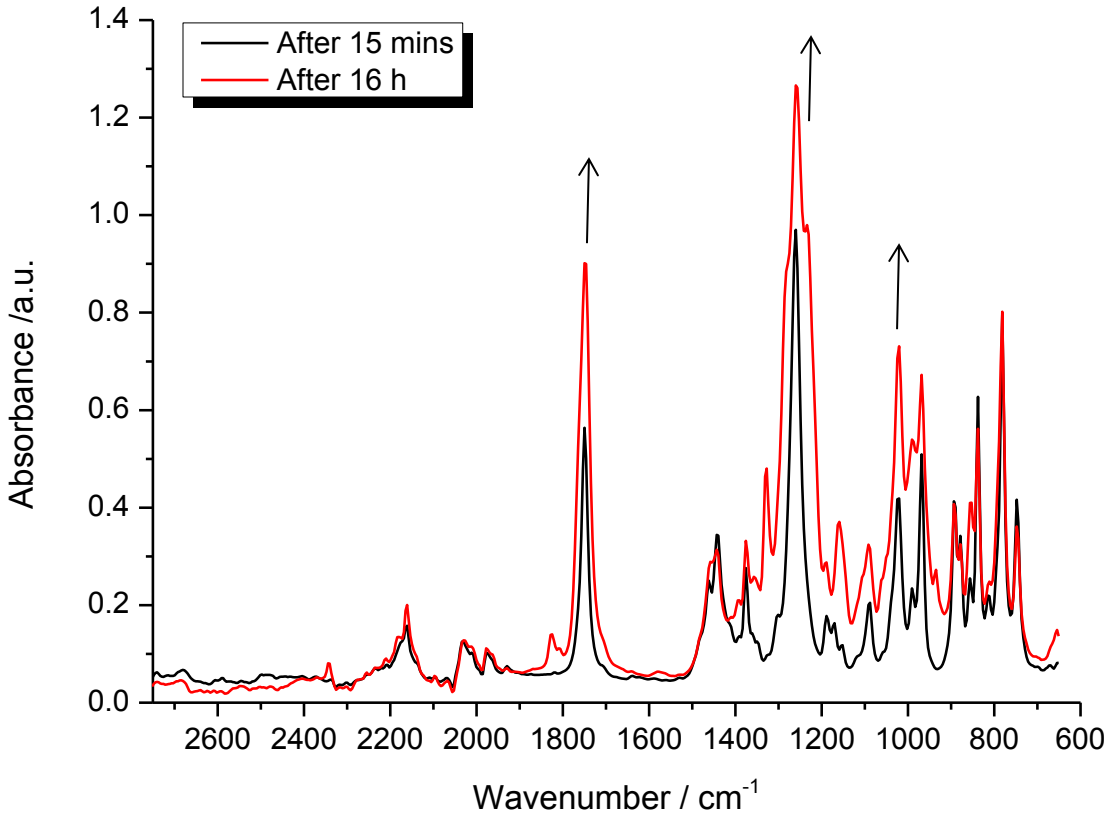

Figure 2.12: Typical ATIR-IR spectra recorded during the course of CHO/CO_2 copolymerisation reactions at 80 °C and 1 bar CO_2 pressure. The increase in absorbance for the three signals annotated with the arrows was monitored. The C=O stretching mode (1787-1731 cm^{-1}), the C-O stretching mode in O-C=O at 1014 cm^{-1} and the C-O-C asymmetric mode (1239-1176 cm^{-1}) part of the PCHC product. The signals at 1750 cm^{-1} and 1825 cm^{-1} are due to the C=O stretching mode of DEC and cyclic carbonate, respectively.

The change in absorbance for each vibrational mode at a particular catalyst concentration was sigmoidal in shape (Figure 2.13). There is a clear initiation period at the start of the reaction (45 mins to 1 h), followed by a linear increase in intensity. Once the conversion of CHO reaches high values (> 40 %), the viscosity of the reaction mixture becomes too high for efficient stirring and thus the plot of the change in absorbance *vs.* time for all three vibrational modes starts to plateau (Figure 2.13). Initiation periods have also been seen with the chromium salen complexes and the length of the initiation period changes with co-catalyst used.[20]

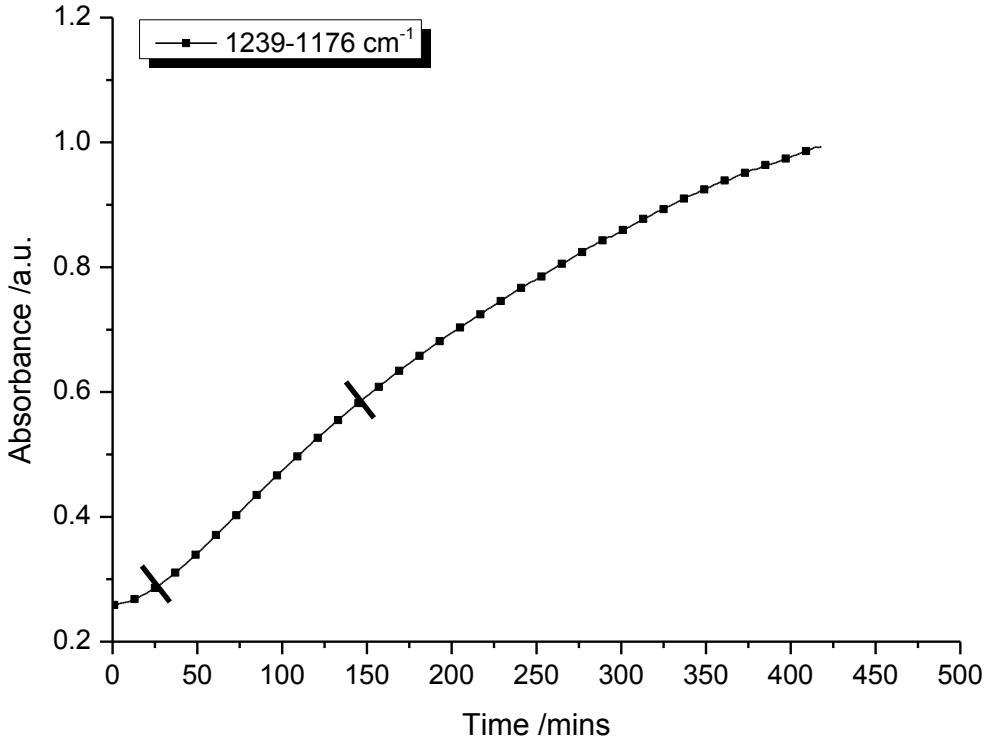

Figure 2.13: Change in absorbance *vs.* time plot of vibrational mode 1239-1176 cm^{-1} for a single CHO/CO_2 copolymerisation reaction, but repeated in triplicate. Reaction conditions: 80 °C, 1 bar CO_2 pressure, $[CHO]_0$ = 8.24 M in DEC, [**1a**] = 8.3 mM. Only 50 % of the data points are shown for clarity. The line markings represent 5-20 % CHO conversion (tangent to the curve to calculate initial rate).

The initial rate for a particular concentration of catalyst **1a** was determined by linearly fitting the change in absorbance *vs.* time plot (Figure 2.13) between 5-20 % CHO conversion (linear part of sigmoidal curve marked in Figure 2.13). The gradient value obtained represents the initial rate for a particular catalyst concentration for that specific vibrational mode (Figure 2.14). Each vibrational mode produced an initial rate for a particular catalyst concentration.

Therefore, three initial rate values for a particular catalyst concentration were recorded (see Appendix A for all plots).

.

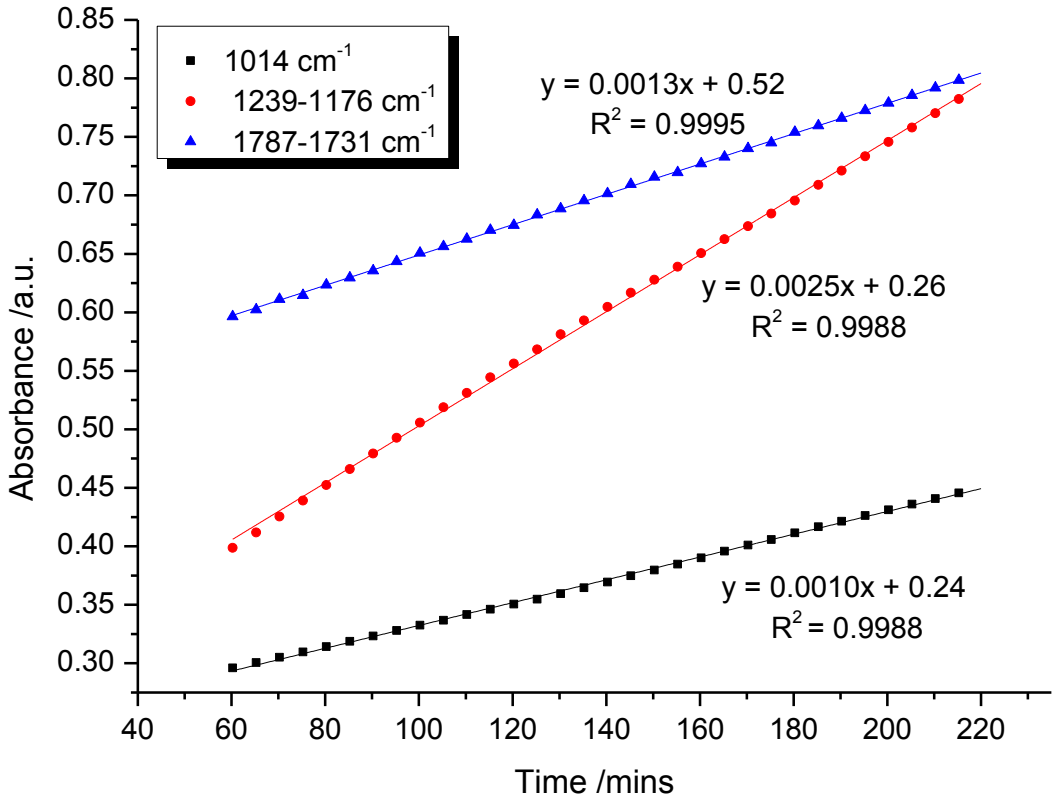

Figure 2.14: Change in absorbance *vs.* time plot for three vibrational modes during a single CHO/CO_2 copolymerisation reaction, but repeated in triplicate. Reaction conditions: [**1a**] = 12.5 mM, $[CHO]_0$ = 8.24 M in DEC, 80 °C at 1 bar CO_2 pressure. For clarity 50 % of the data points have been omitted. The gradient values represent the initial rate.

The plot of the initial rate *vs.* catalyst concentration (Figure 2.15) shows a clear linear dependence, therefore, suggesting that the rate of copolymerisation of CHO/CO_2 is first order dependent on catalyst **1a** concentration.

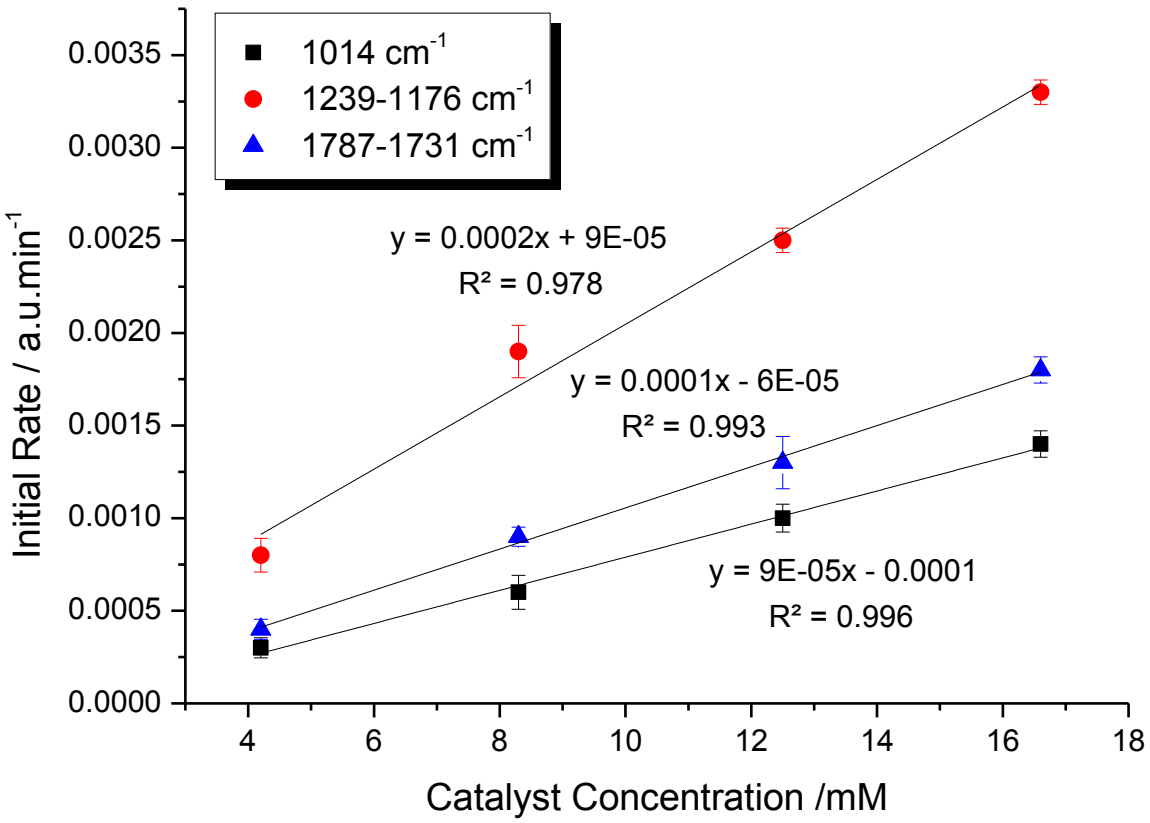

Figure 2.15: Initial rate *vs.* [catalyst **1a**] plot. Reaction conditions: $[CHO]_0$ = 8.24 M in DEC, 80 °C at 1 bar CO_2 pressure. Each experiment was run in triplicate to give the error value for each data point. The gradient values correlate to the k_{obs} values.

This first order dependence was also observed for catalyst **2** (di-zinc analogue). However, the data reported previously by our group used a different ATR-IR probe and thus comparing the k_{obs} values (gradient of initial rate *vs.* catalyst concentration plot) obtained for catalyst **2** with those for catalyst **1a** (Figure 2.15) might be inaccurate. Therefore, the k_{obs} values of catalyst **2** were also investigated. The plot obtained for catalyst **2** (Figure 2.16) confirmed the first order dependence.[11]

Moreover, the k_{obs} values obtained for each vibrational mode (1239-1176, 1787-1731 and 1014 cm^{-1}) are 9 x 10^{-5} ± 5 x 10^{-6}, 5 x 10^{-5} ± 4 x 10^{-6} and 4 x 10^{-5} ± 3 x 10^{-6} $mMa.u.^{-1}min$, respectively for catalyst **2** (Figure 2.16). These values are approximately half the k_{obs} values obtained with catalyst **1a** (2 x 10^{-4} ± 8 x 10^{-5}, 1 x 10^{-4} ± 8 x 10^{-5} and 9 x 10^{-5} ± 6 x 10^{-6} $mMa.u.^{-1}min$). More accurately, the magnesium derivative of the catalyst is between 2.0-2.25 times faster than the zinc analogue of the catalyst. From the TOF values reported in literature, the di-magnesium catalyst was shown to be 1.9 times faster than the di-zinc catalyst. The

good agreement suggests that in this case TOF values can give a good indication of the difference in activity of different catalysts.

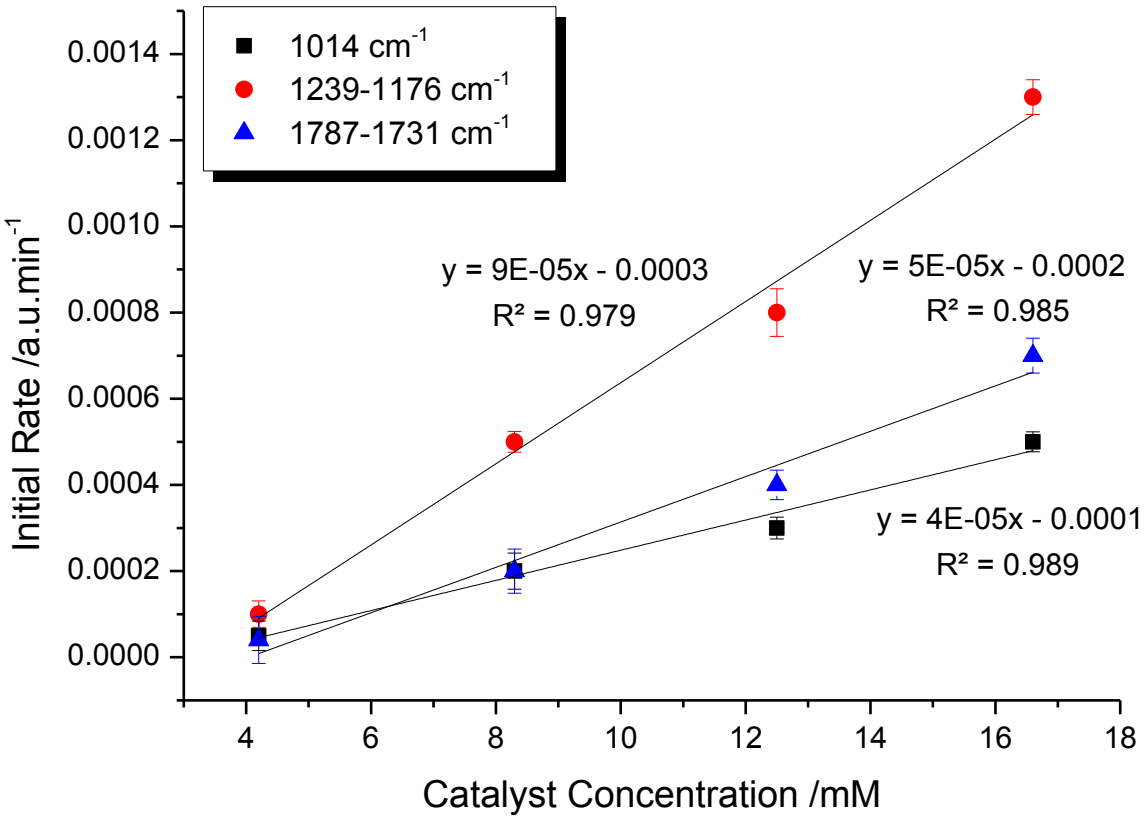

Figure 2.16: Initial rate *vs.* [catalyst **2**] plot. Reaction conditions: $[CHO]_0$ = 8.24 M in DEC, 80 °C at 1 bar CO_2 pressure. Each experiment was run in triplicate to give the error value for each data point. The gradient values correlate to the k_{obs} values.

2.3.2 Reaction Order in [CHO]

An integrated rate law method was applied to determine the reaction order in the concentration of monomer (CHO). The conditions for the CHO/CO_2 copolymerisation reaction were: [catalyst **1a**] = 4.98 mM, $[CHO]_0$ = 4.94 M in DEC at 80 °C and 1 bar CO_2 pressure. The reaction was left for 53 hours, which allowed a high conversion to be reached (88% CHO conversion determined by ^{1}H NMR spectroscopy) in order to ensure that several reaction half-lives had been exceeded. A plot of ln[CHO] *vs.* time was produced (Figure 2.17), which shows a clear linear dependence and thus suggests that rate of CHO/CO_2 copolymerisation reactions using catalyst **1a** is first order dependent on CHO concentration.

Furthermore, the slope of the linear plot (Figure 2.17) corresponds to the k_{obs} value. This value is -0.0453 h^{-1} for catalyst **1a**, which is double the value obtained for catalyst **2** (-0.0225 h^{-1}, Figure 2.18).[11] Additionally, from the k_{obs} value and the set of conditions specified, the reaction half-life when using catalyst **1a** is 15 h, which is half the reaction half-life for when the di-zinc catalyst (**2**) is used in CHO/CO_2 copolymerisation reactions (31 h).[11] Both the k_{obs} and reaction half-life values suggest that catalyst **1a** is twice as fast as catalyst **2** in CHO/CO_2 copolymerisation reactions at 80 °C and 1 bar CO_2 pressure.

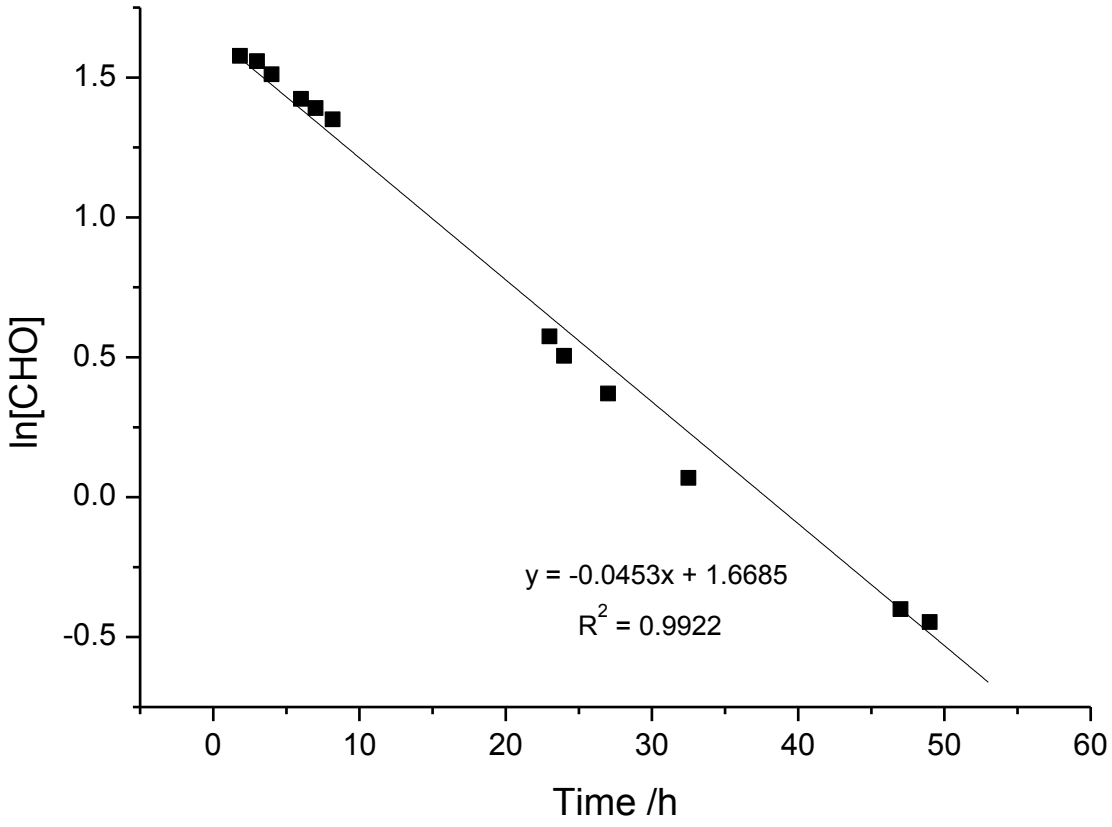

Figure 2.17: ln[CHO] *vs.* time plot. Copolymerisation conditions: $[CHO]_0$ = 4.94 M, [catalyst **1a**] = 4.94 mM in DEC at 80 °C and 1 bar CO_2 pressure.

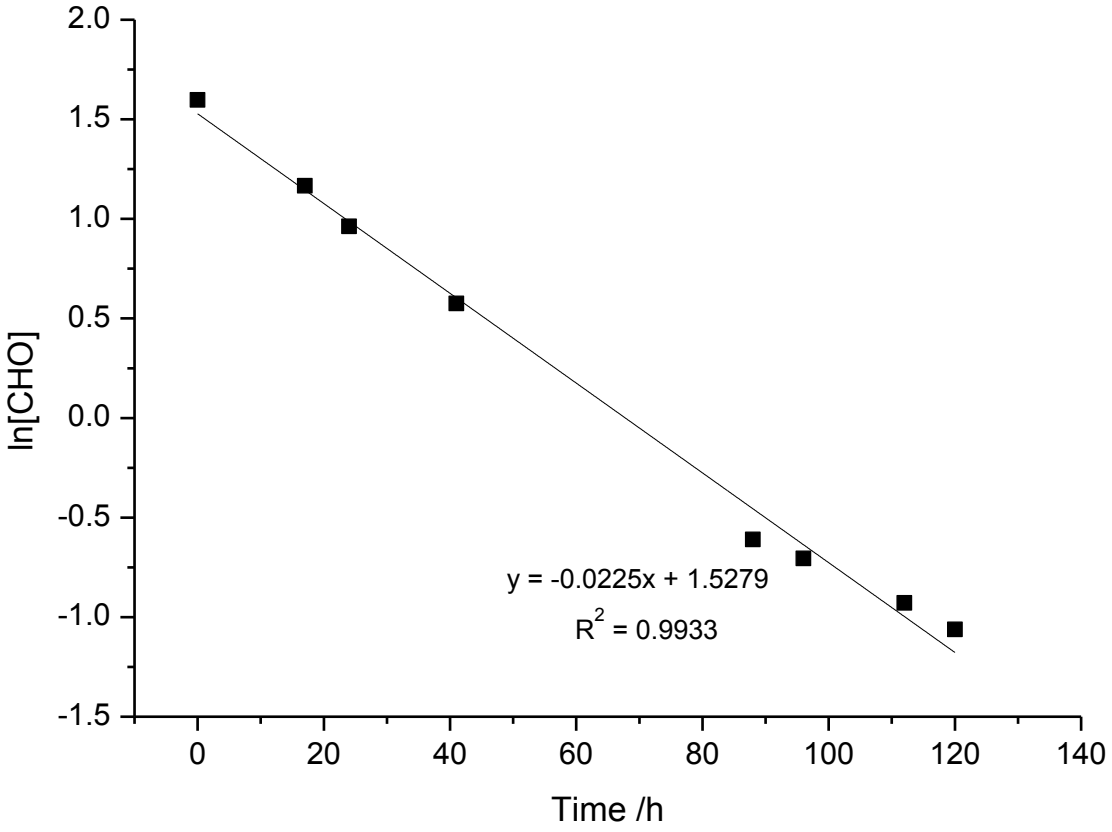

Figure 2.18: ln[CHO] *vs.* time plot produced by Williams and co-workers.[11] Copolymerisation conditions: $[CHO]_0$ = 4.94 M, [catalyst **2**] = 4.94 mM in DEC at 80 °C and 1 bar CO_2 pressure.

2.3.3 Reaction Order in CO_2 Pressure

The rate dependence on CO_2 pressure was determined by using the initial rate method. Various CO_2 pressures (10, 20, 30 40 and 50 bar CO_2 pressure) were investigated. This was done with a 1:1000 catalyst:CHO loading at 80 °C, in a Paar reactor vessel. The initial rate of the copolymerisation reaction at each pressure was calculated by carrying out several copolymerisations at a particular pressure and stopping these reactions at various different times and hence a plot of conversion *vs.* time was produced (Appendix A for plots). The slope from these plots represents the initial rate of the reaction for a particular pressure. Additionally, a copolymerisation reaction at 1 bar CO_2 pressure in a Schlenk tube was also carried out at 80 °C and aliquots were taken at regular time intervals to obtain an initial rate.

A plot of initial rate *vs.* CO_2 pressures was obtained (*vide infra* – Figure 2.19) and shows that the rate of CHO/CO_2 copolymerisation using catalyst **1a** does not vary with pressure of CO_2 and thus is zero order dependent with respect to CO_2 pressure. The slight discrepancies in the

initial rate values are due to experimental error. A zero order dependence was also observed previously with catalyst **2** and the data points within the plot are also slightly scattered (Figure 2.20).[11]

However, the initial rate values obtained at 1 bar and 50 bar CO_2 pressure for catalyst **1a** are slightly lower than expected. The copolymerisation reaction at 1 bar CO_2 pressure was carried out in a Schlenk tube, rather than a Paar reactor vessel and hence the stirring was much less efficient. The initial rate at 50 bar CO_2 pressure is also slightly lower than expected and this could be because the reaction tends towards a supercritical regime (supercritical point of CO_2 is at 31 °C and 73.9 bar), which may affect activity.[29]

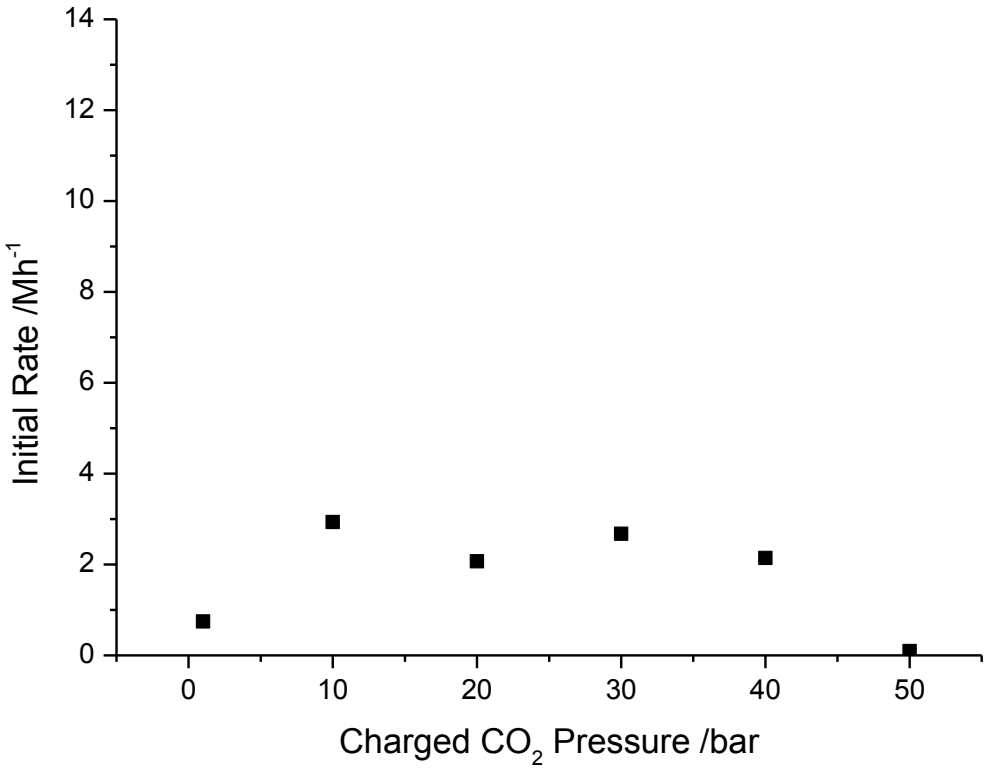

Figure 2.19: Initial rate *vs*. charged CO_2 pressure plot for catalyst **1a**. Reaction conditions: 1:1000 catalyst:CHO loading at 80 °C.

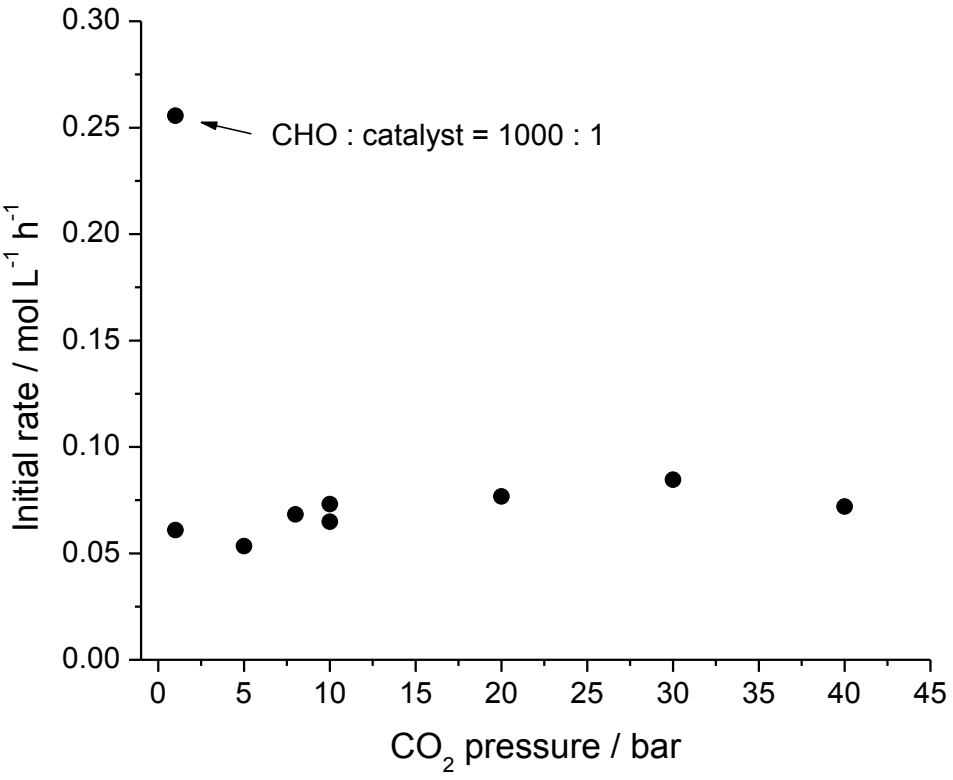

Figure 2.20: Initial rate *vs*. CO_2 pressure plot for catalyst **2** produced by Williams and co-workers.[11] Reaction conditions: 1:8000 catalyst:CHO loading at 80 °C.

2.4 Copolymerisation Mechanism

From the reaction orders determined in Section 2.3, the rate law for CHO/CO_2 copolymerisations using **1a** is:

$$\text{Rate} = k_p[\text{CHO}][\text{catalyst}] \qquad (9)$$

As the rate law is the same for catalyst **2**, it is hypothesised that catalyst **1a** undergoes the same mechanism that has already been proposed previously for catalyst **2** (Section 2.1).[11] From the rate law, it is assumed that the rate determining step of the reaction involves the ring opening of the epoxide. Additionally, it is believed that CO_2 insertion is pre-rate determining and occurs very rapidly.

It is hypothesised that during CHO/CO_2 copolymerisation reactions using catalyst **1a**, one of the acetate co-ligands initiates the copolymerisation reaction by ring opening a metal bound CHO molecule. A metal alkoxide species is formed on one of the metal centres (M_b – Figure 2.21) and this undergoes CO_2 insertion, which is rapid. This causes a metal-carbonate species

to form on the other metal centre within catalyst **1a** (M_a – Figure 2.21). The growing copolymer is thought to 'shuttle' twice between both metal centres within one catalytic cycle. The cycling between metal alkoxide and carbonate intermediates produces a perfectly alternating polycarbonate chain. According to our hypothesis, one acetate co-ligand remains bridging between the metal centres (normally on the concave face of the catalyst structure) and does not initiate copolymerisation.The role of this co-ligand is to maintain the coordination number and electronics of the metal centres (Figure 2.21).[10,11]

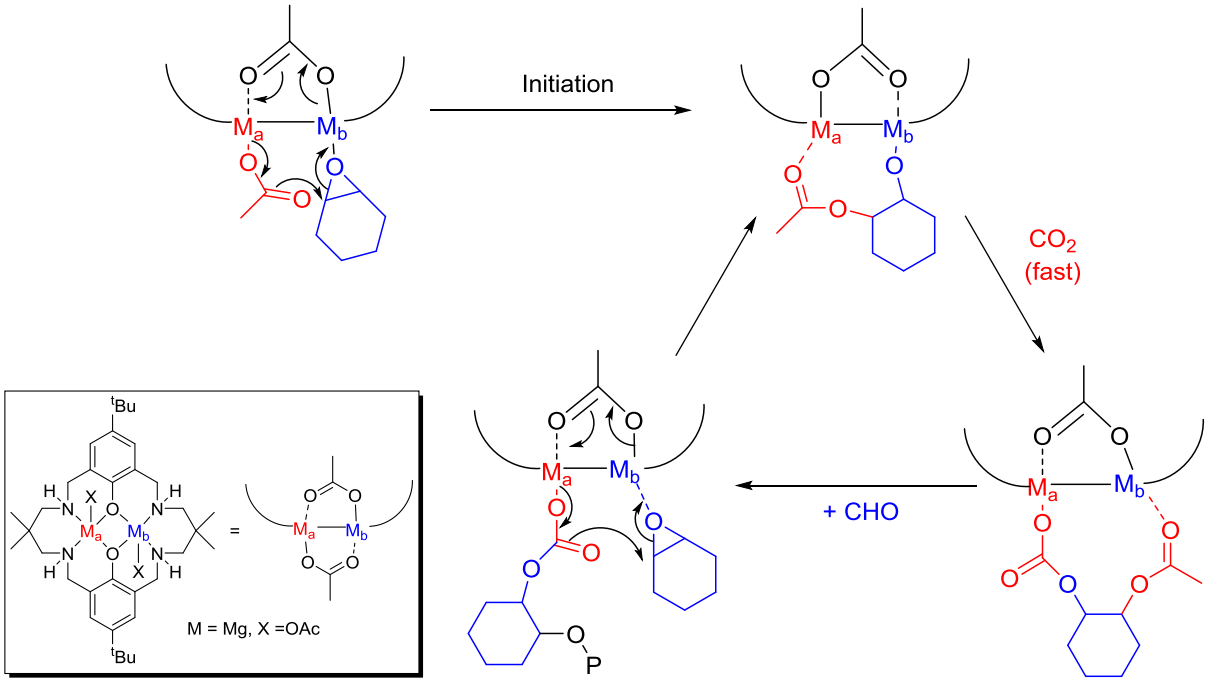

Figure 2.21: Proposed mechanism for catalyst **1a**.

2.5 Kinetic Investigations for Other Di-magnesium Complexes

The second aim of this chapter, to investigate if a co-ligand effect occurs during copolymerisation reactions, was conducted by using seven di-magnesium catalysts with different co-ligands (X in Figure 2.22). These catalysts were synthesised by Dr. Andrew Chapman, Econic Technologies. Most of these analogues are known and were prepared following literature protocols.[4]

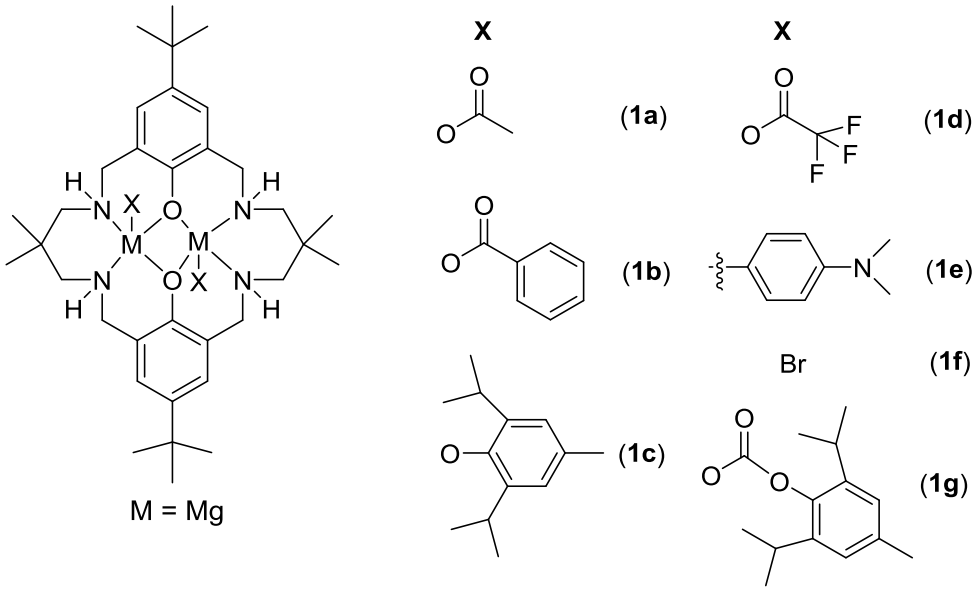

Figure 2.22: Structures of the seven di-magnesium catalyst derivatives investigated. Catalysts synthesised by Dr. Andrew Chapman.

Initiation is likely to differ between the magnesium catalyst derivatives outlined in Figure 2.22. Magnesium catalysts **1a**, **1b**, **1d**, **1f** and **1g** all initiate copolymerisation reactions as shown in Figure 2.21 (directly ring open a metal bound epoxide monomer). However, it is believed that catalysts **1c** and **1e** require CO_2 insertion to occur first before initiation can occur (Figure 2.23). Coates and co-workers have shown that CO_2 insertion occurs within the metal-alkoxide bonds of zinc β-diiminate (BDI) complexes to form metal-carbonate species, which then initiate copolymerisation. The zinc BDI complexes with alkoxide co-ligands did not show any reactivity with CHO.[12]

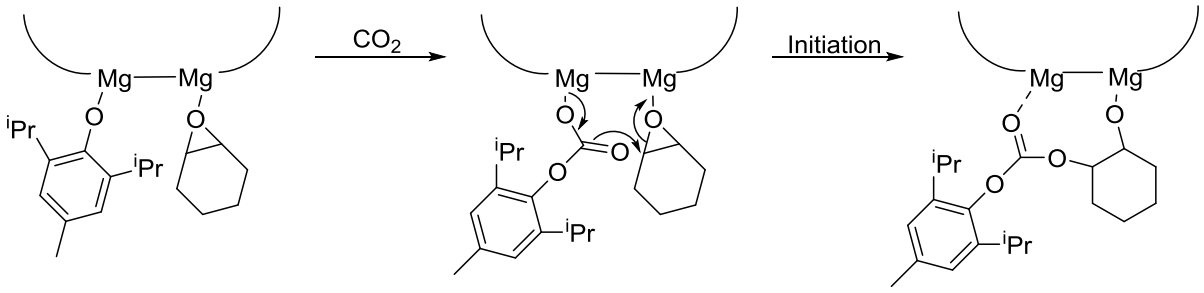

Figure 2.23: Proposed initiation process for di-magnesium catalysts **1c** and **1e**. Macrocyclic ligand architecture simplified and second co-ligand omitted for clarity.

The reaction order in [catalyst] for two of the seven magnesium catalyst derivatives (**1c** and **1d** in Figure 2.22) was investigated. The derivatives used had either an aryl oxide (**1c**) or carboxylate (**1d**) group as the co-ligand instead of the conventional acetate co-ligand (**1a**). The reaction order in [catalyst] was determined by an initial rates method using *in situ* ATR-IR spectroscopy, as described in Sections 2.2.1 and 2.3.1.

The initial rate *vs.* catalyst concentration plots generated (Figure 2.24 and 2.25) show that both analogues have a first order dependence on catalyst concentration. Considering this dependence was also found for the di-magnesium acetate catalyst (**1a**) and di-zinc acetate catalyst (**2**), it is assumed that these other dinuclear magnesium catalyst derivatives follow the same rate law (*vide supra* – equation 9).[11]

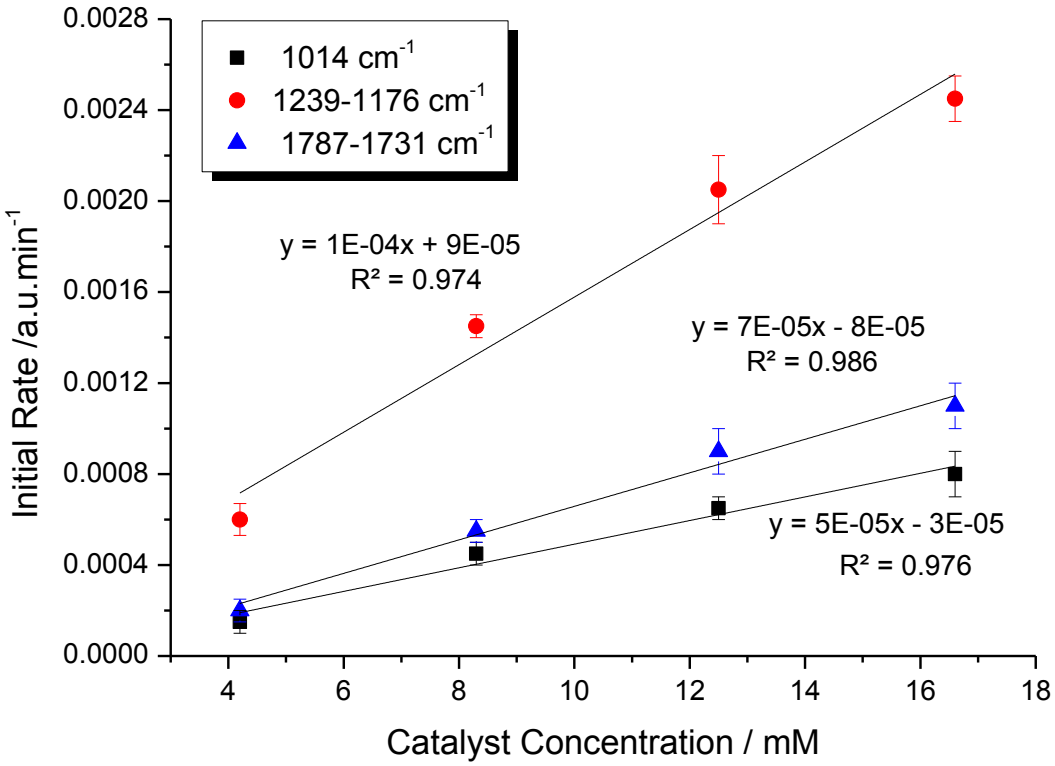

Figure 2.24: Initial rate *vs.* [catalyst **1c**] plot. Reaction conditions: $[CHO]_0$ = 8.24 M in DEC, 80 °C at 1 bar CO_2 pressure. Each experiment was run in triplicate to give the error value for each data point. The gradient values correlate to the k_{obs} values. For raw data plots see Appendix A.

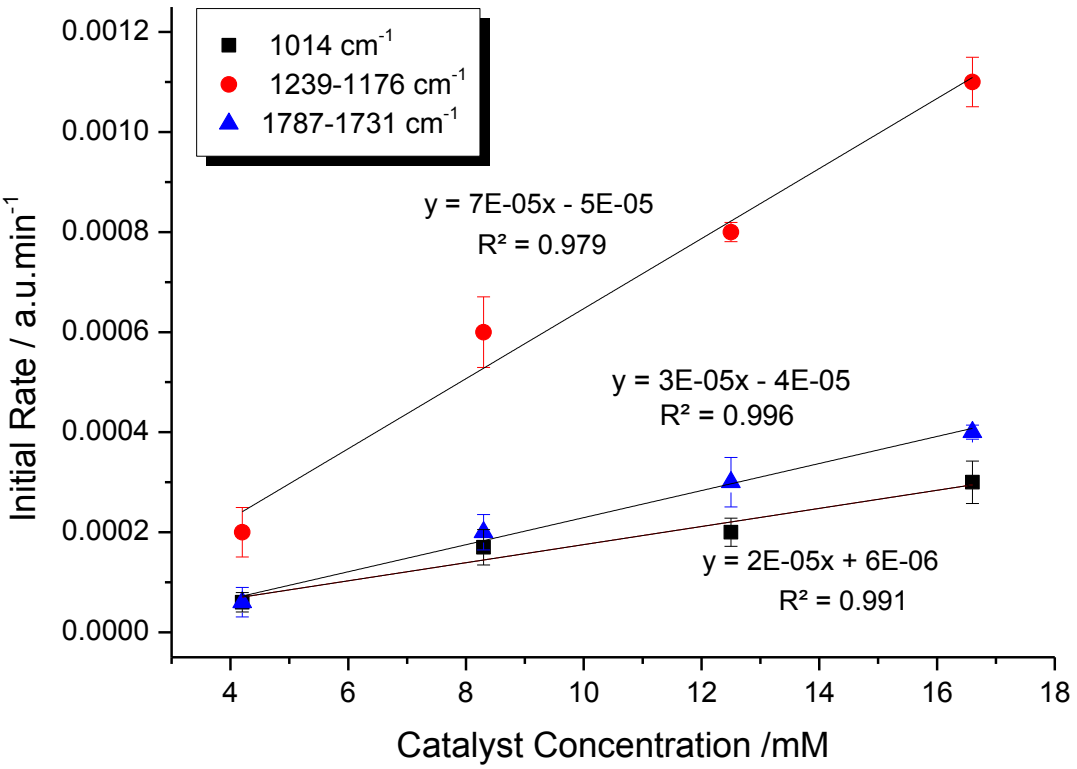

Figure 2.25: Initial rate *vs.* [catalyst **1d**] plot. Reaction conditions: $[CHO]_0$ = 8.24 M in DEC, 80 °C at 1 bar CO_2 pressure. Each experiment was run in triplicate to give the error value for each data point. The gradient values correlate to the k_{obs} values. For raw data plots see Appendix A.

The TOF values obtained for catalysts **1a** (X = acetate), **1c** (X = aryl oxide) and **1d** (X = trifluoroacetate) are 35, 33 and 31 h^{-1}, respectively. The differences are not significant and are within error and therefore the TOF values suggest that catalysts **1a**, **1c** and **1d** are very similar in activity, if not identical.[4]

TOF values are point kinetic measurements and thus combine initiation and propagation rates. Therefore, from the TOF values for **1a**, **1c** and **1d** the rate of propagation and initiation appear to be the same.[4] However, this was surprising because it was thought that the initiation periods would be different for **1a**, **1c** and **1d**. This is because the initiation period represents the time it takes for the metal-co-ligand bond to ring-open a metal bound epoxide monomer. Therefore, different co-ligands should initiate the copolymerisation at different rates. The shorter the initiation period, the easier and more facile the co-ligand is at ring opening the epoxide. Ideally, highly nucleophilic metal-co-ligand bonds will rapidly initiate the copolymerisation. The ability for the epoxide to reach and bind to the metal centre can also

affect the initiation period, but as the reaction conditions (ratio of catalyst to monomer) were the same for all copolymerisation reactions, it is believed that this has a negligible effect on the initiation period.

By looking at the k_{obs} values (gradient values) of the plots of initial rate *vs.* [catalyst] for catalysts **1a**, **1c** and **1d** (Figure 2.15, 2.24 and 2.25), more information was provided. In actual fact, **1a** is roughly 1.5-2 times faster than **1c**, depending on which vibrational mode is monitored. This result was not observed in the TOF values and therefore highlights that TOF values can give an estimate on which catalyst is faster, but for quantitative results more in depth kinetic analysis is required. The **1d** catalyst is also substantially slower than **1a** (0.89 times slower), which is also not shown in the TOF values (31 and 35 h^{-1}).[4]

The TOF values did not show these significant differences in propagation rate because even though catalyst **1a** is more active, it has a substantially longer initiation period (roughly 60 mins) compared to catalysts **1c** and **1d** (≈ 10 mins). Therefore, these different properties averaged out when monitoring TOF values and thus catalysts **1a**, **1c** and **1d** appeared to have similar activities. From these observations, it seems that TOF values can be a rough guide to investigate catalytic activity and rate, but a more accurate comparison is required (initial rate study).

Furthermore, it is interesting to see that the initiation time for **1c** and **1d** are similar even though **1c** needs to undergo CO_2 insertion to form a carbonate species first before initiating copolymerisation.[12] This is because alkoxides cannot initiate this copolymerisation process. This suggests that CO_2 insertion is very rapid and does not affect the initiation period (Figure 2.23).

2.6 Different Co-Ligands

Section 2.5 has outlined that varying co-ligands within the di-magnesium catalyst not only affects the initiation rate, but also affects the propagation rate (initial rate) of copolymerisation. This observation further supports the hypothesis that one co-ligand remains bound to the metal centres during CHO/CO_2 copolymerisation reactions. It is proposed that this difference in propagation rate occurs because different co-ligands have different electronic properties and thus affect the electrophilicity of the metal centres in the catalyst structure. Any difference in electronics at the metal centres would, in turn, affect the nucleophilicity of the metal carbonate bond required to ring open the metal bound epoxide molecules. Additionally, this will also affect the binding capabilities of the epoxide monomer to the metal centre.[8,20,30] Therefore, different co-ligands should change the rate of propagation of the catalyst in CHO/CO_2 copolymerisation reactions as well as the initiation rate.[10,11]

However, predicting the precise nature of the rate of acceleration/deceleration for particular co-ligands may be complex. Therefore, to further investigate this co-ligand effect in copolymerisation reactions, the initial rate for all seven di-magnesium catalyst derivatives (Figure 2.22) was recorded.

Several CHO/CO_2 copolymerisation reactions were carried out at 80 °C, 1 bar CO_2 pressure with $[CHO]_0$ of 8.24 M in DEC and a catalyst concentration of 8.3 mM. The copolymerisation reactions were monitored with an *in situ* ATR-IR probe and the C=O stretching vibrational mode (1787-1731 cm^{-1}) was monitored. The gradients (initial rate) were plotted against catalyst analogue (Appendix A for absorbance *vs.* time plots). The graph (Figure 2.26) shows that di-magnesium catalysts with different co-ligands have different initial rates.

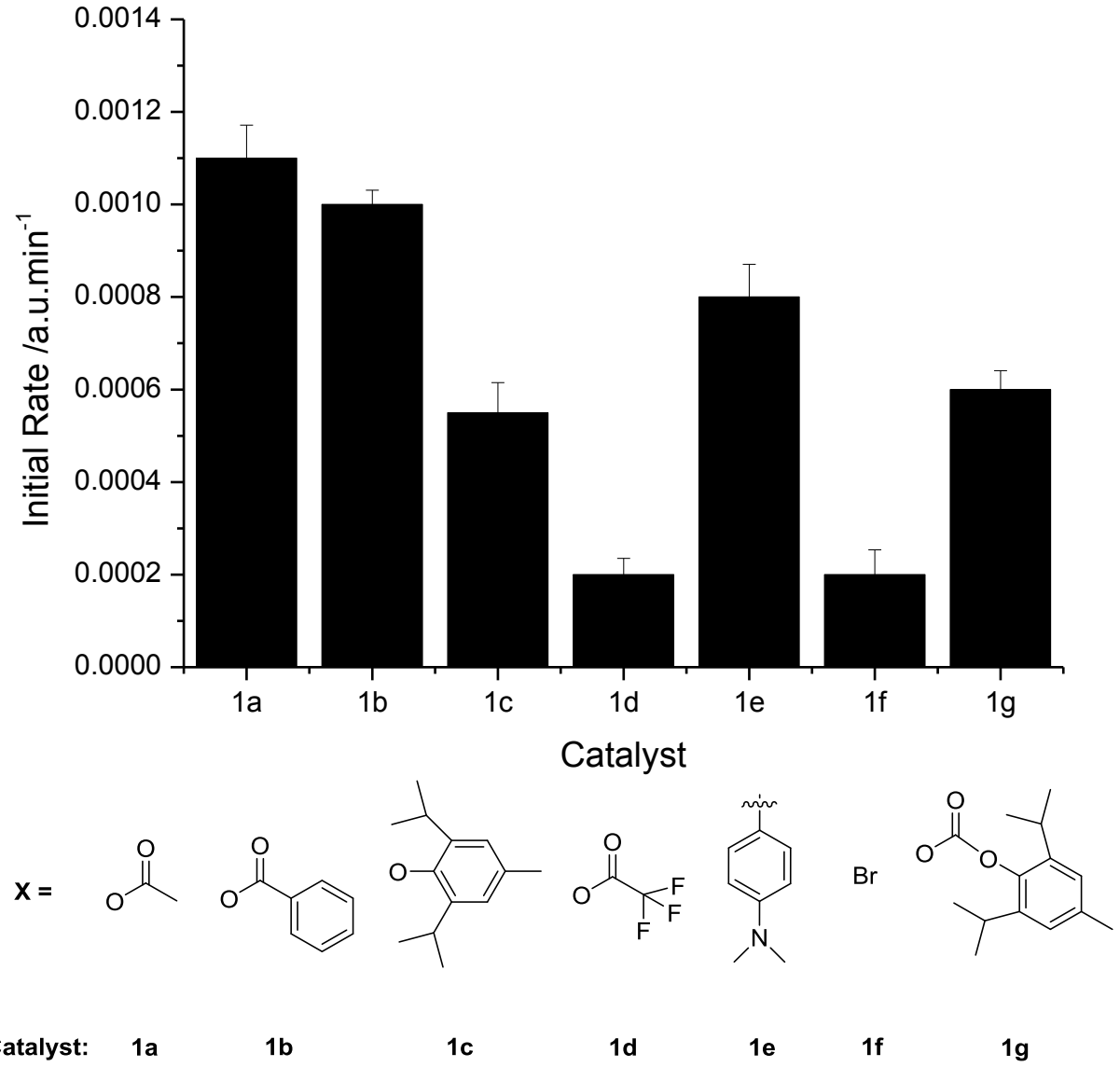

Figure 2.26: Graph of initial rate *vs.* different magnesium catalyst derivatives. Initial rates taken from monitoring the C=O stretching mode at 1787-1731 cm^{-1}. Reaction conditions: $[CHO]_0$ = 8.24 M in DEC, [catalyst] = 8.3 mM, 80 °C at 1 bar CO_2 pressure. Each experiment was run in triplicate to give the error value for each data point. For raw data plots see Appendix A.

The data (Figure 2.26) also shows that the least active catalysts are the catalysts with highly electron withdrawing co-ligand groups (**1d** – trifluoroacetate and **1f** – bromide). This suggests that co-ligands which increase the metal electrophilicity reduce the rate of copolymerisation. One explanation may be that even though such increased electrophilicity is expected to increase the rate of epoxide binding to the metal centre (which might be expected to benefit the polymerisation cycle), this increased electrophilicity may also stabilise the

metal-carbonate bond, which could decrease the rate. There is a subtle and delicate balance between sufficient electrophilicity for epoxide binding and the need for labile metal-carbonate bonds.

The more electron donating co-ligands (**1c** – aryl oxide and **1e** – dimethyl aniline) showed higher initial rates compared to the electron withdrawing groups (Figure 2.26), but the activities of these complexes were not as a high as catalysts **1a** (acetate) and **1b** (benzoate). One reason for this may be that the binding of the epoxide to the metal centres is weakened due to the electron donation and hence reduces the rate of ring opening of the epoxide.

The co-ligands with intermediate pKa values and thus the correct balance of electron withdrawing and donating abilities, have the best activity. The acetate and benzoate catalyst derivatives are the most active, which suggests the metal centres in these catalyst derivatives have the correct electrophilicity to aid epoxide binding and facilitate nucleophilic attack of the metal carbonate bond to ring open the metal bound epoxide.

Finally, catalysts **1c** and **1g** have similar initial rates, if not identical. This is not surprising because CO_2 insertion is expected to occur within the metal-aryloxide bond of **1c** before initiation occurs (Figure 2.23).[12] Once CO_2 insertion occurs, catalyst **1c** would have transformed into catalyst **1g** and thus the co-ligands are identical and hence the rate of copolymerisation should be the same for these catalysts even if a co-ligand remains bound to the metal centres. Even more interestingly, the initiation periods for **1c** and **1g** are similar (≈ 10 mins), which indicates CO_2 insertion within the metal-aryloxide bond occurs more rapidly and thus does not affect the initiation period (Figure 2.23).[31]

2.7 Conclusions and Future Work

Kinetic and mechanistic investigations have been carried out using catalysts **1a**-**1f** and **2**. The results have revealed that catalyst **1a** is approximately twice as fast as catalyst **2**, which suggests that the electrophilicity of the metal centres is an important feature and affects the catalyst activity for epoxide/CO_2 copolymerisation reactions. The correct electrophilicity is needed to aid epoxide binding and facilitate nucleophilic attack by the metal co-ligand or metal-carbonate bond to ring open the metal bound epoxide molecule.[7] In this case, the more electrophilic zinc centres of **2** hinder the activity of the catalyst. The less electrophilic magnesium centres in catalyst **1a** favour the key processes within CHO/CO_2 copolymerisation reactions and hence improve the activity of the catalyst.[32]

Additionally, catalysts **1a** and **2** follow the same rate law (rate = k_p[CHO][catalyst]) and hence are proposed to operate by the same reaction mechanism during the copolymerisation of CHO/CO_2. It is hypothesised that one co-ligand remains bound to the catalyst structure and the other co-ligand initiates copolymerisation. The growing copolymer chain 'shuttles' twice between the metal centres during a catalytic cycle. Both metals are involved in the catalytic process and each metal centre has a distinctive role (epoxide ring opening or CO_2 insertion). The rate determining step within the copolymerisation reaction was found to be the ring opening of the epoxide and that CO_2 insertion is facile and non-rate determining.[10,11]

Moreover, the use of TOF values in determining activity of catalysts in the ROCOP of CHO/CO_2 has been shown to be somewhat inaccurate for different catalysts and thus initial rates need to be recorded for a more accurate comparison. The TOF values for **1a** and **2** did in fact show that the magnesium derivative is twice as fast as the zinc analogue. However, when comparing catalysts **1a**, **1c** and **1d**, the TOF values showed that all three magnesium complexes had similar activities, but a more detailed rate study revealed more subtle effects. The different magnesium catalyst derivatives all had different initial rates (1×10^{-4}, 7×10^{-5} and 3×10^{-5} mMa.u^{-}min for **1a**, **1c** and **1d**, respectively looking at 1787-1731 cm^{-1} vibrational mode). This indicates that the co-ligand affects the rate of copolymerisation.

Figure 2.26 conveys that the electron donating and withdrawing nature of the co-ligand influences the rate of copolymerisation. It is proposed that this happens because one co-ligand may remain bound to the metal centres and thus changes the electrophilicity of the

metal centres, which affects the epoxide binding and metal-carbonate nucleophilic attack steps. The most active magnesium catalyst contains an acetate co-ligand and hence this co-ligand (**1a**) appears to have an optimum electronic balance to aid both the epoxide binding and metal-carbonate nucleophilic attack steps.

The comparison of the initial rates for seven magnesium catalyst derivatives confirmed that co-ligands with different electronic properties affect the rate of propagation, which suggests that one co-ligand may remain bound to the metal centres during copolymerisation. However, the different co-ligands investigated not only have different electronic properties, but they also have different steric properties. This could affect the conformation of the catalyst structure, which might in turn, affect the rate of copolymerisation. Therefore, for more accurate comparisons, similar co-ligand structures need to be investigated (benzoate, *para*-methoxy benzoate, penta-fluoro benzoate) and thus the sterics and catalyst conformation should be maintained.

Moreover, the initiation period has been observed to be different for various co-ligands, but the rate has not been investigated in detail. This can be observed by monitoring the ring opening of epoxide by the co-ligands *via* ATR-IR spectroscopy. Using a high catalyst to CHO loading, under N_2, at 80 °C, may enable the rate of ring opening of the epoxide by the co-ligand to be evaluated. This will shed light on the different initiation periods observed with different catalyst derivatives and produce an in depth analysis on which co-ligands should be used to minimise the initiation period and increase catalytic activity.

Additionally, as discussed briefly in Section 2.5 and 2.6, certain co-ligands require CO_2 insertion to occur before they can initiate the copolymerisation reaction. On initial inspection, this does not seem to extend the initiation period and thus CO_2 insertion into metal alkyl, phenyl and alkoxide bonds seems to be very facile. However, this needs to be probed more. The initiation rates for alkyl, phenyl and alkoxide co-ligands and their corresponding carboxylate and carbonate derivatives need to be recorded and compared in order to verify if CO_2 insertion does not affect the initiation period.[31]

Even though several investigations have led to the hypothesis that one co-ligand remains bound to the metal centres during copolymerisation reactions, no structure has been obtained to verify this. Therefore, attempts to crystallise the product obtained when a catalyst molecule

ring opens one epoxide monomer should be carried out in order to support the hypothesis that one co-ligand remains bound to the catalyst during copolymerisation reactions.

Sections 2.5 and 2.6 have shown that co-ligands with short initiation periods have slow rates of propagation and *vice versa*. The reason for this is because the electronic demands for initiation and propagation are opposite. The more electron withdrawing co-ligands may initiate faster *via* nucleophilic attack. However, as one co-ligand remains bound to the metal centres during copolymerisation, an electron withdrawing co-ligand may increase the electrophilicity of the metal centres, which may strengthen the metal-carbonate bond and hence reduce propagation rates. Catalysts with two different co-ligands should be targeted and then investigated. Ideally, one co-ligand should be more electron withdrawing than the other and hence the activity of the catalyst should improve as both initiation and propagation rates will be optimised. This target may be difficult to obtain as the co-ligands are thought to be very labile, but if synthesised, in depth kinetic studies need to be carried out on these species.[12]

Furthermore, kinetic and mechanistic studies on other new catalyst structures, some described in Chapter 3, should be carried out. In particular, heterodinuclear catalysts and homodinuclear catalysts with asymmetrical macrocyclic ligands need to be investigated in order to see if the same mechanism and rate law applies to these analogues.

The co-ligands investigated thus far are conventionally carboxylates, but other co-ligands, such as amides, thio-esters, sulfinates and phosphinates could be investigated. A new series of analogues should be synthesised. The use of new co-ligands that are not conventionally used in catalysts for CHO/CO_2 copolymerisation will be interesting to monitor kinetically.

Finally, an attempt to quantify the electrophilicity (Lewis acidity) required to produce an active catalyst should be carried out. This may be done by looking at the association and dissociation of various donors (phosphines, N-bases) to the metal centres of the catalyst structure.

2.8 References

1. A. Buchard, M. R. Kember, K. G. Sandeman and C. K. Williams, *Chem. Commun.,* 2011, ***47***, 212-214.

2. M. R. Kember, F. Jutz, A. Buchard, A. J. P. White and C. K. Williams, *Chem. Sci.,* 2012.

3. M. R. Kember, P. D. Knight, P. T. R. Reung and C. K. Williams, *Angew. Chem. Int. Ed.,* 2009, ***48***, 931-933.

4. M. R. Kember and C. K. Williams, *J. Am. Chem. Soc.,* 2012, ***134***, 15676-15679.

5. M. R. Kember, A. J. P. White and C. K. Williams, *Inorg. Chem.,* 2009, ***48***, 9535-9542.

6. M. R. Kember, A. J. P. White and C. K. Williams, *Macromolecules,* 2010, ***43***, 2291-2298.

7. T. Bok, H. Yun and B. Y. Lee, *Inorg. Chem.,* 2006, ***45***, 4228-4237.

8. M. R. Kember, A. Buchard and C. K. Williams, *Chem. Commun.,* 2011, ***47***, 141-163.

9. M. R. Kember, J. Copley, A. Buchard and C. K. Williams, *Polym. Chem.,* 2012.

10. A. Buchard, F. Jutz, M. R. Kember, A. J. P. White, H. S. Rzepa and C. K. Williams, *Macromolecules,* 2012, ***45***, 6781-6795.

11. F. Jutz, A. Buchard, M. R. Kember, S. B. Fredrickson and C. K. Williams, *J. Am. Chem. Soc.,* 2011, ***133***, 17395–17405.

12. D. R. Moore, M. Cheng, E. B. Lobkovsky and G. W. Coates, *J. Am. Chem. Soc.,* 2003, ***125***, 11911-11924.

13. B. Y. Lee, H. Y. Kwon, S. Y. Lee, S. J. Na, S.-i. Han, H. Yun, H. Lee and Y.-W. Park, *J. Am. Chem. Soc.,* 2005, ***127***, 3031-3037; Y. Xiao, Z. Wang and K. Ding, *Chem. Eur. J.,* 2005, ***11***, 3668-3678.

14. C. T. Cohen, T. Chu and G. W. Coates, *J. Am. Chem. Soc.,* 2005, ***127***, 10869-10878.

15. K. Nakano, S. Hashimoto and K. Nozaki, *Chem. Sci.,* 2010, ***1***, 369-373; S. I. Vagin, R. Reichardt, S. Klaus and B. Rieger, *J. Am. Chem. Soc.,* 2010, ***132***, 14367-14369.

16. X.-B. Lu, L. Shi, Y.-M. Wang, R. Zhang, Y.-J. Zhang, X.-J. Peng, Z.-C. Zhang and B. Li, *J. Am. Chem. Soc.,* 2006, ***128***, 1664-1674; D.-Y. Rao, B. Li, R. Zhang, H. Wang and X.-B. Lu, *Inorg. Chem.,* 2009, ***48***, 2830-2836; C. Chatterjee and M. H. Chisholm, *Inorg. Chem.,* 2011, ***50***, 4481-4492; T. Aida and S. Inoue, *J. Am. Chem. Soc.,* 1983, ***105***, 1304-1309.

17. D. J. Darensbourg, R. M. Mackiewicz, J. L. Rodgers and A. L. Phelps, *Inorg. Chem.,* 2004, ***43***, 1831-1833.

18. D. J. Darensbourg and J. C. Yarbrough, *J. Am. Chem. Soc.,* 2002, ***124***, 6335-6342.

19. D. J. Darensbourg, J. C. Yarbrough, C. Ortiz and C. C. Fang, *J. Am. Chem. Soc.,* 2003, ***125***, 7586-7591.

20. D. J. Darensbourg, *Chem. Rev.,* 2007, ***107***, 2388-2410.

21. D. J. Darensbourg, Mackiewicz and J. L. Rodgers, *J. Am. Chem. Soc.,* 2005, ***127***, 17565-17565; D. J. Darensbourg, R. M. Mackiewicz, J. L. Rodgers, C. C. Fang, D. R. Billodeaux and J. H. Reibenspies, *Inorg. Chem.,* 2004, ***43***, 6024-6034.

22. J. O'Donnell, *J. Am. Chem. Soc.,* 2010, ***132***, 10206-10207.

23. S. Inoue, *J. Polym. Sci. A Polym. Chem.,* 2000, ***38***, 2861-2871.

24. B. Iván, *Macromol. Symp.,* 1994, ***88***, 201-215.

25. K. Nakano, M. Nakamura and K. Nozaki, *Macromolecules,* 2009, ***42***, 6972-6980; S. J. Na, S. S, A. Cyriac, B. E. Kim, J. Yoo, Y. K. Kang, S. J. Han, C. Lee and B. Y. Lee, *Inorg. Chem.,* 2009, ***48***, 10455-10465; E. K. Noh, S. J. Na, S. S, S.-W. Kim and B. Y. Lee, *J. Am. Chem. Soc.,* 2007, ***129***, 8082-8083.

26. J. K. Varghese, A. Cyriac and B. Y. Lee, *Polyhedron,* 2012, ***32***, 90-95.

27. X.-B. Lu and D. J. Darensbourg, *Chem. Soc. Rev.,* 2012, ***41***, 1462-1484.

28. P. Atkins and J. d. Paula *Elements of Physical Chemistry*; Fourth ed.; W.H. Freeman and Company: New York, 2005.

29. F. Rindfleisch, T. P. DiNoia and M. A. McHugh, *J. Phys. Chem.,* 1996, ***100***, 15581-15587; A. J. Ragauskas, M. Nagy, D. H. Kim, C. A. Eckert, J. P. Hallett and C. L. Liotta, *Ind. Biotech.,* 2006, ***2***, 55-65; C. Swalina, S. Arzhantsev, H. Li and M. Maroncelli, *J. Phys. Chem. B,* 2008, ***112***, 14959-14970.

30. G. W. Coates and D. R. Moore, *Angew. Chem. Int. Ed.,* 2004, ***43***, 6618-6639.

31. X. Yin and J. R. Moss, *Coord. Chem. Rev.,* 1999, ***181***, 27-59.

32. J. Mullay, *J. Am. Chem. Soc.,* 1984, ***106***, 5842-5847.

Chapter 3

Synthesis of Heterodinuclear Complexes for Epoxide/CO_2 Ring Opening Copolymerisation Reactions

"Learn from yesterday, live for today, hope for tomorrow. The important thing is to not stop questioning."

Relativity: The Special and the General Theory by Albert Einstein

3.1 Introduction

3.1.1 Heterodinuclear Catalysts for Epoxide/CO_2 Copolymerisation Reactions

Coates and co-workers observed that zinc β-diiminate complexes can exist as dimers, which enhanced their catalytic activity (Chapter 1). These findings led to a surge in the synthesis and use of homogeneous bimetallic complexes for epoxide/CO_2 copolymerisation reactions.[1] A more in depth analysis of these bimetallic catalyst systems is outlined in Chapter 1. However, there are three main types of bimetallic catalysts for epoxide/CO_2 copolymerisation reactions (Figure 3.1). Type I is based on binucleating ligands, such as, macrocycles.[2-6,7] Type II is based on tethering mononucleating ligands, such as, salens or propyhrins.[8,9] Type III involves monometallic complexes, which can form dimeric species in solution.[1]

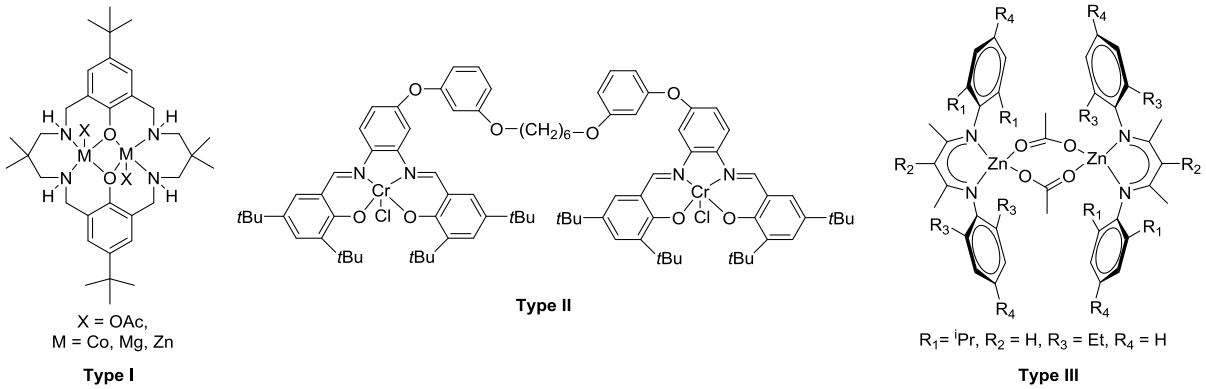

Figure 3.1: Examples of different types of bimetallic complexes for epoxide/CO_2 ring opening copolymerisation reactions.[1,2-5,9]

However, all these catalysts have one feature in common, which is that they are all homodinuclear complexes. To date, no heterodinuclear complexes have been synthesised for epoxide/CO_2 copolymerisations.[2-6,8,9,10] All bimetallic catalysts contain two metal centres of the same metal. Catalysts for epoxide/CO_2 copolymerisation reactions containing different metal centres have only come in the form of heterogeneous double metal cyanides (DMCs).[11-13]

These DMCs have a generic structure of an oxophilic metal ion [M_1] bound to a transition metal [M_2] present as a cyanide salt and thus have a generic formula of $[M_1]_n[M_2(CN)_6]_m$.[14] All of these DMCs also require the addition of organic compounds, including salts and alcohols.[14-16] The most frequently used metals in DMCs are Zn bound to either $[Fe(CN)_6]^{3-}$ or

$[Co(CN)_6]^{3-}$. Generally the proposed structure for these DMCs involves the CN groups bridging between the M_1 and M_2 metal centres.[14,15]

These heterogeneous DMCs have shown good activity for epoxide/CO_2 copolymerisation reactions. Even though the catalyst is in a different phase to the monomers, the zinc metal centres within DMCs are able to facilitate epoxide binding and polymer propagation.[16] DMCs were initially used for epoxide homopolymerisation, in particular for propylene oxide (PO).[15] When used for PO or cyclohexene oxide (CHO) and CO_2 copolymerisation reactions, the Fe-Zn DMCs showed lower productivities compared to the Co-Zn derivatives, which possessed productivities between 500-1000 g of copolymer/ g of Zn.[11,16,17] The activity of the DMCs is drastically influenced by the crystallinity of the sample. The more amorphous the sample the more active the DMCs are because it is believed that the reduction in crystallinity increases the catalyst surface area.[16,18] Moreover, the addition of additives, such as alcohol, dramatically improves the activity of the DMCs.[14,19]

However, the disadvantage of using DMCs as catalysts for epoxide/CO_2 copolymerisation reactions is that the incorporation of CO_2 in the growing copolymer chain is low and thus the polycarbonate chains formed have high ether content (from sequential epoxide enchainment). PO is easier to homopolymerise and thus the % carbonate present in poly(propylene) carbonate (PPC) is typically lower than for poly(cyclohexene) carbonate (PCHC), 20-40 % compared to up to 90 %, respectively.[12,16,17] Additionally, DMCs require very high temperatures (80-130 °C) and high pressures (50-100 atm), which is not ideal as it increases process costs.[11,12,16,17,20]

High ether linkages are not always desirable because the incorporation of ether linkages in polycarbonate chains lowers the T_g of the copolymer and thus affects the material properties of the polycarbonate. However, ether linkages can improve the polymer chain solubility in supercritical CO_2 and therefore it can be used as a 'CO_2-phile'.[20,21] Lee and co-workers have used dual catalyst systems (bifunctional cobalt salen complexes with a DMC) in order to deliberately introduce certain amounts of ether linkages in the polycarbonate chains produced and thus tune the copolymer properties.[20]

Understanding the mechanism of DMCs and modifying the catalyst system to enhance activity is extremely difficult for such ill-defined heterogeneous catalysts. Therefore,

Darensbourg and others tried to synthesise well-defined Zn-Fe DMCs by incorporating phosphine ligands into the DMC structure and making the DMCs soluble in acetonitrile or THF ([CpFe(CO)(μ-CN)$_2$ZnI(THF)]$_2$). These derivatives were less active, but showed good CO_2 incorporation in the copolymer product (> 85 % carbonate linkages in PCHC).[14,18,22]

3.1.2 Other Heterodinuclear Complexes

In other areas of Chemistry, heterodinuclear complexes have been synthesised and used in various reactions. Some have shown an enhanced activity compared to their homodinuclear or monometallic counterparts.

One example of this cooperativity has been observed in the field of C-H bond cleavage. Usually, C-H bond cleavage or deprotonation by metallation occurs by the formation of reactive $C^{\delta+}$-$M^{\delta-}$ bonds. These bonds are formed by reacting an organic compound with either organolithium, organomagnesium or organozinc species.[23] This reactive $C^{\delta+}$-$M^{\delta-}$ bond can then undergo conversion to C-C or C-X bonds, which are used in many organic synthetic processes adopted by industry to synthesise common drug molecules.[23,24]

The conventional metallation reagents are effective, but have their shortcomings, which are primarily issues with functional group tolerance and selectivity. Organolithium reagents, such as, *n*BuLi or ^{t}BuLi are the most reactive reagents for C-H bond cleavage. Even though this process is very facile, this high reactivity causes these organolithium reagents to have poor functional group tolerance and expensive cooling procedures are required to prevent decomposition occurring.[25] Organomagnesium reagents, such as, Grignards (RMgX) and Hauser bases (R_2NMgX) have moderate activity, but low functional group tolerance and selectivity.[26,27] Organozinc species have low reactivity, but good selectivity and functional group tolerance.[28]

The field of C-H bond activation by metallation have been developing organometallic reagents that show good selectivities, good functional group tolerance and are able to dimetallate organic molecules. The latter allows multi-substituted products to be synthesised *via* a single reaction.[29] Therefore, the field of C-H bond activation have slowly moved away from monometallic reagents and have been developing heterobimetallic reagents for C-H

bond cleavage. Heterobimetallic reagents have shown synergistic effects, which have led to good activity, selectivity and functional group tolerance.[30]

Many heterobimetallic reagents have been developed, one example being, the turbo-Grignards and turbo-Hauser bases ((TMP)MgCl·LiCl).[31,32] Grignard reagents are usually synthesised by inserting Mg within an alkyl halide bond. However, Knochel and co-workers found that by adding a salt to the Grignard, in particular LiCl, the activity, selectivity and functional group tolerance improved. These new derivatives of Grignards were called turbo-Grignards and have a generic structure of RMgX·LiCl. It seems that the LiCl enhances the reactivity of the Grignard reagent by disrupting the aggregation present in the Grignard and hence increases the solubility.[27,31,33]

Sigma Aldrich have managed to commercialise TMPMgCl·LiCl (turbo-Hauser base) and Mulvey and co-workers have been successful in crystallising this compound. They have found that the sample contained both $[(THF)Mg(\mu\text{-}Cl)(TMP)]_2$ and $[(THF)_2Li(\mu\text{-}Cl)_2Mg(THF)(TMP)]$ complexes.[34] This finding suggests that the LiCl is involved in the turbo-Hauser base structure. The lithium-magnesium co-complex structure has a TMP (2,2,6,6-tetramethylpiperidine) molecule bound in the terminal position to the Mg metal centre (Figure 3.2), which also has a terminally bound THF molecule. The chloride ions bridge the Mg and Li metal centres and the Li also has two THF molecules terminally bound to it (Figure 3.2). The activity of this turbo-Hauser reagent is hypothesised to occur due to the facile dissociation of the Mg bound THF molecule in solution, which allows substrates to approach the Mg metal centre before metallation occurs.[34]

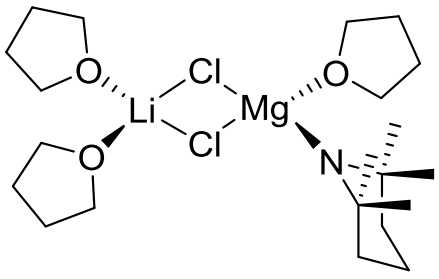

Figure 3.2: Structure of turbo-Hauser base $[(THF)_2Li(\mu\text{-}Cl)_2Mg(THF)(TMP)]$.

Another example of where heterodinuclear complexes have shown enhanced activity over their monometallic counterparts is in the field of olefin polymerisation.[35] Marks and co-workers have shown that by covalently tethering Ti and Zr monometallic catalysts for ethylene polymerisation, the resulting heterodinuclear catalyst has an enhanced activity compared to the Ti and Zr monometallic counterparts (Figure 3.3). This heterodinuclear catalyst also displayed the ability to produce high M_n (number average molecular weight) branched polyethylene chains. This is thought to occur due to the spatial confinement of the Ti and Zr catalytic sites, which may increase the chance of intramolecular oligomer enchainment.[35]

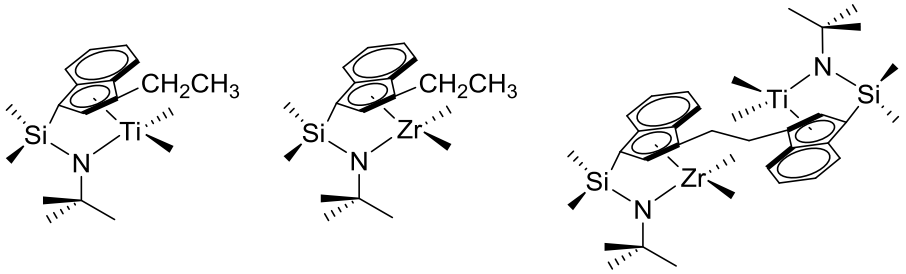

Figure 3.3: Ti and Zr monometallic and heterodinuclear catalysts synthesised by Marks and co-workers.[35]

3.1.3 Background and Aims

Extensive research into the mechanism adopted by the homogeneous homodinuclear catalysts synthesised by Williams and co-workers for CHO/CO_2 copolymerisation reactions have been carried out.[36,37] The hypothesised mechanism has been discussed in detail in Chapter 2. The main aspect of the mechanism is that both metal centres in the bimetallic complex are believed to be involved in the copolymerisation reaction and that the copolymer chain 'shuttles' twice between the metal centres per catalytic cycle.[36,37] This therefore also suggests that one metal centre (M_b – Figure 3.4) aids epoxide binding and ring opening, whereas the second metal centre (M_a – Figure 3.4) carries out CO_2 insertion.

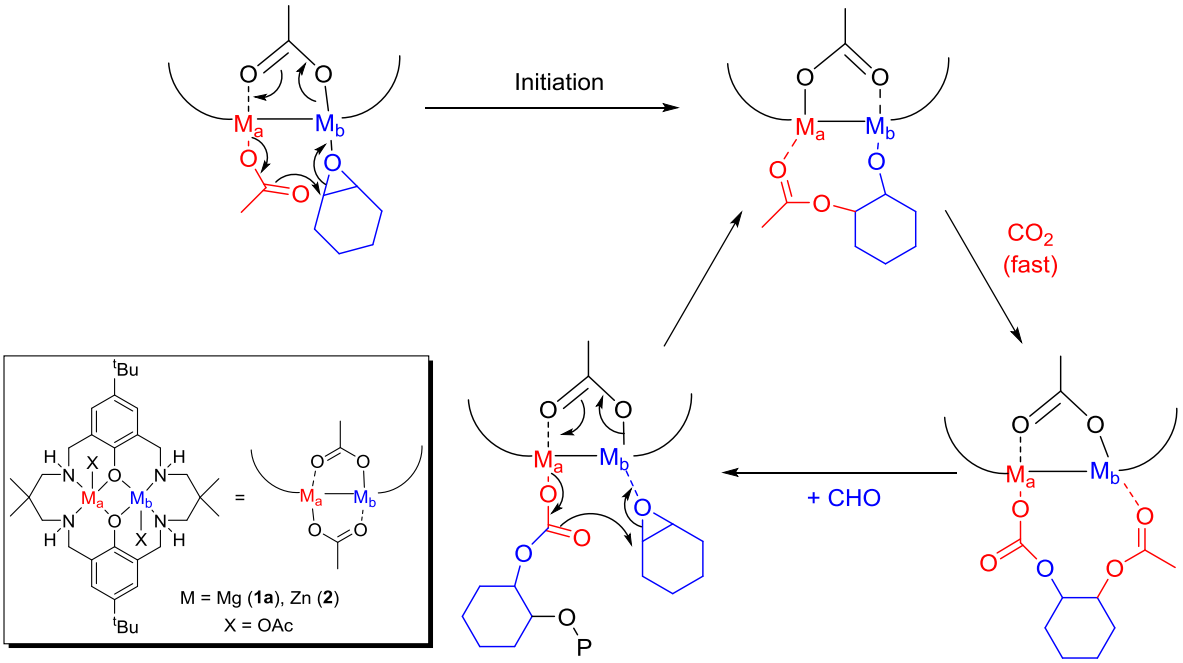

Figure 3.4: Proposed mechanism for bimetallic catalysts synthesised by Williams and co-workers.[36]

It is believed that by using two different metals within the symmetrical macrocyclic ligand (heterodinuclear complex) or synthesising asymmetric macrocyclic ligands and thus asymmetric homodinuclear complexes, would cause each metal centre to have different electronic properties. Therefore, it may be possible to bias one metal to carry out epoxide binding and ring opening and the other to facilitate CO_2 insertion and hence the activity of the catalyst may be improved by a positive cooperativity effect.

This chapter reports the attempts to synthesise heterodinuclear Zn-Mg complexes, surrounded by a symmetrical macrocyclic ligand, and homodinuclear zinc complexes, coordinated by asymmetrical macrocyclic ligands. The chapter also describes the activity, if any, of these complexes in epoxide/CO_2 copolymerisation reactions, in particular when using CHO or PO as the epoxide monomer.

Relevant heterodinuclear complexes coordinated by macrocyclic ligands were reported in the literature by Bosnich and others.[38,39-41] The complexes are all based around asymmetrical macrocyclic ligands or symmetrical tetra-imine macrocyclic ligands (Figure 3.5 and Section 3.2.2).[38,39-41] Therefore, these reports have been essential in the development of symmetrical heterodinuclear and asymmetrical homodinuclear complexes (Section 3.2 and 3.6).

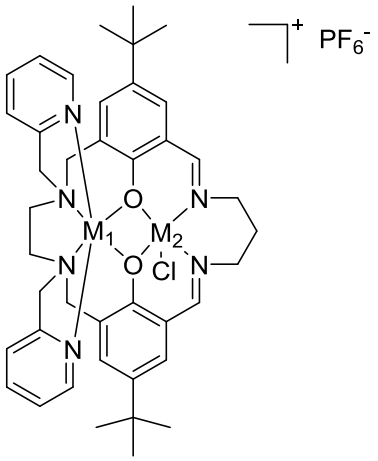

Figure 3.5: Heterodinuclear asymmetrical complexes synthesised by Bosnich and co-workers.[40,41]

3.2 Synthesising Heterodinuclear Complexes *via* Stepwise Route

3.2.1 Synthesis of Monometallic Complexes

The synthesis of heterodinuclear derivatives of catalysts **1a** and **2** was attempted *via* a stepwise route. The synthesis generally involved the formation of half a macrocyclic ligand, which has two different compartments (N_2O_2 and O_4) and thus it is believed that the addition of one equivalent of one metal precursor should favour coordination to the N_2O_2 compartment. Once the monometallic complex had formed, cyclisation of the half macrocycle by the addition of a diamine would have been attempted. The addition of another equivalent of a different metal precursor and reduction of the ligand would then have been carried out, in order to yield the desired heterodinuclear complex surrounded by the same macrocyclic ligand used previously by our group.[2-5] The reason for maintaining the same ligand motif is to ensure that if the activity of the heterodinuclear complex is different to the homodinuclear derivatives, this change in activity is solely due to having two different metals within the catalyst structure and not due to any ligand modification. Two routes were adopted (Scheme 3.1) to prepare heterodinuclear complexes.

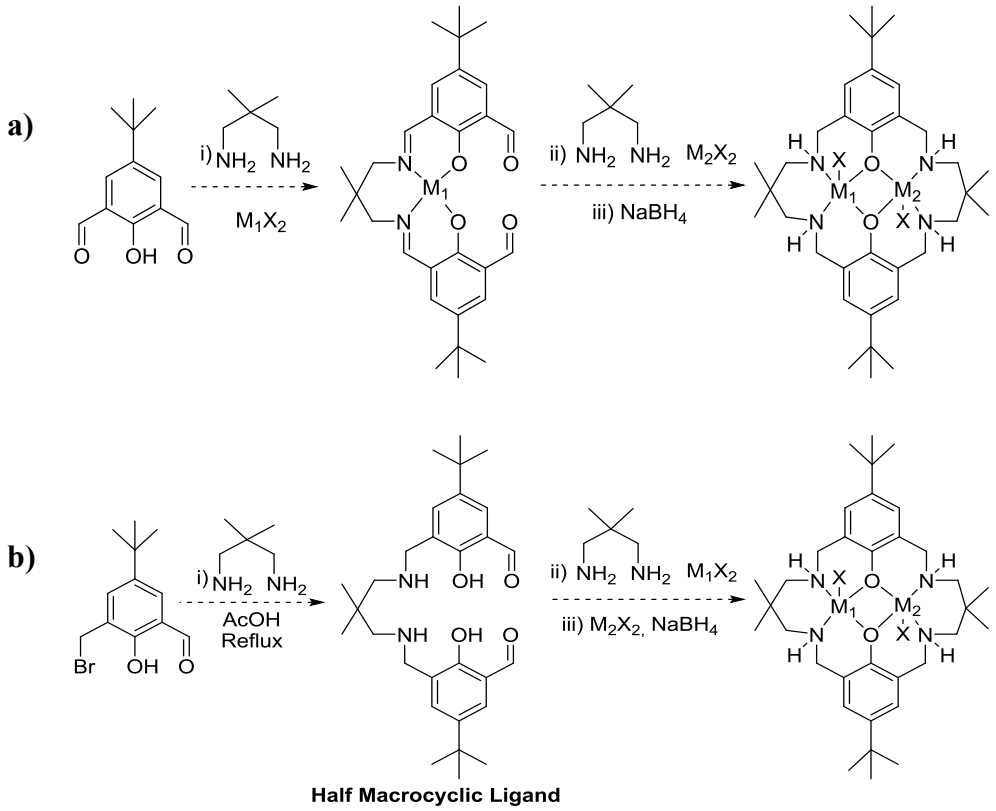

Scheme 3.1: Synthetic routes attempted to produce heterodinuclear catalysts.

Route a) (Scheme 3.1) involved reacting a 4-tert-butyl-2,6-diformylphenol with 2,2-dimethyl-1,3-propanediamine and a metal precursor to form a diimine monometallic complex. This was tried with four different metal precursors ($Zn(OAc)_2$, $Cu(OAc)_2$, $MgNO_3.6H_2O$ and $Zn(BF_4)_2$). This route was not successful with any of the metal precursors. The reaction with $Zn(OAc)_2$ produced a bimetallic tetra-imine complex. A monometallic copper complex was obtained in low yield, but the reaction was not reproducible and when reacted with $Zn(OAc)_2$, a heterodinuclear complex did not form. With both $MgNO_3.6H_2O$ and $Zn(BF_4)_2$, the monometallic product was the minor product. The major product was polymer, which is difficult to separate from the desired product.

Route b) entailed reacting 3-bromo-5-*t*-butylsalicylaldehyde with 2,2-dimethyl-1,3-propanediamine in the presence of several drops of AcOH. The acid in this reaction is acting as a templating agent, like the metal precursor in route a), to favour the formation of the half macrocycle over polymer. Once this half macrocyclic ligand had formed, a metal precursor would have been added to form a monometallic complex, which would then undergo cyclisation, reduction of the imine bonds and the addition of another metal precursor to form

the desired heterodinuclear complex. However, the first step was problematic, it was repeated several times and each time a mixture of products was obtained, which included a large proportion of polymer.

An attempt to promote the reaction between the Br functional group of 3-bromo-5-*t*-butylsalicylaldehyde with 2,2-dimethyl-1,3-propanediamine and thus remove the tendency for the amine to react with the aldehyde functionality was carried out. This involved protecting the amine with BOC (Scheme 3.2). This secondary amine can therefore only react with the Br functional groups of 3-bromo-5-*t*-butylsalicylaldehyde and hence prevent a mixture of products being formed. However, the BOC (*t*-butyloxycarbonyl) group reduced the activity of the amine groups and hence no reaction was observed. Several attempts to protect the aldehyde group were also carried out, but this was also unsuccessful, as the starting material was always recovered at the end of the reaction (Scheme 3.3).

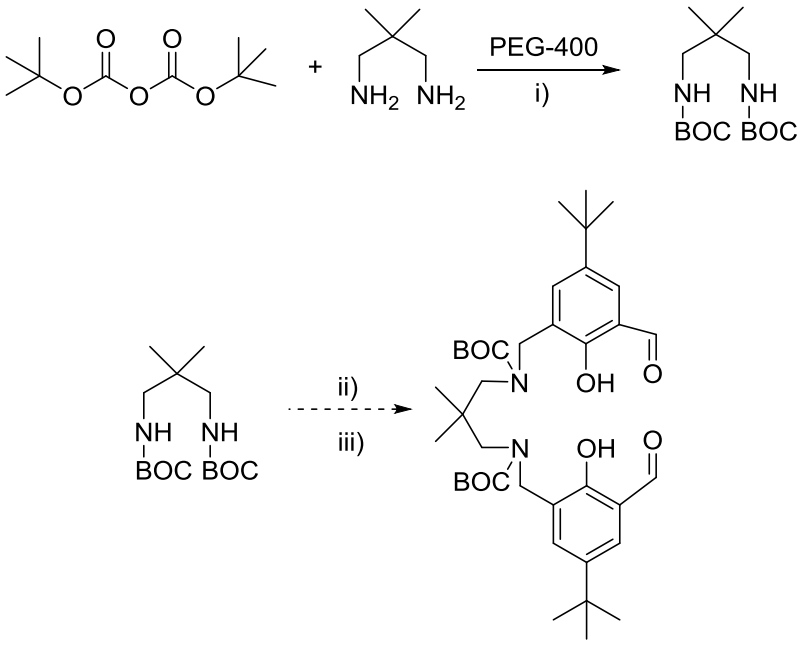

Scheme 3.2: Illustrates the unsuccessful attempt to react a BOC protected diamine with 3-bromo-5-*t*-butylsalicylaldehyde; Reaction conditions: i) 25 °C, 2h; ii) $N^{i}Pr_2Et$, MeOH, 25 °C, 0.5 h; iii) 3-bromomethyl-5-*t*-butylsalicylaldehyde, reflux, 16 h.

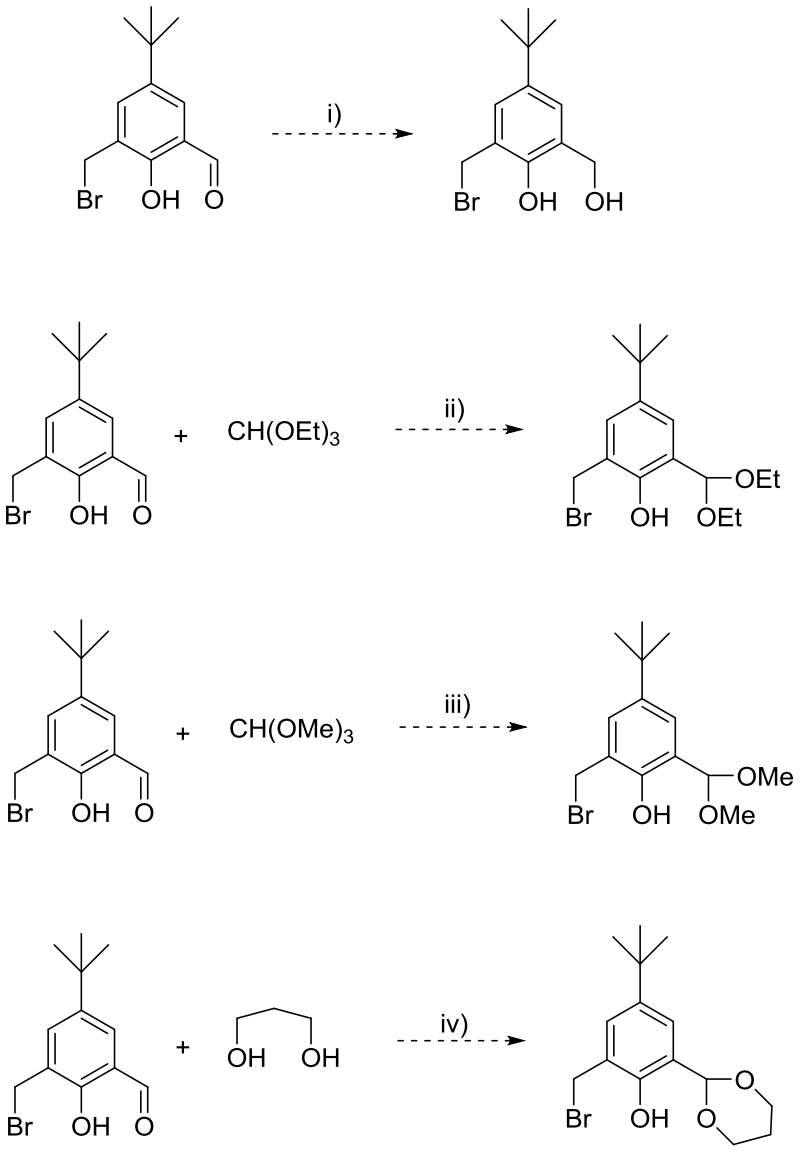

Scheme 3.3: Illustrates the attempts to protect the aldehyde moiety of 3-bromo-5-*t*-butylsalicylaldehyde; Reaction conditions: i) $NaBH_4$, MeOH, 25 °C, 16 h; ii) 5 mol % TsOH, MeOH, mol. sieves, 25 °C, 16 h; iii) 5 mol % TsOH, dry MeOH, N_2, 25 °C, 16 h; iv) 5 mol % TsOH, dry toluene, N_2, reflux, 16 h.

3.2.2 Synthesis of Monometallic Complex 3 & Heterodinuclear Complex 4

From the lack of success of making the half macrocyclic ligand and monometallic complexes based on the symmetrical macrocyclic ligand used by Williams and co-workers, a stepwise synthesis adopted by Bosnich and co-workers was modified and attempted.[2-5] Bosnich and others managed to synthesise heterodinuclear complexes *via* a similar stepwise route to Scheme 3.1 with a slightly modified macrocyclic ligand.[39-41] The possible reason for the

reaction success is that there are pyridyl arms instead of protons on the amine moieties of the macrocyclic ligand (Scheme 3.4). The pyridyl arms aid the formation of a hexadentate N_4O_2 compartment, which will prefer the coordination of metal ions that favour an octahedral environment (Co^{2+} and Mn^{2+}). The other compartment in the macrocycle is a tetradentate N_2O_2 compartment, which is favoured by certain metal ions (Zn^{2+}) and hence stabilises the resultant heterodinuclear complex.[39-41]

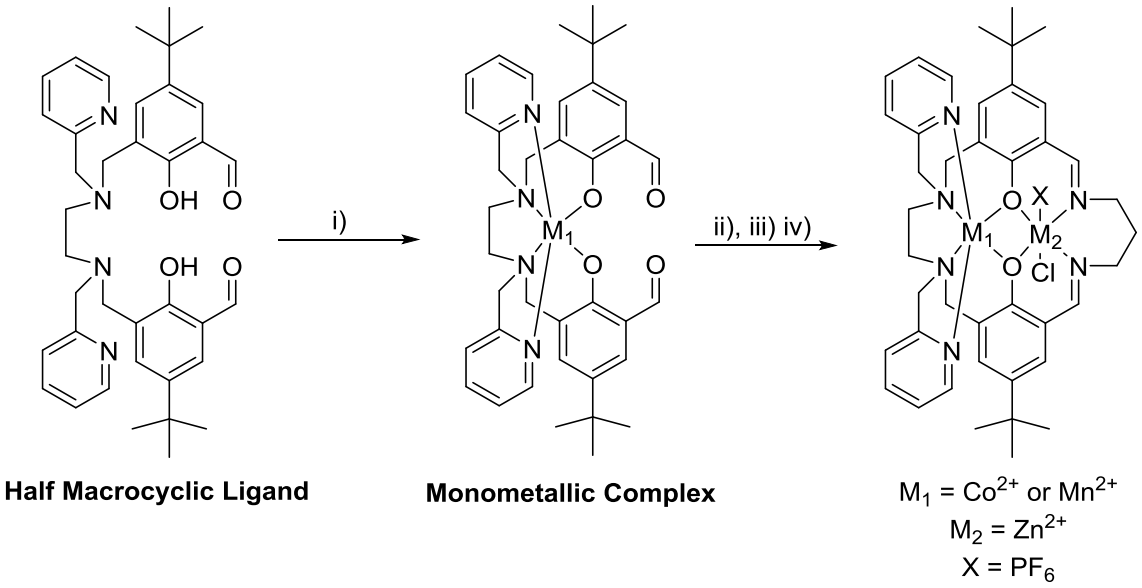

Scheme 3.4: Synthesis route for heterodinuclear complexes adopted by Bosnich and co-workers. Reaction conditions: i) Et_3N, EtOH/MeOH, $M_1(OAc)_2$, 25 °C; ii) AcOH, MeOH, 1,3-propanediamine, 25 °C; iii) Et_3N, MeOH, 25 °C, $M_2(OAc)_2$; iv) NH_4PF_6, LiCl, MeOH, 50-60 °C.[39-41]

Bosnich and co-workers found that cyclisation of the monometallic complex followed by a second complexation was more successful compared to the reverse order because the latter process undergoes a substantial amount of scrambling (Scheme 3.4).[39-41] The macrocyclic ligand used by Bosnich had different *para*-phenyl substituents and alkyl backbones of the amine and imine bridges compared to the macrocycle used previously by our group (Figure 3.1 & Scheme 3.1).[2-5] Additionally, the literature synthesis of the Zn-Co heterodinuclear complex, reported by Bosnich, involved a complicated 13 step procedure, 9 of these steps were carried out to produce the initial half macrocycle needed for the formation of the monometallic complex (Scheme 3.4).[40]

A modified version of Bosnich's procedure was carried out in order to produce the half macrocycle in fewer steps.[39-41] Moreover, the half macrocycle synthesised had ^{t}Bu groups in the *para* position of the phenol groups and 2,2-dimethyl-1,3-propanediamine was used for both the amine and imine bridges (Scheme 3.5). These modifications were carried out in order to keep a similar ligand motif to the macrocyclic ligand used previously by our group. The pyridyl arms were still present in the modified half macrocycle ligand (Scheme 3.5).

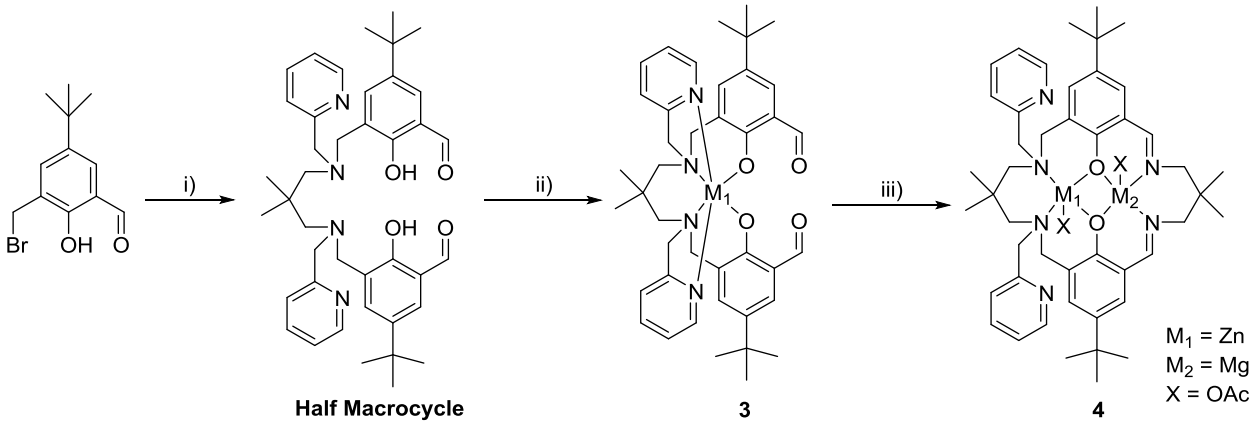

Scheme 3.5: Modified synthesis route for heterodinuclear complexes. Reaction conditions: i) 2,2-dimethyl-N_1,N_3-bis(pyridin-2-ylmethyl)-1,3-diaminopropane, Et_3N, THF, 25 °C, 16 h; ii) Et_3N, EtOH/MeOH, $Zn(OAc)_2$, 25 °C, 24 h; iii) MeOH, 2,2-dimethyl-1,3-propanediamine $Mg(OAc)_2$, 25 °C, 16 h.

The half macrocycle was synthesised by reacting 3-bromomethyl-5-*t*-butylsalicylaldehyde with 2,2-dimethyl-N_1,N_3-bis(pyridin-2-ylmethyl)-1,3-diaminopropane *via* an S_N2 reaction (Scheme 3.5). The half macrocycle was synthesised in a moderate yield (64 %) and in good purity, as the calculated and recorded elemental analysis values matched well. The ^{1}H NMR spectrum of the half macrocycle (Figure 3.6) shows that both starting materials were consumed. The product signals are distinctly shifted and all assignments are correct relative to the structure of the half macrocycle. Additionally, the ESI mass spectrum (Appendix B) shows a signal at 665 amu, which correlates to the mass of the half macrocycle plus a proton and thus confirms the presence of the product.

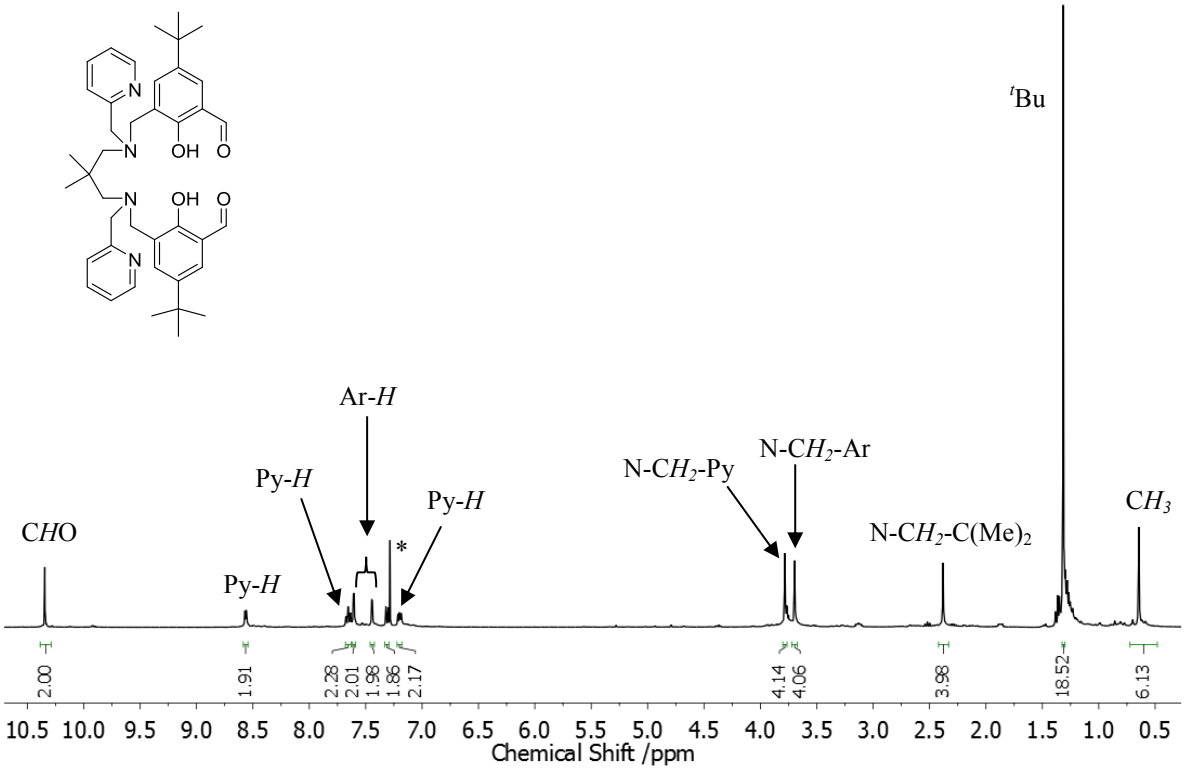

Figure 3.6: ^{1}H NMR spectrum of the half macrocycle in $CDCl_3$.

To this half macrocycle, one equivalent of $Zn(OAc)_2$ was added to form monometallic complex **3** in a good yield (68 %). The ^{1}H NMR spectrum (Figure 3.7) recorded for complex **3** shows two distinct differences compared to the ^{1}H NMR spectrum recorded for the half macrocycle pro-ligand (Figure 3.6). Firstly, the signals for the pyridyl protons are significantly shifted (8.89, 7.52, 7.10 and 6.79 ppm compared to 8.54, 7.63, 7.28 and 7.18 ppm). Additionally, the spectrum shows two signals for both the NC*H*$_2$Py and NC*H*$_2$Ar protons, which indicates that each set of C*H*$_2$ protons are chemically inequivalent. These differences indicate that the monometallic complex has been synthesised. The formation of complex **3** was also confirmed by mass spectrometry (Appendix B). A signal at 727 amu was observed, which represents the mass of the monometallic complex plus a proton.

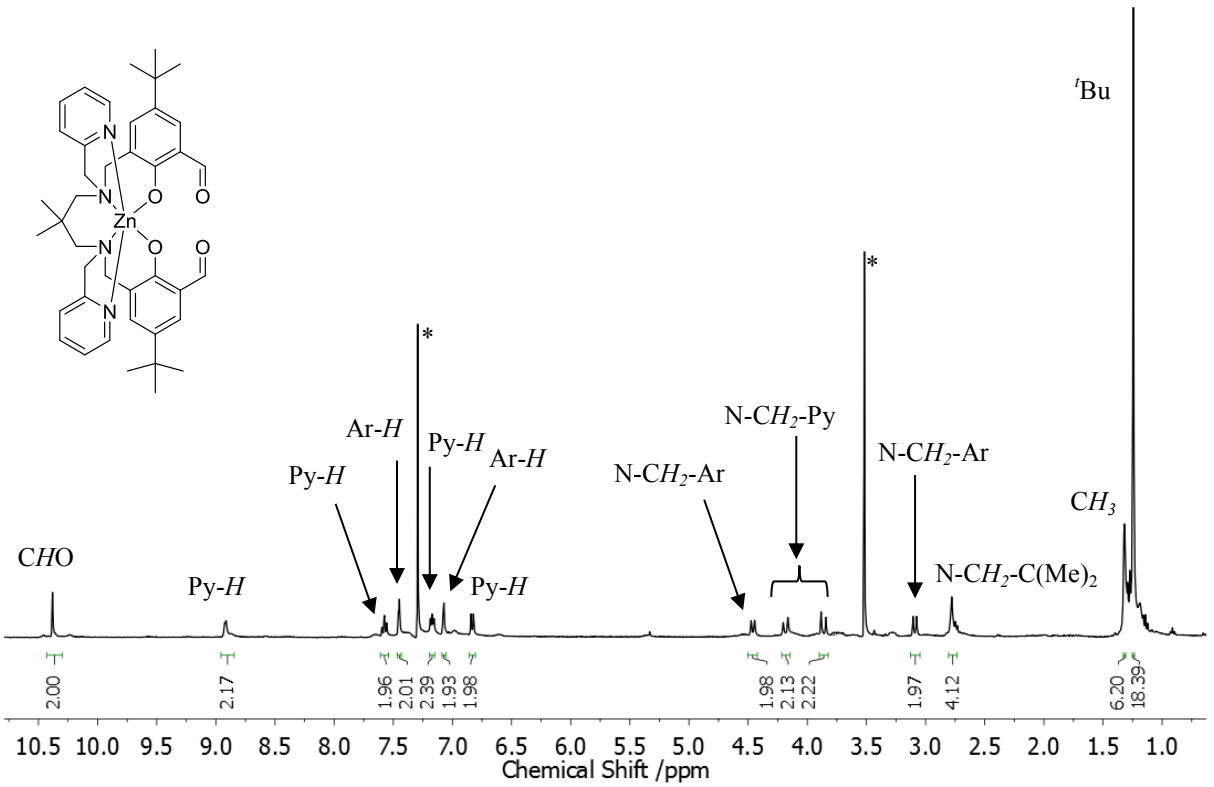

Figure 3.7: ^{1}H NMR spectrum of the complex **3** in $CDCl_3$.

Complex **3** was then simultaneously cyclised by the addition of 2,2-dimethyl-1,3-propanediamine and coordinated to $Mg(OAc)_2$ to yield heterodinuclear complex **4**. The heterodinuclear Zn-Mg complex was successfully synthesised in a moderate yield (54 %, 130 mg). The purity of the complex was verified by elemental analysis; the values obtained are in good agreement with the calculated values. MALDI-ToF mass spectrometry also confirmed the presence of the heterodinuclear complex because the molecular ion peak observed at 877 amu correlates to the heterodinuclear complex (**4**) without one acetate co-ligand (Appendix B). Moreover, the IR spectrum of complex **4** shows a signal at 1630 cm^{-1} (Appendix B), which is indicative of an imine bond and thus suggests that the desired macrocyclic ligand formed.

^{1}H NMR spectroscopy (Figure 3.8) proved to be useful as the spectrum shows a signal at 8.13 ppm, which correlates to an imine proton and therefore confirms that the cyclisation of the half macrocycle was successful. Cyclisation was also confirmed by the lack of a signal representing an aldehyde proton. The ^{1}H NMR spectrum also shows the correct number of signals and expected integrals for the macrocycle, which indicates that the heterodinuclear complex has successfully been synthesised. Furthermore, two signals were observed for both

the aromatic protons and methyl groups, which suggest there is asymmetry within the molecule, further confirming that the complex has been made.

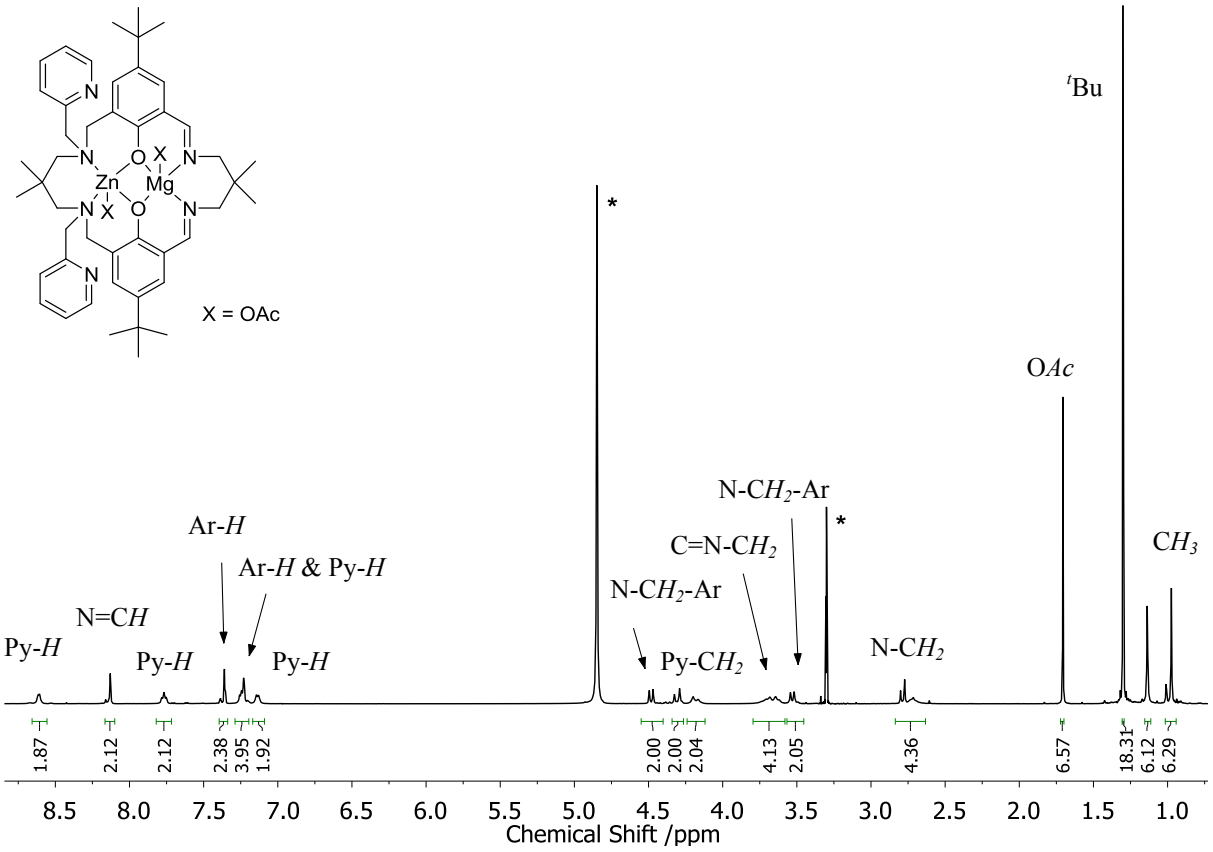

Figure 3.8: ^{1}H NMR spectrum of heterodinuclear complex **4** in CD_3OD.

The ^{1}H NMR spectra of complex **3** and **4** could not be compared because they were recorded in different deuterated solvents, and therefore it is not easily verified if the pyridyl arms are coordinated to the zinc centre or not in complex **4**. However, the pyridyl signals in Figure 3.8 are broad, which may suggest that fluxional coordination and exchange of these groups is occurring on the NMR timescale. Variable temperature (VT) may shed light on this and should be carried out in the near future.

A single signal for the OAc co-ligand groups at 1.72 ppm indicates that both OAc groups are in the same chemical environment. This is curious because two distinct OAc signals are expected if the heterodinuclear complex has the proposed structure in Figure 3.8. Therefore, another possible structure might be the one shown in Figure 3.9. In order to distinguish which structure is present, VT NMR needs to be carried out on complex **4**.

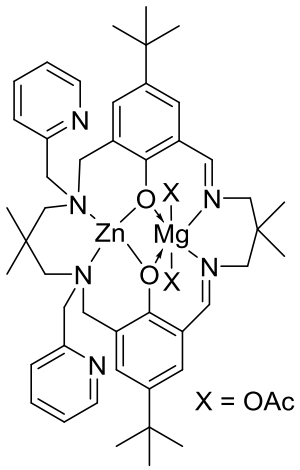

Figure 3.9: Other proposed structure for heterodinuclear complex **4**.

Even though the exact coordination of the pyridyl and co-ligand groups in heterodinuclear complex **4** are not yet fully known, the complex has still been synthesised successfully and therefore was used in CHO/CO_2 ring opening copolymerisation reactions at 80 °C, 1 bar CO_2 pressure for 24 h. The complex is not an active catalyst for this copolymerisation reaction. No polycarbonate and cyclic carbonate by-product was observed. Therefore, complex **4** was used in a copolymerisation reaction at 80 °C and 50 bar CO_2 pressure in order to see if high pressure promoted any activity, but again no copolymer or cyclic carbonate formed.

The potential reasons for the inactivity of complex **4** could be the presence of the pyridyl arms or imine moieties in the macrocyclic ligand. It was assumed that two different metals within the ligand cavity (Zn-Mg) did not cause this inactivity because both homodinuclear di-zinc and di-magnesium catalysts work for CHO/CO_2 copolymerisation reactions.

A control CHO/CO_2 copolymerisation reaction with the di-magnesium catalyst (**1a**) and 2 equivalents of pyridine at 80 °C, 1 bar CO_2 pressure for 6 h was carried out. The turnover frequency (TOF) value recorded is 42 h^{-1}, which is slightly lower than the TOF observed for **1a** with no equivalents of pyridine (52 h^{-1}). Therefore, this suggests that the presence of the pyridyl arms in complex **4** probably reduce of the activity of the catalyst, but do not completely stop activity.

Another control reaction was carried out with a tetra-imine derivative of the di-magnesium catalyst (**5** – Figure 3.10). This complex also shows no activity in CHO/CO_2 copolymerisation reactions at 1 bar CO_2 pressure and at 80 °C, which implies that the imine

moieties have caused the inactivity of heterodinuclear complex **4**. This is surprising because the imine moieties are thought to be more electron donating and therefore facilitate nucleophilic attack, which leads to the ring opening of the epoxide.

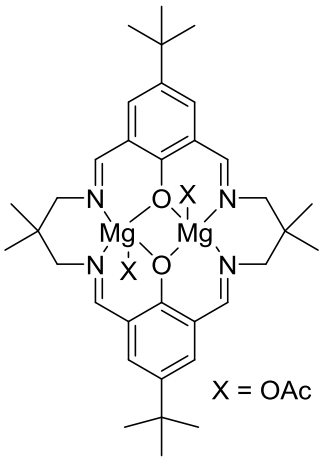

Figure 3.10: Illustrates complex **5** (tetra-imine complex).

Therefore, an attempt to reduce the imine moieties of complex **4** was carried out. However, as only 130 mg of complex **4** was produced, the reduction reaction was carried out on a Zn salen complex (**6** – Scheme 3.6). If successful, it would have been carried out on heterodinuclear complex **4**. The reduction of imine bonds of a ligand bound to a metal has to be carried out carefully in order to prevent the metal centre from being displaced.

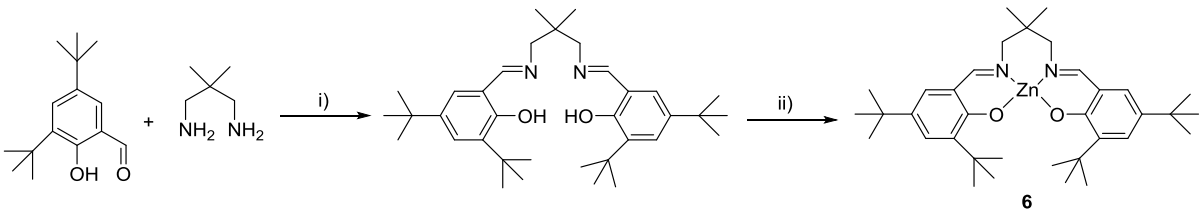

Scheme 3.6: Illustrates the synthesis of a zinc salen complex; Reaction conditions: i) MeOH, few drops of formic acid, reflux for 2 h; ii) Et_2Zn, hexane, 25 °C, 16 h.

Initially, $NaBH_4$ was used in excess to reduce the Zn salen complex, but the imine bonds did not reduce. Then 10 wt % of Pd/C with 1 bar and 4 bar H_2 pressure was used to reduce the Zn salen complex. However, both reduction reactions did not work because the starting zinc salen complex was recovered. Due to time constraints this reduction could not be further investigated, but should be probed in the future (Section 3.8).

3.3 *In Situ* Route to Heterodinuclear Mixed Catalyst System

Section 3.2 revealed that it is essential to maintain the same ancillary ligand when trying to synthesise a heterodinuclear catalyst for CHO/CO_2 copolymerisation reactions. Modification of the N_4O_2 ligand can significantly influence the catalytic activity and selectivity, which has also been observed by Williams and co-workers.[3,42] Many unsuccessful attempts to synthesise a heterodinuclear Zn-Mg analogue of catalysts **1a** and **2** were carried out, which entailed synthesising the catalyst in a step-wise manner (Section 3.2.1). The main problems with these reactions were: 1) the facile formation of homodinuclear complexes and 2) the ability to form polymer over the desired macrocycle (Section 3.2.1).

Due to these difficulties, a strategy was developed, which attempted to use the conventional macrocyclic ligand (H_2L – Scheme 3.7) and coordinate a single metal ion within one cavity of the ligand (Scheme 3.7). The monometallic complex would then undergo a second addition of another metal ion to form the desired heterodinuclear complex. Initially, the addition of one equivalent of zinc or magnesium acetate to H_2L to yield the desired monometallic complex was carried out, but resulted in the formation of the homodinuclear complexes and excess ligand.

However, by reacting H_2L with one equivalent of diethyl zinc at -40 °C and allowing the solution to warm to 25 °C and then followed by the addition of one equivalent of magnesium acetate, resulted in the formation of a white powder. The powder was isolated in 85% yield, which assumes a 1:2:1 mixture of $LMg_2(OAc)_2$, $LZnMg(OAc)_2$, $LZn_2(OAc)_2$ (Scheme 3.7).

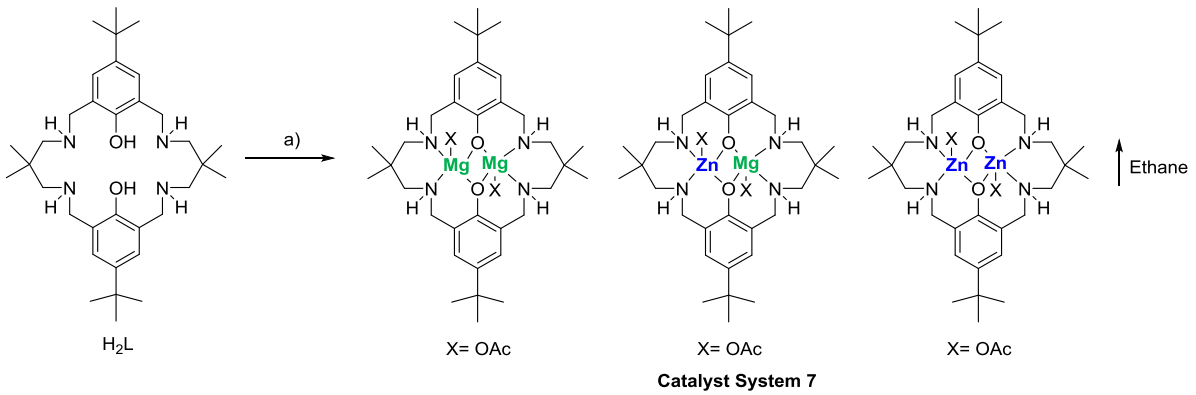

Scheme 3.7: Illustrates the synthesis of mixed catalyst system **7**; a) Reagents and Conditions: i) 1 eq. Et_2Zn, THF - 40 °C to 25 °C, 4 h; ii) 1 eq. $Mg(OAc)_2$, THF 25 °C, 16 h.

The characterisation data recorded for this white powder is different compared to the data recorded for either $LMg_2(OAc)_2$ (**1a**) or $LZn_2(OAc)_2$ (**2**). The ^{1}H NMR spectrum of the white powder shows the full consumption of the zinc bound ethyl group and the ligand signals broadened, which is indicative of metal coordination.[3,5,43] These broad signals did not coalesce when the solvent was changed (e.g. benzene, THF, tetrachloroethane) or by increasing or decreasing the temperature (-50 to 80 °C). This is opposite to the behaviour of the homodinuclear complexes, which showed resolved signals in the ^{1}H NMR spectrum at elevated temperatures.[3,5,43]

Elemental analysis recorded indicates that the white powder contained the expected quantities of Zn and Mg. Mass spectrometry was the most informative analysis technique (Figure 3.11). The MALDI-ToF mass spectrum shows a peak at 697 amu, which corresponds to the heterodinuclear Zn-Mg complex cation $[LZnMg(O_2CCH_3)]^+$. The MALDI-ToF mass spectrum of the white powder also revealed that both homodinuclear complexes **1a** and **2** were present within the product sample (657 and 739 amu, due to $[LMg_2(O_2CCH_3)]^+$ and $[LZn_2(O_2CCH_3)]^+$, respectively).

To ensure that the signal representing the heterodinuclear complex did not arise from scrambling within the MALDI-ToF mass spectrometry analysis technique, a control mass spectrum was recorded. An equimolar mixture of $[LMg_2(OAc)_2]$ and $[LZn_2(OAc)_2]$ was analysed (Figure 3.12). The equimolar mixture of complexes only shows signals for the two homodinuclear complexes (**1a** and **2**). There was no evidence for any heterodinuclear complex cations. Moreover, the equimolar mixture of the two homodinuclear complexes was heated at 80 °C for 16 h (copolymerisation conditions) and the MALDI-ToF mass spectrum also only shows the two homodinuclear complexes (Appendix B). Therefore, these mass spectra suggest that catalyst system **7** contains a novel Zn-Mg heterodinuclear complex, which is part of a mixture that also contains two homodinuclear complexes (**1a** and **2**).

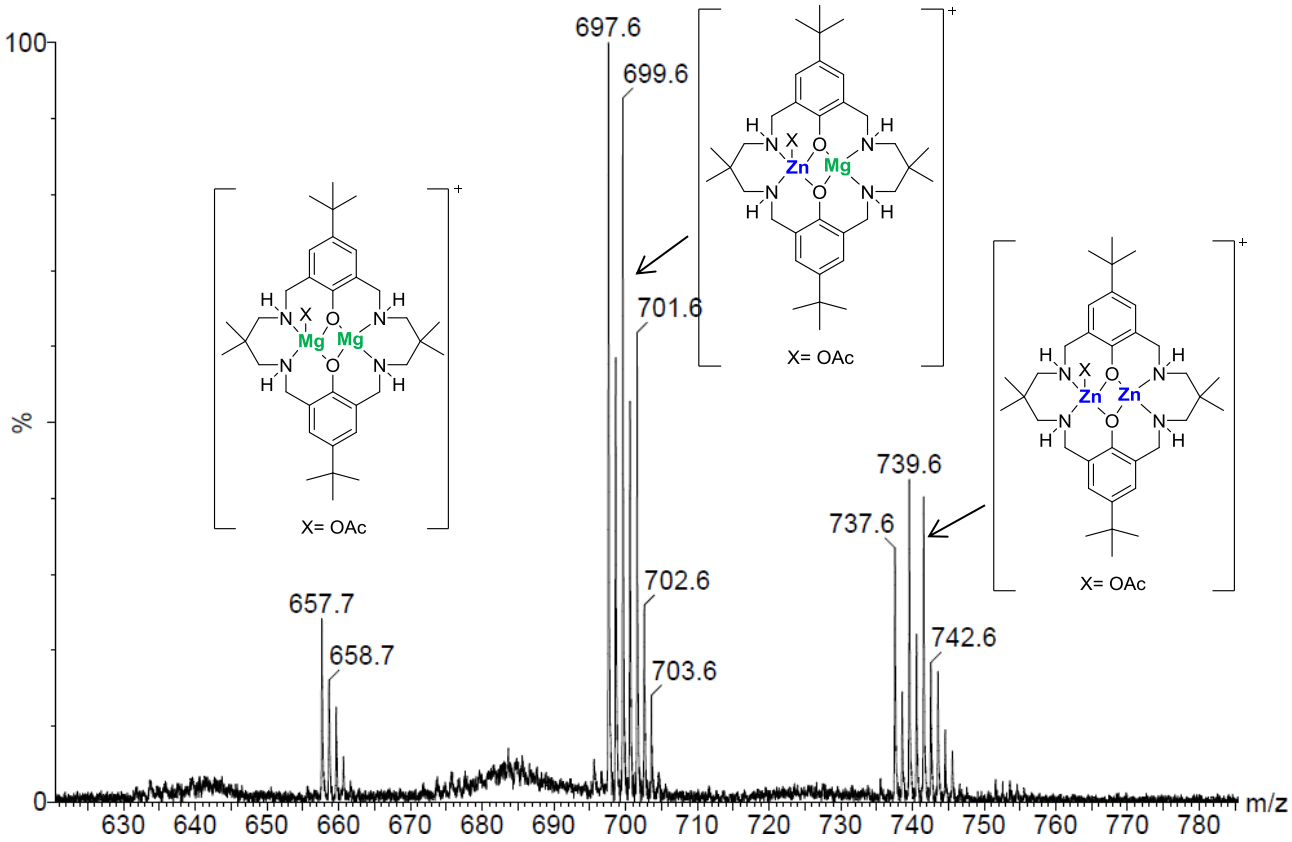

Figure 3.11: Part of the MALDI-ToF mass spectrum for catalyst system **7**, with the structures for the molecular ions illustrated. The full spectrum is available in Appendix B.

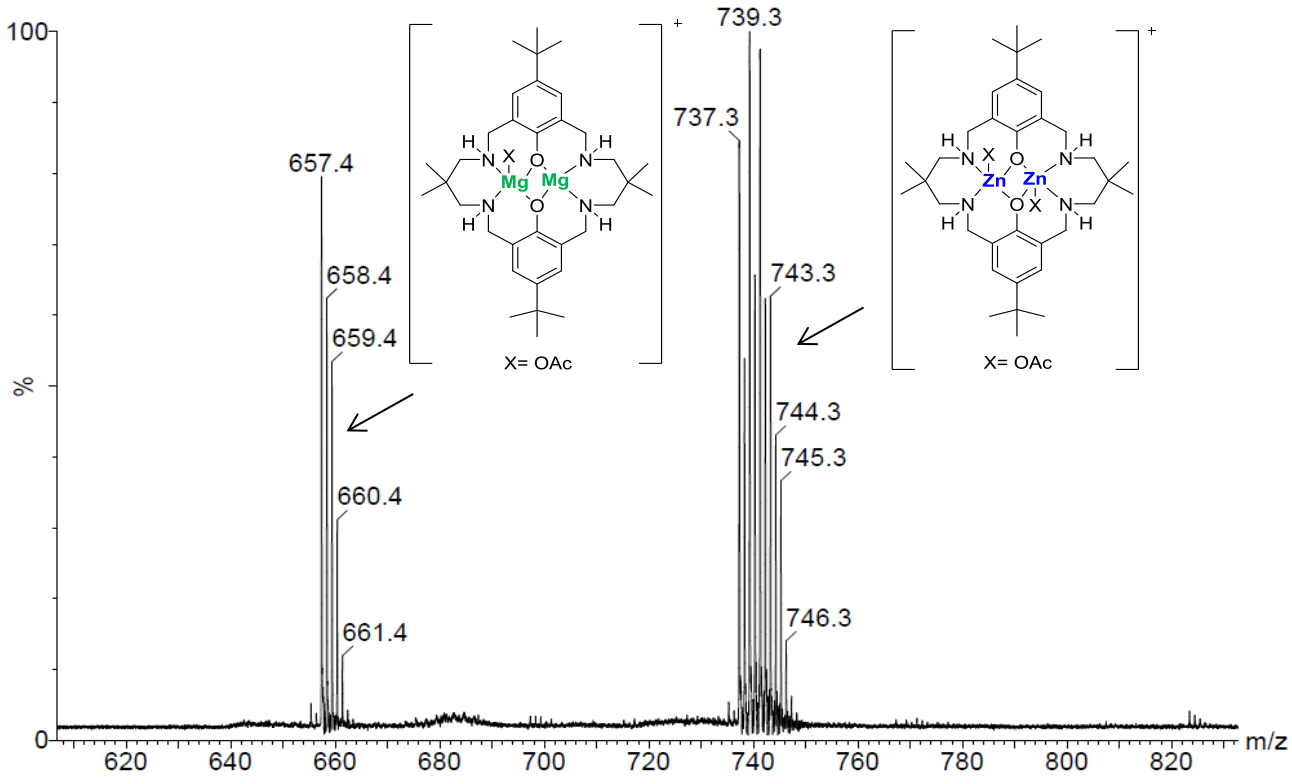

Figure 3.12: MALDI-ToF spectrum of 50:50 mixture, $LMg_2(OAc)_2$) (**1a**):($LZn_2(OAc)_2$) (**2**).

It has not yet been possible to accurately determine the exact composition of the mixture due to the nature of the NMR signals (v. broad). However, a likely stoichiometry would be 1:2:1 ($LZn_2(OAc)_2$:$LZnMg(OAc)_2$:$LMg_2(OAc)_2$) in order to be in line with the elemental analysis results recorded. Several attempts to separate this mixture by selective crystallisation were carried out, but were unsuccessful. This type of separation is very challenging due to the individual complexes having very similar structures. Therefore the mixed catalyst system (**7**) was used for epoxide/CO_2 copolymerisation reactions.

The same synthesis was repeated with $Co(OAc)_2$ instead of $Mg(OAc)_2$, in order to form a Zn-Co heterodinuclear complex and as expected a mixed catalyst system **8** was formed. MALDI-ToF mass spectrometry conveys that the product contains a Zn-Co heterodinuclear complex, with homodinuclear Zn and Co catalysts (Appendix B).

3.4 CHO/CO_2 Ring Opening Copolymerisation Results Using 7

3.4.1 Comparative Studies

The activity of catalyst system **7** in the copolymerisation of CHO and CO_2 was monitored using 0.1 mol % of catalyst in relation to epoxide (assuming a 1:2:1 composition) at 1 bar CO_2 pressure, 80 °C for 6 h. These conditions have been previously reported to be very effective for catalysts **1a** and **2**.[3,5]

The results revealed that catalyst system **7** is more active than either **1a** or **2**, more specifically nearly twice the activity of **1a** and four times more active than **2** (Table 3.1) which is one of the most active derivatives of the bimetallic catalysts synthesised by Williams and co-workers.[5]

Furthermore, catalyst system **7** has an increased activity (double) compared to an equimolar mixture of catalysts **1a** and **2** (Table 3.1). The productivity (TON) and activity (TOF) value for the equimolar mixture of catalysts **1a** and **2** closely matches the expected value based on the composition mixture ($TON_{mixture} = (TON_{\mathbf{1a}} + TON_{\mathbf{2}})/2$). This supports the idea that no metal exchange occurs between catalysts **1a** and **2** to form a heterodinuclear species, which was also outlined by MALDI-ToF mass spectrometry (Figure 3.11 and 3.12). The increased activity for catalyst system **7** further confirms the presence of the heterodinuclear complex in

the catalyst system. Moreover, the increased activity for catalyst system **7** is assumed to be due to the extra heterodinuclear species present in the catalyst system, which indirectly supports the hypothesis that the polymer chain 'shuttles' between the two metals in the catalyst structure (Chapter 1 and 2).

Table 3.1: Illustrating the catalytic activity, productivity, selectivity and M_n data for copolymerisation reactions using catalysts **1a**, **2** and **7**.

Catalyst	TON[a)]	TOF[b)] /h^{-1}	% Polymer[c)]	% Ether[c)]	M_n[d)] /gmol^{-1}	PDI[d)]
1a	309 ± 34	52 ± 5	> 99	< 1	5600	1.04
2	99 ± 11	17 ± 2	> 99	< 1	1300	1.23
7	476 ± 31	79 ±5	> 99	< 1	5200	1.12
50:50 of 1a:2	239 ±36	40 ± 6	> 99	< 1	2900	1.18

All copolymerisations were conducted in a Schlenk tube at 0.1 mol % catalyst loading (vs. CHO), 80 °C, 1 bar CO_2 for 6 h. a) The turn over number (TON) = number of moles of cyclohexene oxide consumed/number of moles of catalyst. b) The turn over frequency (TOF) = TON/6. c) This is determined by comparing the relative integrals of the ^{1}H NMR resonances due to carbonate (δ: 4.65 ppm) and ether (δ: 3.45 ppm) linkages in the polymer backbone. d) Determined by SEC, in THF, using narrow M_n polystyrene standards as the calibrant.

The Zn-Co catalyst system **8** was also used in a CHO/CO_2 copolymerisation reaction for 6 h at 80 °C and 1 bar CO_2 pressure. The activity of this catalyst system was recorded to be 34 h^{-1}, which is lower than catalyst system **7** (TOF = 79 h^{-1}). Moreover, catalyst system **8** only shows an increased activity compared to the di-zinc catalyst (TOF = 18 h^{-1}). The activity of the di-cobalt catalyst was recorded, previously by our group, to be 172 h^{-1} and thus mixed catalyst system **8** does not show an improved activity compared the di-cobalt catalyst.[4,44]

This is opposite to what was observed for catalyst system **7**, which highlighted positive cooperativity occurring during copolymerisation reactions. It was initially thought that this lower than expected activity for **8** may be due to the oxygen content in the CHO used in the copolymerisation reaction. The CHO is always degassed three times *via* freeze pump thaw cycles. However, Co^{2+} is very sensitive to oxidation and it has been reported that changing one of the cobalt metal centres from 2+ to 3+, in the homodinuclear di-cobalt complex, reduces the TOF from 172 to 156 h^{-1}.[4,44] Therefore, the copolymerisation was repeated with

extra degassed CHO (ten freeze pump thaw cycles). The TOF improved slightly (45 h^{-1}), but still was not as high as the di-cobalt catalyst. It seems that catalyst system **8** is not as thermally robust compared to catalyst system **7** and this may give rise to the reduced activity.

3.4.2 Polymer Characteristics

All catalysts, more specifically catalyst system **7**, have shown good selectivity towards polycyclohexene carbonate (PCHC) production (> 99 %). Very low quantities of ether linkages or cyclic carbonate were observed (< 1 %), which arise due to sequential epoxide enchainment or backbiting reactions within the growing copolymer chain, respectively (Table 3.1). This was determined by ^{1}H NMR spectroscopy of the crude copolymer sample. The relative integrals of the distinctive cyclohexene methine protons in polycarbonate (δ = 4.65 ppm), ether (3.45 ppm) and *trans*-cyclic carbonate (4.0 ppm) were calculated (Figure 3.13). *Trans*-cyclic carbonate almost only forms in these copolymerisation reactions due to the inversion of stereochemistry occurring when the ring opening of the epoxide occurs in the copolymerisation process. This also suggests that the backbiting reaction occurs from the alkoxide propagating copolymer species instead of the carbonate propagating copolymer (Figure 3.14).[2]

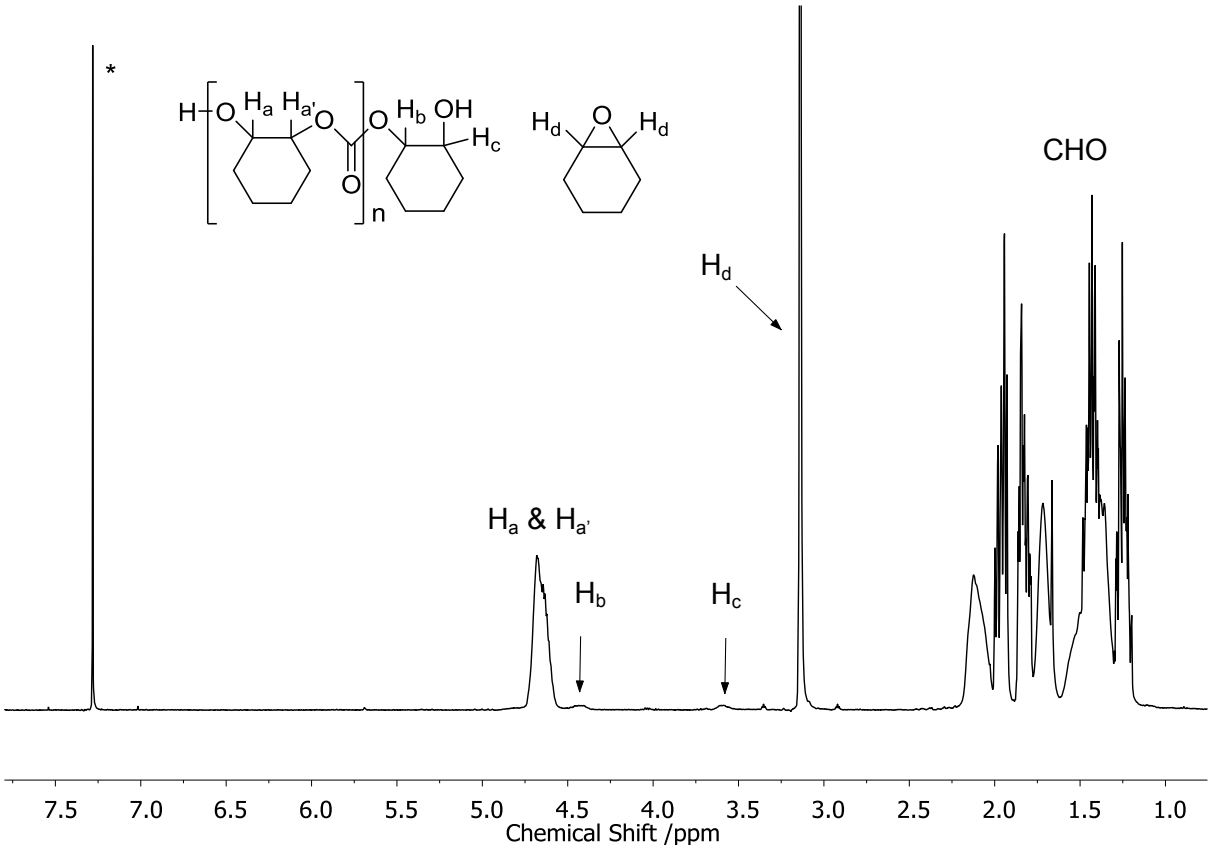

Figure 3.13: ^{1}H NMR spectrum of crude CHO/CO_2 copolymerisation reaction mixture used to calculate the catalyst's TON and TOF. Also, the spectrum confirms the absence of signals due to cyclic carbonate (4.0 ppm) or ether linkages (3.45 ppm) as by-products.

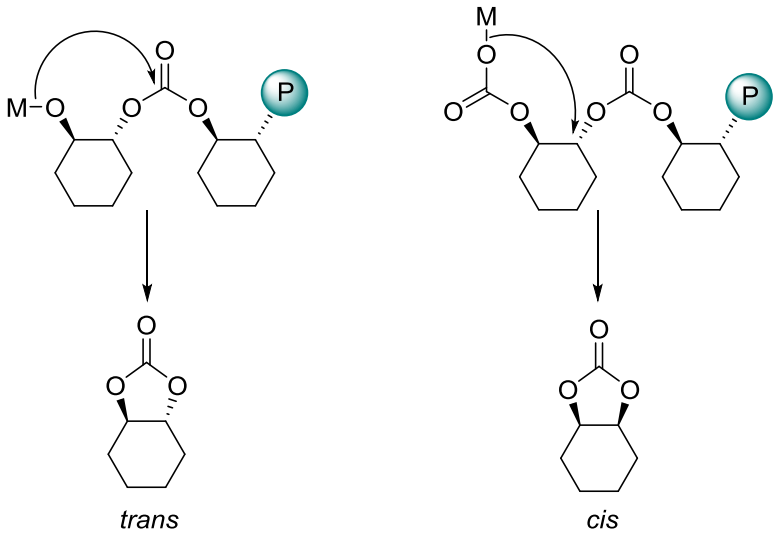

Figure 3.14: *Trans*- and *cis*-cyclic carbonate by-product formation from metal bound copolymer chains.

All the polycarbonate samples produced have low M_n (M_n < 6000 g/mol). This is due to efficient chain transfer reactions occurring during the copolymerisation reactions with protic impurities (alcohols).[37,45,46] The chain transfer agent present in these copolymerisation reactions is cyclohexane-1,2-diol (CHD), which is believed to form from water reacting with CHO. Trace amounts of water seem to present in these copolymerisation reactions even though the CHO monomer is dried and distilled before use. The contamination of water is thought to come from the CO_2 used. These chain transfer reactions and hence low M_n polycarbonate samples have been previously observed in field, with other catalysts, such as, chromium salen and zinc β-diiminate complexes.[1,47] Low M_n polycarbonate chains are highly desirable by industry because these polymers can be used for higher polymer synthesis, such as, polyurethanes.[45,48]

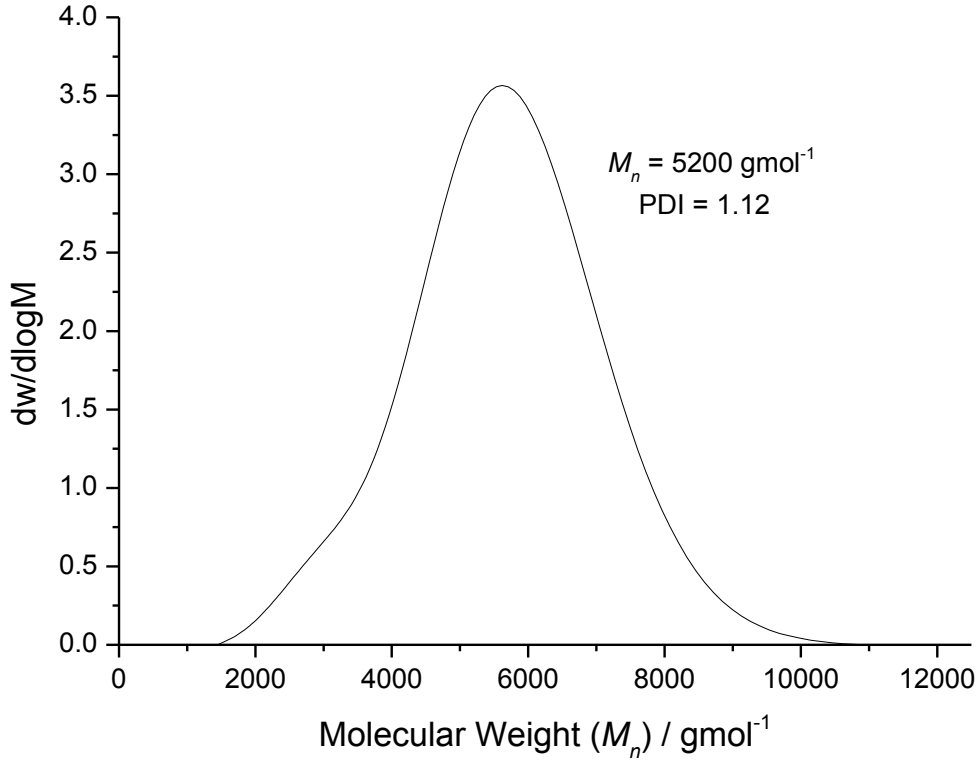

Figure 3.15: SEC trace of polycarbonate formed using catalyst system **7**.

Moreover, the PCHC samples produced by catalyst system **7** have monomodal molecular weight distributions with narrow polydisperity indices (PDIs), which indicate a high degree of polymerisation control (Figure 3.15). Initially, this was surprising because there are three different catalysts species present in catalyst system **7**. However, the rapid rate of chain transfer *vs.* propagation and rapid interconversion between all propagating chains with all the catalysts species, gives rise to the narrow M_n distributions.[49] This observation conveys the

vast potential of mixed catalyst systems for epoxide/CO_2 copolymerisation. Lee and others have reported mixed homogeneous and heterogeneous catalyst systems that produce polymer samples with specific properties.[20] Catalyst system **7** has highlighted the ability to improve catalytic activity *via* mixed catalyst systems. Using catalyst system **7** allows the formation of PCHC with decent M_n and PDI values.

Furthermore, the MALDI-ToF mass spectrum (Figure 3.16) shows that the polycarbonate samples produced contain two series of chains; both with > 99 % carbonate linkages, but differ by the chain end groups. One series is α-acetyl-ω-hydroxyl, which implies that this chain was initiated by the acetate co-ligand present in the catalyst structures. However, the other chain is α,ω-di-hydroxyl end-capped, which arises from chain transfer reactions with CHD. Even though the rate of propagation is assumed to be the same for both acetate and CHD initiated polymer chains, the polymer chains initiated by CHD can grow from both OH groups and hence produce telechelic PCHC chains, which have approximately double the M_n of the acetate end-capped PCHC chains (Figure 3.17).

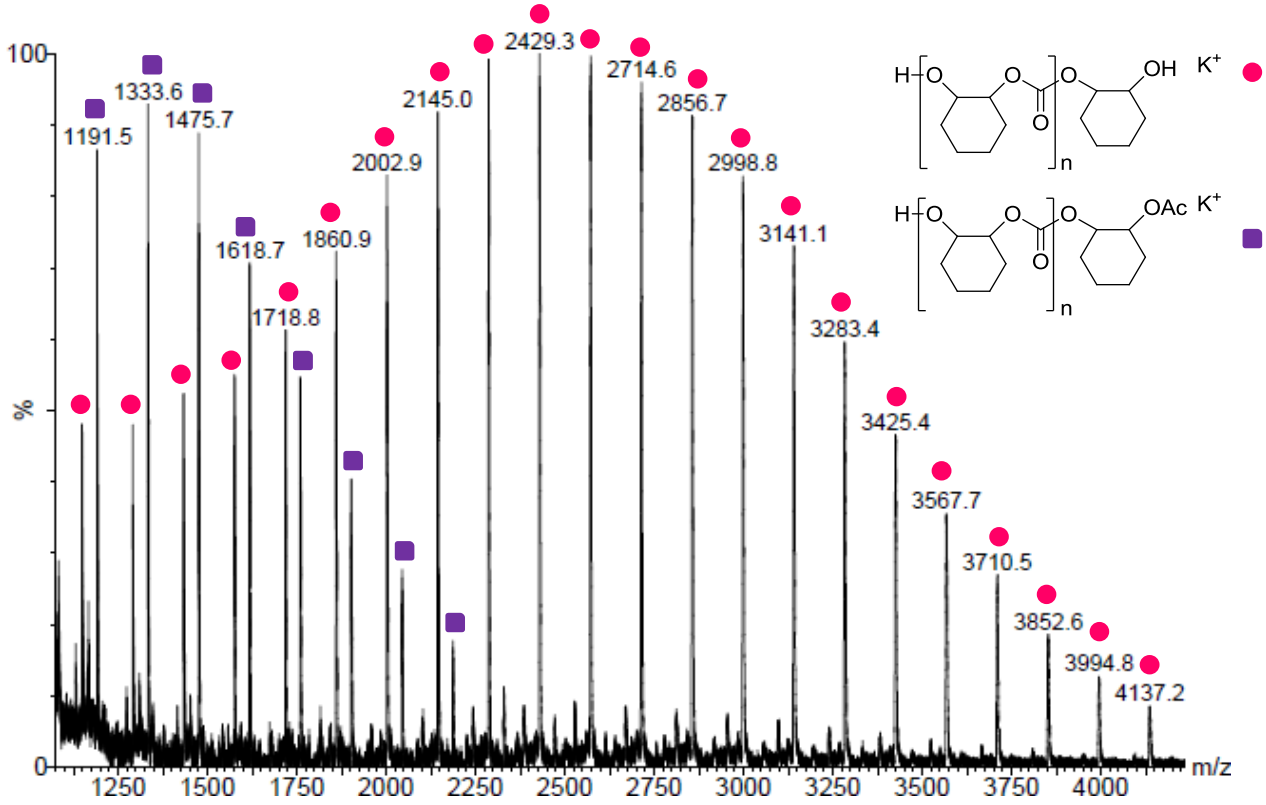

Figure 3.16: MALDI-ToF mass spectrum of the poly(cyclohexene carbonate) produced by using catalyst system **7**.

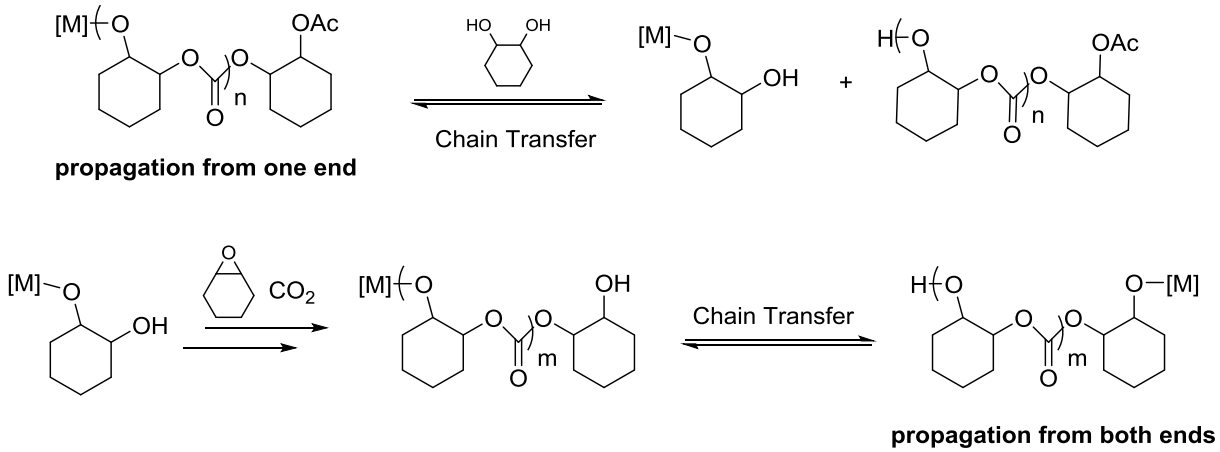

Figure 3.17: Illustrates chain transfer reactions in CHO/CO_2 copolymerisation reactions with cyclohexane-1,2-diol (CHD).

3.4.3 Optimisation Study

Many optimisation CHO/CO_2 copolymerisation reactions were carried out with catalyst system **7** in order to understand and establish the activity of this catalyst system relative to other known catalysts in literature. A wide range of conditions were investigated and under all conditions, **7** shows very high activity. When the temperature of the copolymerisation reactions was increased, as expected, the activity of **7** significantly improves. The optimum temperature for catalyst system **7** is 90 °C, as the TOF increases from 71 (at 80 °C) to 105 h^{-1}, whilst maintaining > 99 % selectivity towards copolymer formation. However, at 100 °C the TOF further improves to 134 h^{-1}, but 4 % cyclic carbonate by-product formation occurs, which is not desirable (Table 3.2).

Table 3.2: CHO/CO_2 copolymerisation reactions with **7** at different temperatures.

Temperature /°C	TON[a)]	TOF[b)] /h^{-1}	% Carbonate[c)]	% Ether[c)]	M_n[d)] /$gmol^{-1}$	PDI[d)]
80	286	71	>99	<1	4000	1.16
90	419	105	>99	<1	5500	1.18
100	535	134	96	4	6300	1.17

All copolymerisations were conducted in a Schlenk tube at 0.1 mol % catalyst loading (vs. CHO), 1 bar CO_2 for 4 h. a) The turn over number (TON) = number of moles of cyclohexene oxide consumed/number of moles of catalyst. b) The turn over frequency (TOF) = TON/4. c) This is determined by comparing the relative integrals of the ^1H NMR resonances due to carbonate (δ: 4.65 ppm) and ether (δ: 3.45 ppm) linkages in the polymer backbone. d) Determined by SEC, in THF, using narrow M_n polystyrene standards as the calibrant.

Catalyst system **7** shows no difference in activity when changing the CO_2 pressure at a fixed catalyst concentration (Table 3.3), which is consistent with the findings in Chapter 2, that the rate of copolymerisation is independent of CO_2 pressure for catalysts **1a** and **2**.[37] Therefore, this also suggests that catalyst system **7** may undergo the same mechanism hypothesised for catalysts **1a** and **2**.

Table 3.3: CHO/CO_2 copolymerisation reactions with **7** at CO_2 pressures.

Catalyst Loading	TON[a)]	TOF[b)] /h^{-1}	% Carbonate[c)]	% Ether[c)]	Mn[d)] /$gmol^{-1}$	PDI[d)]
1:10000	196	33	>99	<1	800	1.18
1:10000*	196	33	>99	<1	710	1.19

All copolymerisations were conducted in a Schlenk tube at 1 bar CO_2 for 4 h at 80 °C. a) The turn over number (TON) = number of moles of cyclohexene oxide consumed/number of moles of catalyst. b) The turn over frequency (TOF) = TON/4. c) This is determined by comparing the relative integrals of the ^{1}H NMR resonances due to carbonate (δ: 4.65 ppm) and ether (δ: 3.45 ppm) linkages in the polymer backbone. d) Determined by SEC, in THF, using narrow M_n polystyrene standards as the calibrant. Copolymerisation carried out in a 100 mL Parr vessel at 50 bar CO_2 for 6 h at 80 °C.*

From these investigations, catalyst system **7** was used in CHO/CO_2 copolymerisation reactions under all optimised conditions and a TOF of 292 h^{-1} was obtained. Comparing this system with some of the best catalysts for CHO/CO_2 copolymerisation reactions in the literature, under their optimised reaction conditions, this new catalyst system shows good activity, selectivity and productivity. Catalyst system **7** shows similar productivity and activity to one of the most active cobalt salen catalysts in literature.[50] Moreover, catalyst system **7** is 2.5 times faster than the di-magnesium catalyst coordinated by a Trost's phenolate ligand, whilst operating at 5 times lower catalyst loadings (Figure 3.18 and Table 3.4).[51]

Table 3.4: Optimised CHO/CO_2 copolymerisation reactions with **7** and comparison with literature catalysts.

7:CHO (Molar Ratio)	Time /h, Temp. /°C, Pressure /bar	TON[a)]	TOF[b)] /h^{-1}	% Carbonate[c)]	M_n[d)] /$gmol^{-1}$	PDI[d)]
1:10,000	6, 90, 50	1379	230	>99	2900	1.09
1:1000	3, 90, 50	875	292	>99	15400	1.03
(di-Mg) 1:200[51]	6, 60, 1	194	32	>99	42800	1.56
(Co salen) 1:5000[50]	5, 50, 1	1315	263	>99	48000	1.16

All copolymerisations carried out at in a 100 mL Parr vessel. a) The turn over number (TON) = number of moles of cyclohexene oxide consumed/number of moles of catalyst. b) The turn over frequency (TOF) = TON/reaction period. c) This is determined by comparing the relative integrals of the ^1H NMR resonances due to carbonate (δ: 4.65 ppm) and ether (δ: 3.45 ppm) linkages in the polymer backbone. d) Determined by SEC, in THF, using narrow M_n polystyrene standards.

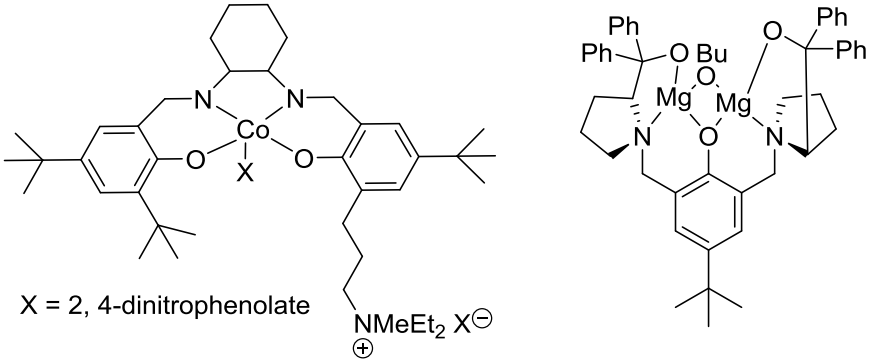

Figure 3.18: Cobalt salen and di-magnesium Trost phenolate catalysts.[50,51]

3.4.4 Polyol Selectivity

The ability for catalyst system **7** to produce low M_n PCHC chains led to investigations which focused on selectively producing PCHC chains that are α,ω-di-hydroxyl end-capped. This is because low M_n, di-hydroxyl terminated polycarbonates (polycarbonate polyols) have the potential to replace polyether polyols that are normally used in polyurethane synthesis.[45,48] In order to try and force catalyst system **7** to selectively produce PCHC polyols, 16 equivalents of H_2O (*vs*. catalyst) were added to the copolymerisation reaction (Table 3.5).

The activity of catalyst system **7** did not diminish significantly (Table 3.5) with the addition of H_2O. This high tolerance to water is highly desirable because it removes the need for drying the epoxides and CO_2. However, by adding protic reagents, such as water, to the copolymerisation reaction, the number of chain transfer reactions increases due to the formation of cyclohexane-1,2-diol, which aids the production of telechelic dihydroxyl terminated polymers.[37] When 16 equivalents of water were added to the copolymerisations catalysed by **7**, the M_n of the polycarbonate reduced from 4000 to 1300 g/mol and the PDI remained narrow (1.16 to 1.14).

Table 3.5: CHO/CO_2 copolymerisation data for catalyst system **7** with 16 eq. of H_2O.

Catalyst 7	TON[a)]	TOF[b)] /h^{-1}	% Carbonate[c)]	% Ether[c)]	M_n[d)] /$gmol^{-1}$	PDI[d)]
Without H_2O	286	71	>99	<1	4000	1.16
With 16 eq. H_2O	248	62	>99	<1	1300	1.14

All copolymerisations carried out at in a Schlenk tube for 4h at 80 °C and 1 bar CO_2, at a 1:1000 catalyst:CHO loading. a) The turn over number (TON) = number of moles of cyclohexene oxide consumed/number of moles of catalyst. b) The turn over frequency (TOF) = TON/reaction period. c) Determined by the relative integrals of the signals at 3.45 ppm (ether linkages) and 4.65 ppm (polycarbonate). d) Determined by SEC in THF, using narrow M_n polystyrene standards.

Furthermore, this reaction with catalyst system **7** has shown potential to selectively producing α,ω-di-hydroxyl end-capped PCHC chains. From ^{1}H NMR spectroscopy it was observed that the relative proportion of α,ω-di-hydroxyl end-capped PCHC chains in the copolymer sample, produced by catalyst **7**, increased from 34 % to 55 % (Appendix B). This was determined by integrating the cyclohexene methine proton signal for acetate end groups (4.43 ppm) and the methine proton signal for OH end groups (3.59 ppm). This polyol selectivity was also observed by MALDI-ToF mass spectrometry (Figure 3.19), as the acetate end-capped polycarbonate series seemed to be significantly suppressed.

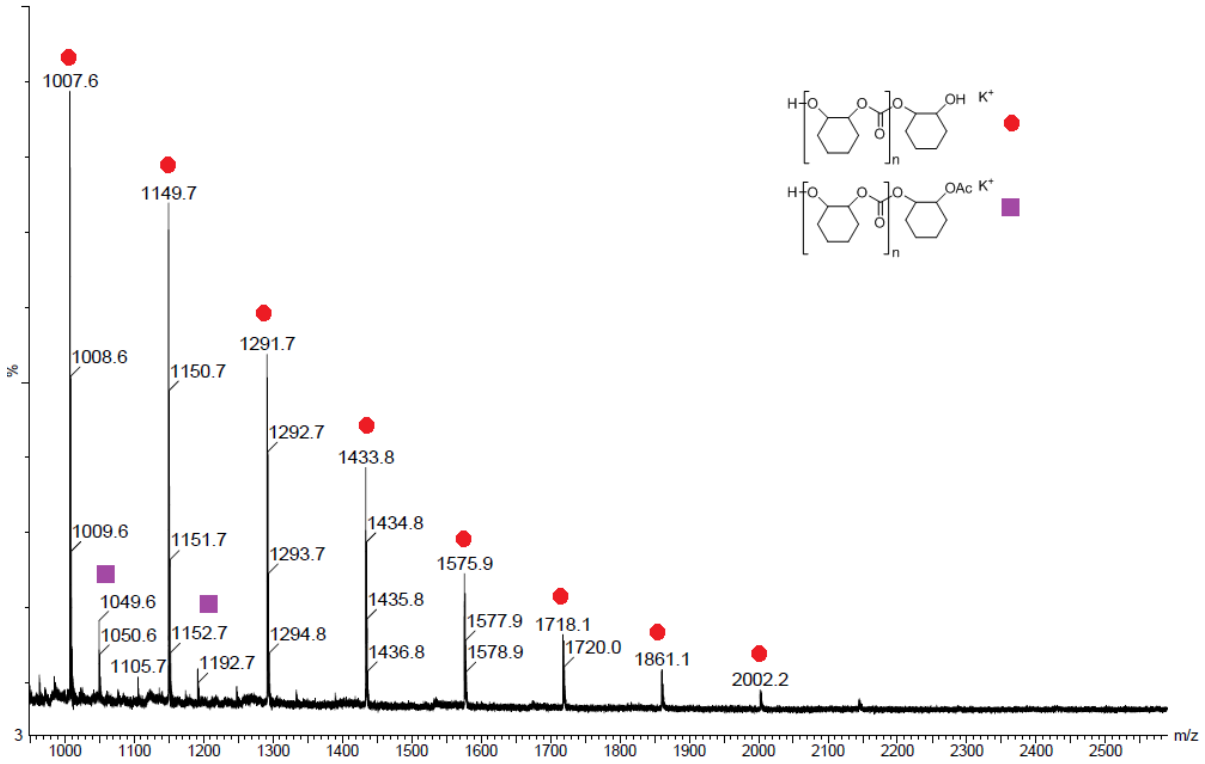

Figure 3.19: MALDI-ToF spectrum of the poly(cyclohexene carbonate) produced by using catalyst system **7**, with 16 equivalents of water (Table 3.5, Entry 2).

3.5 PO/CO_2 Ring Opening Copolymerisation Results Using 7

Catalyst system **7** was also tested for the copolymerisation of PO/CO_2 at 60 °C, 50 bar CO_2 pressure. Catalyst **7** shows moderate activity (TON = 248 and TOF = 11 h^{-1}), but low selectivity for PPC (9 %), the major product was a five-membered ring, cyclic propylene carbonate (PC), which is the thermodynamic product and arises due to backbiting reactions within the growing copolymer chain (Table 3.6). At 70 °C, the TOF rose to 19 h^{-1} and no selectivity towards PPC was observed; only cyclic carbonate by-product was formed. This was determined by ^{1}H NMR spectroscopy (Appendix B) and integrating the propylene methine proton signals of the polymer (5.0 ppm) and the cyclic carbonate (4.85 ppm) products.

However, this low selectivity towards PPC formation is unprecedented with these catalyst systems, as both **1a** and **2** and an equimolar mixture of **1a** and **2** show no formation of PPC (only PC formation) under identical conditions.

Table 3.6: PO/CO_2 copolymerisation reactions with catalyst system **7**.

Temperature /°C	Time /h	TON[a)]	TOF[b)] /h^{-1}	% Conversion[c)]	% PPC[c)]	% PC[c)]
60	22.5	248	11	25	9	91
70	22.5	435	19	44	0	>99
60*	22.5	115	5	12	0	>99

*All copolymerisations were conducted in a 100 mL Paar reactor vessel at 50 bar CO_2 at a 1:1000 catalyst:PO loading. a) The turn over number (TON) = number of moles of propylene oxide consumed/number of moles of catalyst. b) The turn over frequency (TOF) = TON/reaction period. c)Determined by the relative integrals in ^1H NMR spectrum of crude reaction mixture 5.0 ppm (PCC), 4.85 ppm, (PC), 2.99 ppm (PO). * Copolymerisation using 50:50 mixture of catalyst **1a**:**2**.*

3.6 Synthesis of Asymmetric Macrocycles and Complexes

An alternative to synthesising heterodinuclear complexes, in order to improve catalytic activity, was to synthesise asymmetric macrocycles and thus complexes. By introducing asymmetry into the macrocyclic ligand, the electronic properties of the metal centres in the macrocycle cavity will be different and hence hopefully favour one metal to do one process (epoxide binding and ring opening) and the other metal to carry out the other process (CO_2 insertion) and hence the activity of the complex should increase.

Therefore, an attempt to make macrocyclic ligands with imine and amine moieties was carried out (Scheme 3.8). The logic to this is that the imine moiety is more electron donating than the amine and therefore may cause the adjacent metal centre to facilitate nucleophilic attack/CO_2 insertion. Whereas, the amine coordinated metal centre is proposed to favour epoxide binding and ring opening.

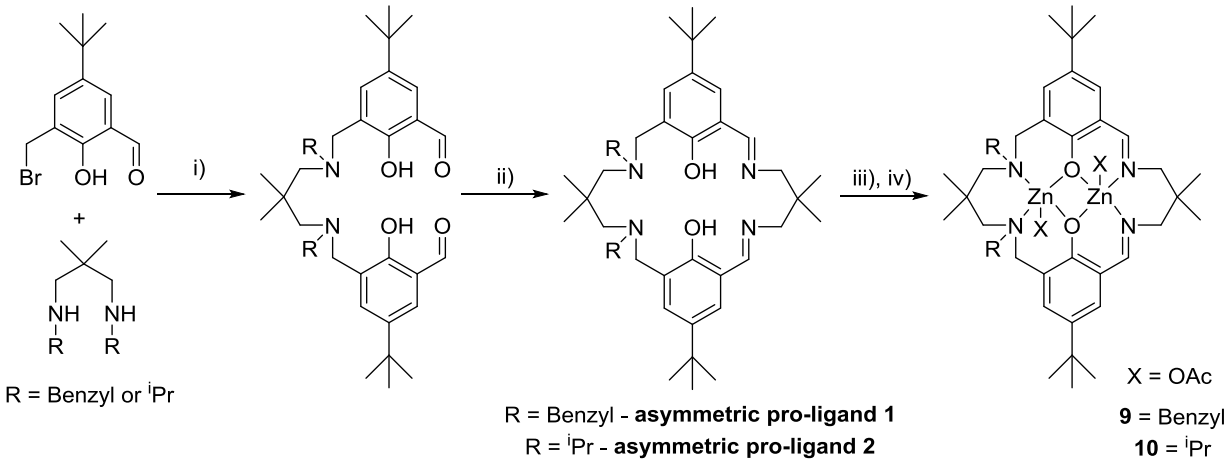

Scheme 3.8: Illustrates the synthesis of asymmetric complexes; Reaction conditions: i) *N*,*N*-diisopropylethylamine, THF, 25 °C, 16 h; ii) 2,2-dimethyl-1,3-propanediamine, MeOH, 25 °C, 16 h; iii) 3 equivalents of KH, dry THF, 25 °C, 3 h; iv) $Zn(OAc)_2$, dry THF, 25 °C, 16 h.

The synthesis of the asymmetric macrocyclic pro-ligands was similar to the attempted stepwise synthesis to form heterodinuclear complexes outlined in Section 3.2. The synthesis involved reacting 3-bromomethyl-5-*t*-butylsalicylaldehyde with one equivalent of *N*,*N*'-dibenzyl-2,2-dimethylpropane-1,3-diamine or 2,2-dimethyl-*N*,*N*'-di(propan-2-yl)propane-1,3-diamine to form half macrocyclic ligands. The use of secondary amines ensured that a mixture of products did not form because the diamines will only react with the Br group of 3-bromomethyl-5-*t*-butylsalicylaldehyde. Once the half macrocycle was formed, it was cyclised by the addition of 2,2-dimethyl-1,3-propanediamine to form asymmetric pro-ligands **1** and **2**.

Both asymmetric macrocyclic pro-ligands were produced in reasonable yields (89 % and 49 % for pro-ligand **1** and **2**, respectively) and in reasonably good purity, as the calculated and recorded elemental analysis values matched fairly well. The ^{1}H NMR spectra for both asymmetric pro-ligands (Figure 3.20 – pro-ligand **1** and Appendix B – pro-ligand **2**) show signals for the diagnostic imine protons (8.34 and 8.40 ppm respectively), which confirms that the macrocyclic pro-ligands had been synthesised. The IR spectra (Appendix B) also show signals for the imine bonds at 1631 cm^{-1}. Furthermore, ESI mass spectrometry for asymmetric pro-ligands **1** and **2** revealed signals at 729 and 633 amu respectively, which represent the mass of the macrocyclic pro-ligands plus a proton (Appendix B).

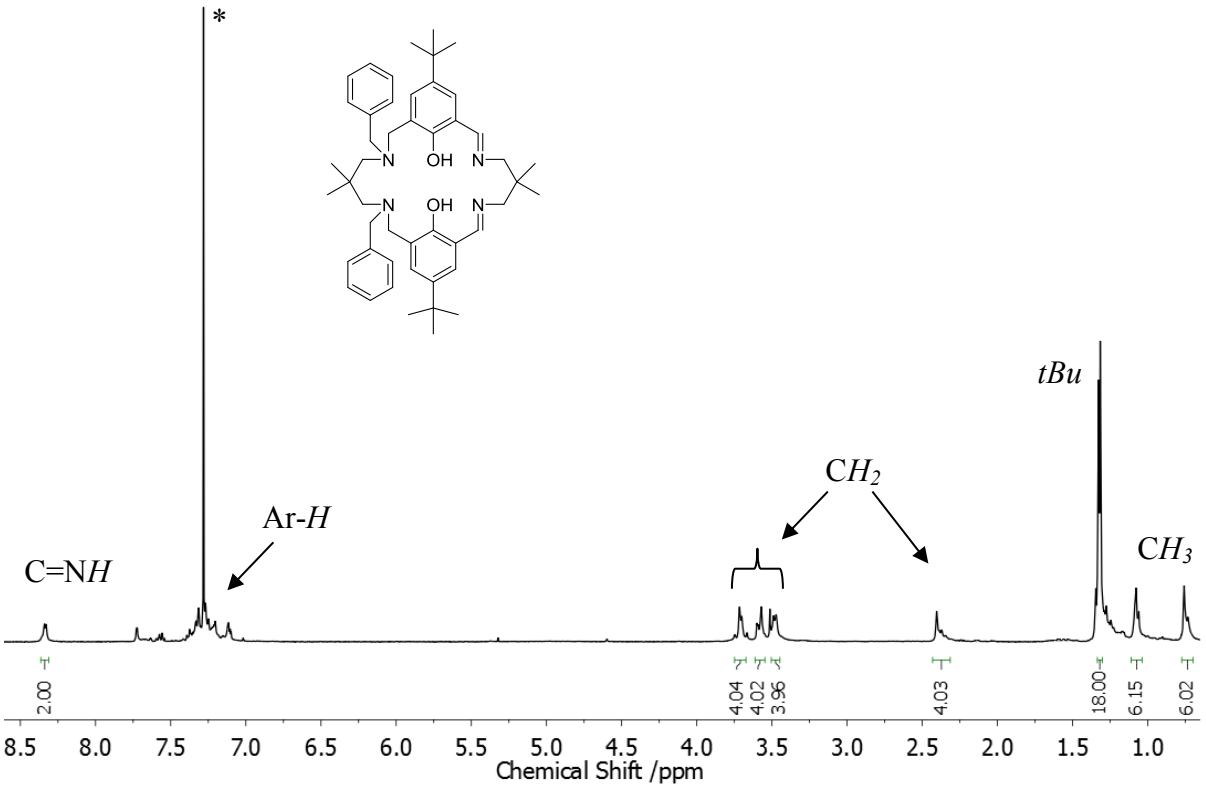

Figure 3.20: ^{1}H NMR Spectrum of asymmetric macrocyclic pro-ligand **1** in $CDCl_3$.

The asymmetric macrocyclic pro-ligands obtained were then complexed to zinc by the conventional route of deprotonating the macrocyclic ligand with KH, followed by transmetallation with $Zn(OAc)_2$. Complexes **9** and **10** were synthesised in low to moderate yield (35 % and 50 %, respectively). The complexes were characterised by ESI mass spectrometry and signals at 903 and 805 amu were observed for **9** and **10**, respectively, which represent the complex without the OAc co-ligands, but with a formate ion. The formate is present within the molecular ion fragment due to formic acid being used in the mass spectrometry analysis technique (Appendix B).

The complexes (**9** and **10**) were also analysed by IR spectroscopy and both spectra show C=N stretches at 1622 and 1625 cm^{-1}, respectively (Appendix B). Both complexes have shown little back bonding character occurring between the metal and the C=N bond. This is because the C=N stretch for both free macrocyclic ligands was recorded at 1631 cm^{-1}. This decrease in wavenumbers for the C=N stretch, when the ligand becomes coordinated to zinc, suggests that a little π back donation of the electrons in the d orbitals of the zinc metal centre to the empty π^* orbitals of the C=N bond occurs and thus the C=N bond weakens slightly.

Moreover, elemental analysis results recorded for the complexes are in good agreement with the calculated values, indicating good purity of complexes **9** and **10**. However, the ^{1}H NMR spectra were less informative because the spectra are very complex. The ligand signals are very broad, which arises due to the metal coordination. In addition, the broad signals also occur due to the many different conformations the ligand can undergo. An attempt to resolve the signals in the spectra was carried out by using variable temperature ^{1}H NMR spectroscopy, but this was unsuccessful.

Both complexes were used in CHO/CO_2 copolymerisation reactions at 80 °C, 1 bar CO_2 or 50 bar CO_2 pressure for 16 h and neither showed activity. The inactivity could be due to the two modifications of the macrocyclic ligands (either the R groups on the amine groups or the imine moieties). It is likely that the R groups reduce the activity of the complex by adding steric bulk to the ligand and that the imine moieties have caused the inactivity.

3.7 Conclusions

From the mechanistic and kinetic studies outlined in Chapter 2 for the di-magnesium catalyst (**1a**) and the investigations reported for the di-zinc catalyst (**2**) in literature,[36,37] the hypothesised mechanism for these catalysts in CHO/CO_2 copolymerisation reactions involves both metal centres. One metal centre aids epoxide binding and ring-opening, whilst the other facilitates CO_2 insertion. The growing copolymer chain 'shuttles' twice between the metal centres per catalytic cycle. Due to this observation, attempts to make heterodinuclear and asymmetrical derivatives of catalysts **1a** and **2** were carried out. The motivation for synthesising these analogues was that the metal centres in these complexes will have different electrophilicities (either due to being different metals or being surrounded by different electron donors) and hence one metal centre may favour epoxide binding and ring opening (most electrophilic metal centre) and the other may favour CO_2 insertion.[52]

Several attempts to producing a heterodinuclear complex *via* a stepwise route and using the same macrocycle of catalysts **1a** and **2** were carried out. The general route involved making half of the macrocycle, complexing this ligand to one metal centre and then the monometallic complex would have been cyclised and another metal centre would have been coordinated to the empty cavity. However, making the half macrocycle and monometallic complex proved to be difficult and a lack of product selectivity was observed.

Therefore, the synthesis of a heterodinuclear complex with a modified version of the macrocycle was synthesised. Following an adapted procedure from Bosnich and co-workers, heterodinuclear complex **4** was synthesised.[39-41] This Zn-Mg complex was easily obtained due to the presence of pyridyl arms on the amine moieties, which favoured metal coordination and thus promoted the formation of a monometallic complex. Once the monometallic complex formed, the cyclisation of the macrocycle and second metallation was fairly straight forward. The complex is inactive in CHO/CO_2 copolymerisation reactions. This could be due to the pyridyl arms or the imine moieties, but from control reactions it looks more likely to be due to the imine bonds. Attempts to reduce the imine bonds have been carried out with $NaBH_4$ or low pressure hydrogenation with a Pd/C catalyst, but these were unsuccessful.

Due to the fact that ligand modification has such a drastic effect on the activity of the complex, an attempt to synthesise a heterodinuclear derivative of catalysts **1a** and **2** using the same macrocycle, previously used by our group, was carried out by an *in situ* method.[3,42] This involved reacting the symmetrical macrocycle with the sequential addition of different metal precursors ($ZnEt_2$ and $Mg(OAc)_2$). This procedure yielded a mixed catalyst system (**7**), which was characterised by mass spectrometry. This catalyst system contains a Zn-Mg heterodinuclear complex and the homodinuclear Zn and Mg catalysts. The catalyst system was used in CHO/CO_2 copolymerisation reactions and has shown high activity (TOF = 292 h^{-1} under optimised conditions).

Moreover, catalyst system **7** is much more active compared to the di-magnesium (**1a**) and the di-zinc (**2**) catalysts alone or in a 50:50 mixture. The TOF values obtained for these catalysts are 52, 17 and 40 h^{-1}, respectively. The TOF value obtained for catalyst system **7** (79 h^{-1}) is double the activity seen for a 50:50 mixture of catalysts **1a** and **2**. This result shows that the presence of the Zn-Mg heterodinuclear species has improved the activity of the catalyst system.

Optimisation reactions with this catalyst system have also been investigated and the optimum temperature for this system is 90 °C. The catalyst system is not as robust at very low catalyst loadings and thus the ideal catalyst to epoxide ratio is 1:1000. The CO_2 pressure does not affect the activity of catalyst system **7**, as the activity is the same at 1 and 50 bar of CO_2 pressure.

The poly(cyclohexene) carbonate produced with catalyst system **7** were low in M_n and had narrow PDIs, which is due to chain transfer reactions occurring within the copolymerisation reaction. Chain transfer reactions also caused the formation of two copolymer series within the polycarbonate samples produced. One series is α-acetyl-ω-hydroxyl end-capped and the other series is α,ω-di-hydroxyl end-capped. Low M_n α,ω-di-hydroxyl polycarbonate chains (polycarbonate polyols) are highly desirable for polyurethane synthesis, as they can substitute polyether polyols used in this process.[45,48] Therefore in an attempt to selectively produce polycarbonate polyols with catalyst system **7**, 16 equivalents of H_2O were added to the copolymerisation reaction. The catalyst system seems to be robust to water and also shows promise to forming polycarbonate polyols selectively.

Furthermore, this catalyst system has also shown very low selectivity towards polypropylene carbonate formation in PO/CO_2 copolymerisation reactions (9 %), which has not been seen by catalysts **1a** and **2** and a 50:50 combination of these two homodinuclear catalysts. Additionally, catalyst system **7** (TOF = 11 h^{-1}) has a better activity for PO/CO_2 copolymerisation reactions compared to a 50:50 combination of **1a** and **2** (TOF = 5 h^{-1}), thus suggesting that the heterodinuclear species in this mixed catalyst system is the reason for the improved selectivity and activity.

A Zn-Co mixed catalyst system was also synthesised, but did not show enhanced activity compared to the homodinuclear di-cobalt catalyst. This mixed catalyst system **8** seems to be unstable under the copolymerisation reactions.

Other work to promote one metal centre to carry out epoxide binding and ring opening and the other metal centre to facilitate CO_2 insertion was carried out by producing asymmetrical macrocyclic ligands, which thus possess two cavities with different electronic properties. This therefore should affect the two zinc metal centres within the macrocyclic ligand and thus cause each metal centre to carry out a specific process. Two asymmetric ligands and thus di-zinc complexes were synthesised (**9** and **10**), but these were inactive in CHO/CO_2 copolymerisation reactions. The reason for this could be due to the imine moieties in the ligand framework or the benzyl and *iso*-propyl groups on the amine moieties of the macrocyclic ligand.

3.8 Future Work

Time constraints did not allow the reduction of the imine bonds in complexes **4**, **9** and **10** to occur and therefore this needs to be carried out in order to verify if the inactivity of these complexes in CHO/CO_2 copolymerisation reactions is due to the imine bonds or due to the other macrocyclic ligand modifications (R groups on the amine moieties). These complexes may be degrading in copolymerisation reactions and thus this needs to be fully investigated. The degradation temperature of these complexes needs to be investigated and the sensitivity of these complexes towards particular compounds, such as epoxides, also needs to be probed.

Moreover, the synthesis of catalyst system **7** can be further investigated in order to try and synthesise a pure Zn-Mg heterodinuclear complex without contamination with homodinuclear catalysts **1a** and **2**. The reason for the presence of homodinuclear catalysts **1a** and **2** in catalyst system **7** is that when one equivalent of Et_2Zn is added to the macrocyclic ligand, both the mono-zinc and di-zinc complexes form along with the presence of free ligand and therefore, the formation of di-zinc, di-magnesium and a heterodinuclear species occurs.

Therefore, the addition of Et_2Zn can be done at lower concentrations, over a longer period of time and at lower temperatures in order to promote the sole formation of the mono-zinc complex. Moreover, different zinc precursors can be used ($Zn(OAc)_2$, $Zn(OC_6H_5)_2$, $Zn(OCOC_6H_5)_2$ or $Zn(N(Si(Me)_3)_2)_2$) in order to promote the formation of a mono-zinc complex. Additionally, monitoring the reaction progress over time when one equivalent of Et_2Zn is added to the macrocyclic ligand would also help shed light on when the second metal precursor should be added to the reaction in order to maximise the amount of heterodinuclear species formed.

Another route can also be adopted to synthesise the heterodinuclear complexes with the symmetrical macrocyclic ligand. This involves using different metal precursors which may more easily form monometallic complexes ($TiCl_2$ or *n*BuLi) and then by adding an equivalent of either a zinc or magnesium precursor will yield a heterodinuclear complex, with Ti(IV) or Li in one of the cavities. Even though the latter metals are not usually used for epoxide/CO_2 copolymerisation reactions, these complexes can still be investigated.

Furthermore, heterodinuclear metal precursors can be synthesised first, which have been reported extensively by Mulvey and Hevia and then added to the macrocyclic ligand. The heterodinuclear metal precursors (lithium or sodium zincates and magnesates) may prevent the formation of homodinuclear complexes.[30,53] Once synthesised, these Li-Zn, Li-Mg, Na-Zn or Na-Mg heterodinuclear complexes can be used in copolymerisation reactions and an attempt to transmetallate the Li or Na with Zn and Mg can also be carried out. The synthesis of a lithium zincate (**11** – Figure 3.21) was carried out and was added to the macrocyclic ligand and a complex did form, as the ligand signals broadened in the ^{1}H NMR spectrum recorded. However due to time constraints, purification, full characterisation and testing of this complex in copolymerisation reactions were not carried out.

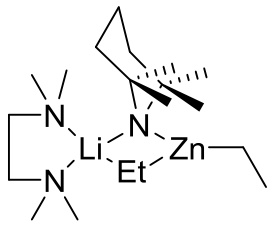

11

Figure 3.21: Lithium-zincate synthesised and used to make a Li-Zn heterodinuclear complex.

Once a synthetic route for synthesising heterodinuclear complexes cleanly has been established, then many more heterodinuclear complexes can be synthesised, not just Zn-Mg complexes, but other metal combinations, such as Zn-Co, Fe-Zn, Co-Fe and Fe-Mg. In particular Co-Mg complexes would be of great interest because the most active homodinuclear catalysts, using this symmetrical macrocyclic ligand, are the di-magnesium and di-cobalt derivatives.[4,5,44]

3.9 References

1. M. Cheng, E. B. Lobkovsky and G. W. Coates, *J. Am. Chem. Soc.,* 1998, ***120***, 11018-11019; M. Cheng, D. R. Moore, J. J. Reczek, B. M. Chamberlain, E. B. Lobkovsky and G. W. Coates, *J. Am. Chem. Soc.,* 2001, ***123***, 8738-8749; D. R. Moore, M. Cheng, E. B. Lobkovsky and G. W. Coates, *J. Am. Chem. Soc.,* 2003, ***125***, 11911-11924.

2. A. Buchard, M. R. Kember, K. G. Sandeman and C. K. Williams, *Chem. Commun.,* 2011, ***47***, 212-214.

3. M. R. Kember, P. D. Knight, P. T. R. Reung and C. K. Williams, *Angew. Chem. Int. Ed.,* 2009, ***48***, 931-933.

4. M. R. Kember, A. J. P. White and C. K. Williams, *Macromolecules,* 2010, ***43***, 2291-2298.

5. M. R. Kember and C. K. Williams, *J. Am. Chem. Soc.,* 2012, ***134***, 15676-15679.

6. B. Y. Lee, H. Y. Kwon, S. Y. Lee, S. J. Na, S.-i. Han, H. Yun, H. Lee and Y.-W. Park, *J. Am. Chem. Soc.,* 2005, ***127***, 3031-3037; M. W. Lehenmeier, S. Kissling, P. T. Altenbuchner, C. Bruckmeier, P. Deglmann, A.-K. Brym and B. Rieger, *Angew. Chem. Int. Ed.,* 2013, ***52***, 9821-9826.

7. Y. Xiao, Z. Wang and K. Ding, *Chem. Eur. J.,* 2005, ***11***, 3668-3678.

8. C. E. Anderson, S. I. Vagin, M. Hammann, L. Zimmermann and B. Rieger, *ChemCatChem,* 2013, ***5***, 3269-3280; S. I. Vagin, R. Reichardt, S. Klaus and B. Rieger, *J. Am. Chem. Soc.,* 2010, ***132***, 14367-14369.

9. K. Nakano, S. Hashimoto and K. Nozaki, *Chem. Sci.,* 2010, ***1***, 369-373.

10. M. F. Pilz, C. Limberg, B. B. Lazarov, K. C. Hultzsch and B. Ziemer, *Organometallics,* 2007, ***26***, 3668-3676.

11. S. Chen, Z. Hua, Z. Fang and G. Qi, *Polym. J.,* 2004, ***45***, 6519-6524.

12. I. Kim, M. J. Yi, K. J. Lee, D.-W. Park, B. U. Kim and C.-S. Ha, *Catal. Today,* 2006, ***111***, 292-296.

13. J. Sebastian and D. Srinivas, *Appl. Catal., A.,* 2014, ***482***, 300-308; Y.-Y. Zhang, X.-H. Zhang, R.-J. Wei, B.-Y. Du, Z.-Q. Fan and G.-R. Qi, *R. Soc. Chem. Adv.,* 2014, ***4***, 36183-36188.

14. D. J. Darensbourg, M. J. Adams and J. C. Yarbrough, *Inorg. Chem.,* 2001, ***40***, 6543-6544.

15. M. R. Kember, A. Buchard and C. K. Williams, *Chem. Commun.,* 2011, ***47***, 141-163.

16. S. Chen, G.-R. Qi, Z.-J. Hua and H.-Q. Yan, *J. Polym. Sci. A Polym. Chem.,* 2004, ***42***, 5284-5291.

17. I. Kim, M. J. Yi, S. H. Byun, D. W. Park, B. U. Kim and C. S. Ha, *Macromolecular Symp.,* 2005, ***224***, 181-192.

18. N. J. Robertson, Z. Qin, G. C. Dallinger, E. B. Lobkovsky, S. Lee and G. W. Coates, *Dalton Trans.,* 2006, 5390-5395.

19. X.-K. Sun, X.-H. Zhang, F. Liu, S. Chen, B.-Y. Du, Q. Wang, Z.-Q. Fan and G.-R. Qi, *J. Polym. Sci. A Polym. Chem.,* 2008, ***46***, 3128-3139.

20. J. K. Varghese, A. Cyriac and B. Y. Lee, *Polyhedron,* 2012, ***32***, 90-95.

21. T. Sarbu, T. Styranec and E. J. Beckman, *Nature,* 2000, ***405***, 165-168.

22. D. J. Darensbourg, M. J. Adams, J. C. Yarbrough and A. L. Phelps, *Inorg. Chem.,* 2003, ***42***, 7809-7818.

23. J. A. Labinger and J. E. Bercaw, *Nature,* 2002, ***417***, 507-514.

24. T. R. Verhoeven and D. Askin, *U.S. Pat. 4,820,850,* 1989.

25. J. Clayden; *Organolithiums: Selectivity for Synthesis*; 1st ed. Oxford, U.K., 2002; T. Stey and D. Stalke *The Chemistry of Organolithium Compounds* Chichester, U.K., 2004; H. W. Gschwend and H. R. Rodriguez *Heteroatom-Facilitated Lithiations Organic Reactions* Hoboken, New Jersey, 2005.

26. V. Grignard, *Ann. Chim. Phys.,* 1901, ***24***, 433-490; F. C. Frostick and C. R. Hauser, *J. Am. Chem. Soc.,* 1949, ***71***, 1350-1352; C. R. Hauser and H. G. Walker, *J. Am. Chem. Soc.,* 1947, ***69***, 295-297.

27. E. C. Ashby, J. Laemmle and H. M. Neumann, *Acc. Chem. Res.,* 1974, ***7***, 272-280; P. Knochel, W. Dohle, N. Gommermann, F. F. Kneisel, F. Kopp, T. Korn, I. Sapountzis and V. A. Vu, *Angew. Chem. Int. Ed.,* 2003, ***42***, 4302-4320.

28. D. Seyferth, *Organometallics,* 2001, ***20***, 2940-2955; E. von Frankland, *Liebigs Ann.,* 1849, ***71***, 171-213.

29. J. A. Garden In *Pure and Applied Chemistry*; University of Strathclyde, 2014; Vol. Ph.D. Thesis.

30. F. Mongin and A. Harrison-Marchand, *Chem. Rev.,* 2013, ***113***, 7563-7727; R. E. Mulvey, *Organometallics,* 2006, ***25***, 1060-1075; R. E. Mulvey, *Acc. Chem. Res.,* 2009, ***42***, 743-755.

31. A. Krasovskiy and P. Knochel, *Angew. Chem. Int. Ed.,* 2004, ***43***, 3333-3336.

32. Y. Kondo, M. Shilai, M. Uchiyama and T. Sakamoto, *J. Am. Chem. Soc.,* 1999, ***121***, 3539-3540.

33. B. Haag, M. Mosrin, H. Ila, V. Malakhov and P. Knochel, *Angew. Chem. Int. Ed.,* 2011, ***50***, 9794-9824.

34. D. R. Armstrong, P. García-Álvarez, A. R. Kennedy, R. E. Mulvey and J. A. Parkinson, *Angew. Chem. Int. Ed.,* 2010, ***49***, 3185-3188; P. García-Álvarez, D. V. Graham, E. Hevia, A. R. Kennedy, J. Klett, R. E. Mulvey, C. T. O'Hara and S. Weatherstone, *Angew. Chem. Int. Ed.,* 2008, ***47***, 8079-8081.

35. J. Wang, H. Li, N. Guo, L. Li, C. L. Stern and T. J. Marks, *Organometallics,* 2004, ***23***, 5112-5114.

36. A. Buchard, F. Jutz, M. R. Kember, A. J. P. White, H. S. Rzepa and C. K. Williams, *Macromolecules,* 2012, ***45***, 6781-6795.

37. F. Jutz, A. Buchard, M. R. Kember, S. B. Fredrickson and C. K. Williams, *J. Am. Chem. Soc.,* 2011, ***133***, 17395–17405.

38. H. Wada, T. Aono, K.-i. Motoda, M. Ohba, N. Matsumoto and H. Okawa, *Inorg. Chim. Acta.,* 1996, ***246***, 13-21; H. Ōkawa, H. Furutachi and D. E. Fenton, *Coord. Chem. Rev.,* 1998, ***174***, 51-75; H. Okawa, J. Nishio, M. Ohba, M. Tadokoro, N. Matsumoto, M. Koikawa, S. Kida and D. E. Fenton, *Inorg. Chem.,* 1993, ***32***, 2949-2957; H. Golchoubian, E. Baktash and R. Welter, *Inorg. Chem. Commun.,* 2007, ***10***, 120-124; J. Nishio, H. Ōkawa, S.-i. Ohtsuka and M. Tomono, *Inorg. Chim. Acta.,* 1994, ***218***, 27-32.

39. C. Fraser and B. Bosnich, *Inorg. Chem.,* 1994, ***33***, 338-346.

40. C. Fraser, L. Johnston, A. L. Rheingold, B. S. Haggerty, G. K. Williams, J. Whelan and B. Bosnich, *Inorg. Chem.,* 1992, ***31***, 1835-1844.

41. C. Fraser, R. Ostrander, A. L. Rheingold, C. White and B. Bosnich, *Inorg. Chem.,* 1994, ***33***, 324-337; D. G. McCollum, G. P. A. Yap, A. L. Rheingold and B. Bosnich, *J. Am. Chem. Soc.,* 1996, ***118***, 1365-1379.

42. M. R. Kember, A. J. P. White and C. K. Williams, *Inorg. Chem.,* 2009, ***48***, 9535-9542.

43. P. K. Saini, C. Romain and C. K. Williams, *Chem. Commun.,* 2014, ***50***, 4164-4167.

44. M. R. Kember, F. Jutz, A. Buchard, A. J. P. White and C. K. Williams, *Chem. Sci.,* 2012.

45. A. Cyriac, S. H. Lee, J. K. Varghese, E. S. Park, J. H. Park and B. Y. Lee, *Macromolecules,* 2010, ***43***, 7398-7401.

46. W. J. van Meerendonk, R. Duchateau, C. E. Koning and G.-J. M. Gruter, *Macromolecules,* 2005, ***38***, 7306-7313; K. Nakano, M. Nakamura and K. Nozaki, *Macromolecules,* 2009, ***42***, 6972-6980.

47. D. J. Darensbourg and R. M. Mackiewicz, *J. Am. Chem. Soc.,* 2005, ***127***, 14026-14038; D. J. Darensbourg, J. C. Yarbrough, C. Ortiz and C. C. Fang, *J. Am. Chem. Soc.,* 2003, ***125***, 7586-7591.

48. J. Langanke, A. Wolf, J. Hofmann, K. Bohm, M. A. Subhani, T. E. Muller, W. Leitner and C. Gurtler, *Green Chem.,* 2014, ***16***, 1865-1870.

49. S. Inoue, *J. Polym. Sci. A Polym. Chem.,* 2000, ***38***, 2861-2871.

50. W.-M. Ren, X. Zhang, Y. Liu, J.-F. Li, H. Wang and X.-B. Lu, *Macromolecules,* 2010, ***43***, 1396-1402.

51. Y. Xiao, Z. Wang and K. Ding, *Macromolecules,* 2005, ***39***, 128-137.

52. J. Mullay, *J. Am. Chem. Soc.,* 1984, ***106***, 5842-5847.

53. E. Hevia, K. W. Henderson, A. R. Kennedy and R. E. Mulvey, *Organometallics,* 2006, ***25***, 1778-1785; F. Mongin, A. Bucher, J. P. Bazureau, O. Bayh, H. Awad and F. Trécourt, *Tetrahedron Lett.,* 2005, ***46***, 7989-7992.

Chapter 4

Homodinuclear Metal Catalysts for Epoxide/Anhydride Ring Opening Copolymerisation Reactions

"Nothing in life is to be feared, it is only to be understood. Now is the time to understand more, so that we may fear less."

Marie Curie quoted in *Our Precarious Habitat* by Melvin A. Benarde

4.1 Introduction

4.1.1 General Introduction

Polyesters are a useful commodity to society and are produced on a 50 million tonne scale annually.[1] The conventional route to synthesising polyesters involves polycondensation reactions between carboxylic acids and alcohols. The vast variety of carboxylic acids and alcohols available gives rise to the formation of polyesters with different backbones and side chains and thus different mechanical, thermal and chemical properties. This considerable catalogue of polyesters allows them to be used in an extensive range of applications, such as, textiles and packaging.[2,3] Additionally, the good biodegradability and biocompatibility of polyesters has prompted their use in medical applications, such as, sutures and bone screws.[4,5]

Generally, polyesters are formed from homopolymerisation reactions of monomers containing both carboxylic acid and alcohol functional groups, such as glycolic acid, or by copolymerisation reactions between diacids and diols, for example, polyethylene terephthalate is formed by reacting terephthalic acid and ethylene glycol.[6,7] Both polymerisation processes occur *via* a step-growth manner and minimal side reactions, such as cyclisation reactions, occur. However, the polymers produced from polycondensation reactions do not have controlled number average molecular weights (M_n) and the molecular weight distributions of these polymers are usually large (polydispersity index (PDI) = 2). Thus, the preparation of well-defined polyesters with sophisticated molecular architectures is usually complicated with step-growth routes. Moreover, precise stoichiometries of the diacids and diols are also required in polycondensation reactions.

Additionally, another concern for producing polyesters *via* this method is that in polycondensation reactions, water or small alcohol molecules are generated as a by-product. These small molecules need to be driven off in order to push the equilibrium of the polycondensation reaction to the right and thus favour polyester formation. Therefore, high temperatures are often required, which is expensive and energy inefficient.

To synthesise well controlled polyesters with a narrow polydispersity index and at lower temperatures, an initiator is required. Polymerisation reactions using initiators are well controlled because they occur *via* a chain growth manner and are usually living polymerisations because no disproportionation or termination reactions occur. Many initiators

have been discovered for the ring opening polymerisation (ROP) of cyclic esters in order to produce highly desirable polyesters, such as, polylactide from lactide.[8,9] However, there are only a limited number of cyclic esters and hence only certain polyesters can be synthesised.[10] These polymers are useful and some are derived from biodegradable starting materials (lactide from the fermentation of starch), but the resulting polyesters have limited mechanical, thermal and chemical properties and therefore cannot be used in as many different applications as the polyesters generated from polycondensation reactions.

A solution to this problem is the ring opening copolymerisation (ROCOP) of epoxides and anhydrides (Scheme 4.1).[2,11-17] As there are a wide variety of commercially available epoxides and anhydrides, a vast variety of polyesters with many different properties and uses can be produced. The ROCOP of epoxides and anhydrides can also facilitate the synthesis of polyesters with aromatic backbones, which cannot be accessed by the ROP of cyclic esters, but are useful due to their thermal and mechanical properties.[14,17-19] Furthermore, this route can also use renewable monomers, such as, limonene oxide and maleic anhydride and thus improve the sustainability of the polyester formed.[2,16-20]

Additionally, this method (ROCOP) is also seen as a desirable alternative because it is highly controlled unlike polycondensation reactions. This is because these copolymerisation reactions require initiators. Research in academia and industry has led to the discovery of highly active and robust initiators for the ROCOP of epoxides and anhydrides.[2,11-17] However, there are still far fewer initiators for the ROCOP of epoxide and anhydrides compared for the ROP of cyclic esters.[9]

R_1, R_2, R_3 & R_4 = Aliphatic or Aromatic Groups

Scheme 4.1: Illustrates the ROCOP (ring-opening copolymerisation) of epoxides/anhydrides.

4.1.2 Catalysts for Epoxide/Anhydride Ring Opening Copolymerisation Reactions

Homogeneous catalysts for the ROCOP of epoxides and anhydrides generally consist of a Lewis acid metal centre(s), such as Zn(II), Cr(III), Co(III), Mn(III) or Al(III) coordinated to a

ligand, which is either a salen,[17] salan,[21] β-diimine[2,18] or porphyrin.[5,14,16,19,22] The metal catalyst used in the ROCOP of epoxide/anhydride is vital in controlling the polymerisation rate, the degree of polymerisation and monomer selectivity. The coupling of epoxide and anhydride was first reported in the 1960's by Inoue and Fischer.[23,24] However, a low M_n polymer sample was obtained with a high contamination of polyether, which is formed from the homopolymerisation of epoxides.[23,24]

After 20 years of these initial findings, Inoue managed to synthesise an alternating copolymer between propylene oxide (PO) and phthalic anhydride (PA) with an aluminium tetraphenylporphyrin (TPP) complex and a quaternary organic salt (Figure 4.1). However, the copolymer samples produced still had low M_n values (around 3000 g/mol).[11,12]

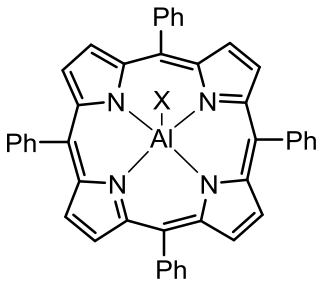

X= Cl, OMe, Me, OR

Figure 4.1: Aluminium tetraphenylporphyrin complex.

Coates and co-workers used their well-documented zinc β-diiminate (BDI) complexes for epoxide/anhydride copolymerisations instead of the conventional epoxide/CO_2 copolymerisation reactions.[15] It was found that complexes with a CN group in the R_2 position were the most stable and thus the most active in these copolymerisation reactions (Figure 4.2). It was hypothesised that electron withdrawing groups in this position prevented ligand degradation and hence enhanced the stability of the complex. Additionally, steric bulk in the R_1 and R_3 positions lowered the activity of these complexes, whilst intermediate groups were most favourable (Figure 4.2). More importantly, Coates and co-workers found that these complexes worked with a wide range of epoxides (cyclohexene oxide (CHO), limonene oxide, vinyl CHO and PO), with diglycolic anhydride (DGA) and maleic anhydride (MA) as the anhydrides of choice.[2,15] The copolymers synthesised had exceptionally high M_n values (up to 55 000 g/mol), which had not been observed previously.[15]

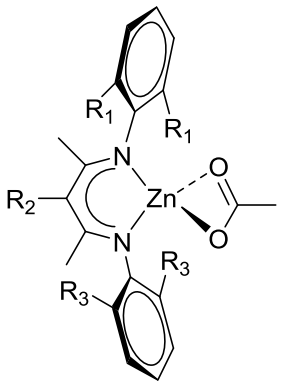

R_1 = Et, R_2 = CN, R_3 = ^{i}Pr

Figure 4.2: Zinc BDI complex by Coates and co-workers.[15]

Heterogeneous catalysts have also been reported for the copolymerisation of epoxides and anhydrides. These double metal cyanides (DMCs) were found to be much more active (≈ 90 % conversion in approximately 2 h) compared to the homogeneous BDI catalysts reported (≈ 90 % conversion in up to 24 h). Even though these DMCs ($Zn_3[Co(CN)_6]_2$ and $Zn_{2.3}Cl_{1.0}[Co(CN)_6]_{1.0}.2.0^{t}BuOH{\cdot}1.0H_2O$) are active when used with a wide variety of anhydrides (maleic anhydride (MA), succinic anhydride (SA) and PA) and PO as the epoxide; the copolymers synthesised were of low M_n and contained a high percentage of ether linkages (3000 g/mol and 10-60 %, respectively).[25,26] This is not desirable as these polyester chains have low T_d and T_g values, which limits number of applications the polyester sample can be used for.

4.1.3 Proposed Mechanism

The proposed mechanism for epoxide/anhydride copolymerisation reactions involves a coordination and insertion process. A metal alkoxide species is generated by the ring-opening of an epoxide molecule bound to the metal centre of the catalyst by either the co-ligand present within the catalyst structure or a co-catalyst. Subsequently, an anhydride molecule inserts within the metal alkoxide bond to generate a metal carboxylate intermediate, which can nucleophilically attack another epoxide bound to the metal to regenerate the metal alkoxide species. Thus there is a cycling between metal alkoxide and metal carboxylate species in order to generate an alternating copolymer (Figure 4.3).

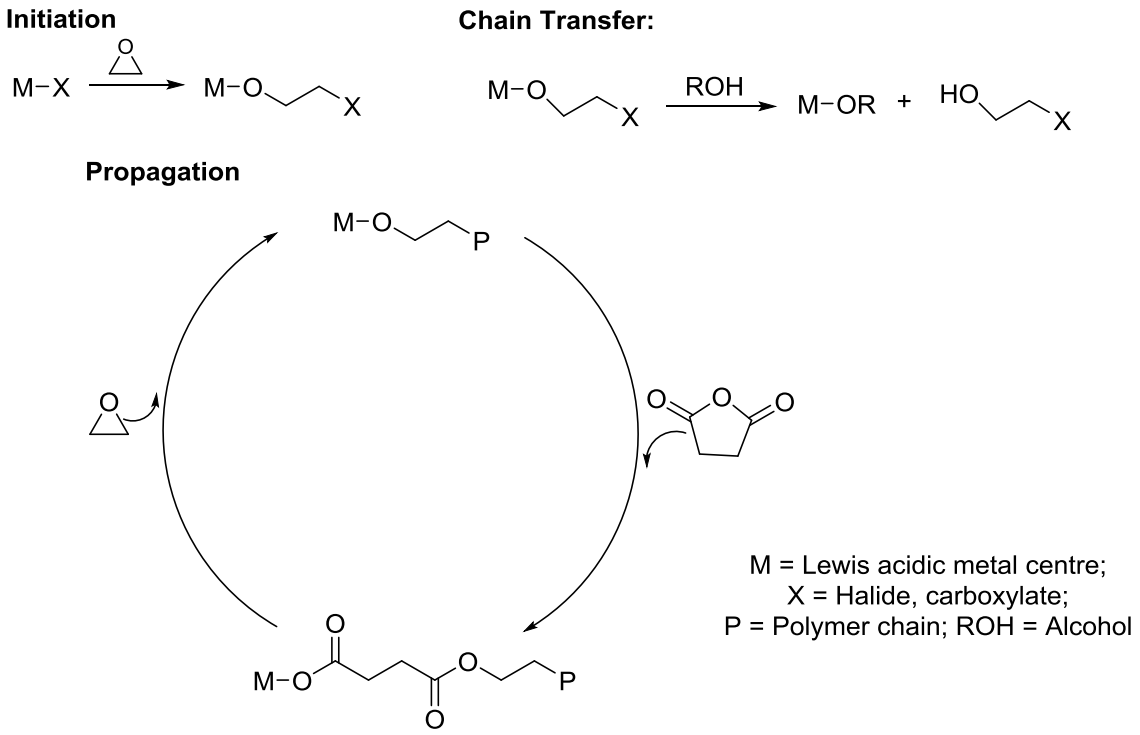

Figure 4.3: Proposed mechanism for epoxide/anhydride copolymerisation.

4.1.4 Terpolymerisation Reactions of Epoxide/Anhydride/CO_2

Most of the catalysts reported for the copolymerisation of epoxide and anhydride are also active catalysts for the copolymerisation of epoxide and CO_2, which also occurs *via* a coordination-insertion pathway.[5,17,18] In this mechanism there is a rapid interchange between metal alkoxide and metal carbonate species.

The introduction of carbonate linkages into a polyester chain has been found to lower the rate of hydrolytic degradation of the polymer and the autocatalytic degradation, which is of particular interest and importance in biomedical applications.[27] These polymers can be accessed by either the copolymerisation of cyclic esters and cyclic carbonates, by sequential addition of monomers, or by combining the ROCOP of epoxide/anhydride and of epoxide/CO_2, which results in the terpolymerisation of epoxide, CO_2 and anhydride.

Very few homogenous catalysts have been reported for these terpolymerisations. The zinc BDI complexes reported by Coates and co-workers (Figure 4.2) not only worked for the copolymerisation of epoxide and anhydride, but also for the terpolymerisation of CHO/SA/CO_2 or CHO/DGA/CO_2. These reactions were carried out in one pot and thus it was expected that random poly(ester-carbonate) chains would form. However, ^{1}H NMR and IR

spectroscopy revealed that a diblock copolymer had formed and that the formation of the polyester block occurred first, albeit at a slower rate compared to the formation of the polycarbonate block. The terpolymer formed had high M_n values (≈ 30 000 g/mol) and narrow PDI values (1.2-1.3).[18]

Duchateau and co-workers used chromium, manganese and cobalt tetraphenylporphyrin (Figure 4.4, left) and salphen complexes (Figure 4.4, right) in PA/styrene oxide (SO) copolymerisation reactions and these complexes showed good activity (50-100 % conversion of 250 equivalents of SO and PA in 100 mins, in neat conditions). Additionally, these catalysts also worked well, but with a slightly lower activity in toluene solutions. All these complexes required the presence of co-catalysts, most commonly 4-dimethylaminopyridine (DMAP). The most active catalysts were the chromium complexes, with the chromium salphen complex displaying higher activity compared to the chromium porphyrin complex.[14]

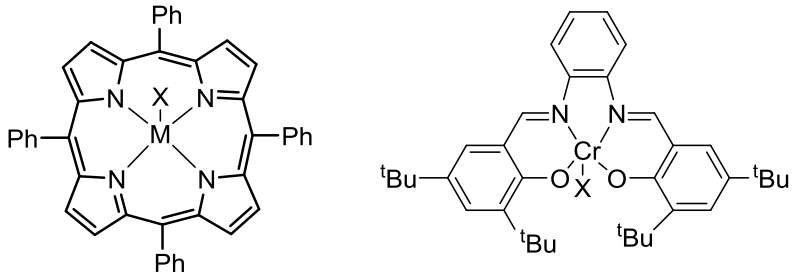

X= Cl; M = Cr, Mn, Co

Figure 4.4: Cr, Mn and Co salphen and tetraphenylporphyrin (TPP) complexes.

The chromium salphen and TPP complexes were further investigated in copolymerisations with CHO and other cyclic anhydrides (PA, SA, cyclopropane-1,2-dicarboxylic acid anhydride (CPrA) and cyclopentane-1,2-dicarboxyclic acid anhydride (CPA)) and both catalysts worked well with all reagents. Again, both catalysts performed better in neat conditions than in toluene solutions. Low M_n copolymers were produced (1000-10000 g/mol) with high ester content (70-100 %) and minimal ether linkage by-product formation.[5]

When the chromium complexes were used in terpolymerisation reactions of CHO, SA or PA and CO_2, similar observations to the findings of Coates and co-workers were recorded. A diblock copolymer formed during the reaction. The polyester block formed first and minimal carbonate linkages were observed until approximately 90 % of the anhydride had been consumed to form the polyester block.[5] Darensbourg has also shown that another chromium

salen complex (*N,N'*-bis(3,5-di-*tert*-butylsalicylidine)-1,2-cyclohexanediaminochromium(III) chloride complex – Figure 4.5), with bis(triphenylphosphine)iminium salts as co-catalysts, has good activity for the terpolymerisation of CHO/PA/CO_2.[17]

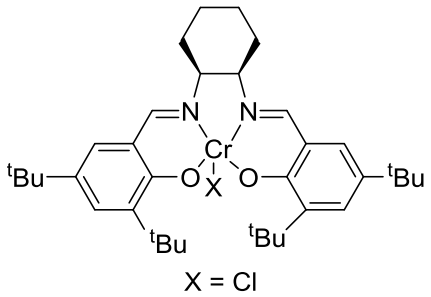

Figure 4.5: *N,N'*-bis(3,5-di-*tert*-butylsalicylidine)-1,2-cyclohexanediaminochromium(III) chloride complex.[17]

4.1.5 Chapter Aims

This chapter describes the reactivity of magnesium and zinc based catalysts (**1a** and **2**, respectively), which are known catalysts for the ROCOP of CHO/CO_2, during copolymerisation reactions of CHO and PA in neat and solution conditions (Scheme 4.2). Additionally, catalysts **1a** and **2** have also been used in the terpolymerisation of CHO/PA/CO_2. The results obtained highlight the importance of the choice of metal within the catalyst structure and how different metals affect the rate and selectivity in polymerisation reactions.

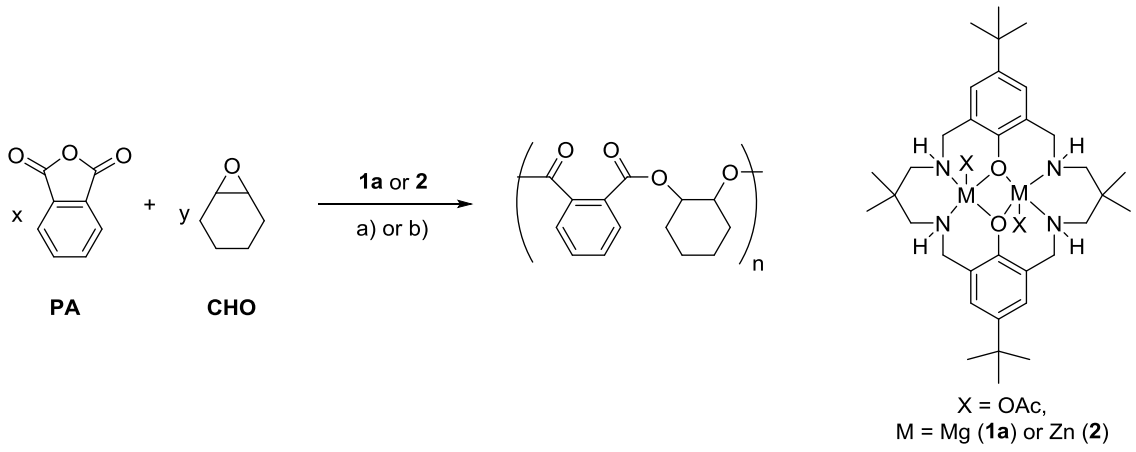

X = OAc,
M = Mg (**1a**) or Zn (**2**)

Scheme 4.2: Illustrates ROCOP of cyclohexene oxide (CHO) and phthalic anhydride (PA), initiated by complexes **1a** or **2**. Reagents and conditions: a) 100 °C, N_2, toluene, [PA] = 2.5 M, catalyst:CHO:PA = 1:100:100; b) 100 °C, N_2, neat CHO as the solvent, catalyst:CHO:PA = 1:800:100.

4.2 ROCOP of CHO/PA in Neat Conditions

4.2.1 Rate: Point Kinetics

Both catalysts (**1a** or **2**) are active in the ROCOP of CHO/PA in neat conditions at 100 °C and thus produce the desired polyester, poly(1,2-cyclohexylene-1,2-phthalate) (PE). The magnesium catalyst (**1a**) is approximately four times faster than the zinc analogue (**2**) in neat conditions. Catalyst **1a** converts ≈ 97 % of PA in 1 h, compared to **2** which converts 24 % in 1 h, giving respective turnover frequencies (TOFs) of 97 h^{-1} and 24 h^{-1}. This trend is also observed with the relative rates for catalysts **1a** and **2** in the ROCOP of CHO/CO_2, where catalyst **1a** operates six times faster than **2** (TOF = 152 h^{-1} and 25 h^{-1} for **1a** and **2** at 100 °C, respectively).[28,29]

Table 4.1: Data for the ROCOP of CHO/PA initiated by catalysts **1a** or **2** in neat conditions.

Cat.	Cat./CHO/PA	t /h	% PA Conversion[a), b)]	% Ester linkages[c)]	M_n[d)] /gmol^{-1}	PDI[d)]
1a	1/800/100	1	97	>99	12670	1.10
					5470	1.06
2	1/800/100	1	24	>99	2570	1.20
2	1/800/100	4	100	>99	13220	1.06
					6190	1.08

Reactions were conducted at 100 °C, under N_2 atmosphere, in neat CHO as the solvent. a) Determined by ^{1}H NMR spectroscopy ($CDCl_3$) by integrating the normalized resonances for PA (7.97 ppm) and the phenylene signals in PE (7.83-7.30 ppm). b) % Error in PA conversion was <3% in all cases. c) Determined by ^{1}H NMR spectroscopy (DMSO-d_6) by integrating the normalized resonances for ester linkages (5.10-4.85, 4.66 and 3.46 ppm) and ether linkages (3.59 ppm). d) Determined by SEC in THF at 40 °C, calibrated using polystyrene standards.

The TOF values obtained reveal that the magnesium catalyst (**1a**) is more active in the ROCOP of CHO/CO_2 compared to that of CHO/PA (TOF = 152 h^{-1} and 97 h^{-1}, respectively). However, even though the zinc catalyst (**2**) has similar TOF values for both the ROCOP of CHO/CO_2 and CHO/PA (TOF = 25h^{-1} and 24h^{-1}, respectively); the zinc catalyst (**2**) also seems to be more active in the ROCOP of CHO/CO_2 compared to that of CHO/PA. This is because it is assumed that rate is proportional to the catalyst concentration (as per the kinetic study using **1a** discussed in Chapter 2) and the catalyst loading in the CHO/CO_2

copolymerisation reactions was 0.1 mol %, whereas the catalyst loading in the CHO/PA copolymerisation reactions was ten times higher (1 mol %). Therefore, for both catalysts the ROCOP of CHO/CO_2 is substantially faster than the ROCOP of CHO/PA. In the case of the magnesium catalyst, the ROCOP of CHO/CO_2 is around 1.5 times faster than CHO/PA at ten times lower catalyst loading.

As discussed previously (Section 4.1.2 and 4.1.4), there are several catalysts for the ROCOP of CHO/PA, but only a few of these catalysts have been compared in both ROCOP processes (CHO/PA and CHO/CO_2). Coates and co-workers discovered that the [(BDI)ZnOAc] catalysts were active in both the ROCOP of epoxide/CO_2 and epoxide/anhydride, but like catalysts **1a** and **2**, the zinc BDI catalysts (Figure 4.2) have a lower activity in the copolymerisation of epoxide/anhydride compared to epoxide/CO_2. This observation was attributed to the fact that the ring opening of an epoxide is carried out faster by a zinc-carbonate species compared to a zinc-carboxylate bond.[18]

The activities observed for catalysts **1a** and **2** in the copolymerisation of CHO/PA (TOF = 97 h^{-1} and 24 h^{-1}) are similar to the activities of the catalysts reported in literature. Homogeneous catalysts, [(salphen)CrCl] and [(TPP)CrCl], have TON and TOF values between 150-250 and 50 h^{-1}-71 h^{-1}, respectively. However, unlike catalysts **1a** and **2**, these Cr catalysts are only effective upon the addition of a co-catalyst. The use of these co-catalysts is undesirable because side reactions can be initiated by these species, which can affect the end groups of the copolymer synthesised and hence cause uncertainty.[16,29]

Moreover, catalyst **1a** is one of the first examples of a well-defined magnesium catalyst for epoxide/anhydride copolymerisations. There has been one example of a magnesium alkoxide catalyst ($Mg(OEt)_2$), which is known to aggregate and thus is not as well-defined, as the nuclearity and the structure of the catalyst is unclear.[30] Magnesium is an attractive metal of choice within catalysts because it has a low cost, low toxicity and is naturally abundant. Additionally, magnesium catalysts are colourless and hence do not colour the polymer they produce. These robust catalysts are also inert to redox chemistry.

4.2.2 Polymer Characterisation

According to the literature, the polymer produced from the ROCOP of CHO/PA can vary in composition. It may possess a perfectly alternating polyester structure due to the sequential epoxide/anhydride copolymerisation, or alternatively, ether linkages can be dispersed within the polyester structure due to the sequential enchainment of epoxides.[2,14-16,19] The relative ratio of ester and ether repeat units was determined by comparing the integrals of the polyester and ether signals in the ^{1}H NMR spectra recorded of the copolymer samples.

It was discovered that when the copolymer sample was dissolved in $CDCl_3$, the ^{1}H NMR spectrum obtained gave indistinguishable resonances for the ether linkages (3.5-3.3 ppm) and the end group signals of the polyester (3.6-3.4 ppm), as they significantly overlapped. However, the ^{1}H NMR spectrum recorded for a mixture of polyether and polyester in DMSO-d_6 showed no such overlap (Figure 4.6, polyester signals observed at 3.46 ppm and polyether linkages at 3.59 ppm). Hence, by recording a ^{1}H NMR spectrum of the copolymer samples in DMSO-d_6, the ether content could be determined by comparing the relative integrals of the polyester and ether resonances.

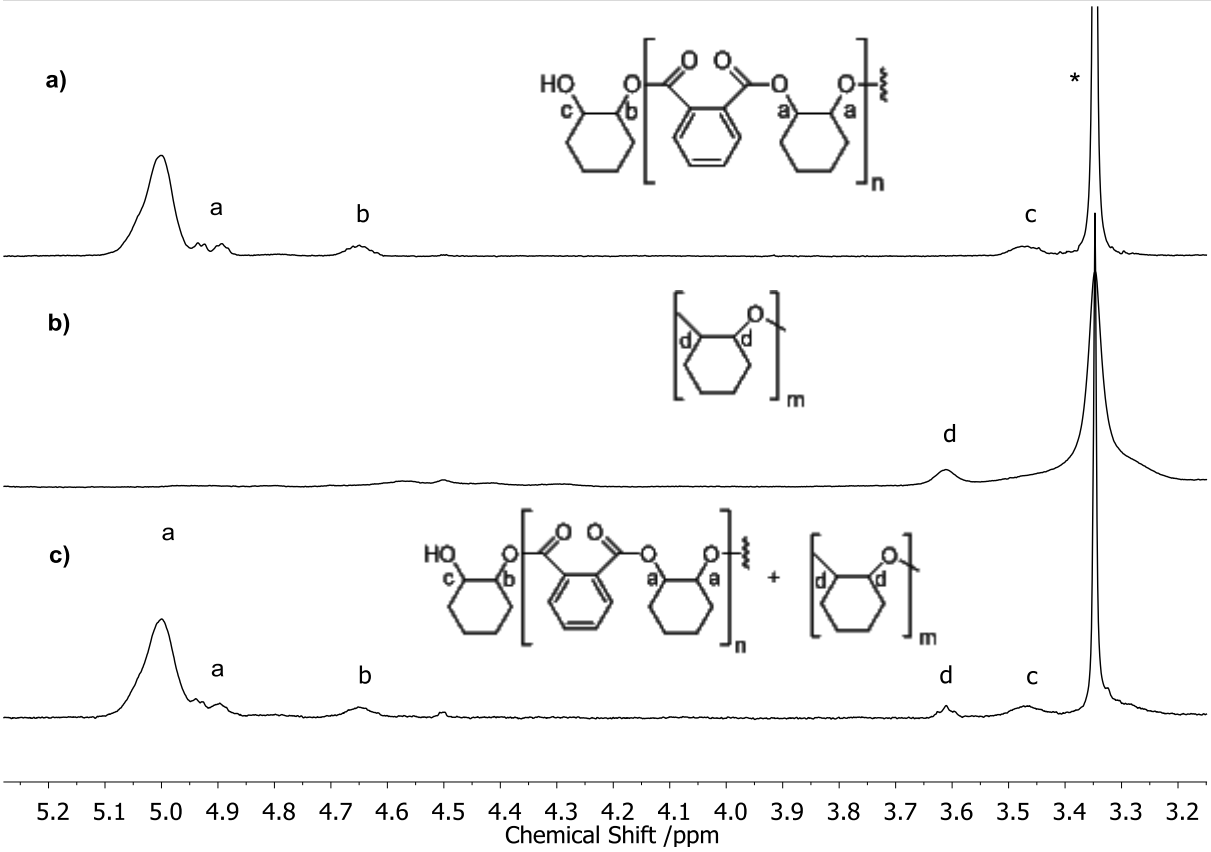

Figure 4.6: a) ^{1}H NMR spectrum of polyester (PE) (without any ether linkages) in DMSO-d_6; b) ^{1}H NMR spectrum of polyether in DMSO-d_6; c) ^{1}H NMR spectrum of a mixture of PE and polyether in DMSO-d_6.

When CHO was used as the solvent, the polyester samples formed using catalysts **1a** and **2** show perfectly alternating structures with no detectable ether linkages (Table 4.1). This high selectivity for polyester formation implies that catalysts **1a** and **2** have the correct balance of electrophilicity (to aid epoxide and anhydride binding) and lability (to aid carboxylate attack of the epoxide or alkoxide attack of the anhydride).

4.2.3 Molecular Weight (M_n)

The polyester samples produced were analysed by SEC (size exclusion chromatography) and have low M_n and bimodal molecular weight distributions (Figure 4.7). The higher M_n polymer series is approximately double the M_n of the lower M_n polymer series. This bimodal M_n distribution is also observed for both catalysts **1a** and **2** for CHO/CO_2 copolymerisation reactions.[31]

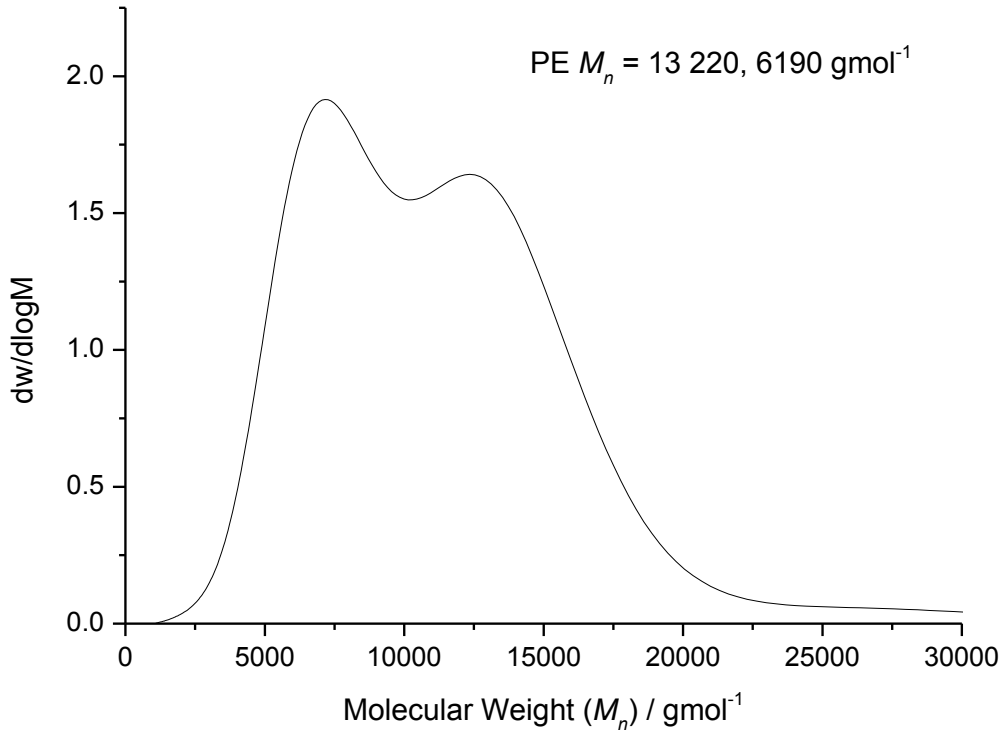

Figure 4.7: SEC trace for PE sample produced using **2**.

Additionally, the M_n values obtained for the polyester samples are lower than expected. This observation is typical in the field and has also been observed by other researchers using many different catalysts.[2,5,15]

SEC analysis is able to separate species due to size and the machine is calibrated using polystyrene standards. Therefore, the behaviour of PE and polystyrene are assumed to be alike. In actual fact, it is likely that the different polymers behave differently within the chromatography column and thus the M_n values recorded for PE are only a rough guide. However, the difference between polystyrene and PE cannot be solely responsible for the lower than expected M_n values recorded.

The unexpectedly low M_n for these polyester chains can also be explained by chain transfer reactions, which occur due to the presence of protic impurities, such as water, in the copolymerisation reaction. The source of water in these copolymerisation reactions is believed to be the solvent/monomer (CHO). Although it should be noted that the CHO is dried over $MgSO_4$ and fractionally distilled under N_2 and despite a lack of spectroscopic (^{1}H NMR spectroscopy) evidence of water, it may still be present within the monomer because the integrals of ^{1}H NMR spectroscopy are only accurate to ± 5 %. Additionally, it has been calculated that seemingly low levels of water (0.06 mol % or < 10 ppm by mass), in

comparison to the total amount of epoxide present, are all that is needed to produce polyester samples with an observed reduction in M_n.[5]

4.2.4 MALDI-ToF Mass Spectrometry

The MALDI-ToF spectrum of the polyester sample produced by catalyst **1a** (Table 4.1, Entry 1, M_n (PDI): 12670 (1.10) and 5470 (1.06) g/mol) conveys a bimodal distribution. The higher M_n polymer series (12670 g/mol by SEC) is not fully observed in the spectrum (only the lower molecular weight tail is recorded - red circles in Figure 4.8), which is likely to be due to the fact that the high M_n series have a lower propensity to volatilise. This is a commonly observed feature in MALDI-ToF analysis.[29]

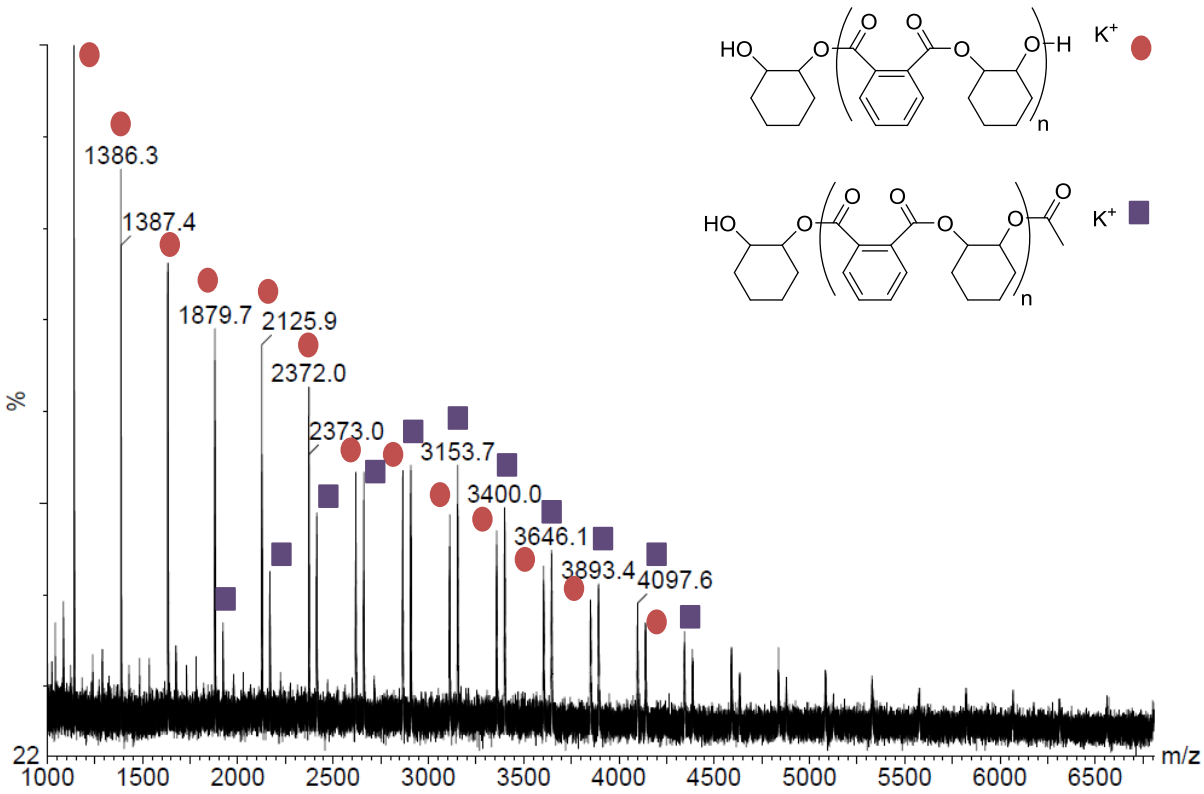

Figure 4.8: MALDI-ToF mass spectrum of the polyester sample formed by complex **1a** (Table 4.1, Entry 1).

The lower M_n polymer series (5470 g/mol by SEC) are α-acetyl-ω-hydroxyl end-capped and correspond well with the series observed in the MALDI-ToF mass spectrum with M_n of around 3153 amu. The higher M_n polymer series are α,ω-di-hydroxyl end-capped. The presence of the latter series infers that chain transfer reactions with cyclohexane-1,2-diol

(CHD) occur within the copolymerisation reactions. Therefore, suggesting that the water present in the CHO monomer reacts with CHO to form CHD, which acts as the chain transfer agent. The direct chain transfer with water seems unlikely because Zn-OH bonds are rare and unstable.[32]

Chains initiated from cyclohexane-1,2-diol are expected to have the same rate of propagation as chains initiated from the acetate groups (co-ligand of catalysts **1a** and **2**). However, the chains growing from cyclohexane-1,2-diol can do so from both hydroxyl moieties and thus form a telechelic polymer (Figure 4.9).[33] Therefore, the higher M_n series is associated with the telechelic polyester and thus the lower M_n series corresponds to chains initiated by the acetate co-ligand.[5,31]

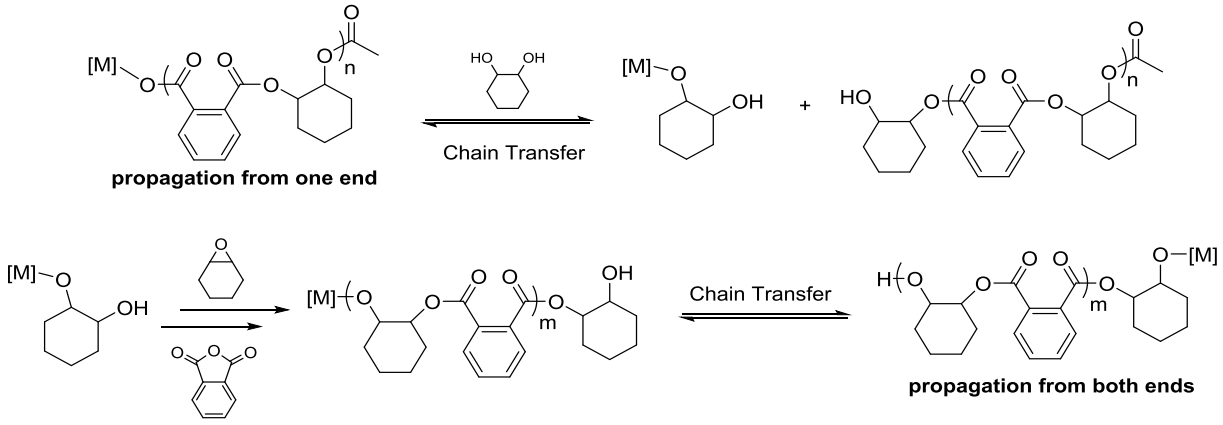

Figure 4.9: Illustrates chain transfer reactions in CHO/PA copolymerisation reactions with cyclohexane-1,2-diol (CHD).

4.3 ROCOP of CHO/PA in Toluene Solutions

The ROCOP of CHO/PA in toluene solutions ([PA] = 2.5 M) at 100 °C using both catalysts (**1a** or **2**) also produced polyester, poly(1,2-cyclohexylene-1,2-phthalate) (PE). However, under these reaction conditions the conversion of PA was very low even after 22 h. The observed conversions were 19 and 15 % for catalyst **1a** and **2**, respectively (determined by comparison of the integrals of the aromatic protons in phthalic anhydride and the polyester, in the ^{1}H NMR spectrum recorded). Compared to the reactions in neat conditions (97 % and 24 % PA conversion for catalyst **1a** and **2**, respectively, after 1 h), the copolymerisation reactions were much slower in toluene. Not only were low conversions obtained, but longer reaction times were required to achieve these poor conversions. These observations suggest

that the rate is proportional to CHO concentration, as when toluene is used as the solvent, the CHO monomer is in a diluted environment and thus unable to readily be in contact with the catalyst and hence the reaction rate becomes slower.

Table 4.2: Data for the ROCOP of CHO/PA initiated by catalysts **1a** or **2** in toluene solutions.

Cat.	Cat./CHO/PA	t /h	% PA Conversion [a), b)]	% Ester linkages[c)]	M_n[d)] /gmol^{-1}	M_n Calc. /gmol^{-1}	PDI[d)]
1a	1/100/100	22	19	83	3800	4670	1.11
2	1/100/100	22	15	82	2250	3690	1.17

Reactions were conducted at 100 °C, under N_2 atmosphere, in toluene (solvent), [PA] = 2.5 M. a) Determined by ^{1}H NMR spectroscopy ($CDCl_3$) by integrating the normalized resonances for PA (7.97 ppm) and the phenylene signals in PE (7.83-7.30 ppm). b) % Error in PA conversion was <3 % in all cases. c) Determined by ^{1}H NMR spectroscopy (DMSO-d_6) by integrating the normalized resonances for ester linkages (5.10-4.85, 4.66 and 3.46 ppm) and ether linkages (3.59 ppm). d) Determined by SEC in THF at 40 °C, calibrated using polystyrene standards.

The composition of the copolymer structures was determined by recording the ^{1}H NMR spectrum of the copolymer samples in DMSO-d_6. The resultant spectra show that in all cases the content of ester linkages is high (> 80 %), with a moderate (< 20 %) contamination of ether linkages in the polyester samples synthesised in toluene solutions (a representative example of a copolymer sample with ether linkage contamination is shown in Figure 4.10). This ether linkage contamination was not observed in the polyester samples produced in neat conditions and thus can also be attributed to dilution.

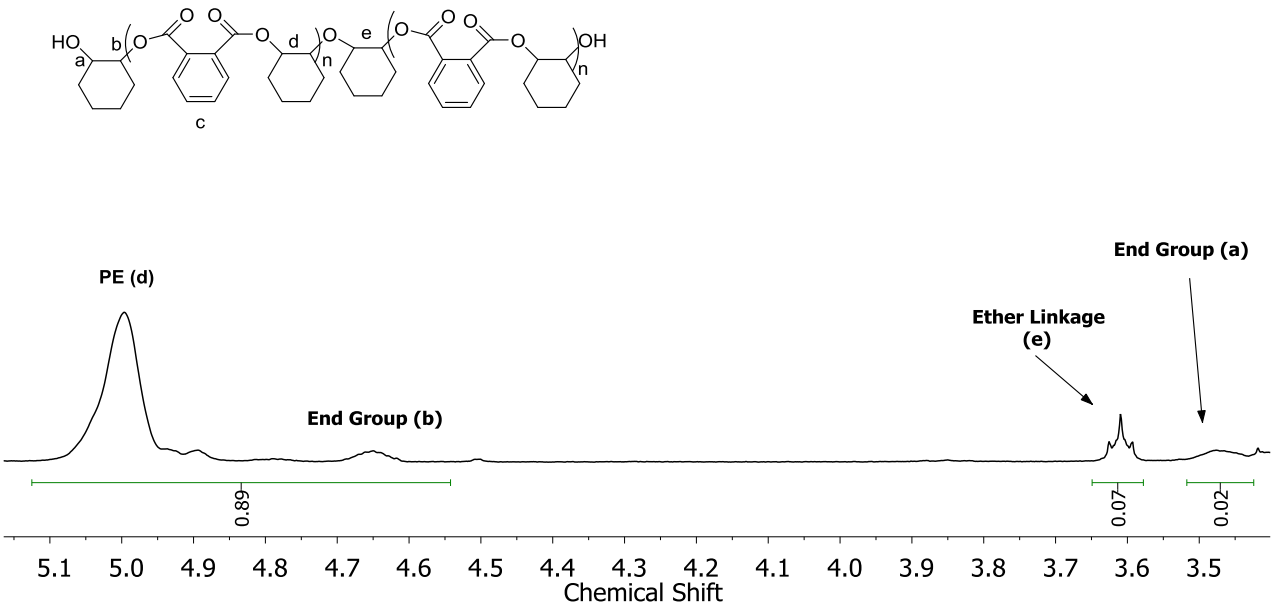

Figure 4.10: ^{1}H NMR spectrum of polyester (PE) in DMSO-d_6 (Table 4.2, Entry 1).

The polyester samples produced in toluene solutions have low M_n (< 5000 g/mol), which is due to the low conversion of PA achieved. SEC analysis showed monomodal distributions instead of bimodal distributions, which were observed in the polyester samples synthesised in neat conditions. It seems likely that this occurs because the conversions are sufficiently low that the two polymer series overlap and hence cannot be distinguished by SEC analysis. Additionally, the polyester samples have narrow polydispersity indices (< 1.2).

Interestingly, only a small number of chain transfer reactions seem to occur in the reactions performed in toluene solutions, unlike in the neat conditions, because the M_n values recorded are in good agreement with the calculated values (without any calibration correction), which assumes that on average one polymer chain is initiated per catalyst.[33]

4.4 Copolymerisation Kinetic Study

4.4.1 Aliquoting Reactions

A kinetic study of the ROCOP of CHO/PA in neat conditions was carried out by monitoring the copolymerisation reaction through aliquoting. Each aliquot was analysed by ^{1}H NMR spectroscopy to produce PA conversion *vs.* time plots. The PA conversion was determined by integrating the normalized phenylene resonances for PA (7.97 ppm) and for PE (7.83-7.30 ppm) in the ^{1}H NMR spectra recorded.

The PA conversion *vs.* time plots revealed a linear relationship (Figure 4.11), which indicates that for both catalysts **1a** and **2**, the rate of copolymerisation has a zero order dependence on PA concentration. The gradient values of these linear plots also verified that the magnesium catalyst (**1a** – 1.327 M/h) is roughly four times faster than the zinc catalyst (**2** – 0.324 M/h).

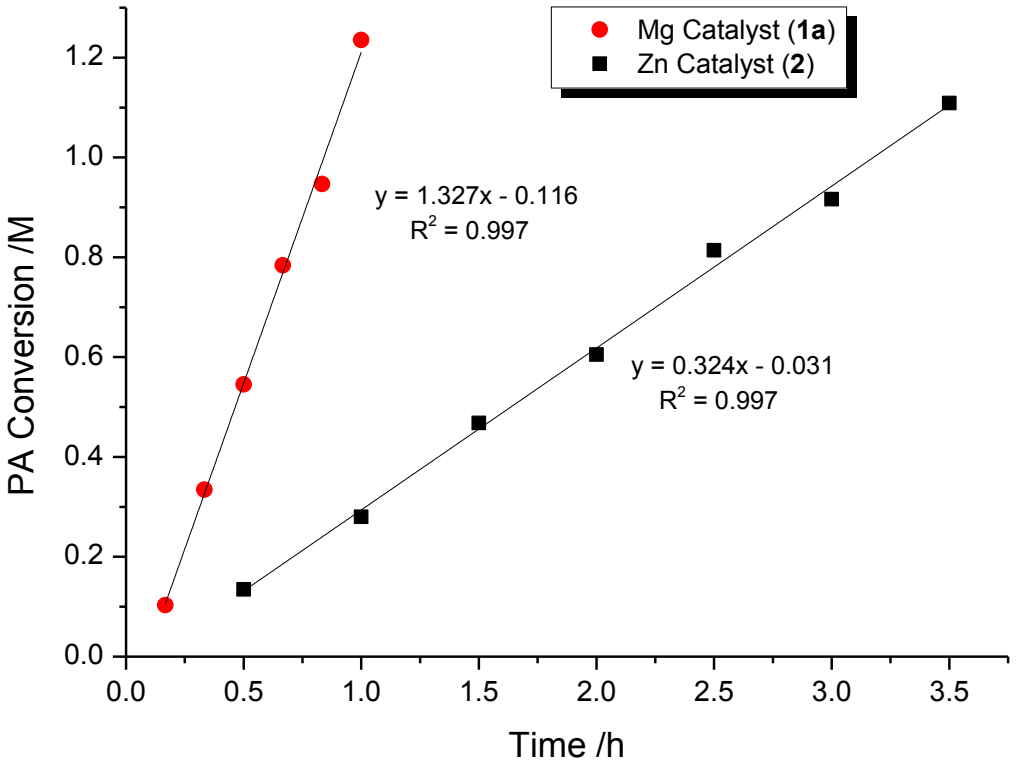

Figure 4.11: PA conversion *vs.* time plot for catalysts **1a** and **2** (determined by integrating the phenylene proton resonances in PA (7.97 ppm) and PE (7.83-7.30 ppm) in ^{1}H NMR spectra).

The aliquots taken from the CHO/PA copolymerisation reactions using catalysts **1a** and **2** were also analysed by SEC. The M_n *vs.* % PA conversion plots for both catalysts show a linear correlation (Figure 4.12), which indicates that both catalysts are able to exert good polymerisation control. Further evidence to support that these polymerisation reactions using catalysts **1a** and **2** are well controlled comes from the narrow polydispersity indices observed for the polyester samples produced (< 1.5).

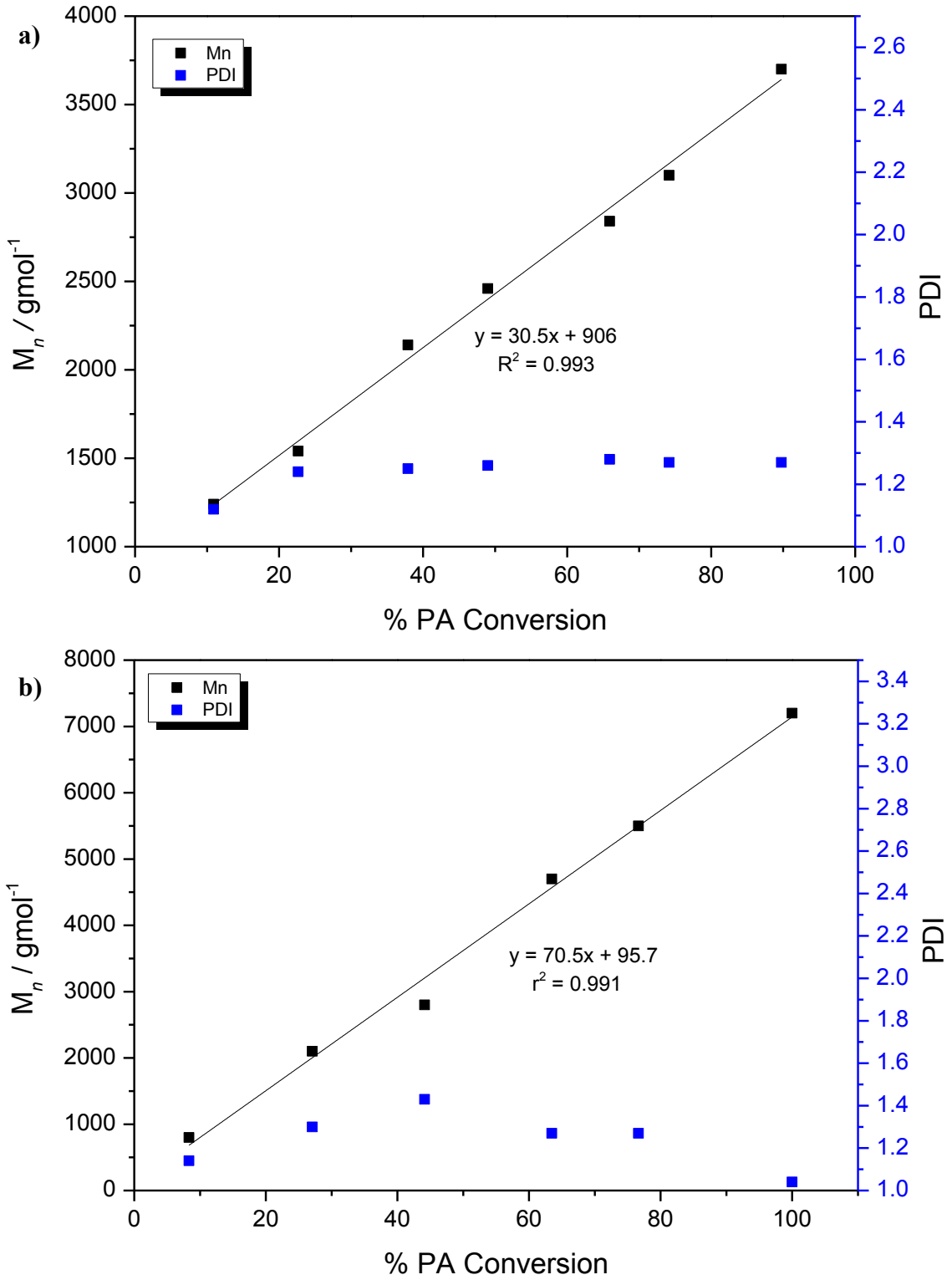

Figure 4.12: Evolution of M_n against PA conversion for ROCOP of CHO/PA initiated by catalyst **1a** (a) and **2** (b). Polymerisation conditions: catalyst:CHO:PA = 1:800:100, 100 ° C. At higher PA conversions, SEC data becomes bimodal and thus the higher M_n of the two peaks was plotted.

4.4.2 Monitoring by ATR-IR Spectroscopy

The concentration of PA, during CHO/PA copolymerisation reactions, was also monitored by an *in situ* ATR-IR probe, which enables continual monitoring of the IR spectra as the copolymerisation progresses (Figure 4.13). By observing the intensity of the resonances associated with PA (1860 and 1800-1770 cm^{-1}), a linear reduction in PA concentration *vs.* time was observed, which also supports the zero order rate dependence with respect to PA concentration found by ^{1}H NMR spectroscopy.

Thus, both ^{1}H NMR and IR spectroscopic data show that the rate of copolymerisation does not depend on the concentration of PA, indicating that PA insertion occurs faster than epoxide ring-opening and thus is not involved in the rate determining step in the ROCOP of CHO/PA (Figure 4.14). In previous polyester copolymerisation studies, the [(BDI)ZnOAc] catalyst also showed a zero order rate dependence on PA concentration.[18]

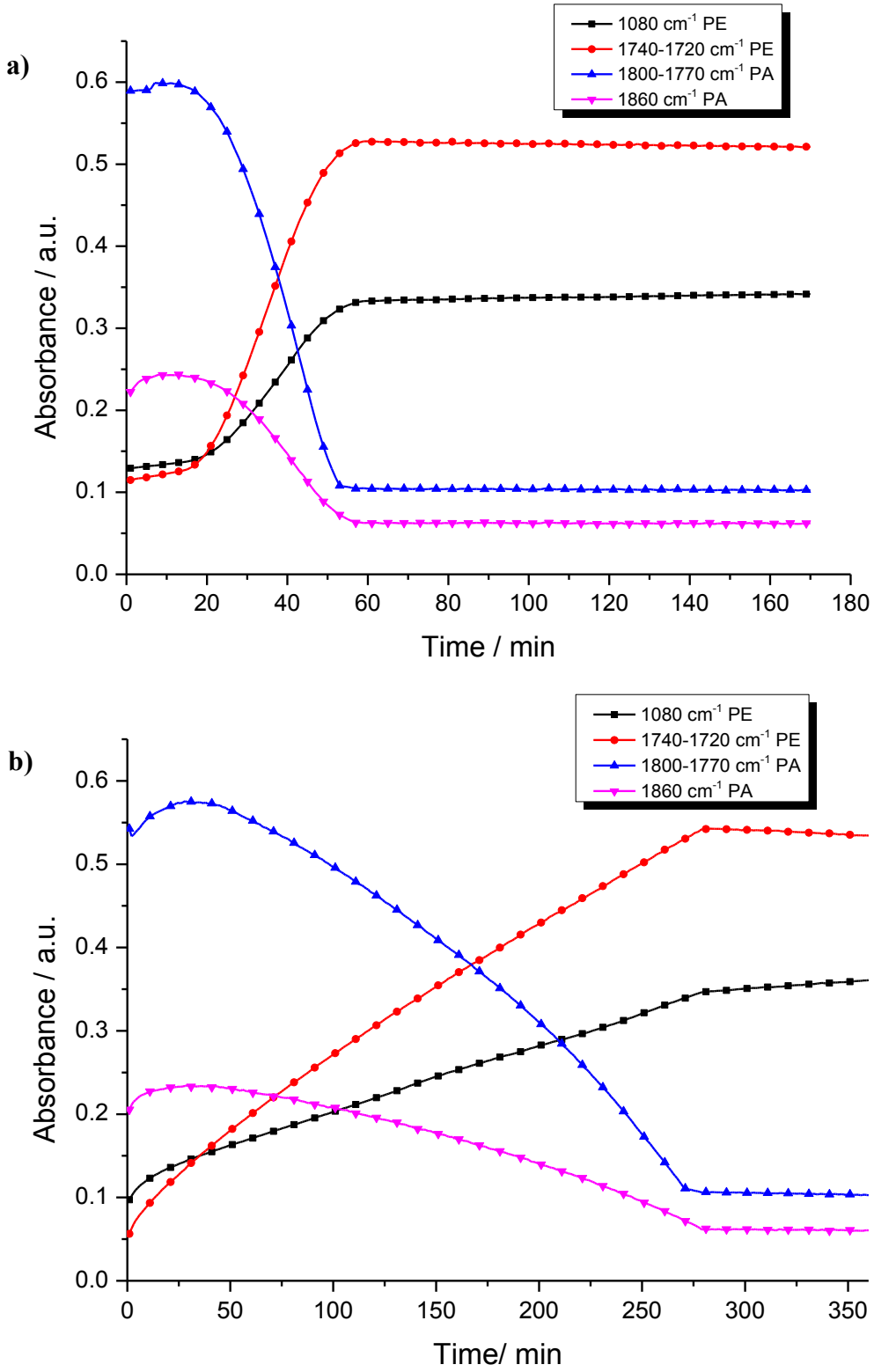

Figure 4.13: Graphs illustrating the change in intensity *vs.* time for various signals in the IR spectra recorded for the ROCOP of CHO/PA, using **1a** (a) and **2** (b). Polymerisation conditions: catalyst:CHO:PA = 1:800:100, 100 °C. Where PA = phthalic anhydride and PE = polyester. The increase in PA concentration observed initially occurs due to the time required for PA to dissolve in the injected CHO.

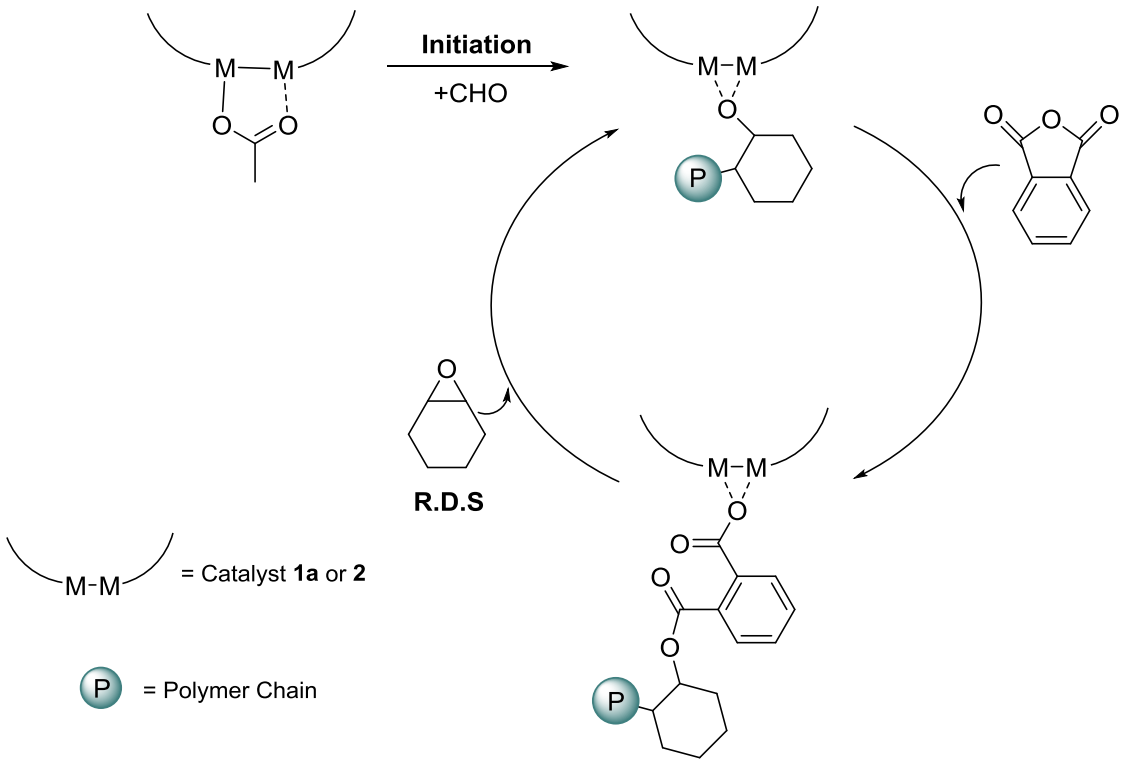

Figure 4.14: Proposed mechanism for CHO/PA copolymerisation reactions using **1a** and **2**, which indicates that the rate determining step is the ring opening of CHO.

4.5 Terpolymerisations

4.5.1 Results

The synthesis of block copolymers is highly desirable as they can be used in membrane synthesis, drug delivery, lithography and thermo-plastic elastomers.[34,35,36,37] Usually, these block copolymers are synthesised by the sequential addition of monomers or by using macroinitiators.[37,38] However, synthesising block copolymers in 'one pot' and without the use of macroinitiators would be highly desirable. This is because it can simplify the synthesis and lower costs. The previous results (Section 4.2-4.4) show the use of catalysts **1a** and **2** for the ROCOP of CHO/PA and these catalysts have been also been used for the ROCOP CHO/CO_2.[31,28] This prompted investigations into using catalysts **1a** and **2** for the terpolymerisation of CHO/PA/CO_2, using CHO as the solvent (Scheme 4.3).

A key question was whether a block or a random poly(ester-carbonate) would be formed. Other literature catalysts (zinc BDI, chromium salen, salphen and tetraphenylporphyrin complexes) active in both the ROCOP of epoxide/anhydride and epoxide/CO_2 have formed block copolymers when used in terpolymerisation reactions of epoxide/anhydride/CO_2 due to the catalyst preferentially reacting with the anhydride first to form a block of polyester and then reacting with CO_2 to form a block of polycarbonate (Section 4.1.4).[5,17,18]

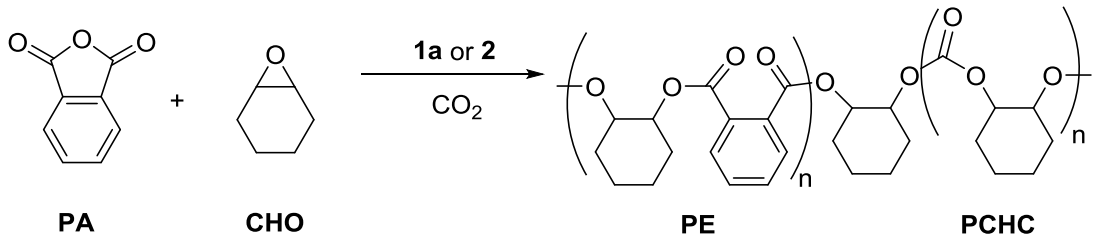

Scheme 4.3: The terpolymerisation of CHO, PA and CO_2 to produce a copoly(ester-carbonate) (PE-PCHC), using catalyst **1a** and **2** (catalyst structure illustrated in Scheme 4.1).

A mixture of CHO/PA (800/100), under 1 bar of CO_2, using either catalysts **1a** or **2** was heated to 100 °C. These polymerisations were monitored using an *in situ* ATR-IR spectroscopic probe. The graphs produced for both catalysts show that there were two stages during these polymerisation reactions. These two distinct stages show which monomer is

enchained within the growing copolymer chain, which is strongly indicative of block copolymer formation (Figure 4.15).

The first stage portrays a decrease in the PA concentration (1860 and 1800-1770 cm^{-1}) and an increase in the polyester (PE) signals is observed (1740-1720 and 1080 cm^{-1}). During the first stage the concentration of polycarbonate (PCHC) did not vary significantly (1014 and 1239-1176 cm^{-1}), which suggests little or no CO_2 was incorporated within the copolymer chain. Thus, the first stage of the polymerisation involves only the copolymerisation CHO/PA to form a block of polyester. There is a slight increase in the intensity of the signal at 1014 cm^{-1} during this polyester forming stage, which is probably due to the overlap of the PCHC signals with the polyester signals because they have similar frequencies (Figure 4.15).

Once all the PA was consumed (confirmed by ^1H NMR spectroscopy), the second stage of the polymerisation began, which involved an increase in intensity of the signals assigned to PCHC (1239-1176 and 1014 cm^{-1}). In this stage, the PA and polyester signals remained constant (slight increases in these signals are attributed to signal overlap with PCHC absorptions). This, therefore, suggests that the second stage of the polymerisation involves CHO/CO_2 copolymerisation to form a block of PCHC (Figure 4.15).

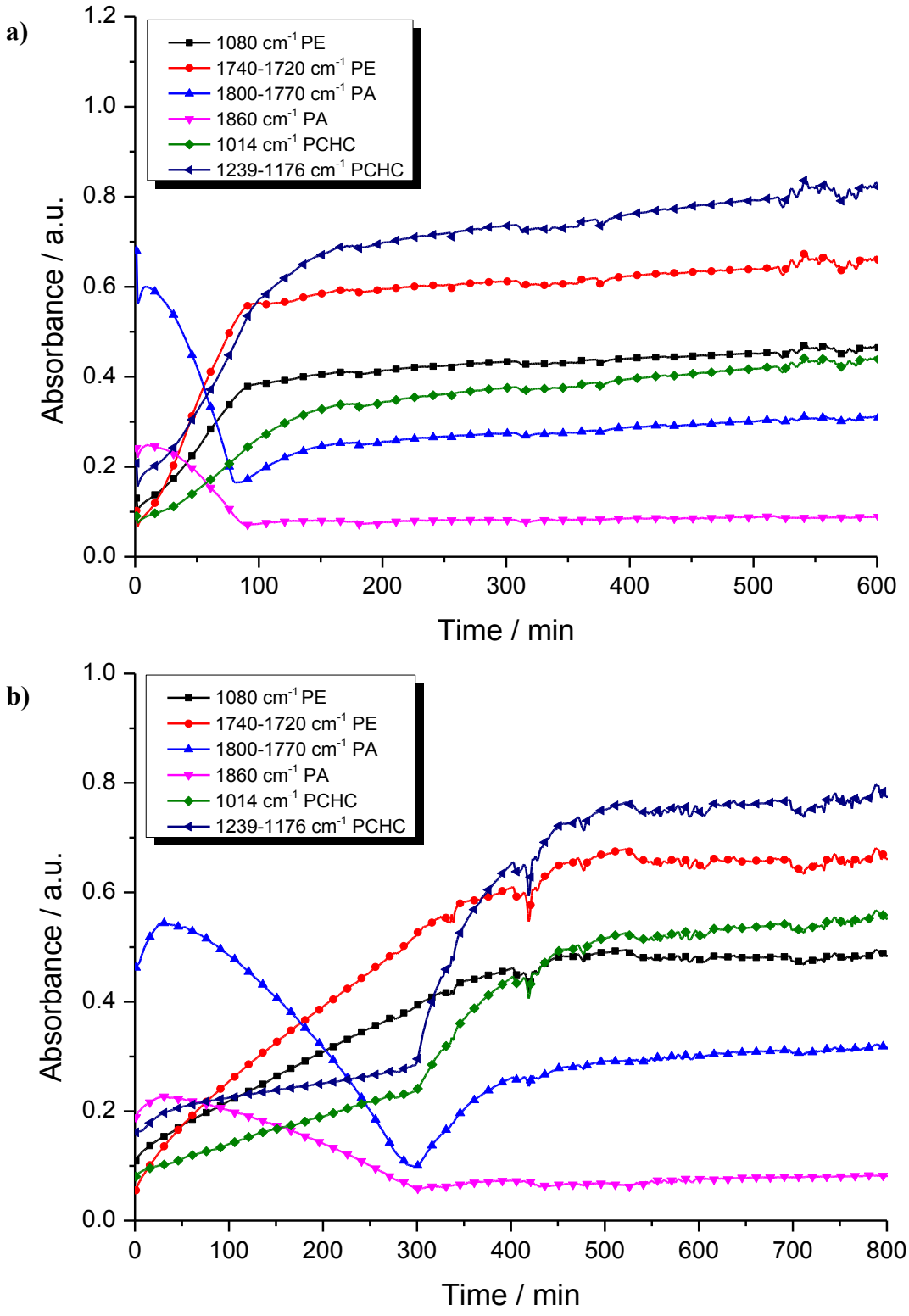

Figure 4.15: Shows the changes in the intensity of the ATR-IR resonances observed during the terpolymerisation of CHO, PA and CO_2 using catalyst **1a** (a) or **2** (b). Polymerisation conditions: catalyst:CHO:PA = 1:800:100 under 1 bar CO_2 at 100 °C. The baseline 'noise' observed after 500 mins (a) and 400 mins (b) results from an increase in sample viscosity due to the polymerisation reaction reaching relatively high conversions. Increase in PA concentration at the start is due to the time required for PA to dissolve in the injected CHO.

From the ATR-IR study (Figure 4.15), it seems likely that a block copoly(ester-carbonate) formed, particularly considering that PCHC is only formed after the PA is fully consumed. To further provide evidence for the formation of a block copolymer, aliquots were taken during the reaction and analysed by ^{1}H NMR spectroscopy. The first stage of the polymerisation, using catalyst **2**, only showed polyester signals at 7.83-7.30 ppm (aromatic protons) and 5.26-4.80 ppm (C*H* protons of the cyclohexyl unit in PE). Once the PA was fully consumed (loss of resonance at 7.97 ppm), the formation of PCHC occurred, which was observed by the evolution of a signal at 4.60 ppm. This, thus, further confirms that a block of polyester forms first and then the formation of a block of PCHC occurs.

However, in the case of catalyst **1a**, which is substantially faster than catalyst **2**, some carbonate repeat units were observed by ^{1}H NMR spectroscopy once the conversion of phthalic anhydride exceeded 95%. In the case of catalyst **2**, there is no evidence for the formation of any carbonate linkages until the PA was completely consumed (Figure 4.16). Both catalysts show < 5 % of cyclic carbonate by-product, and thus display a high selectivity for copolymer formation.

Other catalysts in the literature have also shown similar monomer selectivity in the terpolymerisations of CHO/PA/CO_2, such as, zinc β-diiminate,[18] chromium tetraphenylporphyrin,[5] chromium salen[17] and chromium salphen[5] catalysts (Section 4.1.4).

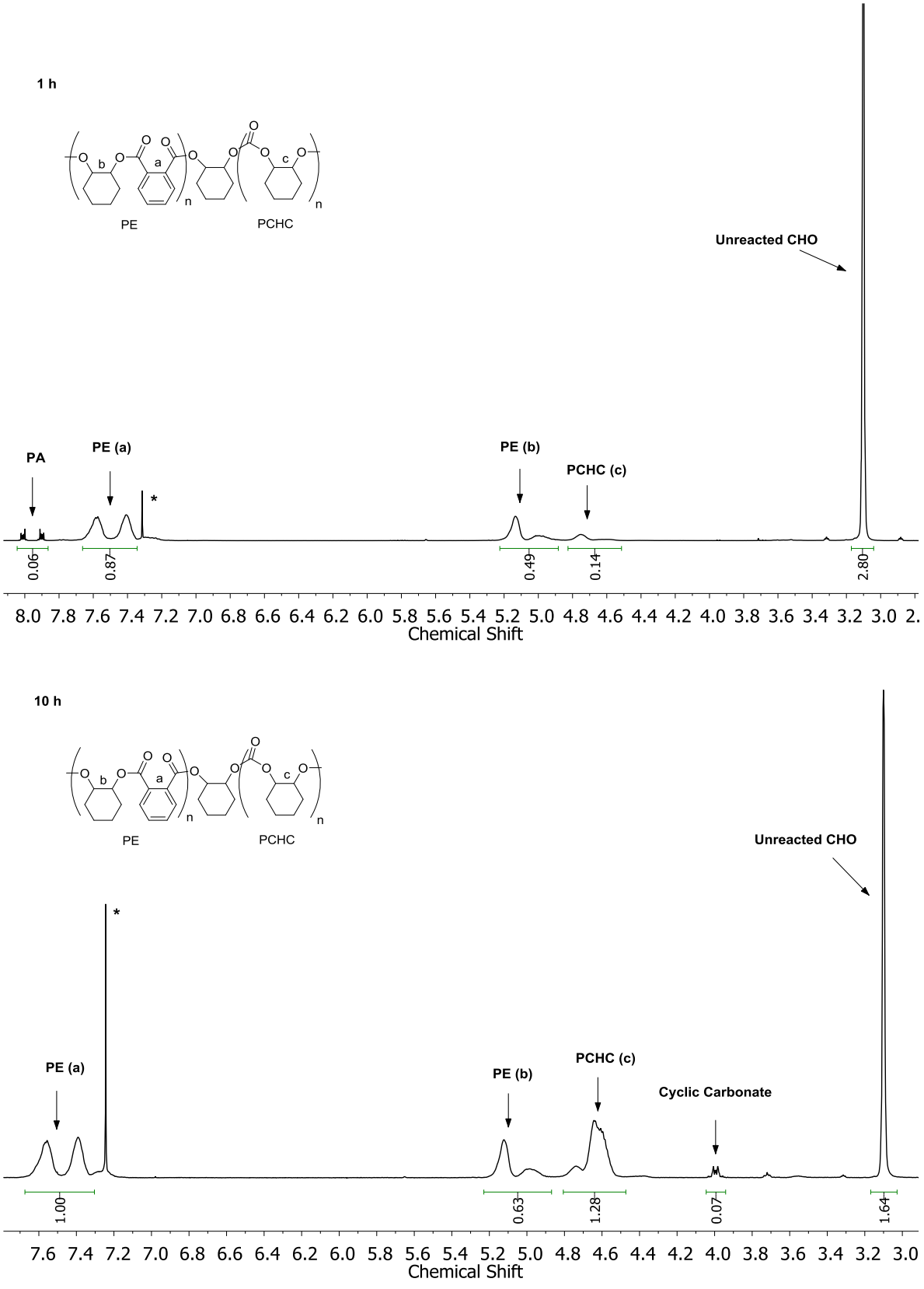

Figure 4.16: ^{1}H NMR spectra for terpolymerisation of CHO/PA/CO_2 using **1a** after 1 h (top) and 10 h (bottom). Reaction conditions: 1:800:100, catalyst:CHO:PA, 100 °C under 1 bar CO_2. Spectra show that PCHC forms when PA is still present in a low concentration (95% PA conversion).

4.6 Discussion

The observation discussed in Section 4.2, which shows that the rate of ROCOP of CHO/CO_2 is faster than the rate of the ROCOP of CHO/PA using **1a** and **2**, suggests that the activation energy barrier for the ring opening of CHO by a zinc/magnesium carboxylate group (k_2 in Figure 4.17) is higher compared to a zinc/magnesium carbonate group ($k_{2'}$ in Figure 4.17).

Moreover, the selectivity of enchaining PA into the growing copolymer chain before CO_2 (terpolymerisation reactions – Section 4.5) suggests that the rate of insertion of anhydride is considerably faster than that of CO_2 ($k_1 > k_{1'}$ in Figure 4.17). Kinetic studies using catalyst **1a** (Chapter 2) and catalyst **2** for CHO/CO_2 copolymerisations have shown that there is a zero order dependence of the rate on CO_2 pressure, over the range 1-40 bar.[33] Therefore, both the PA and CO_2 insertion steps are pre-rate determining steps. Additionally, the presence of the CO_2 does not significantly affect the polymerisation kinetics of polyester formation because the complete consumption of PA occurs approximately within 1 h for catalyst **1a** and 4 h for catalyst **2** as observed under a N_2 atmosphere (Table 4.1, Figure 4.13 and 4.15).

Within the terpolymerisation reactions for both catalysts, the metal alkoxide intermediate formed by the ring-opening of CHO can react either with PA or CO_2. However, the rate of the reaction with PA must be faster than that of CO_2 and hence a metal carboxylate species forms. The carboxylate reacts with CHO to form a metal alkoxide again. Only when all of the PA is consumed, the insertion of CO_2 into the metal alkoxide can occur to form polycarbonate.

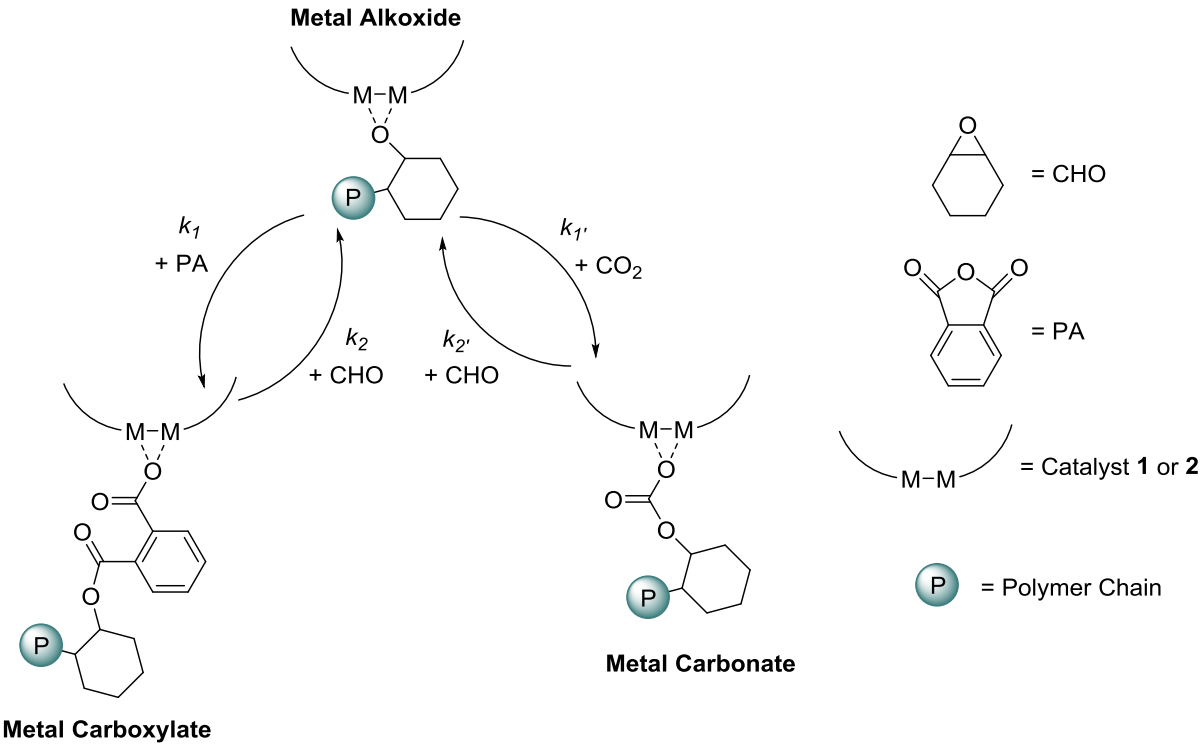

Figure 4.17: Proposed pathways for the ROCOP of CHO/CO_2 and CHO/PA. It is hypothesised that the relative order of rates is: $k_1 > k_1' >> k_2' > k_2$.

4.7 Characterisation of Block Copolymer

Verification of whether the PE and PCHC chains are attached to one another in the block copolymer synthesised, from terpolymerisation reactions of CHO/PA/CO_2, was carried out by MALDI-ToF mass spectrometry, SEC analysis, DOSY and ^{1}H NMR spectroscopy.

4.7.1 Molecular Weight (M_n)

MALDI-ToF mass spectrometry carried out on the block copolymers was unsuccessful and this could be due to the M_n of the block copolymers being too high (21600 and 22150 g/mol for **1a** and **2**, respectively) for this analytical technique.

The aliquots taken during the terpolymerisation reactions were not only analysed by ^{1}H NMR spectroscopy (Figure 4.16) but also by SEC analysis. An aliquot was taken after the complete consumption of PA (first stage) and after the formation of PCHC (second stage). Both traces obtained show a bimodal distribution (Figure 4.18), which arises due to chain transfer reactions occurring during the terpolymerisation reaction (*vide supra*). The M_n of both signals increase in the second aliquot, taken after PCHC formation, which suggests that both polymer

series can initiate and grow a carbonate block. This increase in M_n also indicates that the PCHC chains are likely to be attached to the PE chains (Figure 4.18). However, the highest M_n signal in the first trace overlaps with the lower M_n signal of the second trace and therefore contamination by homopolymers cannot be completely ruled out.

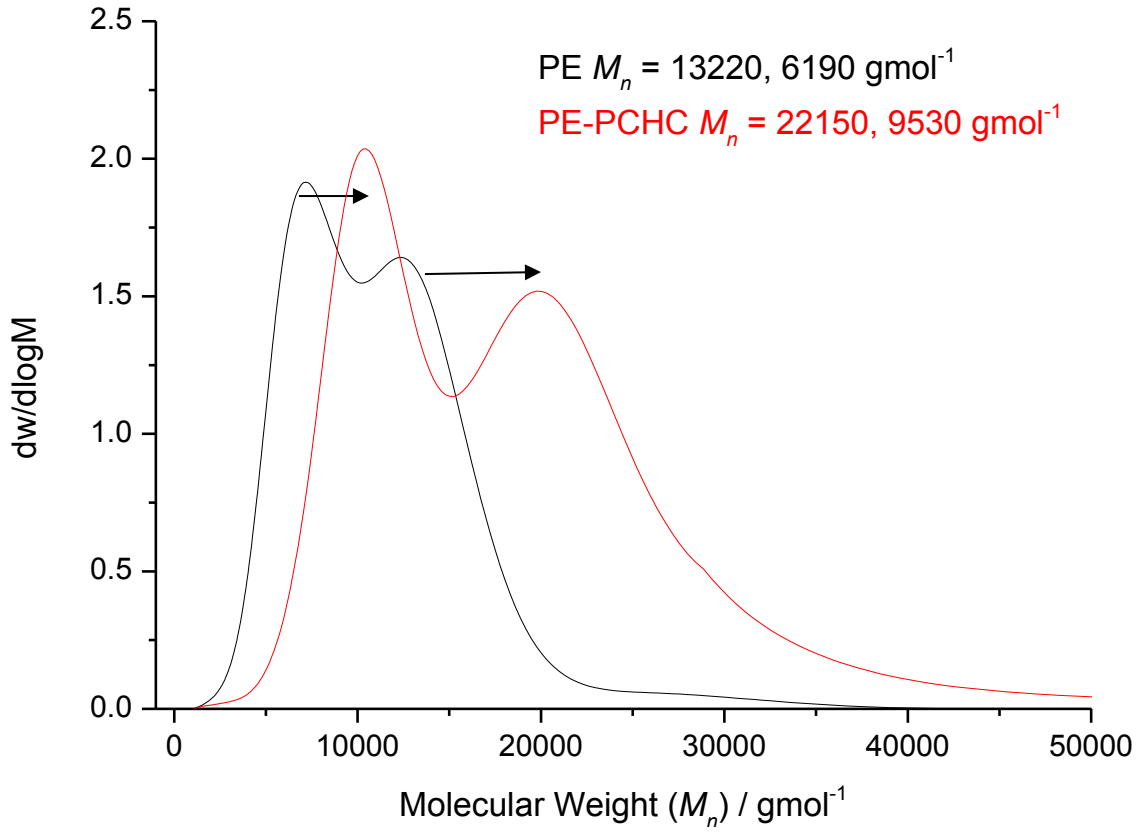

Figure 4.18: SEC trace for PE formation and PE-PCHC block copolymer formation using **2**.

4.7.2 NMR Spectroscopy

^{1}H NMR spectroscopy also suggests that there may be a slight contamination in the block copolymer with low M_n PE and PCHC chains. The relative composition of the PE and PCHC blocks in the block copolymer was calculated by integrating the PE signal at 5.26-4.80 ppm and the PCHC signal at 4.80-4.40 ppm. The ^{1}H NMR spectrum of the purified block copolymer samples showed that the PCHC integral reduced by 10 % compared to the crude block copolymer. Therefore, this indicates that after washing, some low M_n 'free' PCHC chains have been removed from the block copolymer sample.

The DOSY (diffusion ordered spectroscopy) spectra of the purified block copolymers and of a mixture of PE and PCHC with similar M_n values (≈ 8000 g/mol) were also recorded. The

DOSY spectrum (Figure 4.19) shows that the diffusion coefficient of the block copolymer synthesised by **1a** or **2** is smaller (1.23-1.18 x 10^{-10} m^2s^{-1}) compared to the diffusion coefficients of the PE and PCHC polymer chains in the mixture (1.69-1.67 x 10^{-10} and 1.89 - 1.86 x 10^{-10} m^2s^{-1}, respectively). This suggests that the block copolymer has a higher M_n than the individual PE and PCHC chains and thus diffuses more slowly. This also indicates that the PE and PCHC chains in the block copolymer are linked.

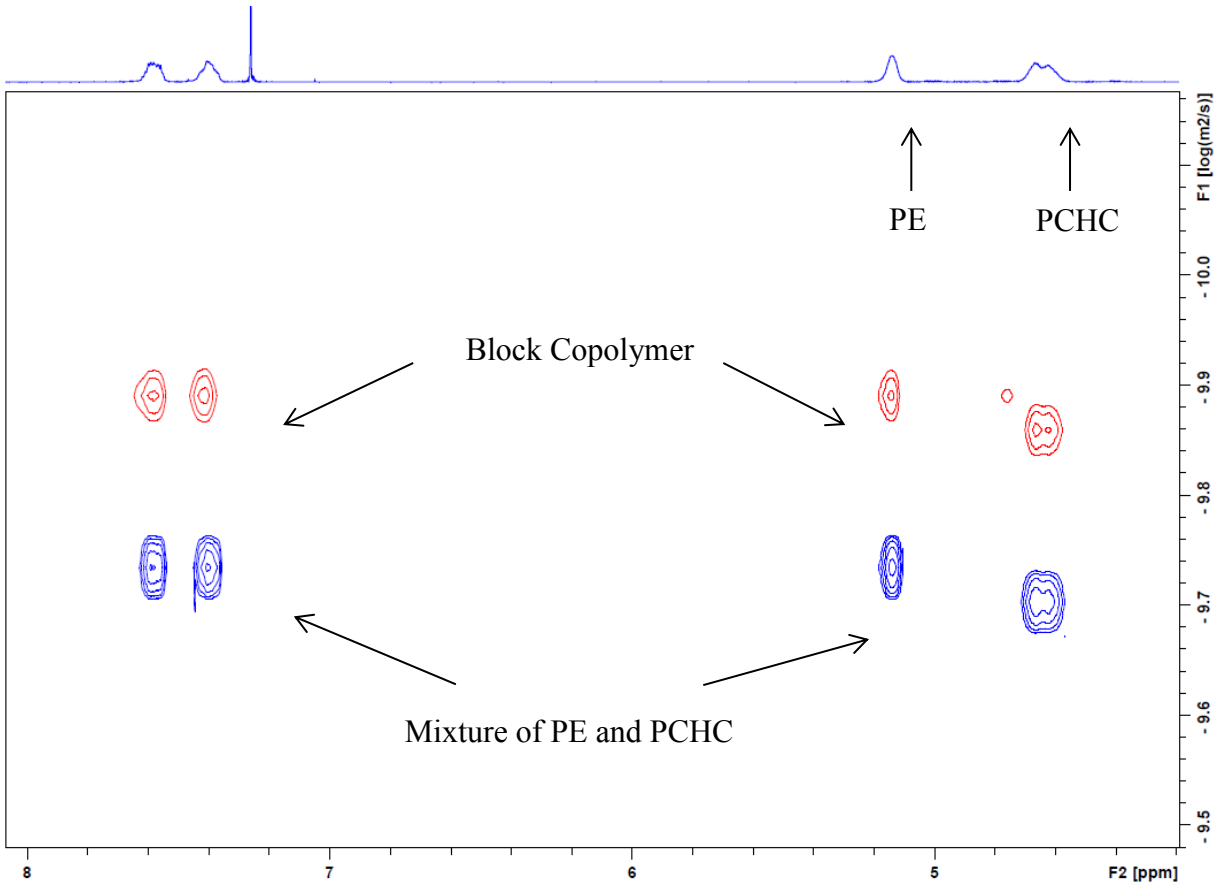

Figure 4.19: DOSY spectrum of block copolymer (red) and a mixture of PE and PCHC (blue) in $CDCl_3$. A ledbpgp2s pulse programme and an exponential method, with a one component fitting mode, diffusion time of 50 ms and gradient impulsion of 4 ms were used.

4.8 Thermal and Optical Analysis of Polymers

The polyester and block copolymers samples synthesised by both catalysts **1a** and **2** were analysed by thermal gravimetric analysis (TGA) and differential scanning calorimetry (DSC). The glass transition temperatures (T_g) of the polyester formed by catalyst **1a** and **2** are 57 and 84 °C, respectively and a T_g of 66 °C for PCHC using catalyst **2** was observed. These T_g values for PE and PCHC are lower than the values reported in literature (107 °C and 115 °C, respectively).[10,12] This is probably due to the lower M_n of the samples obtained. The literature PE sample had a M_n = 19 000 g/mol, which is substantially higher than the M_n of the PE obtained with catalysts **1a** and **2** (12 700 and 4200 g/mol, respectively).[5,17] A lowering in T_g values can also be due to the presence of metal in the copolymer samples from the catalyst used, but as these polymers were purified, the lower values are more likely to be due to the low M_n. Darensbourg and co-workers synthesised a PE sample with M_n of 18 000 g/mol, which had a T_g of 48 °C and thus it appears that the T_g values are somewhat dependent on the M_n and metal compositions. An important, unambiguous conclusion from all the data is that the T_g of PE is lower than the T_g of PCHC.[17]

The block copoly(ester-carbonates) (PE-PCHC) synthesised by catalysts **1a** and **2** show two T_d values (199/317 °C and 167/291 °C, respectively), which was expected as the constituent blocks should decompose at different temperatures. However, both block copolymers have only a single T_g value of 97 and 104 °C, for the copolymers produced by catalyst **1a** and **2**, respectively. This single T_g value therefore suggests that the blocks are miscible. This was also observed for the block copoly(ester-carbonates) synthesised using [TPPCrCl] by Duchateau and co-workers.[5] However, Darensbourg and co-workers obtained a block copolymer of CHO/PA/CO_2 with two T_g values of 48 °C and 115 °C (the former attributed for the PE block and the latter associated for the PCHC block).[17] This discrepancy again could be due to the difference in M_n, but these values were not reported in the literature.

The results in Table 4.3 also show that the block copolymers have substantially higher T_g values compared to the T_g values obtained for individual PE and PCHC chains. This is predominantly due to the M_n of the block copolymers being higher than the M_n of the PE and PCHC copolymer chains; however such high M_n values cannot easily be accessed whilst synthesising PE and PCHC individually due to chain transfer reactions. The significant

increase in T_g for the block copolymers is highly desirable as it widens the scope of applications that block copolymers can be used for.

Table 4.3: Thermal properties of selected polymers obtained from catalysts **1a** and **2**.

Polymers	M_n[a)] /gmol^{-1}	PDI	% ester[b)]	% carbonate[b)]	% ether[b)]	T_g /°C	T_d /°C
PCHC (Zn)	4040	1.16	0	> 99	<1	66	162
PE (Zn)	4200	1.14	>99	0	<1	57	316
PE (Mg)	12670 5470	1.03 1.08	>99	0	<1	84	351
PE-PCHC (Zn)	22150 9530	1.01 1.03	30	56	<1	104	199/317
PE-PCHC (Mg)	21610 8760	1.10 1.06	28	66	<1	97	167/291

a) Determined by SEC using polystyrene standards to calibrate the instrument. b) Determined by ^{1}H NMR spectroscopy by integrating the normalized resonances for ester (5.26-4.80 ppm), carbonate (4.80-4.40 ppm) and ether linkages (3.64-3.22 ppm). The T_d is reported at 50 % decomposition.

The polyester samples and block copolymers were also spin coated to form thin films. This was carried out by using 45 µL of a 10 mg/mL solution of the polymer in THF on a glass slide. The glass slide was spun in a spin coater at 500 rpm for 1 minute to form a thin film. The thin films appeared to be transparent from visual inspection (Figure 4.20) and the UV-Vis spectra of the thin films show that the films do not absorb light between 320-900 nm in wavelength (Appendix C).

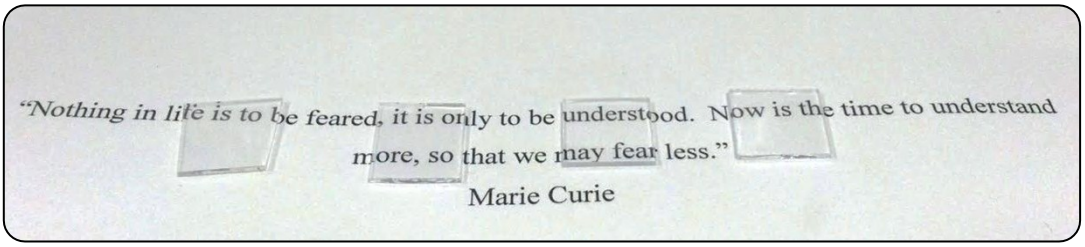

Figure 4.20: Photograph of thin films produced from PE, PCHC and block copolymer samples, overlaying a quote, which demonstrates their transparency.

4.9 Catalyst Sensitivity to Acid Impurities

Both Darensbourg and Duchateau have reported the use of phthalic anhydride in the copolymerisation of epoxide and anhydride to form polyesters. Additionally, both groups either used PA from Sigma Aldrich without further purification or recrystallized the PA once from chloroform.[5,14,16,17,19]

Initially, the PA used with catalysts **1a** and **2** was purified by sublimation (twice) and ^{1}H NMR spectroscopy showed no phthalic acid was present in the PA. Surprisingly, when using PA purified in this manner, the magnesium catalyst was four times slower than the zinc catalyst, which is opposite to the results found for these catalysts in CHO/CO_2 copolymerisation reactions.[28] Therefore, alternative purification routes were investigated. It was found that by dissolving PA in hot benzene, filtering the impurities and then recrystallizing the PA in chloroform, followed by subliming the anhydride once was sufficient in removing any impurities that could be inhibiting the magnesium catalyst.

The impurity removed was analysed by ^{1}H NMR spectroscopy and it was found to be phthalic acid and thus it seems that the magnesium catalyst is more sensitive to acidic impurities compared to the zinc counterpart. The zinc catalyst showed a very slight decrease in activity and thus is more robust compared to the magnesium catalyst.

4.10 Conclusions

Catalysts **1a** and **2** have shown activity in the ring opening copolymerisation (ROCOP) of CHO/PA. Observing activity in epoxide/anhydride copolymerisation reactions with catalyst **1a** is a significant result. This is because until now, magnesium catalysts (heterogeneous or homogeneous) have not been frequently used in these copolymerisation reactions, even though magnesium is cheap, abundant and its complexes usually lack colour and are redox stable. The magnesium analogue is four times faster than its zinc counterpart, under neat conditions, in CHO/PA copolymerisation reactions. This trend is similar to the relative rates observed with the same catalysts for the copolymerisation of CHO/CO_2. Both catalysts undergo well controlled polymerisation reactions that produce low M_n polyester samples. This arises due to the chain transfer reactions that occur during the polymerisation reactions. This is because cyclohexane-1,2-diol can act as a transfer agent in this polymerisation process and this is generated from the hydrolysis of CHO.

Both catalysts are also active for the terpolymerisations of CHO/PA/CO_2 and thus can form block copoly(ester-carbonates). ATR-IR spectroscopy revealed that the first block formed is PE, followed by PCHC. Therefore, the rate of enchaining PA is more facile compared to CO_2. SEC, DOSY and ^{1}H NMR analysis have shown that a block copolymer has formed. However, it seems that the block copolymer samples produced may be contaminated by homo-polyester and homo-polycarbonate chains.

Additionally, these purified terpolymers have a single glass transition temperature, ≈ 100 °C, which indicates miscibility of the blocks, but these values are higher than the T_g values obtained for individual PE and PCHC chains. This is due to the block copolymers possessing higher M_n, but these values cannot be reached when just copolymerising CHO/PA or CHO/CO_2 due to chain transfer reactions. This opens up many different avenues for the application of this block copolymer because it is more thermally resistant.

The different rates observed for both these catalysts (**1a** and **2**) in the copolymerisation of CHO/PA highlight the importance of which metal to select for these copolymerisations. Additionally, the rate has an effect on the selectivity and thus morphology of the resulting terpolymer produced. When using the magnesium catalyst and when the concentration of PA becomes low (5 % left) the competition between PA and CO_2 increases and hence a small gradient polymer block forms between the polyester and polycarbonate blocks. However, usually the incorporation of PA in the metal alkoxide is much more facile compared to CO_2. CO_2 insertion is highly reversible and non-rate limiting (Chapter 2), thus indicating that PA insertion is also not rate limiting.[17] This has also been suggested from the kinetic study, which revealed that the rate of CHO/PA copolymerisation using **1a** or **2** is zero order dependent on PA concentration.

4.11 Future Work

Further studies need to be carried out in order to gain more insight into the copolymerisation between epoxide and anhydrides. Firstly, different catalysts should be tested for the copolymerisation of epoxide/anhydride. Other zinc and magnesium catalysts reported in literature should be tested first, such as, the dinuclear zinc and magnesium catalysts reported by Xiao *et al.* (Figure 4.21).[39] Moreover, the other dinuclear catalysts reported by Williams and co-workers should also be explored in these copolymerisations, especially the cobalt[40] and heterodinuclear (Chapter 3) derivatives, which have a higher activity in CHO/CO_2 copolymerisation reactions compared to the homodinuclear zinc and magnesium analogues.[28,31,40]

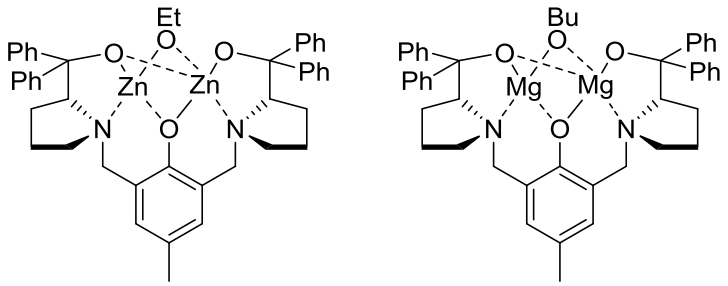

Figure 4.21: Bimetallic catalysts based on Trost's phenolate ligands by Xiao *et al.*[39]

Furthermore, modifying the copolymerisation reaction conditions should be investigated in order to promote polyol selectivity because polyester polyols are a highly desirable commodity. They can be used to synthesise higher polymers, such as, polyurethanes, which are used to make furniture, foams, adhesives and many other applications.[41]

Additionally, different anhydrides and epoxides need to be tested using catalysts **1a** and **2**. Varying the monomers will change the backbone of the copolymers formed and thus their properties, which will enable these polyesters to be used in a large scope of applications. Different properties are required for different applications, but generally, high T_g and T_d values are desired because the polymer can be used at high temperatures without degrading.[42]

Introducing aromaticity and rigid side units within the polyesters formed by using different anhydride and epoxide monomers (e.g. styrene oxide) can improve the T_g of the copolymers. Another modification can be to use unsaturated monomers (maleic anhydride, vinyl CHO) which can then undergo post-polymerisation reactions, such as, the common thiol-ene 'Click'

reaction.[43] These new copolymer structures will be interesting to explore, as their properties may be unique and useful in many different applications. Introduction of alcohol groups in the backbone of the polyesters may also lead to the formation of highly branched copolymers, which may be useful in medical applications.[41]

Finally, it is of interest to see if catalysts (**1a** and **2**) work with different epoxide monomers. When used for epoxide and CO_2 copolymerisation reactions, these catalysts are not easily transferable to different epoxides. However, if this is not observed in epoxide and anhydride copolymerisation reactions, this will be shed light on the reaction energy profiles of both copolymerisations.

4.12 References

1. M. Okada, *Prog. Polym. Sci.,* 2002, ***27***, 87-133; E. M. Aizenshtein, *Fibre Chem,* 2006, ***38***, 264-271; http://www.plasticseurope.org/documents/document/20131014095824-final_plastics_the_facts_2013_published_october2013.pdf, 15th October 2014.

2. A. M. DiCiccio and G. W. Coates, *J. Am. Chem. Soc.,* 2011, ***133***, 10724-10727.

3. N. Alemdar, B. Karagoz, A. T. Erciyes and N. Bicak, *J. Appl. Polym. Sci.,* 2010, ***116***, 165-171.

4. M. S. Kim, J. H. Kim, B. H. Min, H. J. Chun, D. K. Han and H. B. Lee, *Polym. Rev.,* 2011, ***51***, 23-52.

5. S. Huijser, E. HosseiniNejad, R. l. Sablong, C. D. Jong, C. E. Koning and R. Duchateau, *Macromolecules,* 2011, ***44***, 1132-1139.

6. A. Rodríguez-Galán, M. Vera, K. Jiménez, L. Franco and J. Puiggalí, *Macromol. Chem. Phys.,* 2003, ***204***, 2078-2089.

7. S. M. Aharoni In *Handbook of Thermoplastic Polyesters*; Wiley-VCH Verlag GmbH & Co. KGaA, 2005, pp 59-103.

8. M. H. Chisholm and Z. P. Zhou, *J. Mater. Chem.,* 2004, ***14***, 3081-3092.

9. O. Dechy-Cabaret, B. Martin-Vaca and D. Bourissou, *Chem. Rev.,* 2004, ***104***, 6147-6176.

10. C. K. Williams, *Chem. Soc. Rev.,* 2007, ***36***, 1573-1580.

11. T. Aida and S. Inoue, *J. Am. Chem. Soc.,* 1985, ***107***, 1358-1364.

12. T. Aida, K. Sanuki and S. Inoue, *Macromolecules,* 1985, ***18***, 1049-1055.

13. A. Bernard, C. Chatterjee and M. H. Chisholm, *Polym. J.,* 2013, ***54***, 2639-2646.

14. E. Hosseini Nejad, A. Paoniasari, C. E. Koning, R. Duchateau, E. Hosseininejad, A. Paoniasari, C. E. Koning and R. Duchateau, *Polym. Chem.,* 2012, ***3***, 1308.

15. R. C. Jeske, A. M. DiCiccio and G. W. Coates, *J. Am. Chem. Soc.,* 2007, ***129***, 11330-11331.

16. E. Hosseini Nejad, C. G. W. van Melis, T. J. Vermeer, C. E. Koning and R. Duchateau, *Macromolecules,* 2012, ***45***, 1770-1776.

17. D. J. Darensbourg, R. R. Poland and C. Escobedo, *Macromolecules,* 2012, ***45***, 2242-2248.

18. R. C. Jeske, J. M. Rowley and G. W. Coates, *Angew. Chem. Int. Ed.,* 2008, ***47***, 6041-6044.

19. E. H. Nejad, A. Paoniasari, C. G. W. van Melis, C. E. Koning and R. Duchateau, *Macromolecules,* 2013, ***46***, 631-637.

20. K. Yao and C. Tang, *Macromolecules,* 2013, ***46***, 1689-1712.

21. J. Liu, Y.-Y. Bao, Y. Liu, W.-M. Ren and X.-B. Lu, *Polym. Chem.,* 2013, ***4***, 1439-1444.

22. T. Aida and S. Inoue, *Acc. Chem. Res.,* 1996, ***29***, 39-48.

23. R. F. Fischer, *J. Polym. Sci. A Polym. Chem.,* 1960, ***44***, 155-172.

24. T. Tsuruta, K. Matsuura and S. Inoue, *Macromol. Chem. Phys.,* 1964, ***75***, 211-214.

25. Z. Hua, G. Qi and S. Chen, *J. Appl. Polym. Sci.,* 2004, ***93***, 1788-1792.

26. H. S. Suh, J. Y. Ha, J. H. Yoon, C.-S. Ha, H. Suh and I. Kim, *React. Funct. Polym.,* 2010, ***70***, 288-293.

27. J. Xu, Z.-L. Liu and R.-X. Zhuo, *J. Appl. Polym. Sci.,* 2006, ***101***, 1988-1994.

28. M. R. Kember and C. K. Williams, *J. Am. Chem. Soc.,* 2012, ***134***, 15676-15679.

29. P. K. Saini, C. Romain, Y. Zhu and C. K. Williams, *Polym. Chem.,* 2014, ***5***, 6068-6075.

30. K. G. Caulton and L. G. Hubert-Pfalzgraf, *Chem. Rev.,* 1990, ***90***, 969-995.

31. M. R. Kember, P. D. Knight, P. T. R. Reung and C. K. Williams, *Angew. Chem. Int. Ed.,* 2009, ***48***, 931-933.

32. W. Kuran and M. Czernecka, *J. Organomet. Chem.,* 1984, ***263***, 1-7.

33. F. Jutz, A. Buchard, M. R. Kember, S. B. Fredrickson and C. K. Williams, *J. Am. Chem. Soc.,* 2011, ***133***, 17395–17405.

34. G. Krausch and R. Magerle, *Adv. Mater.,* 2002, ***14***, 1579-1583.

35. N. Kumar, M. N. V. Ravikumar and A. J. Domb, *Adv. Drug Deliv. Rev.,* 2001, ***53***, 23-44.

36. D. Zschech, D. H. Kim, A. P. Milenin, R. Scholz, R. Hillebrand, C. J. Hawker, T. P. Russell, M. Steinhart and U. Gösele, *Nano Lett.,* 2007, ***7***, 1516-1520.

37. G. J. Domski, J. M. Rose, G. W. Coates, A. D. Bolig and M. Brookhart, *Prog. Polym. Sci.,* 2007, ***32***, 30-92.

38. N. Hadjichristidis *Block copolymers : synthetic strategies, physical properties and applications*; Wiley: New York; Chichester, 2002.

39. Y. Xiao, Z. Wang and K. Ding, *Chem. Eur. J.,* 2005, ***11***, 3668-3678; Y. Xiao, Z. Wang and K. Ding, *Macromolecules,* 2005, ***39***, 128-137.

40. M. R. Kember, F. Jutz, A. Buchard, A. J. P. White and C. K. Williams, *Chem. Sci.,* 2012; M. R. Kember, A. J. P. White and C. K. Williams, *Macromolecules,* 2010, ***43***, 2291-2298.

41. M. Ionescu *Chemistry and Technology of Polyols for Polyurethanes*; Smithers Rapra Technology.

42. D. Walton and P. Lorimer *Oxford Chemistry Primers:Polymers*; Oxford University Press: New York, 2000.

43. C. E. Hoyle and C. N. Bowman, *Angew. Chem. Int. Ed.,* 2010, ***49***, 1540-1573.

Chapter 5

Conclusion

"If I have seen further it is by standing on the shoulders of giants"
The Correspondence of Isaac Newton by Isaac Newton

5.1 Outlook

The field of ring opening copolymerisation (ROCOP) of epoxide and CO_2 has been developed over the past 45 years in response to the growing concerns of the diminishing supply of fossil fuels and the rising CO_2 levels in the atmosphere, which is triggering global warming.

Due to the high stability of CO_2, many catalysts have been developed for this process (ROCOP of epoxide/CO_2). The polycarbonates produced from these reactions can either be used in construction, textiles, and packaging or used to make higher polymers, such as, polyurethanes, which are used to make foams and adhesives. The most active catalysts to date are the bifunctional metal salen complexes. However, a class of bimetallic complexes have shown promise to becoming competitors to these well-known salen based catalysts. Our group has reported a series of homodinuclear catalysts for cyclohexene oxide (CHO)/CO_2 copolymerisation reactions. These catalysts are remarkable as they are active at only 1 bar CO_2 pressure.

This thesis describes in depth kinetic and mechanistic investigations carried out using the di-magnesium catalyst, previously reported by our group, in CHO/CO_2 copolymerisation reactions. The study reveals that this catalyst probably operates by the same reaction mechanism as the di-zinc catalyst also reported by our group. The TOF values recorded for both catalysts show that the magnesium derivative is in fact twice as fast as the zinc analogue, a finding which was corroborated by detailed kinetic analysis. This result highlights the importance of the metal used in the catalyst structure. There is a fine balance of electrophilicity needed at the metal centres in order to promote both epoxide binding and lability of the propagating bonds. The electrophilicity of the metals is determined by the ligand, co-ligands and the metal itself. In this instance, the ligand and co-ligand remained unchanged, thus establishing that the electrophilicity of the magnesium metal centres is more favourable at accelerating either epoxide binding or ring opening (or both), which require opposite electronic properties.

The mechanism proposed for these homodinuclear catalysts involves both metal centres and suggests that one metal centre carries out the epoxide binding/CO_2 insertion and the other

metal centre carries out the nucleophilic attack of the epoxide to promote ring opening. The copolymer chain 'shuttles' twice between each metal centre per catalytic cycle.

Looking at the initial rate of different di-magnesium catalysts with various co-ligands in CHO/CO_2 copolymerisation reactions has further supported the hypothesis that one co-ligand remains bound to the catalyst structure during copolymerisation reactions. This is because the initial rates recorded for all these catalyst derivatives varied, which suggests that the electronic nature of the metal centres is not the same. The ligand and metal centres remained constant and the only varying factor, which must have caused this difference in rate, is the co-ligand. Therefore, this suggests that a co-ligand remains bound to the metal centres during copolymerisation. It also implies that only one chain grows per catalyst as only one co-ligand seems to initiate the copolymerisation reaction.

The insight gained into the mechanism of these copolymerisation reactions led to several attempts to synthesise heterodinuclear catalysts and asymmetrical homodinuclear catalysts. This is because these changes will cause each metal centre within the macrocyclic cavity to have different electrophilicities. This will hopefully promote one metal centre to carry out one process (epoxide binding/ring opening) and the other metal centre to carry out the other process (nucleophilic attack of the epoxide/CO_2 insertion) and therefore, in theory, should improve the activity of the catalysts.

A heterodinuclear Zn-Mg catalyst was synthesised within a mixture of di-zinc and di-magnesium counterparts. This mixed catalyst system has an improved activity compared to the di-zinc and di-magnesium catalysts on their own and double the activity compared to a 50:50 mixture of these homodinuclear analogues.

Furthermore, this mixed catalyst system is robust to the addition of excess water. When water is added to the copolymerisation reaction, the catalyst system shows promise to forming polycarbonate polyols selectively, which can be used for polyurethane synthesis. This catalyst system also shows low activity for copolymer production in propylene oxide (PO)/CO_2 copolymerisation reactions, which has not been previously observed with the homodinuclear catalysts alone or in combination.

By modifying the macrocyclic ligand another Zn-Mg heterodinuclear complex and two asymmetrical homodinuclear zinc complexes have been synthesised and characterised. These complexes are not catalysts for CHO/CO_2 copolymerisation reactions and this inactivity is most likely to be due to the ligand modifications.

Finally, the homodinuclear di-magnesium and di-zinc catalysts have also been used in epoxide/anhydride copolymerisation reactions. The magnesium derivative is four times faster than the zinc analogue in CHO/phthalic anhydride (PA) copolymerisations under neat conditions. The natural progression to synthesising block copoly(ester-carbonates) by using mixtures of epoxide, anhydride and CO_2 was also successful. The block copolymers formed show distinctively higher T_g values (> 90 °C) compared to their constituent polycarbonate or polyester chains (< 85 °C).

5.2 Future Directions for the Field

As discussed in Chapter 2, 3 and 4, much more work needs to be carried out to further understand the mechanism of epoxide/CO_2 copolymerisation reactions using the bimetallic catalysts synthesised by our group. Additionally, several synthetic routes need to be explored in order to attempt to synthesise a pure sample of a Zn-Mg heterodinuclear catalyst and other heterodinuclear complexes. Moreover, many more epoxides, anhydrides and ring opening copolymerisation reactions need to be tested with these homodinuclear catalysts in order to see how versatile these bimetallic catalysts are and to establish if a diverse range of polymer products can be synthesised with these catalysts.

However, even though the activity of the heterodinuclear mixed catalyst system is superior to its homodinuclear counterparts, it is still not sufficiently active at 1 bar CO_2 pressure. Therefore, next generation catalysts need to be synthesised, which record TOF values exceeding 10 000 h^{-1}. To coincide with this key criterion, the cost and time to synthesise these catalysts needs to be minimised. There are still many parameters that can be investigated, such as, different ligand motifs, co-ligands, co-catalysts and metals.

Furthermore, these new catalysts need to be robust and transferable to many different epoxides. So far, most catalysts are tested using CHO and PO, which are petrochemically

derived. There is an interest and need to attempt copolymerisations using renewable epoxides and more research into using catalysts with such epoxides needs to occur.

Finally, if the catalysts for the ROCOP of epoxide and CO_2 can be used in multiple ring opening copolymerisation reactions, this will enhance the variety of copolymers produced by a single catalyst, which is highly desirable by industry. Moreover, these catalysts will also have the potential to produce block copolymers, which have advantageous properties for industrial applications. Therefore, more investigations into using catalysts in multiple ring opening copolymerisation reactions also needs to occur.

Chapter 6

Experimental

"A man who dares to waste one hour of time has not discovered the value of life."
The Life and Letters of Charles Darwin by Charles Darwin

6.1 General Procedures

6.1.1 Materials and Methods

Unless stated, all reactions were carried out in air. Specifically stated anhydrous reactions were conducted under nitrogen using either a nitrogen filled glovebox or standard anaerobic techniques (Schlenk line). All solvents and reagents were purchased from commercial sources (Alfa Aesar, Sigma Aldrich, Strem and VWR) and were used as received unless otherwise stated.

Solvents hexane, THF and toluene were dried by distilling over sodium and benzophenone and stored under nitrogen. DCM, propylene oxide (PO), d_6-benzene, $CDCl_3$, d_2-TCE, d_8-THF, d_8-toluene were distilled from CaH_2 and stored under nitrogen. Cyclohexene oxide (CHO) was dried over $MgSO_4$ for 16 h and then filtered and distilled and stored under nitrogen. All solvents, CHO and PO were thoroughly degassed, by performing several freeze-thaw cycles. Phthalic anhydride purchased from Sigma Aldrich (98% purity) was purified by dissolving it in hot benzene and filtering impurities, followed by re-crystallising from chloroform and subliming once. CP grade (99.99 %) carbon dioxide (BOC) was used for copolymerisation studies at high pressure, which was passed through a VICI P600-1 CO_2 gas purifying column. Research grade (100 %) carbon dioxide (BOC) was used for low pressure copolymerisation studies, which passed through a drierite column. High pressure copolymerisation reactions were carried out in a Parr 5513 100 mL bench reactor.

6.1.2 Measurements

Unless otherwise stated, ^{1}H and ^{13}C $\{^{1}H\}$ NMR spectra were produced from a Bruker AV-400 instrument and chemical shifts are reported as ppm. Elemental analysis was carried out by Mr. Stephen Boyer at London Metropolitan University, Science Centre, Holloway Road, London, N7 2DD. SEC data was determined by using a Polymer Labs PL GPC-60 instrument, with THF as the eluent, at a flow rate of $1mLmin^{-1}$ and at 40 °C. Two Polymer Labs mixed D columns were used in series. Narrow M_w polystyrene standards were used to calibrate the instrument. MALDI-ToF and ESI mass spectrometry was determined by Ms. Lisa Haigh at Imperial College London. MALDI-ToF was carried out on a Waters/Micromass MALDI micro MX spectrometer using a dithranol matrix, KOAc as the cationizing agent in a 1:1 loading in THF. ESI was carried out on a LCT Premier Waters

machine with a capillary voltage of 2000V, a desolvation gas flow of 400 L/h and source temperature of 120 °C. All IR spectra were performed neat on a Perkin Elmer Spectrum 100 ATR-IR instrument. *In situ* ATR-IR measurements were performed on a Mettler-Toledo ReactIR 4000 spectrometer equipped with a MCT detector and a silver halide DiComp probe. DSC data was recorded on a Perkin Elmer DSC 4000 instrument. TGA measurements were carried out on a Perkin Elmer Pyris 1 TGA 4000 instrument under a flow of nitrogen and a heating rate of 10 °C/min. UV-Vis data was recorded on a Perkin Elmer UV-Vis 450 instrument.

6.2 Synthesis of Pro-Ligands

4-*Tert*-butyl-2,6-diformylphenol[1]

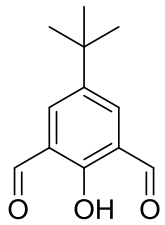

4-*Tert*-butyl-phenol (11.02 mL, 66.6 mmol) and hexamethylenetetramine (14.94 g, 106.6 mmol) were placed in a round bottom flask and TFA (52 mL, 692 mmol) was added slowly to this reaction mixture, whilst stirring. The reaction mixture was left to reflux for 16 h at 125 °C. Then by using a Dean-Stark condenser the mixture was refluxed for 4 h at 150 °C, in order to drive the reaction equilibrium by removal of any water. The reaction mixture was cooled to 100 °C and 3M HCl was added (100 mL). The resulting mixture was refluxed for a further 40 minutes at 100 °C and then cooled to 25 °C and placed in the freezer overnight. The precipitate was filtered, washed with cold MeOH (-78 °C) and dried under vacuum.

4-tert-butyl-2,6-diformylphenol (yellow crystals, 6.41 g, 46 %); δ_H ($CDCl_3$, 400 MHz) 11.50 (s, 1H, O*H*), 10.26 (s, 2H, O=C*H*), 8.00 (s, 2H, Ar-*H*), 1.37 (s, 9H, Ar-C-CH_3); *Literature:* [1] δ_H ($CDCl_3$, 400 MHz) 11.50 (s, 1H, O*H*), 10.27 (s, 2H, O=C*H*), 8.00 (s, 2H, Ar-*H*), 1.38 (s, 9H, Ar-C-CH_3).

5-*Tert*-butylsalicylaldehyde[2]

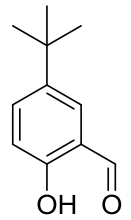

To a mixture of 4-*tert*-butyl-phenol (14.89 mL, 90 mmol), Et_3N (47.7 mL, 337.5 mmol), $MgCl_2$ (12.87 g, 135 mmol) and paraformaldehyde (18.9 g, 607.5 mmol), THF (100 mL) was added. The reaction mixture was refluxed for 24 h. Then the mixture was cooled to 25 °C and 1M HCl (100 mL) was added to quench it. The product was extracted by using EtOAc (3 x 50 mL). The organic layers were washed with brine and dried (Na_2SO_4). The solvent was removed *in vacuo* and the product was purified by flash column chromatography (solvent system 4:1, EtOAc:Hexane).

5-Tert-butylsalicylaldehyde (yellow oil, 13.33 g, 82 %); δ_H ($CDCl_3$, 400 MHz) 10.90 (s, 1H, O*H*), 9.90 (s, 1H, O=C*H*), 7.60 (dd, 1H, Ar-*H*, $^3J_{HH}$ = 8.0 & $^4J_{HH}$ = 3.0 Hz), 7.53 (d, 1H, Ar-*H*, $^4J_{HH}$ = 2.6 Hz), 6.95 (d, 1H, Ar-*H*, $^3J_{HH}$ = 9.0 Hz), 1.35 (s, 9H, Ar-C-CH_3); *Literature:*[2] δ_H ($CDCl_3$, 200 MHz) 10.86 (s, 1H, O*H*), 9.88 (s, 1H, O=C*H*), 7.58 (dd, 1H, Ar-*H*, $^3J_{HH}$ = 10.0 & $^4J_{HH}$ = 2.0 Hz), 7.51 (d, 1H, Ar-*H*, $^4J_{HH}$ = 2.0 Hz), 6.93 (d, 1H, Ar-*H*, $^3J_{HH}$ = 10.0 Hz), 1.32 (s, 9H, Ar-C-CH_3).

3-Bromomethyl-5-*t*-butylsalicylaldehyde[3]

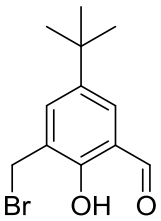

Several drops of conc. H_2SO_4 were added to a mixture of paraformaldehyde (0.76 g, 25.2 mmol), 5-*t*-butylsalicylaldehyde (3.0 g, 16.8 mmol) and 48 wt% HBr (22.5 mL). The reaction mixture was refluxed at 70 °C for 24 h. Then, the reaction mixture was cooled to 25 °C and water (20 mL) was added. The product was extracted with DCM (3 x 20 mL) and the organic layers were dried (Na_2SO_4). After filtration, the solvent was removed to yield a brown oil, which solidified upon standing.

3-Bromomethyl-5-t-butylsalicylaldehyde (brown semi-solid, 3.32 g, 71 %); δ_H ($CDCl_3$, 400 MHz) 11.35 (s, 1H, O*H*), 9.93 (s, 1H, O=C*H*), 7.67 (d, 1H, Ar-*H*, $^4J_{HH}$ = 2.4 Hz), 7.54 (d, 1H, Ar-*H*, $^4J_{HH}$ = 2.6 Hz), 4.63 (s, 2H, CH_2), 1.37 (s, 9H, Ar-C-CH_3); *Literature:*[3] δ_H ($CDCl_3$, 300 MHz) 11.35 (s, 1H, O*H*), 9.92 (s, 1H, O=C*H*), 7.66 (d, 1H, Ar-*H*, $^4J_{HH}$ = 2.5 Hz), 7.53 (d, 1H, Ar-*H*, $^4J_{HH}$ = 2.5 Hz), 4.61 (s, 2H, CH_2), 1.36 (s, 9H, Ar-C-CH_3).

N,N'-dibenzyl-2,2-dimethylpropane-1,3-diamine hydrochloride salt[4]

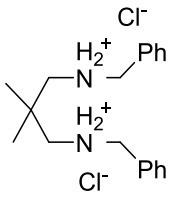

2,2 Dimethyl-1,3-propanediamine (2 mL, 16.6 mmol), benzaldehyde (3.4 mL, 33.2 mmol), triethylamine (5 mL, 36.52 mmol), Na_2SO_4 (1.25 g) and DCM (80 mL) were left to stir at 25 °C for 16 h. The reaction mixture was then filtered and evaporated to dryness, which yielded a pale yellow oil. The product was taken up in MeOH (60 mL) and $NaBH_4$ (2.5 g, 66.1 mmol) was added to the solution slowly. The reaction mixture was then left to stir for two hours and water (30 mL) was added to the reaction mixture and the pH of the solution was recorded to be 10-11. If this pH was not obtained, 2M NaOH was added to the reaction mixture until the desired pH was obtained. The MeOH was then evaporated and the product was extracted with DCM (3 x 20 mL). The organic layers were washed with brine (20 mL) and dried ($MgSO_4$). The filtrate was evaporated to dryness, which produced a clear oil. The product was purified by taking it up in diethyl ether (40 mL) and adding a few drops of conc. HCl. A white precipitate was produced, which was filtered and dried *in vacuo*.

N,N'-dibenzyl-2,2-dimethylpropane-1,3-diamine hydrochloride salt (white powder, 3.98 g, 68 %); δ_H (D_2O, 400 MHz) 7.20-7.35 (m, 10H, Ar-*H*), 3.85 (s, 4H, CH_2), 2.75 (s, 4H, CH_2), 0.90 (s, 6H, CH_3); *Literature (as amine):*[4] δ_H ($CDCl_3$) 7.21 (m, 10H, Ar-*H*), 3.68 (s, 4H, CH_2), 2.37 (s, 4H, CH_2), 0.84 (s, 6H, CH_3).

2,2-Dimethyl-*N*,*N*'-di(propan-2-yl)propane-1,3-diamine oxalic acid salt[5]

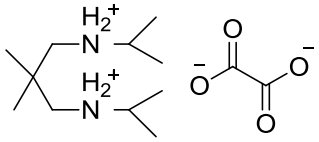

2,2-Dimethyl-1,3-propanediamine (3 mL, 25 mmol), acetone (4.04 mL, 54.97 mmol), acetic acid (5.72 mL, 100 mmol) and $NaBH(OAc)_3$ (15.9 g, 75 mmol) were added to a round bottom flak and left to stir for 3 days. The reaction mixture was quenched with 1M NaOH (400 mL) and the product was extracted with diethyl ether (3 x 40 mL). The organic layers were washed with brine (30 mL) and dried ($MgSO_4$). The filtrate was reduced and a clear oil formed. The crude product was taken up in MeOH (40 mL) and 2 equivalents of oxalic acid (3.20 g, 35.4 mmol) were dissolved in the resulting solution and left to stir for 3 h. The resulting white precipitate was filtered and dried *in vacuo*.

2,2-Dimethyl-N,N'-di(propan-2-yl)propane-1,3-diamine oxalic acid salt (white amorphous powder, 5.31 g, 82 %); δ_H (D_2O, 400 MHz) 3.39 (m, 2H, C*H*), 2.98 (s, 4H, CH_2), 1.26 (d, 12H, CH_3, $^3J_{HH}$ = 6.0 Hz), 1.09 (s, 6H, CH_3).

2,2-dimethyl-N_1,N_3-bis(pyridin-2-ylmethyl)-1,3-diaminopropane[6]

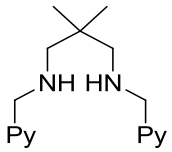

2,2-Dimethyl-1,3-diaminopropane (3.14 mL, 26.2 mmol) was refluxed in methanol (60 mL) and a solution of 2-pyridinecarboxaldehyde (5.00 mL, 52.3 mmol) in methanol (15 mL) was added dropwise to the refluxing solution. The reaction mixture was heated for a further 16 h and then cooled to 0 °C. Then $NaBH_4$ (5.00 g, 132 mmol) was added slowly to the reaction mixture over 2 h. The reaction mixture was then refluxed for 3 h and the solvent was removed. The residue was dissolved in water (100 mL), extracted into DCM (3 x 50 mL), dried (Na_2SO_4) and the solvent removed *in vacuo*.

The crude product was dissolved in methanol (100 mL) and oxalic acid (6.00 g, 66.6 mmol) was added to the solution and stirred at 25 °C for 30 minutes. The resulting, pale yellow precipitate was collected and washed with methanol (3 x 50 mL). The white precipitate was dissolved in water (250 mL), treated with NaOH (6.29 g, 157 mmol) and stirred at 25 °C for

16 h. The product was extracted into DCM (3 x 50 mL), dried (Na_2SO_4) and the solvent removed under reduced pressure to obtain the product as a yellow oil.

2,2-dimethyl-N_1,N_3-bis(pyridin-2-ylmethyl)-1,3-diaminopropane (yellow oil, 3.85 g, 52 %); δ_H ($CDCl_3$, 400 MHz) 8.52 (d, 2H, Py-*H*, $^4J_{HH}$ = 4.4 Hz), 7.57-7.65 (m, 2H, Py-*H*), 7.33 (d, 2H, Py-*H*, $^3J_{HH}$ = 7.8 Hz), 7.08-7.18 (m, 4H, Py-*H*), 3.90 (s, 4H, NCH_2Py), 2.48 (s, 4H,CCH_2N), 0.95 (s, 6H, C(CH_3)$_2$); δ_C ($CDCl_3$, 100 MHz) 160.4 (*CPy*), 149.2 (*CHPy*), 136.5 (*CHPy*), 122.1 (*CHPy*), 121.8 (*CHPy*), 59.0 (C*C*H$_2$N), 56.0 (N*C*H$_2$Py), 35.0 (*C*(CH$_3$)$_2$), 24.8 (C(*C*H$_3$)$_2$); Anal. Calc. for $C_{17}H_{24}N_4$: C, 71.79; H, 8.51; N, 19.70. Found: C, 71.78; H, 8.43; N, 19.68; MS (ESI): m/z 285 ([M+H]$^+$, 100 %).

Preparation of $[H_4L^1](ClO_4)_2$[7]

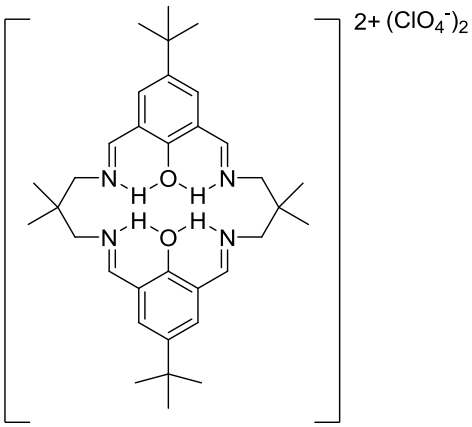

4-*Tert*-butyl-2,6-diformylphenol (1.20 g, 5.8 mmol), $NaClO_4$ (2.81 g, 23.2 mmol), acetic acid (0.66 mL, 11.6 mmol) and MeOH (90 mL) were placed in a round bottom flask and heated to 70 ^oC. When the reaction mixture began to boil, 2,2-dimethyl-1,3-propanediamine (0.70 mL 5.8 mmol) in MeOH (30 mL) was added dropwise over 1 h. After the addition of the amine, the reaction mixture was cooled to 25 °C and stirred for 16 h. The resulting red/orange solution was reduced in volume (by three quarters) and left to stand for 16 h. The red crystalline precipitate formed was filtered and washed with cold MeOH (-78 ^oC).

[H_4L^1](ClO_4)$_2$ (red/orange crystals, 1.85 g, 43 %); δ_H (*d*$_6$-DMSO, 400 MHz) 13.60 (br s, 4H, N*H*/O*H*), 8.70 (d, 4H, N=C*H*, $^3J_{HH}$ = 13.0 Hz), 7.66 (s, 4H, Ar-*H*), 3.88 (s, 8H, CH_2), 1.29 (s, 12H, CH_3), 1.15 (s, 18H, CH_3); *Literature:*[7] δ_H (*d*$_6$-DMSO, 400 MHz) 13.61 (br s, 4H, N*H*/O*H*), 8.68 (d, 4H, N=C*H*), 7.66 (s, 4H, Ar-*H*), 3.87 (s, 8H, CH_2), 1.28 (s, 12H, CH_3), 1.15 (s, 18H, CH_3).

Preparation of $[H_2L^1]$[7]

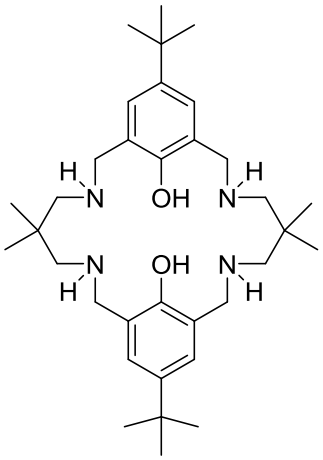

$[H_4L^1](ClO_4)_2$ (1.75 g) was suspended in MeOH (180 mL) and $NaBH_4$ (2.65 g, 70 mmol) was added slowly to the reaction mixture. The resulting colourless solution was left to stir for 1 h. Then, water (approx. 80 mL) was added to the solution until a white precipitate persistently appeared. The mixture was left to crystallise over 16 h. The white crystalline precipitate was filtered and dried under vacuum in the presence of phosphorous pentoxide (desiccant).

[H₂L¹] (white crystals, 1.03 g, 69 %); δ_H ($CDCl_3$, 400 MHz) 6.96 (s, 4H, Ar-*H*), 3.76 (s, 8H, C*H*$_2$), 2.54 (s, 8H, C*H*$_2$), 1.27 (s, 18H, C*H*$_3$), 1.03 (s, 12H, C*H*$_3$); *Literature:*[7] δ_H ($CDCl_3$, 400 MHz) 6.95 (s, 4H, Ar-*H*), 3.76 (s, 8H, C*H*$_2$), 2.53 (s, 8H, C*H*$_2$), 1.27 (s, 18H, C*H*$_3$), 1.02 (s, 12H, C*H*$_3$).

Asymmetric Pro-ligand 1

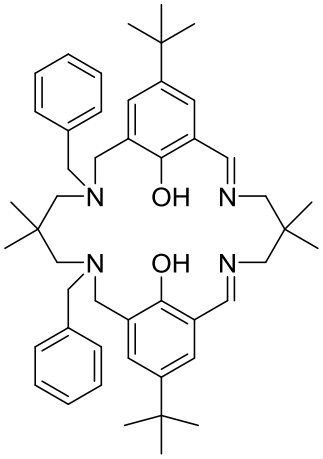

N,*N*'-Dibenzyl-2,2-dimethylpropane-1,3-diamine hydrochloride salt (1.0 g, 2.8 mmol) and caesium carbonate (1.83 g, 5.6 mmol) were added to MeOH (70 mL) and left to stir at 25 °C for 16 h. The solution was reduced and the residue was taken up in DCM (50 mL) and washed with water (3 x 25 mL). The organic layer was then dried ($MgSO_4$) and the solvent was removed *in vacuo*, which yielded *N*,*N*'-dibenzyl-2,2-dimethylpropane-1,3-diamine (a clear oil). This amine (0.52 g, 1.85 mmol) was added to THF (75 mL) containing *N*,*N*-diisopropylethylamine (0.65 mL, 3.70 mmol) and stirred for half an hour. Then, 3-bromomethyl-5-*t*-butylsalicylaldehyde (1.01 g, 3.70 mmol) was added to the solution and this reaction mixture was left to stir for 16 h. The solution turned pale yellow and a white precipitate formed. The reaction mixture was filtered and the filtrate was reduced, which produced a yellow gummy solid. This diformyl product was then dissolved in MeOH (50 mL) and a solution of 2,2-dimethyl-1,3-propanediamine in MeOH (25 mL) was added dropwise. The reaction mixture was then left to stir for 16 h at 25 °C. The yellow precipitate was filtered and dried under vacuum.

Asymmetric Pro-ligand 1 (yellow amorphous powder, 0.90 g, 89 %); δ_H ($CDCl_3$, 400 MHz) 8.34 (br s, 2H, C=N*H*) 7.10-7.70 (m, 14H, Ar-*H*), 3.70 (br s, 4H, CH_2), 3. 60 (br s, 4H, CH_2), 3.50 (br s, 4H, CH_2), 2.40 (br s, 4H, CH_2), 1.33 (s, 18H, CH_3), 1.07 (br s, 6H, CH_3), 0.70 (br s, 6H, CH_3); δ_C ($CDCl_3$, 100 MHz) 166.1 & 165.4 (*C*H=N), 159.0 (Ar-*C*-OH), 157.0 & 156.9 (Ar-*C*-CH=N), 141.7, 140.4, 140.2 & 140.0 (Ar-*C*-CH_2-N), 133.2, 129.3, 128.5, 128.1, 127.8, 126.7 & 126.3 (Ar-*C*H), 118.0 & 117.6 (Ar-*C*-^{t}Bu), 71.8, 68.3, 64.6, 63.9, 60.5, 54.1 & 51.0 (*C*H_2), 36.3 & 36.1 (*C*-Me_2), 34.0 & 33.8 (*C*-^{t}Bu), 31.5 (^{t}*Bu*), 25.6, 24.9, 24.4 & 24.2 (*C*H_3); υ_{max}/cm^{-1} 2960 & 2871 (s, aromatic and aliphatic C-H stretch), 1631 (s, C=N stretch), 1463 (s, aromatic C=C stretch and aliphatic C-H bending), 1362 & 1274 (s, C-N stretch), 733 (s,

aromatic C-H bending); Calc. for $C_{48}H_{64}O_2N_4$: C, 79.08; H, 8.85; N, 7.68; Found: C, 79.49; H, 8.97; N, 7.21 %; MS (ESI): m/z 729 ($[M+H]^+$, 100 %).

Asymmetric Pro-ligand 2

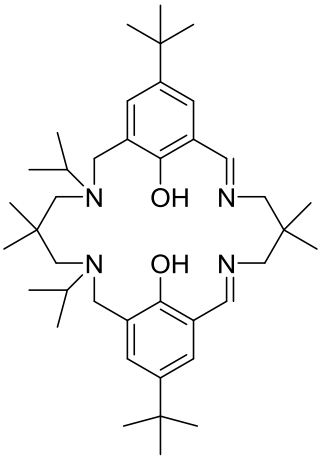

2,2-Dimethyl-*N*,*N*'-di(propan-2-yl)propane-1,3-diamine oxalic salt (1.0 g, 3.6 mmol) and caesium carbonate (2.36 g, 7.2 mmol) were added to MeOH (50 mL) and left to stir at 25 °C for 16 h. The solution was dried *in vacuo* and the residue was taken up in DCM (50 mL) and filtered. The filtrate was evaporated to dryness, which yielded 2,2-dimethyl-*N*,*N*'-di(propan-2-yl)propane-1,3-diamine (a pale yellow oil). This amine (0.38 g, 2.1 mmol) was added to THF (75 mL) containing *N*,*N*-diisopropylethylamine (0.72 mL, 4.1 mmol) and stirred for half an hour. Then 3-bromomethyl-5-*t*-butylsalicylaldehyde (1.12 g, 4.1 mmol) was added to the solution and this reaction mixture was left to stir for 16 h. The solution turned pale yellow and a white precipitate was formed. The reaction mixture was filtered and the filtrate evaporated to dryness, which produced a gummy yellow solid. This diformyl product (1.0 g, 1.8 mmol) was then dissolved in MeOH (75 mL) and a solution of 2,2-dimethyl-1,3-propanediamine (0.22 mL, 1.8 mmol) in MeOH (25 mL) was added dropwise. The reaction mixture was then left to stir for 16 h at 25 °C. The yellow precipitate formed was filtered and dried *in vacuo*.

Asymmetric Pro-ligand 2 (yellow amorphous powder, 0.50 g, 49 %); δ_H ($CDCl_3$, 400 MHz) 8.40 (br s, 2H, C=N*H*) 7.93 (br s, 2H, Ar-*H*), 7.15 (br s, 2H, Ar-*H*), 3.82 (br s, 4H, CH_2), 3.50 (br s, 4H, CH_2), 2.78 (m, 2H, C*H*) 2.43 (br s, 4H, CH_2), 1.35 (s, 18H, CH_3), 1.10 (br s, 6H, CH_3), 1.01 (br s, 12H, CH_3), 0.92 (br s, 6H, CH_3); δ_C ($CDCl_3$, 100 MHz) 166.2 & 166.1 (*C*H=N), 160.1 (Ar-*C*-OH), 157.0 & 156.8 (Ar-*C*-CH=N), 140.7 (Ar-*C*-CH_2-N), 132.1,

129.1, 128.3 & 125.5 (Ar-*C*H), 117.3 (Ar-*C*-^{t}Bu), 68.3, 60.26, 59.4, 58.6, 52.4 & 52.2 (*C*H_2), 50.6 (*C*H-(CH_3)$_2$), 36.3 (*C*-Me_2), 34.1 (*C*-^{t}Bu), 31.6 & 31.4 (*^{t}Bu*), 24.9 & 24.5 (*C*H_3), 18.2 (*C*H_3); υ_{max}/cm^{-1} 2956 & 2874 (s, aromatic and aliphatic C-H stretch), 1631 (s, C=N stretch), 1462 (s, aromatic C=C stretch and aliphatic C-H bending), 1364 & 1270 (s, C-N stretch), 747 (s, aromatic C-H bending); Calc. for $C_{40}H_{64}O_2N_4$: C, 75.90; H, 10.19; N, 8.85; Found: C, 76.43; H, 10.38; N, 8.56 %; MS (ESI): m/z 633 ([M+H]$^+$, 25 %).

Half Macrocycle Pro-Ligand 1

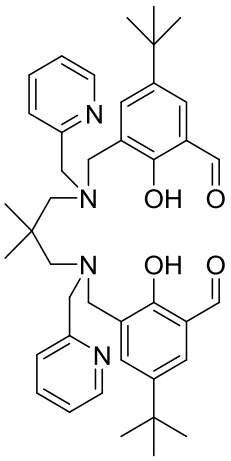

3-Bromomethyl-5-*t*-butylsalicylaldehyde (3.05 g, 11.2 mmol) was dissolved in THF (120 mL) and a solution of 2,2-dimethyl-*N*$_1$,*N*$_3$-bis(pyridin-2-ylmethyl)-1,3-diaminopropane (1.60 g, 5.63 mmol) and Et_3N (4.70 mL, 33.8 mmol) in THF (20 mL) was added over 5 h. The yellow suspension was stirred for 16 h at 25 °C and the yellow precipitate was filtered and washed with THF. The solvent was removed from the filtrate under reduced pressure to produce the crude product as a yellow solid.

To purify the crude product, an aqueous solution of HCl (37 %, 80 mL) was added to the product and the mixture was stirred for 15 min and extracted with DCM (3 × 50 mL). The aqueous phase was made alkaline with an aqueous solution of NaOH (20 %, 200 mL) and the product was extracted into DCM (3 x 100 mL). The organic layers were washed with saturated brine (100 mL) and dried (Na_2SO_4) and the solvent removed under reduced pressure. Then the product was purified by column chromatography, over silica with a mixture of DCM and MeOH (9:1) as the eluent (R_f = 0.54).

Half Macrocycle Pro-Ligand 1 (yellow amorphous solid, 2.41 g, 64 %); δ_H ($CDCl_3$, 400 MHz) 11.81 (br. s, 2H, O*H*), 10.33 (s, 2H, C*H*O), 8.54 (d, 2H, Py-*H*, $^4J_{HH}$ = 3.9 Hz), 7.63 (td,

2H, Py-*H*, $^{3}J_{HH}$ = 7.7 & $^{4}J_{HH}$ = 1.7 Hz), 7.58 (d, 2H, Ar-*H*, $^{4}J_{HH}$ = 2.4 Hz), 7.42 (d, 2H, Ar-*H*, $^{4}J_{HH}$ = 2.0 Hz), 7.28 (d, 2H, Py-*H*, $^{3}J_{HH}$ = 7.8 Hz), 7.18 (t, 2H, Py-*H*, $^{3}J_{HH}$ = 6.0 Hz), 3.76 (s, 4H, NCH_2Py), 3.67 (s, 4H, NCH_2Ar), 2.35 (s, 4H, CCH_2N), 1.28 (s, 18H, C(CH_3)$_3$), 0.61 (s, 6H, C(CH_3)$_2$); δ_C ($CDCl_3$, 100 MHz) 193.3 (*C*HO), 159.3 (Ar-*C*), 158.6 (Py-*C*), 148.2 (Py-*C*H), 141.7 (Ar-*C*), 136.7 (Py-*C*H), 134.7 (Ar-*C*H), 125.8 (Ar-*C*), 125.3 (Ar-*C*H), 123.5 (Py-*C*H), 122.3 (Py-*C*H), 121.9 (Ar-*C*), 64.8 (C*C*H$_2$N), 62.4 (N*C*H$_2$Ar), 58.0 (N*C*H$_2$Py), 38.0 (*C*(CH$_3$)$_2$), 34.2 (*C*(CH$_3$)$_3$), 31.5 (C(*C*H$_3$)$_3$), 24.3 (C(*C*H$_3$)$_2$); Anal. Calc. for $C_{41}H_{52}N_4O_4$: C, 74.06; H, 7.88; N, 8.43. Found: C, 74.44; H, 7.93; N, 8.37; MS (ESI): m/z 665.4 ([M+H]$^+$, 100 %).

Half Macrocycle Pro-ligand 2

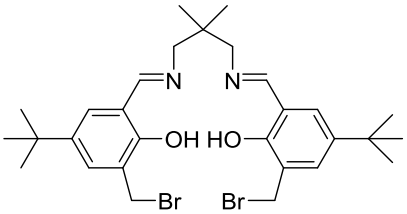

2,2-Dimethyl-1,3-propanediamine (38 mg, 0.37 mmol), 3-bromomethyl-5-*t*-butylsalicylaldehyde (0.2 g, 0.73 mmol) and 3 drops of AcOH were added to MeOH (25 mL) and refluxed for 3 days. The reaction mixture was then cooled to 25 °C and the yellow solution was evaporated to dryness, which produced an orange solid.

Half Macrocycle Pro-Ligand 2 (orange amorphous solid, 0.20 g, 90 %); δ_H ($CDCl_3$, 400 MHz) 11.15 (s, 2H, O*H*), 9.92 (s, 2H, C*H*=N), 7.71 (d, 2H, Ar-C*H*, $^{4}J_{HH}$ = 2.4 Hz), 7.48 (d, 2H, Ar-C*H*, $^{4}J_{HH}$ = 2.4 Hz), 4.61 (s, 4H, CH_2), 3.51 (s, 4H, CH_2), 1.35 (s, 18H, CH_3), 1.10 (s, 6H, CH_3); δ_C ($CDCl_3$, 100 MHz) 196.7 (*C*H=N), 157.0 (Ar-*C*-OH), 142.3 (Ar-*C*-CH$_2$Br), 133.8 (Ar-*C*H), 130.0 (Ar-*C*H), 126.0 (Ar-*C*-CH=N), 119.5 (Ar-*C*-^{t}Bu), 68.99 & 68.36 (*C*H$_2$), 58.3 (*C*H$_3$), 34.96 & 34.1 (*C*-Me), 31.0 (*^{t}Bu*).

Salen Pro-ligand[8]

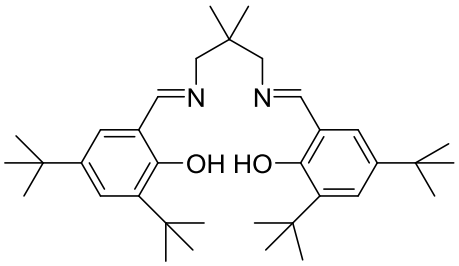

3,5-Ditert-butyl-2-hydroxybenzaldehyde (1.50 g, 6.40 mmol), 2,2-dimethyl-1,3-propanediamine (0.32 g, 3.20 mmol) and several drops of formic acid were dissolved in MeOH (75 mL) and refluxed for 2 h. The solution went from clear to yellow and during the refluxation a yellow precipitate was formed. The reaction mixture was cooled to 25 °C and then filtered under vacuum. The resulting yellow solid was washed with cold MeOH (10 mL) and dried under vacuum.

***Salen Pro-ligand*[8]** (yellow amorphous solid, 1.30 g, 76 %); δ_H ($CDCl_3$, 400 MHz) 11.89 (s, 2H, O*H*), 8.40 (s, 2H, C*H*=N), 7.42 (d, 2H, Ar-C*H*, $^4J_{HH}$ = 2.4 Hz), 7.14 (d, 2H, Ar-C*H*, $^4J_{HH}$ = 2.4 Hz), 1.50 (s, 18H, ^{t}*Bu*), 1.34 (s, 18H, ^{t}*Bu*), 1.13 (s, 6H, CH_3).

6.3 Synthesis of Metal Complexes

Di-magnesium Complex (1a)[9]

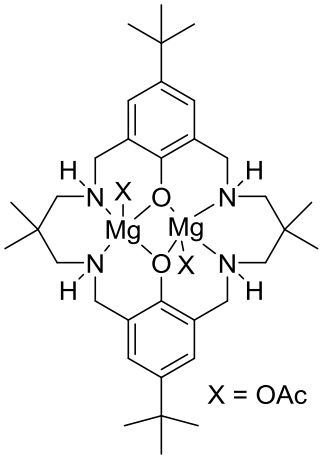

Pro-ligand H_4L^1 (0.6 g, 1.09 mmol) was dissolved in MeOH (35 mL) and $Mg(OAc)_2$ (0.31 g, 2.18 mmol) was added to the reaction mixture and this was left to stir for 16 h. The solvent was then evaporated to produce a white solid, which was dried under vacuum in the presence of phosphorous pentoxide.

Di-magnesium complex (1a) (white amorphous powder, 0.72 g, 93 %); δ_H (d_2-TCE, 400 MHz, 373K) 6.98 (s, 4H, Ar-*H*), 4.25 (br s, 4H, N-*H*), 3.06 (d, 4H, N-CH_2, J_{HH} = 12.0 Hz), 2.97 (t, 4H, N-CH_2, J_{HH} = 12.0 Hz), 2.57 (d, 4H, N-CH_2, J_{HH} = 12.0 Hz), 1.98 (t, 4H, N-CH_2, J_{HH} = 12.0 Hz,), 1.93 (br s, 6H, Ac-CH_3), 1.33 (s, 18H, ^{t}Bu), 1.26 (s, 6H, CH_3), 1.04 (s, 6H, CH_3); *Literature:*[9] δ_H (d_2-TCE, 400 MHz, 373K) 6.95 (s, 4H, Ar-*H*), 4.23 (br s, 4H, N-*H*), 3.06 (br s, 4H, N-CH_2), 2.97 (t, 4H, N-CH_2, J_{HH} = 12.3 Hz), 2.55 (d, 4H, N-CH_2, J_{HH} = 11.2 Hz), 1.97 (t, 4H, N-CH_2, J_{HH} = 13.7 Hz,), 1.84 (br s, 6H, Ac-CH_3), 1.32 (s, 18H, ^{t}Bu), 1.24 (s, 6H, CH_3), 1.03 (s, 6H, CH_3); Anal. Calc. for $C_{38}H_{60}Mg_2N_4O_6$: C, 63.61; H, 8.43; N, 7.81. Found: C, 63.75; H, 8.57; N, 7.81.

Di-zinc Complex (2)[7]

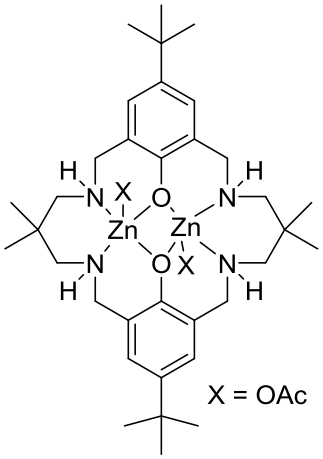

Pro-ligand H_4L^1 (1.0 g, 1.80 mmol) was dissolved in dry THF (25 mL) in a Schlenk tube and KH (0.22 g, 5.40 mmol) was added to the solution. The reaction mixture was left to stir at 25 °C for 2 h, under nitrogen. After filtering off any excess KH, $Zn(OAc)_2$ (0.66 g, 3.60 mmol) was added to the filtrate. The reaction mixture was left to stir for 16 h at 25 °C. The THF was then removed *in vacuo* and the product was taken up in dry DCM (20 mL). The impurities were filtered and the solvent removed under vacuum, which yielded a white powder.

Di-zinc complex (2) (white amorphous powder, 1.24 g, 86 %); δ_H (d_2-TCE, 400 MHz, 373K) 7.00 (s, 4H, Ar-*H*), 4.79 (br s, 4H, N-*H*), 3.34 (br d, 4H, CH_2, J_{HH} = 9.2 Hz), 2.95 (br s, 4H, CH_2), 2.85 (br s, 4H, CH_2), 2.46 (br s, 4H, CH_2), 2.10 (s, ~ 6H, O*Ac*), 1.35 (s, 18 H, ^{t}Bu), 1.30 (s, 6H, CH_3), 1.05 (s, 6H, CH_3); *Literature:*[7] δ_H (d_2-TCE, 400 MHz, 373K) 7.00 (s, 4H, Ar-*H*), 4.78 (br s, 4H, N-*H*), 3.32 (br s, 4H, CH_2), 2.95 (br s, 4H, CH_2), 2.84 (br s, 4H, CH_2), 2.46 (br s, 4H, CH_2), 2.08 (s, ≈ 6H, O*Ac*), 1.35 (s, 18 H, ^{t}Bu), 1.29 (s, 6H, CH_3), 1.05 (s, 6H,

C*H*$_3$); Anal. Calc. for $C_{38}H_{60}Zn_2N_4O_6$: C, 57.07; H, 7.56; N, 7.01%. Found: C, 56.89; H, 7.67; N, 7.07.

Mono-Zinc Complex (3)[10]

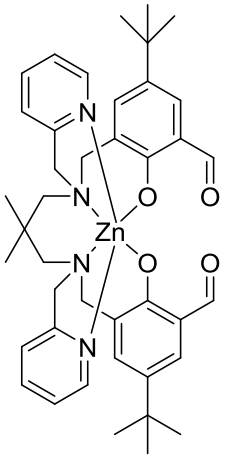

To a solution of the half macrocycle pro-ligand **1** (333 mg, 0.50 mmol) in absolute ethanol (1.3 mL) was added a solution of $Zn(OAc)_2$ (110 mg, 0.50 mmol) and Et_3N (0.14 mL, 1.0 mmol) in methanol (1.30 mL). A pale yellow precipitate appeared almost immediately. The reaction mixture was stirred at 25 °C for 24 h. The mixture was filtered and the precipitate was washed with methanol (2 mL) and Et_2O (2 mL) and dried *in vacuo* to give the monozinc complex.

Mono-Zinc Complex (3) (pale yellow powder, 248 mg, 0.34 mmol, 68 %); δ_H ($CDCl_3$, 400 MHz) 10.37 (s, 2H, C*H*O), 8.89 (d, 2H, Py-*H,* $^4J_{HH}$ = 4.4 Hz), 7.52 (t, 2H, Py-*H,* $^3J_{HH}$ = 7.1 Hz), 7.41 (d, 2H, Ar-*H,* $^4J_{HH}$ = 2.4 Hz), 7.10 (t, 2H, Py-*H,* $^3J_{HH}$ = 6.4 Hz), 7.05 (d, 2H, Ar-*H,* $^4J_{HH}$ = 2.4 Hz), 6.79 (d, 2H, Py-*H,* $^3J_{HH}$ = 7.8 Hz), 4.37 (d, 2H, NCH_2Ar, $^2J_{HH}$ = 11.7 Hz), 4.10 (d, 2H, NCH_2Py, $^2J_{HH}$ =16.1 Hz), 3.84 (d, 2H, NCH_2Py, $^2J_{HH}$ = 16.1 Hz,), 3.05 (d, 2H, NCH_2Ar, $^2J_{HH}$ = 11.7 Hz), 2.68 (br s, 4H, CCH_2N), 1.20 (s, 6H, C(CH_3)$_2$), 1.18 (s, 18H, C(CH_3)$_3$); δ_C ($CDCl_3$, 100 MHz) 193.2 (*C*HO), 171.8 (Ar-*C*), 155.1 158.6 (Py-*C*), 149.6 (Py-*C*H), 138.6 (Py-*C*H), 134.9 (Ar-*C*H), 134.2 (Ar-*C*), 125.8 (Ar-*C*), 124.5 (Ar-*C*H), 124.3 (Ar-*C*H), 123.3 (Py-*C*H), 122.5 (Py-*C*H), 67.3 (C*C*H$_2$N), 65.0 (N*C*H$_2$Py), 56.7 (N*C*H$_2$Ar), 35.1 (*C*(CH$_3$)$_2$), 33.7 (*C*(CH$_3$)$_3$), 32.8 (C(*C*H$_3$)$_2$), 31.7 (C(*C*H$_3$)$_3$); Anal. Calc. for $C_{41}H_{50}N_4O_4Zn$: C, 67.62; H, 6.92; N, 7.69. Found: C, 68.15; H, 7.11; N, 7.31; MS (ESI): m/z 727.3 ($[M+H]^+$, 100 %).

Heterodinuclear Complex (4)

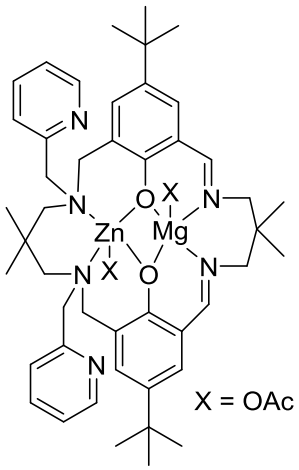

Mono-zinc complex (**3**) (0.20 g, 0.27 mmol) was suspended in dry MeOH (10 mL) in a round bottom flask and a solution of $Mg(OAc)_2$ (39.0 mg, 0.27 mmol), 2,2-dimethyl-1,3-diaminopropane (28 mg, 0.27 mmol) and dry MeOH (5 mL) was added over 3 h using a syringe pump. Upon addition, the suspension turned into a yellow solution, which was left to stir for 16 h. No precipitate formed and therefore the solvent was removed under reduced pressure to yield a yellow solid, which was further dissolved in THF, filtered over celite and the solvent removed under vacuum.

Heterodinuclear Complex (4) (yellow amorphous solid, 130 mg, 54 %); δ_H (CD_3OD, 500MHz,): 8.61 (d, 2H, Py-*H,* $^4J_{HH}$ = 4.5 Hz), 8.13 (s, 2H, N=C*H*), 7.77 (dd, 2H, Py-*H,* $^3J_{HH}$ = 7.2 & 7.2 Hz), 7.36 (d, 2H, Ar-*H,* $^4J_{HH}$ = 2.7 Hz,), 7.28-7.22 (m, 4H, Ar-*H* and Py-*H*), 7.14 (d, 2H, Py-*H,* $^3J_{HH}$ = 7.2 Hz), 4.48 (d, 2H, N-CH_aH$_b$, $^2J_{HH}$ = 12.6 Hz), 4.31 (d, 2H, Py-CH_aH$_b$, $^2J_{HH}$ = 17.6 Hz), 4.19 (d, 2H, Py-CH$_a$$H_b$, $^2J_{HH}$ = 17.6 Hz,), 3.77-3.61 (m, 4H,C=N-CH_2), 3.53 (d 2H, N-CH$_a$$H_b$, $^2J_{HH}$ = 12.6 Hz), 2.82-2.70 (m, 4H, N-CH_2), 1.72 (s, 6H, OAc), 1.31 (br, 18H, ^{t}Bu), 1.15 (s, 6H, CH_3), 0.98 (s, 6H, CH_3); δ_C (CD_3OD, 100 MHz): 180.9 (OO*C*CH_3), 171.6 (*C*H=N), 163.1 (Ar-C_{quat}), 157.4 (Py-C_{quat}), 149.5 (Py-*C*H), 140.9 (Py-*C*H), 140.6 (Ar-C_{quat}), 135.8 (Ar-*C*H), 135.3 (Aryl-*C*H), 124.6 (Py-*C*H), 124.4 (Ar-C_{quat}) 124.2 (Py-*C*H), 122.1 (Ar-C_{quat}), 76.1 (C=N-CH_2), 67.4 (N-CH_2), 65.0 (CH_2-N), 57.0 (*C*H_2-Py), 36.3 (*C*-CH_3), 35.4 (*C*-CH_3), 34.5 (*C*-^{t}Bu), 32.4 (*C*H_3), 31.9 (^{t}*Bu*), 24.8 (*C*H_3), 23.7 (*OAc*); υ_{max}/cm^{-1} 2954 (s, aromatic and aliphatic C-H stretch), 1630 (s, C=N stretch), 1471 (s, aromatic C=C stretch and aliphatic C-H bending), 1278 (s, C-N stretch), 762 (s, aromatic C-H bending); Calc. for $C_{50}H_{66}O_6N_6ZnMg$: C, 64.11; H, 7.10; N, 8.97; Found: C, 63.81; H, 6.85; N, 9.12 %; MS (MALDI-ToF): m/z 877 ([LZnMgOAc]$^+$, 100 %).

Di-magnesium Imine Complex (5)

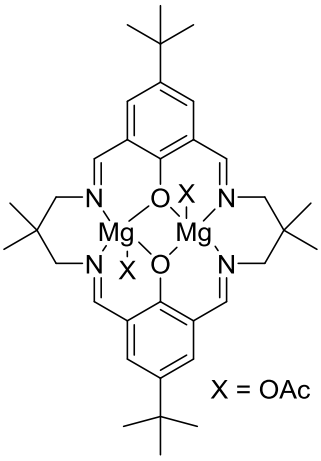

2,2-Dimethyl-1,3-propanediamine and $Mg(OAc)_2$ were placed in a round bottom flask and MeOH (15 mL) was added to the mixture. The reaction mixture was then heated to 40 °C and then a solution of MeOH (10 mL) and 4-*tert*-butyl-2,6-diformylphenol was added dropwise over 3 h. After the addition was complete, the reaction was left to stir for 16 h at 40 °C. The reaction mixture was cooled to 25 °C and then evaporated to dryness, which yielded a yellow crystalline solid.

Di-magnesium Imine Complex (5) (yellow crystalline solid, 0.15 g, 89 %); δ_H (CD_3OD, 500MHz,): 8.20 (s, 4H, C*H*=*N*), 7.51 (s, 4H, Ar-C*H*), 3.70 & 2.78 (br s, 4H, CH_2) 1.75 (br s, 6H, *OAc*), 1.32 (s, 18H, ^tBu), 0.99 (s, 12H, CH_3); δ_C (CD_3OD, 125 MHz): 169.8 (*C*H=N), 164.5 (Ar-*C*-OH), 138.7 (Ar-*C*H), 124.8 (Ar-C_{quat}), 51.0 (*C*H_2), 49.1 (^tBu), 24.1 (*OAc*), 23.3 (*C*H_3); υ_{max}/cm^{-1} 2957 (s, aromatic and aliphatic C-H stretch), 1639 (s, C=N stretch), 1401 (s, aromatic C=C stretch and aliphatic C-H bending), 1226 (s, C-N stretch), 782 (s, aromatic C-H bending); Calc. for $C_{38}H_{52}O_4N_6Mg_2$: C, 64.33; H,7.39; N, 7.90; Found: C, 64.01; H, 7.13; N, 7.56 %; MS (MALDI-ToF): m/z 703 ($[LMg_2(OOCCF_3)]^+$, 100 %).

Salen Complex (6)[8]

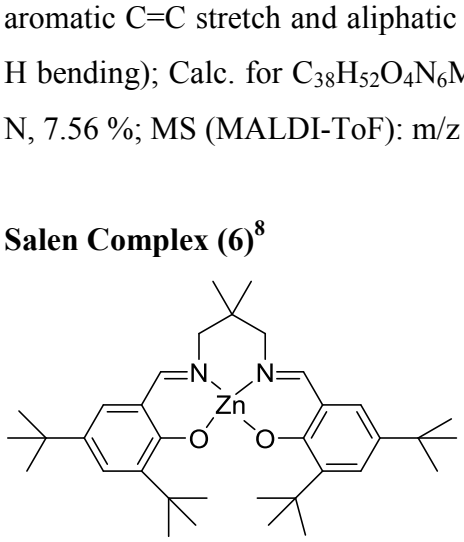

Salen pro-ligand (0.50 g, 0.94 mmol) was dissolved in 10 mL of dry hexane in the glovebox. Then Et_2Zn (116 mg, 0.94 mmol) was added to the solution and immediately a pale yellow

precipitate formed. The reaction mixture was left to stir in the glovebox for 16 h. The precipitate was filtered and washed with dry hexane. The product was dried under vacuum for 16 h.

Salen Complex (6) (pale yellow amorphous solid, 0.42 g, 75 %); δ_H ($CDCl_3$, 400 MHz) 8.23 (s, 2H, C*H*=N), 7.48 (d, 2H, Ar-C*H*, $^4J_{HH}$ = 2.4 Hz), 7.01 (d, 2H, Ar-C*H*, $^4J_{HH}$ = 2.4 Hz), 1.44 (s, 18H, ^tBu), 1.30 (s, 18H, ^tBu), 1.09 (s, 6H, CH_3).

Heterodinuclear Complex (7)

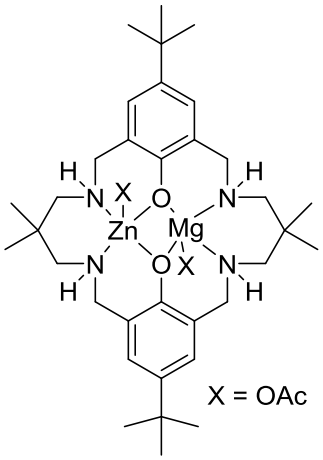

Pro-ligand H_4L^1 (0.6 g, 1.09 mmol) was dissolved in dry THF (30 mL) and placed in the glovebox freezer (-40 °C). Et_2Zn (0.14 g, 1.09 mmol) was dissolved in dry THF (10 mL) and was also placed in the glovebox freezer. Then after two hours the solutions were taken out of the freezer and the Et_2Zn solution was added dropwise to the pro-ligand solution and left to stir for 4 h at 25 °C in the glovebox. $Mg(OAc)_2$ (0.16 g, 1.09 mmol) was added to the reaction mixture and this was left to stir for 16 h in the glovebox. The solvent was then evaporated to produce a white solid.

Heterodinuclear complex (7) (white powder, 0.70 g, 85 %); δ_H spectrum did not provide informative data; δ_C ($CDCl_3$, 100 MHz,): 176.2, 163.5, 135.6, 125.9, 123.6, 62.3, 56.2, 34.2, 32.1, 27.9, 26.5, 24.4, 20.0; Calc. for $C_{38}H_{60}O_2N_2ZnMg$: C, 60.17; H, 7.97; N, 7.39; Found: C, 59.88; H, 7.87; N, 7.31 %; MS (MALDI-ToF): m/z 697 ($[LZnMg(OAc)]^+$, 100%), 657 ($[LMg_2(OAc)]^+$, 25%), 739 ($[LZn_2(OAc)]^+$, 45%).

Heterodinuclear Complex (8)

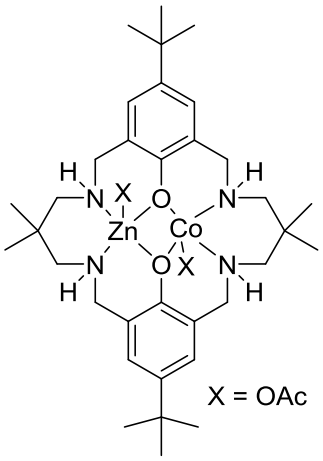

Pro-ligand H_4L^1 (0.2 g, 0.362 mmol) was dissolved in dry THF (15 mL) and placed in the glovebox freezer (-40 °C). Et_2Zn (45 mg, 0.36 mmol) was dissolved in dry THF (5 mL) and was also placed in the glovebox freezer. Then after two hours the solutions were taken out of the freezer and the Et_2Zn solution was added dropwise to the pro-ligand solution and left to stir for 4 h at 25 °C in the glovebox. $Co(OAc)_2$ (64 mg, 0.362 mmol) was added to reaction mixture and this was left to stir for 16 h in the glovebox. The solvent was then evaporated to produce a pink solid.

Heterodinuclear complex (8) (pink powder, 0.20 g, 70 %); δ_H spectrum did not provide informative data; δ_C (C_6D_6, 100 MHz,): 138.4, 126.9, 124.0, 123.3, 67.7, 63.1, 56.3, 44.5, 33.1, 31.5, 27.6, 25.2, 20.9; Calc. for $C_{38}H_{60}O_2N_2CoZn$: C, 57.54; H, 7.62; N, 7.06; Found: C, 57.65; H, 7.54; N, 6.92 %; MS (MALDI-ToF): m/z 727 ($[LCo_2(OAc)]^+$, 65 %), 732 ($[LCoZn(OAc)]^+$, 100 %), 739 ($[LZn_2(OAc)]^+$, 80%), 782 ($[LCo_2(OOCCF_3)]^+$, 3 %), 787 ($[LCoZn(OOCCF_3)]^+$, 10 %), 794 ($[LZn_2(OOCCF_3)]^+$, 3%); $\mu_{(Spin\ Only)}$ = 3.48 BM, $\mu_{(Calc)}$ = 3.87BM.

Asymmetric Complex (9)

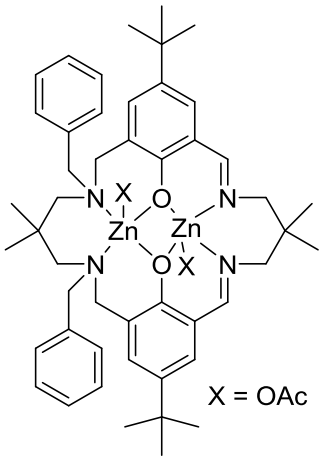

Asymmetric pro-ligand **1** (0.38 g, 0.52 mmol) was dissolved in dry THF (15 mL) in the glovebox. Three equivalents of KH (57 mg, 1.56 mmol) were added slowly to this solution. This reaction mixture was left to stir for 3 h (until the effervescence stopped). The mixture was filtered and the filtrate was added to a Schlenk tube containing zinc acetate (0.19 g, 1.04 mmol) and left to stir in the glovebox for 16 h, at 25 °C. The mixture was filtered and the filtrate was evaporated to dryness. The yellow solid formed was extracted into toluene and filtered. The solvent was then evaporated, which yielded a yellow solid.

Asymmetric Complex (9) (yellow amorphous powder, 180 mg, 35 %), δ_H spectrum did not provide informative data; δ_C ($CDCl_3$, 125 MHz,): 171.2 (*C*H=N), 162.9 (Ar-*C*-OH), 139.3, 138.7 & 135.8 (Ar-*C*-CH_2-N & Ar-*C*-CH=N), 130.5, 129.7, 129.2, 128.1 & 127.9 (Ar-*C*H), 117.5 (Ar-*C*-C^{t}Bu), 66.9, 64.4, 62.8 & 60.8 (*C*H_2), 35.74, 35.0 & 34.0 (*C*-^{t}Bu & *C*-Me_2), 31.4 (^{t}*Bu*), 28.8, 24.9 & 24.3 (*C*H_3); υ_{max}/cm^{-1} 2957 (s, aromatic and aliphatic C-H stretch), 1622 (s, C=N stretch), 1441 (s, aromatic C=C stretch and aliphatic C-H bending), 1362 & 1265 (s, C-N stretch), 739 (s, aromatic C-H bending); Calc. for $C_{52}H_{68}O_6N_4Zn_2$: C, 64.00; H, 7.02; N, 5.74; Found: C, 63.49; H, 7.06; N, 5.14 %; MS (ESI): m/z 903 ($[LZn_2O_2CH]^+$, 100 %).

Asymmetric Complex (10)

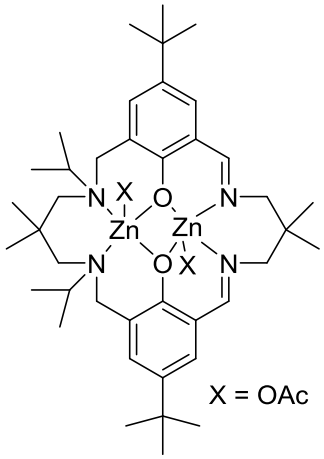

Asymmetric pro-ligand **2** (0.15 g, 0.23 mmol) was dissolved in dry THF (10 mL) in the glovebox and three equivalents of KH (25 mg, 0.69 mmol) were added slowly to this solution. This reaction mixture was left to stir for 3 h, at 25 °C. The mixture was then filtered into another Schlenk tube containing zinc acetate (84 mg, 0.46 mmol) and left to stir in the glovebox for 16 h at 25 °C. The mixture was then filtered and evaporated to dryness. The yellow solid formed was taken up in toluene and the resulting solution was filtered again and evaporated to dryness, which yielded a yellow solid.

Asymmetric Complex (10) (yellow amorphous powder, 100 mg, 50 %), δ_H spectrum did not provide informative data; δ_C ($CDCl_3$, 125 MHz) 168.0 (*C*H=N), 164.3 (Ar-*C*-OH), 138.3 & 137.0 (Ar-*C*-CH=N & Ar-*C*-CH_2-N), 134.5 & 128.0 (Ar-*C*H), 115.0 (Ar-*C*-^{t}Bu), 58.8, 55.5 & 53.7 (*C*H_2), 49.0 (*C*H-(CH_3)$_2$), 37.9 & 37.2 (*C*-Me_2), 35.4 (*C*-^{t}Bu), 31.4 (*^{t}Bu*), 25.0, 24.7 & 23.1 & 22.7 (*C*H_3); υ_{max}/cm^{-1} 2960 & 2868 (s, aromatic and aliphatic C-H stretch), 1625 (s, C=N stretch), 1462 (s, aromatic C=C stretch and aliphatic C-H bending), 1363 & 1267 (s, C-N stretch), 760 (s, aromatic C-H bending); Calc. for $C_{44}H_{68}O_6N_4Zn_2$: C, 60.09; H, 7.79; N, 6.37; Found: C, 60.14; H, 7.81; N, 6.47 %; MS (ESI): m/z 805 ([LZn_2O_2CH]$^+$, 35 %).

Lithium Zincate (11)[11]

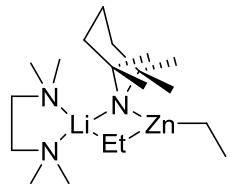

^{n}BuLi (2.94 mL, 4.0 mmols) was added to dry hexane (15 mL) in a Schlenk tube. Then 2,2,6,6-tetramethylpiperidine (0.68 mL, 4.0 mmols) was added to the Schlenk tube and left to stir at 25 °C for 1 hour. In another Schlenk tube, Et_2Zn (0.41 mL, 4.0 mmols) was added to dry hexane (15 mL), which was cannula transferred to the TMPH solution. Tetramethylethylenediamine (0.60 mL, 4.0 mmols) was then added to the Schlenk tube and heated gently, if required, to form a pale yellow solution. The solution was placed in the freezer for 16 h, which yielded a white crystalline solid. The supernatant was removed by cannula filtration and the solid was dried under vacuum for 4 h.

Lithium Zincate (11) (white crystalline powder, 0.83 g, 54 %), δ_H (C_6D_6, 400 MHz) 1.98 (br signal, 4H, β and γ C*H*$_2$ TMP), 1.90 (t, 6H, C*H*$_3$ Et, $^3J_{HH}$ = 8.0 Hz), 1.77 (s, 12H, C*H*$_3$ TMEDA), 1.64 (s, 4H, C*H*$_2$ TMEDA), 1.53 (br d, 2H, β-C*H*$_2$ TMP, $^3J_{HH}$ = 8.0 Hz), 1.21 (s, 12H, C*H*$_3$ TMP), 0.34 (q, 4H, C*H*$_2$ Et, $^3J_{HH}$ = 7.6 Hz,); δ_C (C_6D_6, 100 MHz): 56.8 (*C*H$_2$ TMEDA), 52.8 (α-*C* TMP), 46.4 (*C*H$_3$), 38.7 (β-*C*H$_2$ TMP), 35.4 & 33.7 (*C*H$_3$ TMP), 19.6 (*C*H$_3$ Et), 14.1 (γ-*C*H$_2$ TMP), 5.2 (*C*H$_2$ Et); δ_{Li} (C_6D_6, 155 MHz): 0.78 (^{7}Li).

6.4 Epoxide/CO_2 Copolymerisation Reactions

6.4.1 Low Pressure CHO/CO_2 Copolymerisation Reactions

Distilled and dried cyclohexene oxide (2.5 mL, 25 mmol) and catalyst (0.025 mmol) were placed in a Schlenk tube, under nitrogen. The reaction mixture was degassed and refilled with CO_2 three times. Then, the reaction mixture was heated to 80 °C at 1 bar CO_2 pressure for 6 h. The reaction mixture was quenched by exposure to air and a ^{1}H NMR spectrum of the crude reaction mixture was recorded. Then, the cyclohexene oxide was evaporated under vacuum to yield a white solid (polycarbonate). The PCHC was purified as described in Section 6.8 and analysed by MALDI-ToF mass spectrometry, gel-permeation chromatography, TGA and DSC.

6.4.2 High Pressure CHO/CO_2 Copolymerisation Reactions

A 100 mL Parr reactor was dried in an oven for 16 h at 140 °C. The reactor was then cooled to room temperature by venting CO_2 through it three times. Then, cyclohexene oxide (15 mL, 148 mmol) and the catalyst (0.15 mmol) were added to a Schlenk tube and transferred to the 100 mL Parr reactor, under nitrogen. The reaction mixture was then charged with 50 bar of CO_2 and stirred. Carbon dioxide dissolution was observed by the pressure decreasing. The vessel was then charged again with 50 bar of CO_2 and left to stir. This was carried out several times until CO_2 dissolution reached equilibrium and a 50 bar CO_2 pressure was maintained. The reactor was then heated to the desired temperature for 16 h. The reactor was cooled to room temperature by placing it in ice and then vented slowly to prevent CHO evaporation. A ^{1}H NMR spectrum of the crude reaction mixture was recorded. The mixture was then taken up in DCM and poured into a Schlenk tube and evaporated to dryness. The resulting PCHC was purified (Section 6.8) and analysed by MALDI-ToF mass spectrometry, gel-permeation chromatography, TGA and DSC.

6.4.3 High Pressure PO/CO_2 Copolymerisation Reactions

A 100 mL Parr reactor was dried in an oven for 16 h at 140 °C. The reactor was then cooled to room temperature by venting CO_2 through it three times. Then a solution of propylene oxide (15 mL, 214 mmol) and the catalyst (0.21 mmol) were transferred to the Parr reactor. The reactor was then charged with 50 bar of CO_2 and stirred. The pressure in the reactor head decreased due to CO_2 dissolution in PO occurring. The vessel was then charged again with 50 bar of CO_2 and left to stir. This was carried out several times until CO_2 dissolution reached equilibrium and a 50 bar CO_2 pressure was maintained. The reactor was heated to the desired temperature for 16 h. The reactor was cooled to room temperature by placing in ice. The CO_2 pressure was released by slowly venting the vessel in order to prevent PO evaporation. A ^{1}H NMR spectrum of the crude reaction mixture was recorded. The mixture was then taken up in DCM and poured into a Schlenk tube and evaporated to dryness. The resulting PPC was purified (Section 6.8) and analysed by MALDI-ToF mass spectrometry, gel-permeation chromatography, TGA and DSC.

6.5 Phthalic Anhydride/CHO Copolymerisation Reactions

6.5.1 Copolymerisation Reactions in Toluene Solutions

Cyclohexene oxide (250 μL, 2.5 mmol, 100 eq.), phthalic anhydride (370 mg, 2.5 mmol, 100 eq.), catalyst (25 μmols) and toluene (1 mL, 2.5 M concentration in CHO and PA) were added to a Schlenck tube. The vessel was heated at 100 °C and stirred. The polymerisation was stopped after 16 h by exposure to air. A ^{1}H NMR spectrum of the crude reaction mixture was recorded. The volatile components were removed *in vacuo,* to yield the product as an off white powder. The crude product was purified by the conventional method (Section 6.8).

6.5.2 Copolymerisation Reactions in Neat Conditions

Cyclohexene oxide (2 mL, 19.8 mmol, 800 eq.), phthalic anhydride (366 mg, 2.47 mmol, 100 eq.), and catalyst (25 μmol) were added to a Schlenk tube. The vessel was heated, at 100 °C with constant stirring, for 4 h. The reaction was stopped by exposure to air and a ^{1}H NMR spectrum of the crude reaction mixture was recorded. The volatile components were removed *in vacuo,* to yield the product as an off white powder. The crude product was purified by the conventional method (Section 6.8). The purified polyester was analysed by MALDI-ToF mass spectrometry, gel-permeation chromatography, TGA and DSC.

6.6 Phthalic Anhydride/CHO/CO_2 Terpolymerisation Reactions

6.6.1 General Procedure

Cyclohexene oxide (2 mL, 19.8 mmol), phthalic anhydride (366 mg, 2.47 mmol, 100 eq.), and catalyst (25 μmol) were added to a Schlenk tube in the glovebox. The vessel was degassed and refilled with CO_2 three times at 25 °C. The vessel was left under a CO_2 atmosphere and was then heated to 100 °C, with continuous reaction stirring, for 16 h. The reaction mixture was quenched by exposure to air and a sample of the crude reaction mixture was analysed by ^{1}H NMR spectroscopy to determine the conversion and selectivity. Any unreacted monomers were removed *in vacuo,* to yield the polymer as an off white powder. The polymer was purified (Section 6.8) and analysed by MALDI-ToF, gel-permeation chromatography, TGA and DSC.

6.7 Monitoring Reactions with *In Situ* ATR-IR Spectroscopy

6.7.1 Initial Rates for CHO/CO_2 Copolymerisation Reactions

The React-IR probe was placed in a two neck Schlenk tube and heated under vacuum to 80 °C for 16 h. Then, a solution of CHO (2.5 mL, 148 mmol), diethyl carbonate (0.5 mL, 4.13 mmol) and catalyst (different concentrations) was injected into the Schlenk tube, under CO_2. The reaction mixture was degassed and refilled with CO_2 three times and monitored by the React-IR. The reaction mixture was left stirring and heating for 6 h. The reaction mixture was quenched by exposure to air. A ^{1}H NMR spectrum of the crude reaction mixture was recorded and the volatile CHO was removed under vacuum. The polymer was purified as described in Section 6.8.

6.7.2 Phthalic Anhydride/CHO/CO_2 Terpolymerisation Reactions

The React-IR probe was placed in a two neck Schlenk tube containing phthalic anhydride (366 mg, 2.47 mmol, 100 eq.) and heated under vacuum to 40 °C for 16 h. Then, a solution of CHO (2 mL, 19.8 mmol) and catalyst (25 μmol) was injected into the Schlenk tube under CO_2 at 100 °C. The reaction mixture was degassed and refilled with CO_2 three times and monitored by the React-IR. Aliquots were taken at certain intervals under a positive flow of CO_2. The reaction mixture was left stirring and heating for 16 h. The reaction mixture was quenched by exposure to air. A ^{1}H NMR spectrum of the crude reaction mixture was recorded and the volatile CHO was removed under vacuum. The polymer was purified as described in Section 6.8.

6.8 Purification of Polymers

6.8.1 General Procedure

All crude polymers were purified by dissolving in THF and precipitating from pentane. The resulting white powder was re-dissolved in THF and filtered through a silica plug. The filtrate was evaporated to dryness to yield a white powder.

6.9 References

1. L. F. Lindoy, G. V. Meehan and N. Svenstrup, *Synthesis,* 1998, ***74***, 1029,1032.

2. D. H. T. Phan, B. Kim and V. M. Dong, *J. Am. Chem. Soc.,* 2009, ***131***, 15608-15609.

3. Q. Wang, C. Wilson, A. J. Blake, S. R. Collinson, P. A. Tasker and M. Schröder, *Tetrahedron Lett.,* 2006, ***47***, 8983-8987.

4. F. Qian, J. E. McCusker, Y. Zhang, A. D. Main, M. Chlebowski, M. Kokka and L. McElwee-White, *J. Org. Chem.,* 2002, ***67***, 4086-4092.

5. J. Sandström and U. Sjöstrand, *Tetrahedron,* 1978, ***34***, 371-378.

6. H. Keypour, M. Ahmadi, M. Rezaeivala, A. Chehregani, R. Golbedaghi and A. G. Blackman, *Polyhedron,* 2011, ***30***, 1865-1870.

7. M. R. Kember, P. D. Knight, P. T. R. Reung and C. K. Williams, *Angew. Chem. Int. Ed.,* 2009, ***48***, 931-933.

8. G. A. Morris, H. Zhou, C. L. Stern and S. T. Nguyen, *Inorg. Chem.,* 2001, ***40***, 3222-3227.

9. M. R. Kember, J. Copley, A. Buchard and C. K. Williams, *Polym. Chem.,* 2012.

10. C. Fraser, L. Johnston, A. L. Rheingold, B. S. Haggerty, G. K. Williams, J. Whelan and B. Bosnich, *Inorg. Chem.,* 1992, ***31***, 1835-1844.

11. D. R. Armstrong, J. A. Garden, A. R. Kennedy, S. M. Leenhouts, R. E. Mulvey, P. O'Keefe, C. T. O'Hara and A. Steven, *Chem. Eur. J.,* 2013, ***19***, 13492-13503.

Appendices

"It's not how we fall. It's how we get back up again."
Monsters of Men by Patrick Ness

Appendix A – Raw Data Plots for Chapter 2

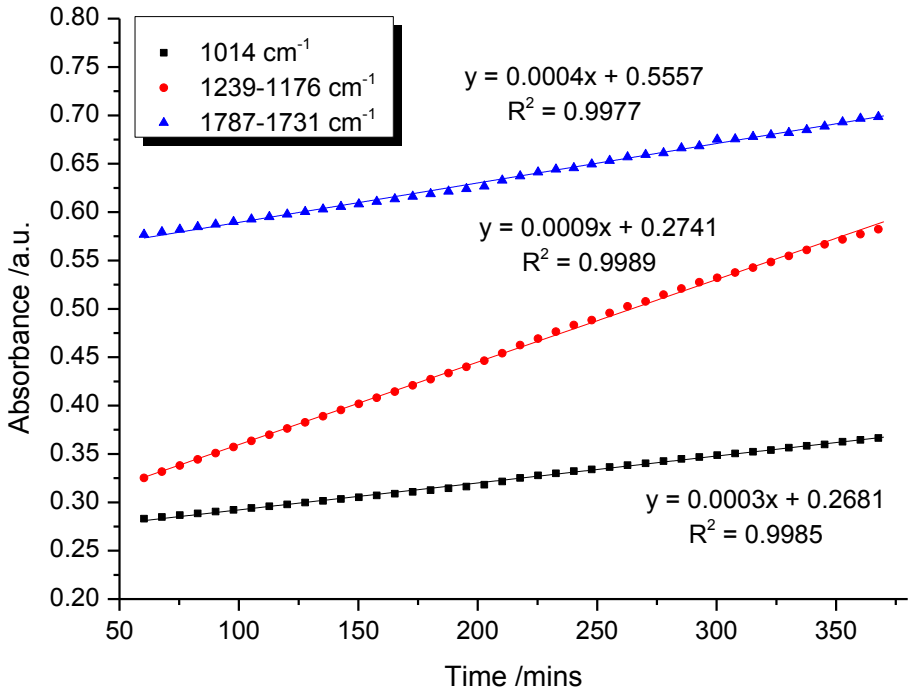

Figure A1: Change in absorbance *vs.* time plot for three vibrational modes. Reaction conditions: [**1a**] = 4.2 mM, $[CHO]_0$ = 8.24 M in DEC, 80 °C at 1 bar CO_2 pressure. For clarity 50 % of the data points have been omitted. The gradient value = initial rate.

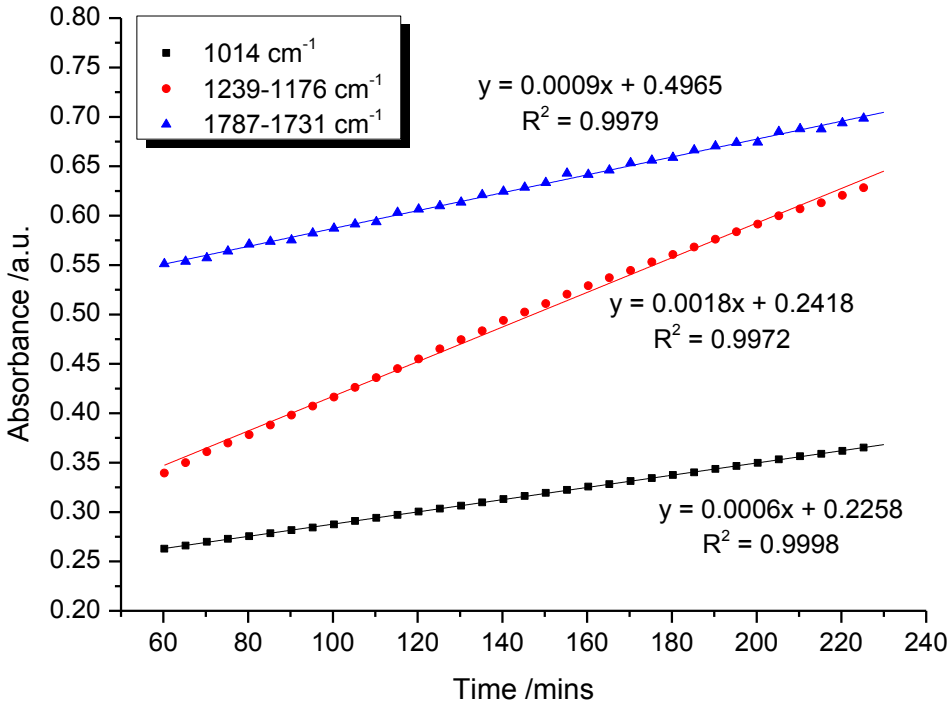

Figure A2: Change in absorbance *vs.* time plot for three vibrational modes. Reaction conditions: [**1a**] = 8.3 mM, $[CHO]_0$ = 8.24 M in DEC, 80 °C at 1 bar CO_2 pressure. For clarity 50 % of the data points have been omitted. The gradient value = the initial rate.

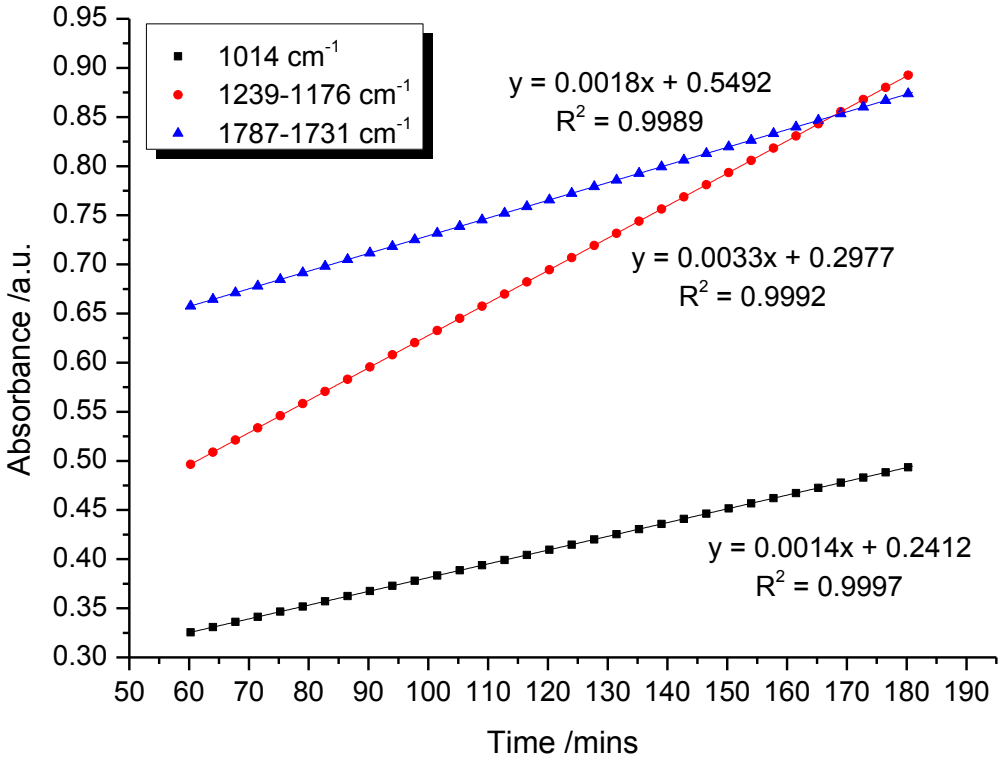

Figure A3: Change in absorbance *vs.* time plot for three vibrational modes. Reaction conditions: [**1a**] = 16.6 mM, $[CHO]_0$ = 8.24 M in DEC, 80 °C at 1 bar CO_2 pressure. For clarity 50 % of the data points have been omitted. The gradient value = initial rate.

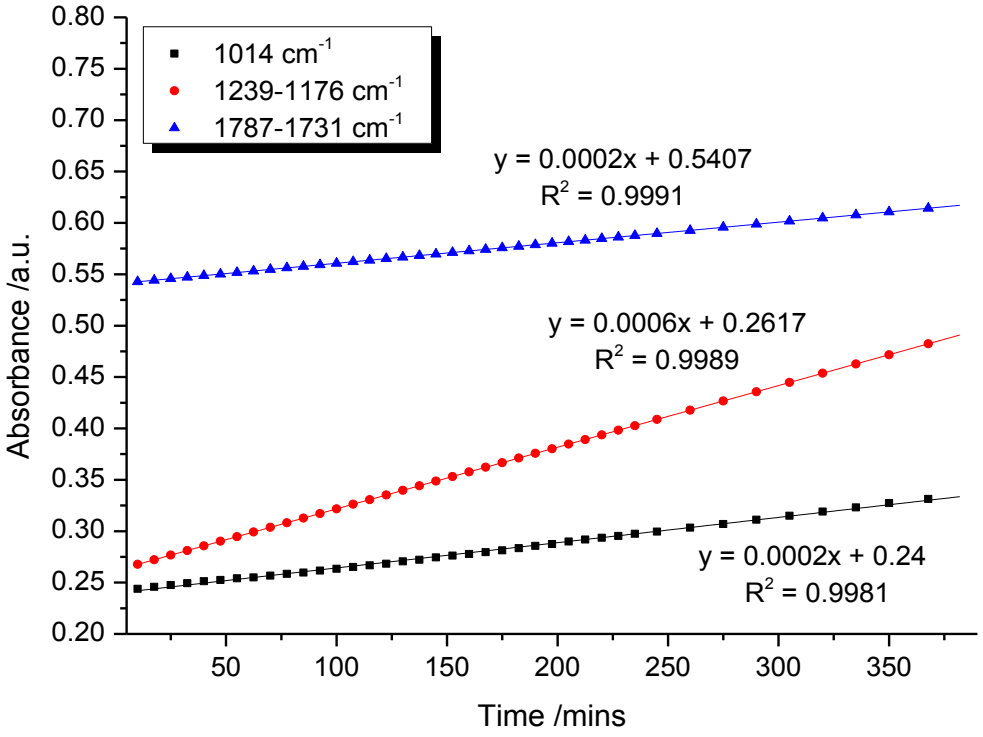

Figure A4: Change in absorbance *vs.* time plot for three vibrational modes. Reaction conditions: [**1c**] = 4.2 mM, $[CHO]_0$ = 8.24 M in DEC, 80 °C at 1 bar CO_2 pressure. For clarity 50 % of the data points have been omitted. The gradient value = initial rate.

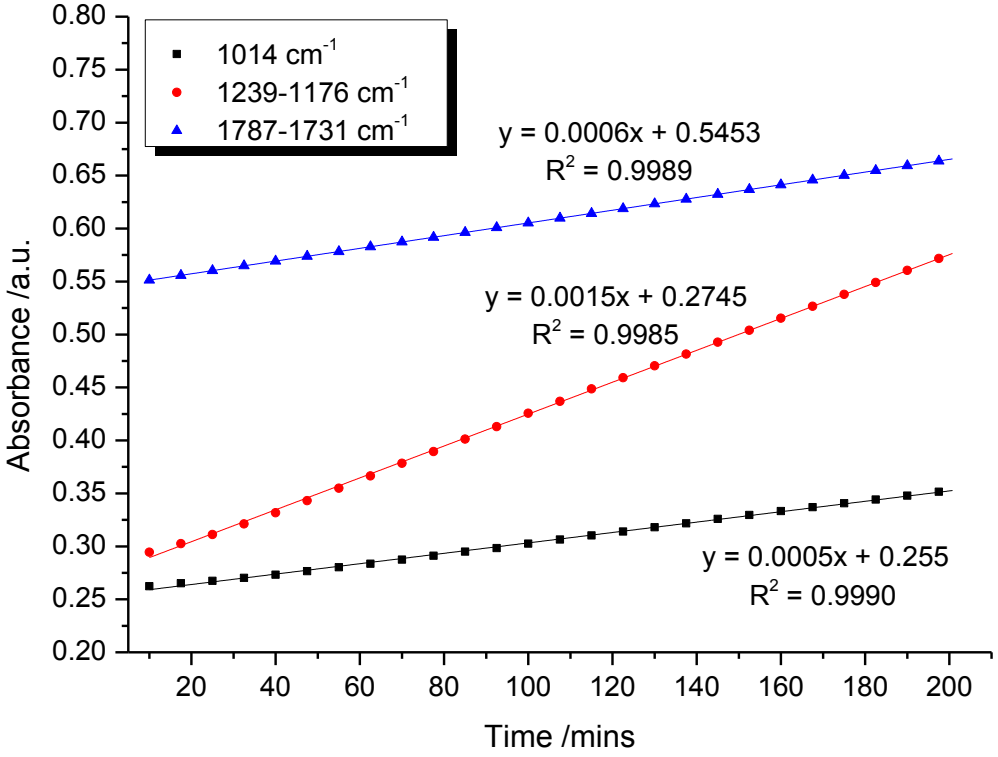

Figure A5: Change in absorbance *vs.* time plot for three vibrational modes. Reaction conditions: [**1c**] = 8.3 mM, $[CHO]_0$ = 8.24 M in DEC, 80 °C at 1 bar CO_2 pressure. For clarity 50 % of the data points have been omitted. The gradient value = initial rate.

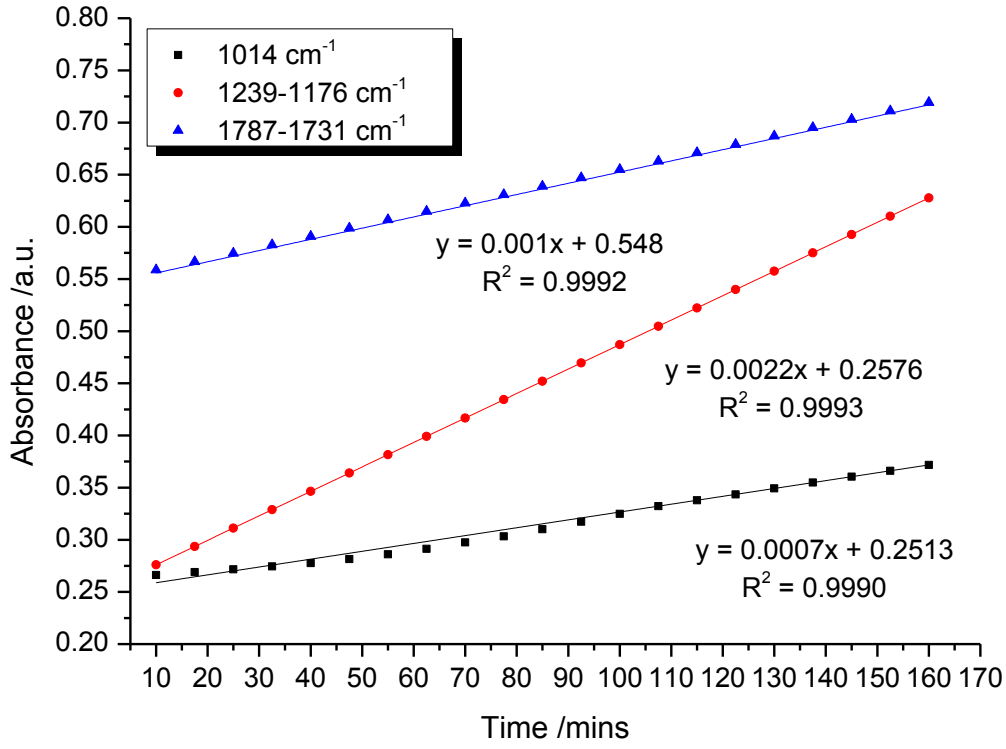

Figure A6: Change in absorbance *vs.* time plot for three vibrational modes. Reaction conditions: [**1c**] = 12.5 mM, $[CHO]_0$ = 8.24 M in DEC, 80 °C at 1 bar CO_2 pressure. For clarity 50 % of the data points have been omitted. The gradient value = initial rate.

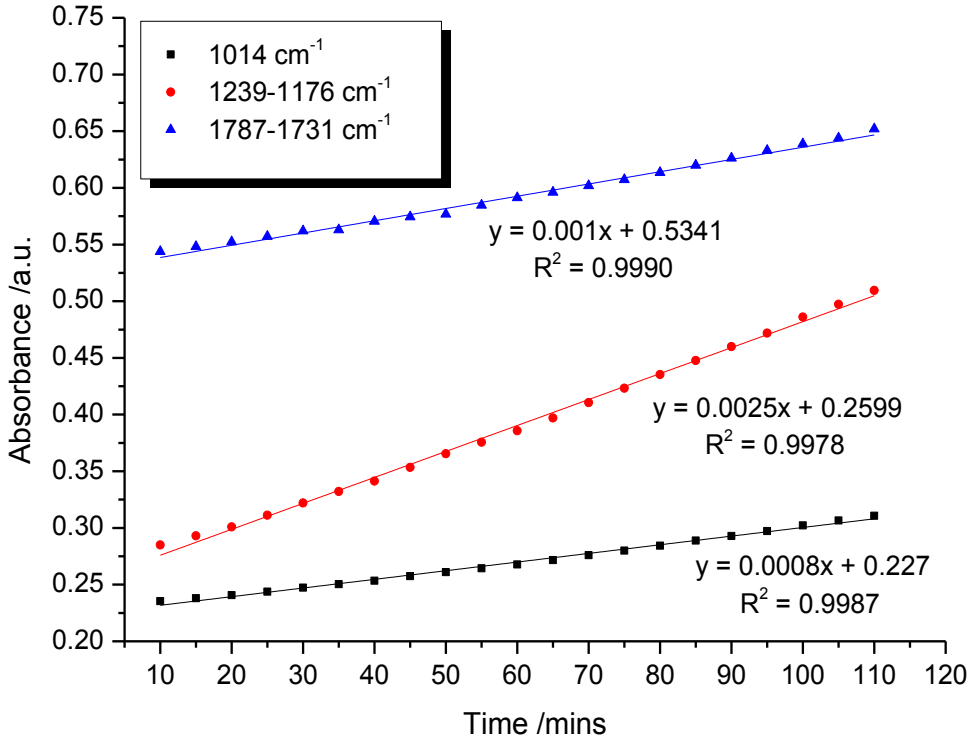

Figure A7: Change in absorbance *vs.* time plot for three vibrational modes. Reaction conditions: [**1c**] = 16.6 mM, $[CHO]_0$ = 8.24 M in DEC, 80 °C at 1 bar CO_2 pressure. For clarity 50 % of the data points have been omitted. The gradient value = initial rate.

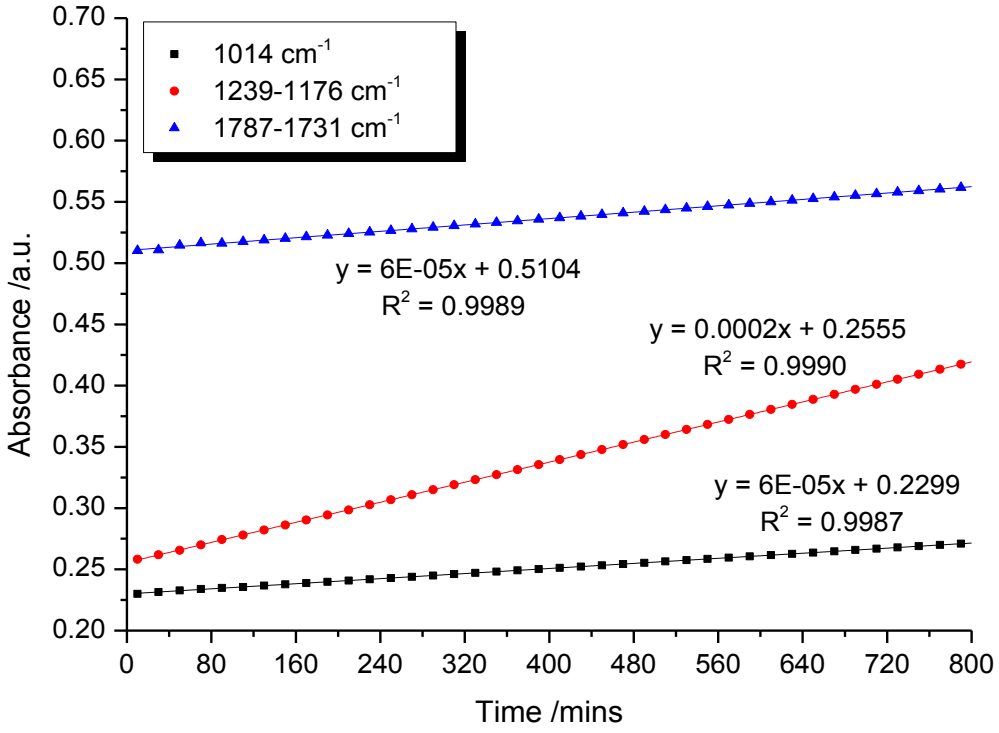

Figure A8: Change in absorbance *vs.* time plot for three vibrational modes. Reaction conditions: [**1d**] = 4.2 mM, $[CHO]_0$ = 8.24 M in DEC, 80 °C at 1 bar CO_2 pressure. For clarity 50 % of the data points have been omitted. The gradient value = initial rate.

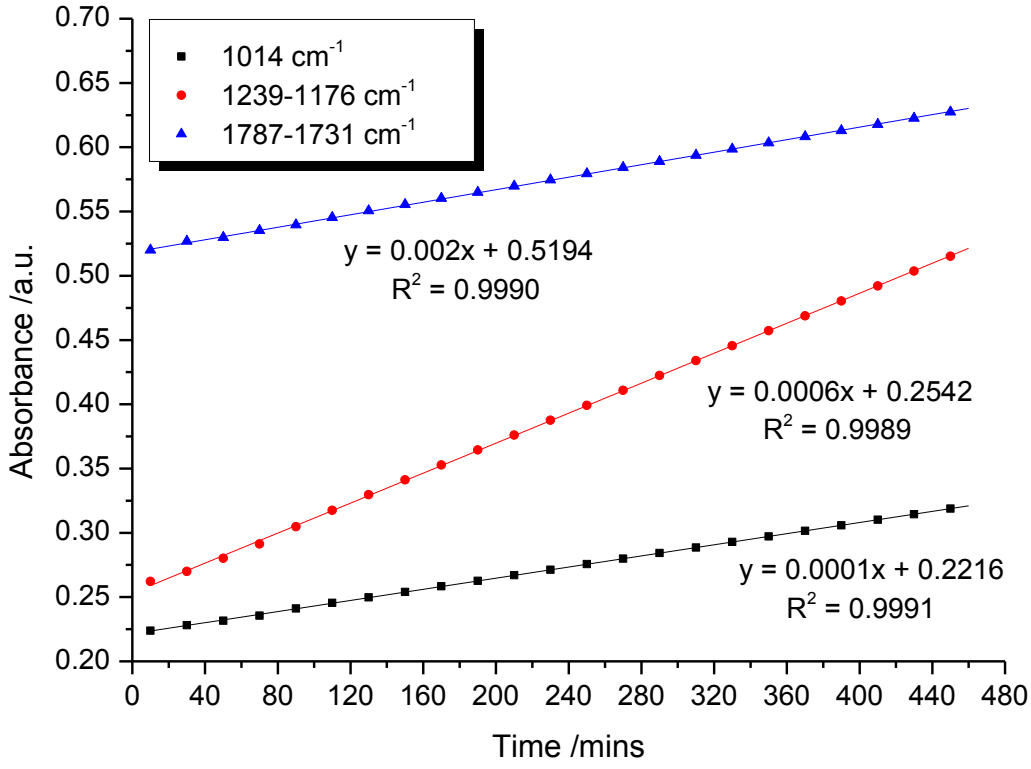

Figure A9: Change in absorbance *vs.* time plot for three vibrational modes. Reaction conditions: [**1d**] = 8.3 mM, $[CHO]_0$ = 8.24 M in DEC, 80 °C at 1 bar CO_2 pressure. For clarity 50 % of the data points have been omitted. The gradient value = initial rate.

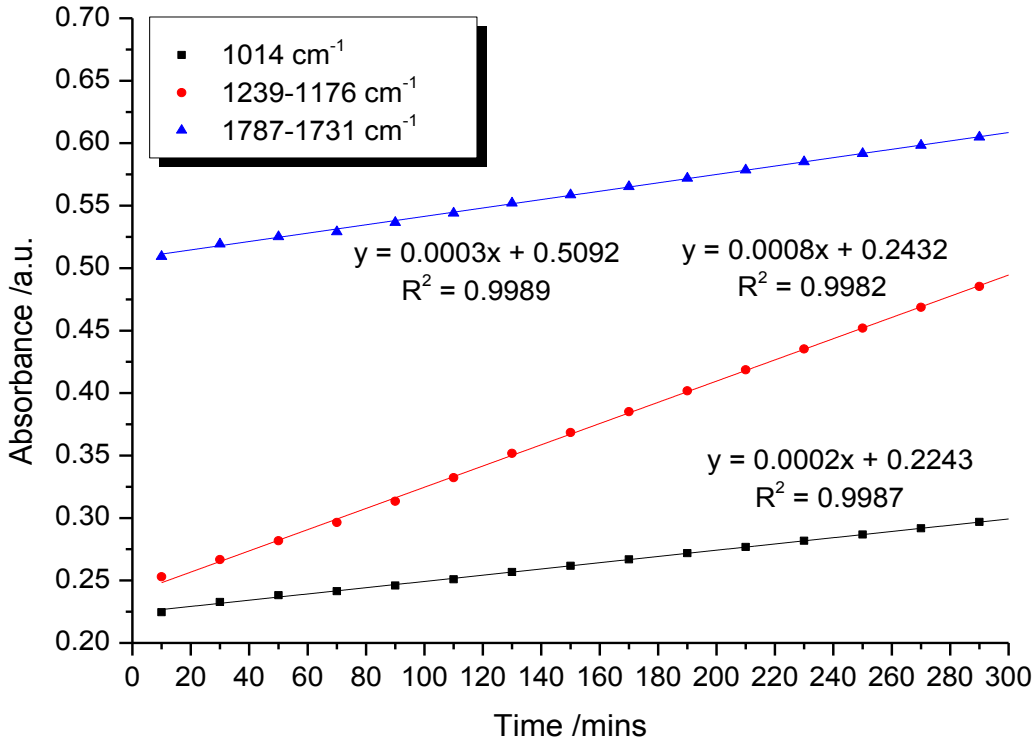

Figure A10: Change in absorbance *vs.* time plot for three vibrational modes. Reaction conditions: [**1d**] = 12.5 mM, $[CHO]_0$ = 8.24 M in DEC, 80 °C at 1 bar CO_2 pressure. For clarity 50 % of the data points have been omitted. The gradient value = initial rate.

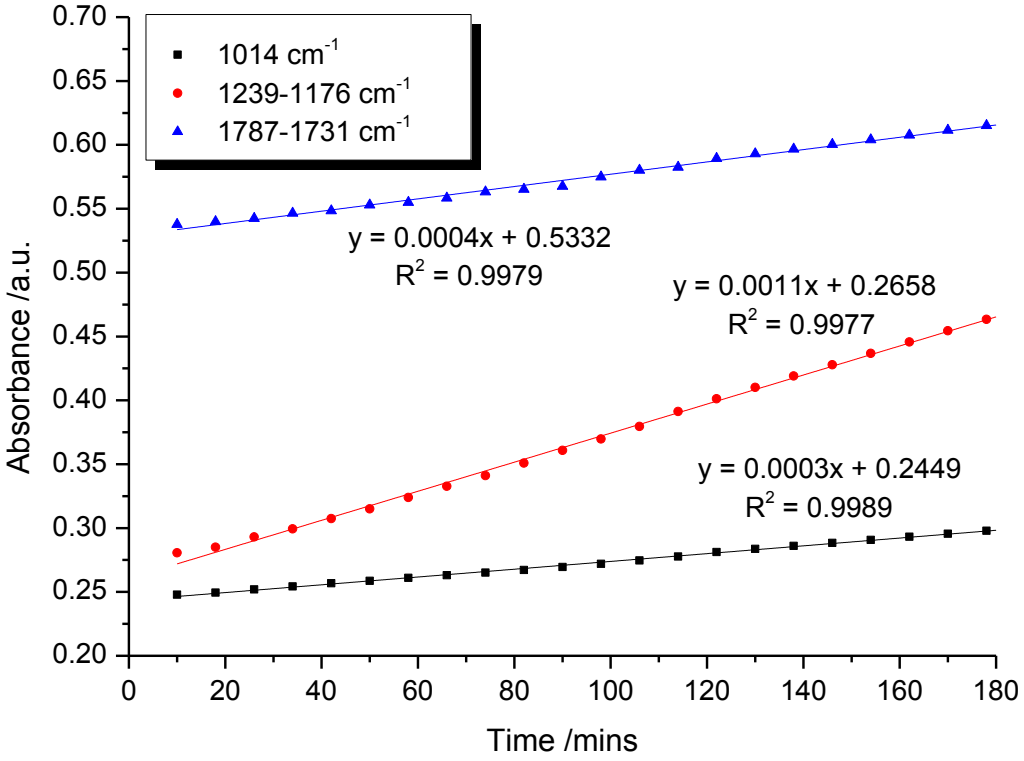

Figure A11: Change in absorbance *vs.* time plot for three vibrational modes. Reaction conditions: [**1d**] = 16.6 mM, $[CHO]_0$ = 8.24 M in DEC, 80 °C at 1 bar CO_2 pressure. For clarity 50 % of the data points have been omitted. The gradient value = initial rate.

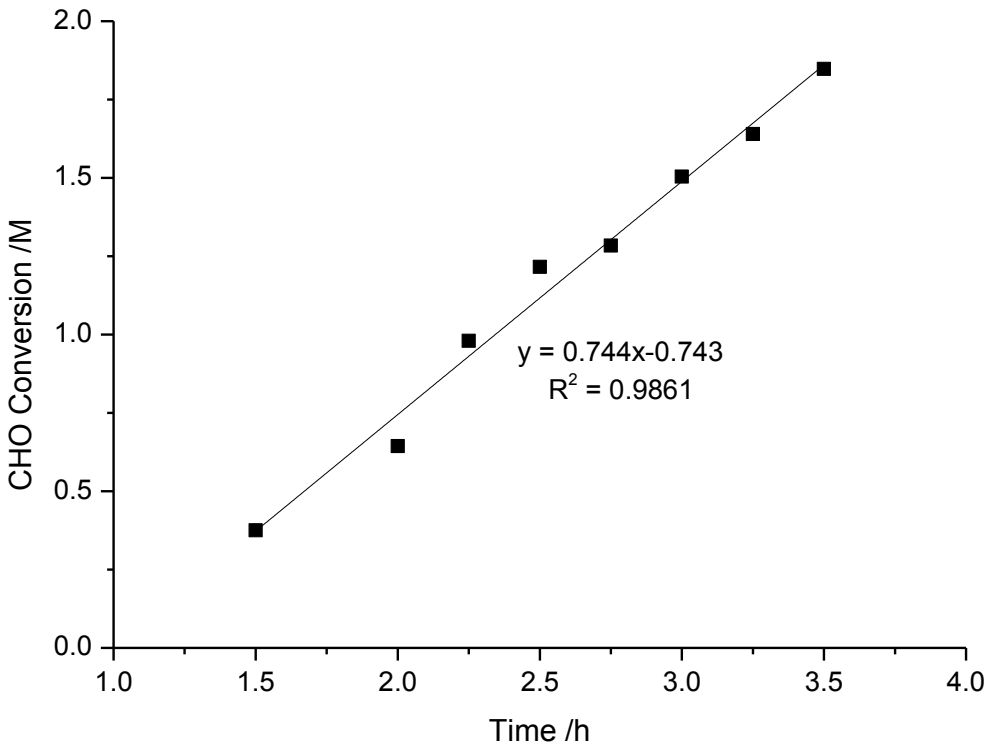

Figure A12: CHO conversion *vs.* time plot. Reaction conditions: 1:1000 (**1a**:CHO) loading at 80 °C and 1 bar CO_2 pressure. The gradient value = initial rate.

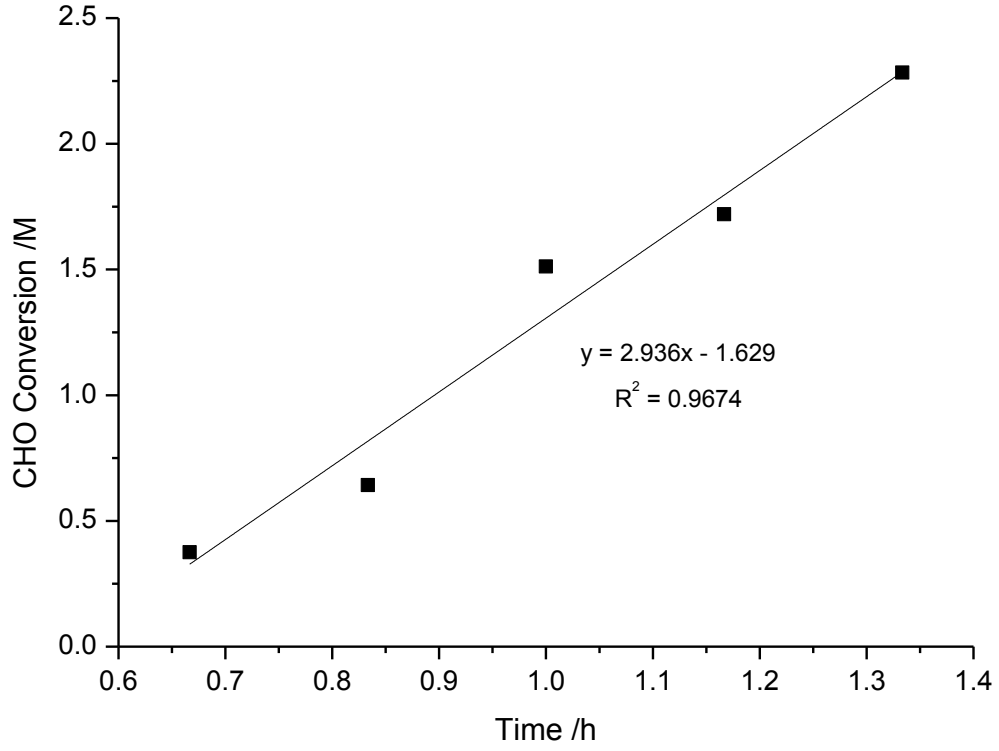

Figure A13: CHO conversion *vs.* time plot. Reaction conditions: 1:1000 (**1a**:CHO) loading at 80 °C and 10 bar CO_2 pressure. The gradient value = initial rate.

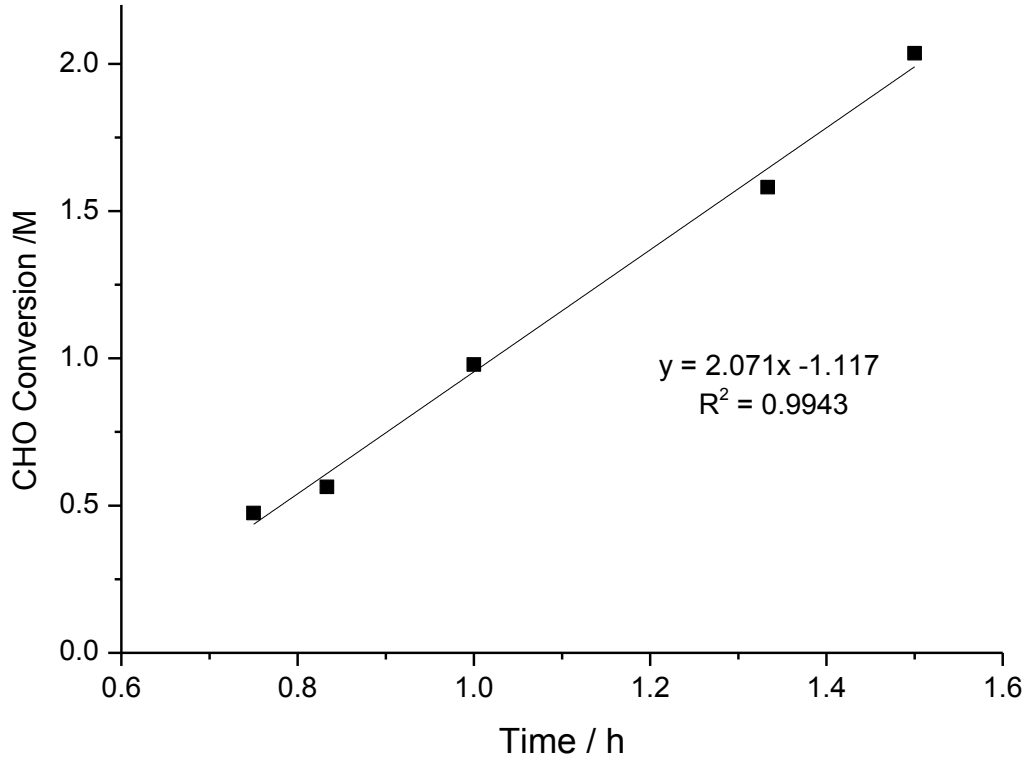

Figure A14: CHO conversion *vs.* time plot. Reaction conditions: 1:1000 (**1a**:CHO) loading at 80 °C and 20 bar CO_2 pressure. The gradient value = initial rate.

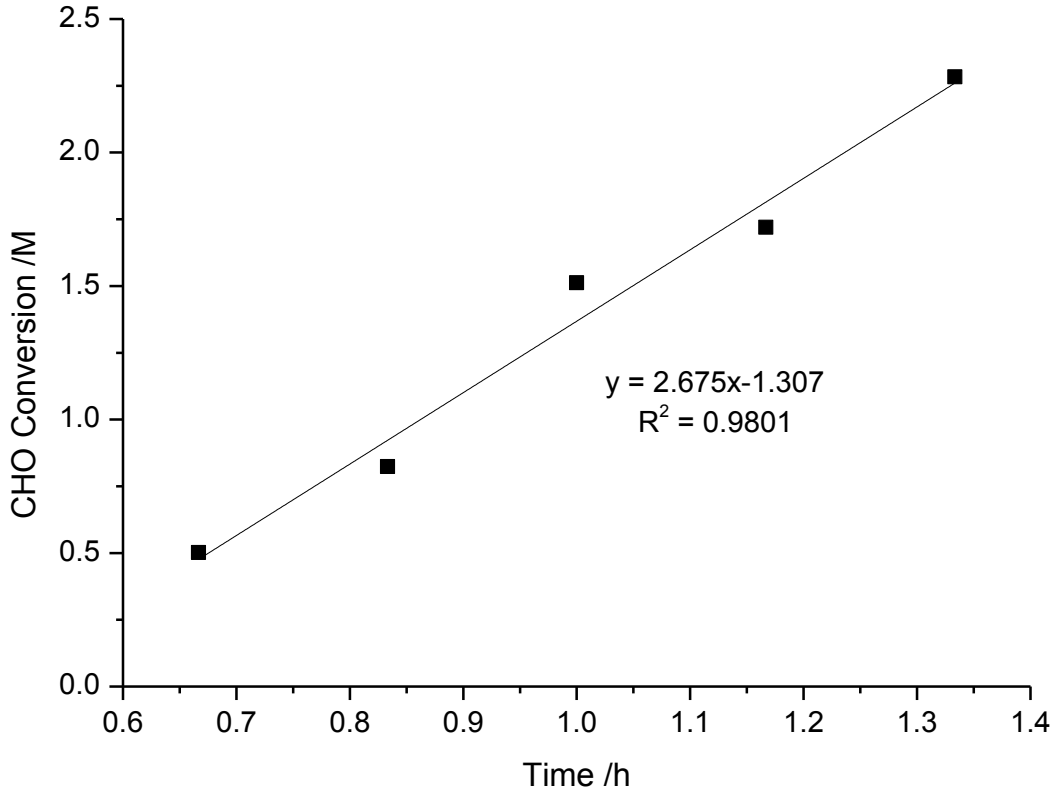

Figure A15: CHO conversion *vs.* time plot. Reaction conditions: 1:1000 (**1a**:CHO) loading at 80 °C and 30 bar CO_2 pressure. The gradient value = initial rate.

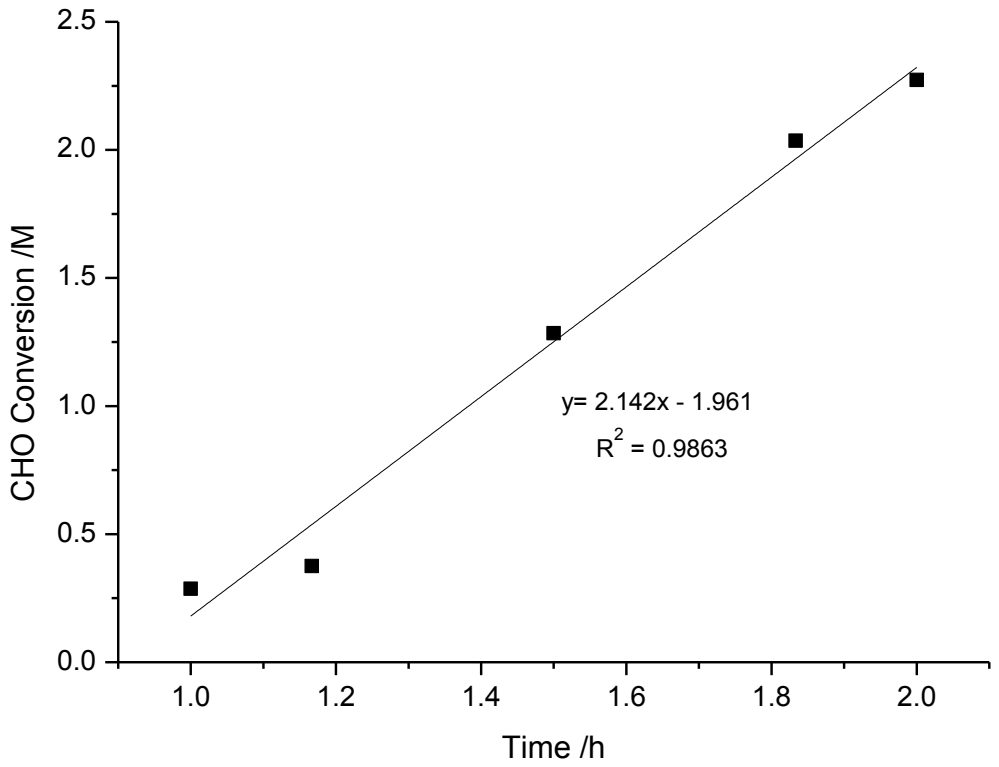

Figure A16: CHO conversion *vs.* time plot. Reaction conditions: 1:1000 (**1a**:CHO) loading at 80 °C and 40 bar CO_2 pressure. The gradient value = initial rate.

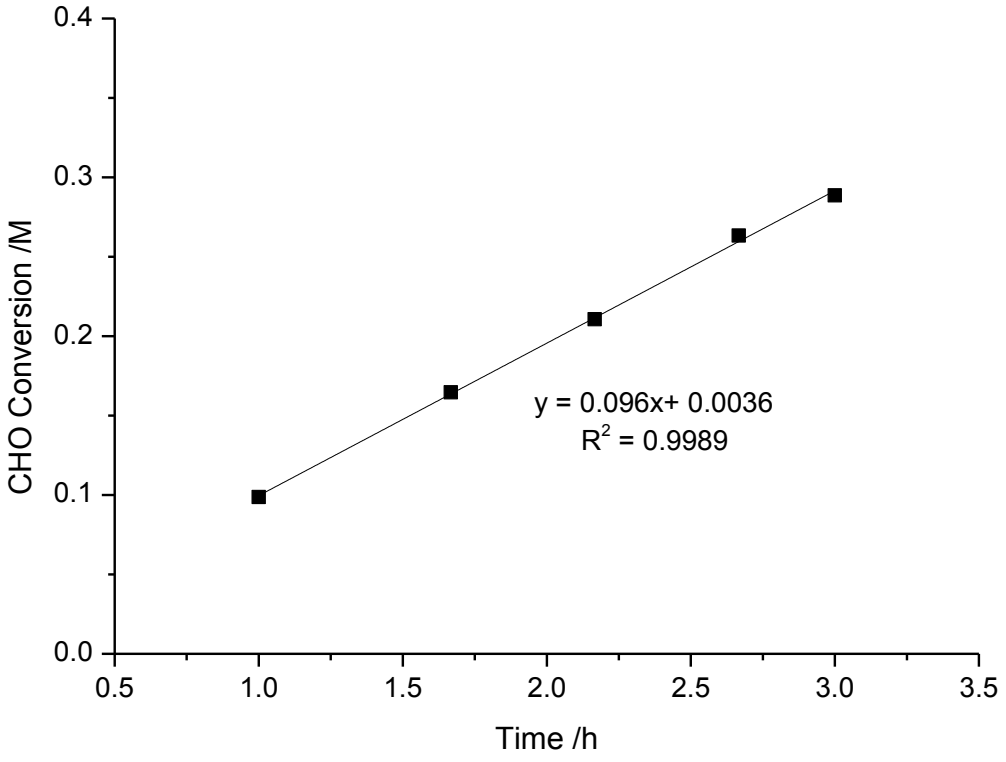

Figure A17: CHO conversion *vs.* time plot. Reaction conditions: 1:1000 (**1a**:CHO) loading at 80 °C and 50 bar CO_2 pressure. The gradient value = initial rate.

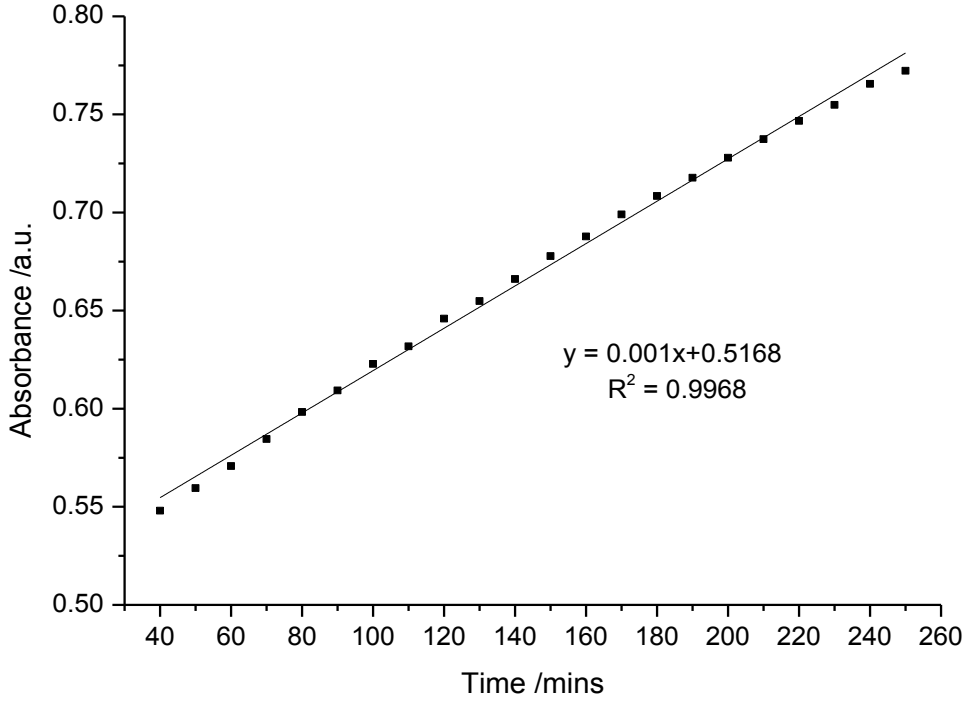

Figure A18: Change in absorbance *vs*. time plot for the 1787-1731 cm^{-1} vibrational mode. Reaction conditions: [**1b**] = 8.3 mM, $[CHO]_0$ = 8.24 M in DEC, 80 °C at 1 bar CO_2 pressure. For clarity 50 % of the data points have been omitted. The gradient value = initial rate.

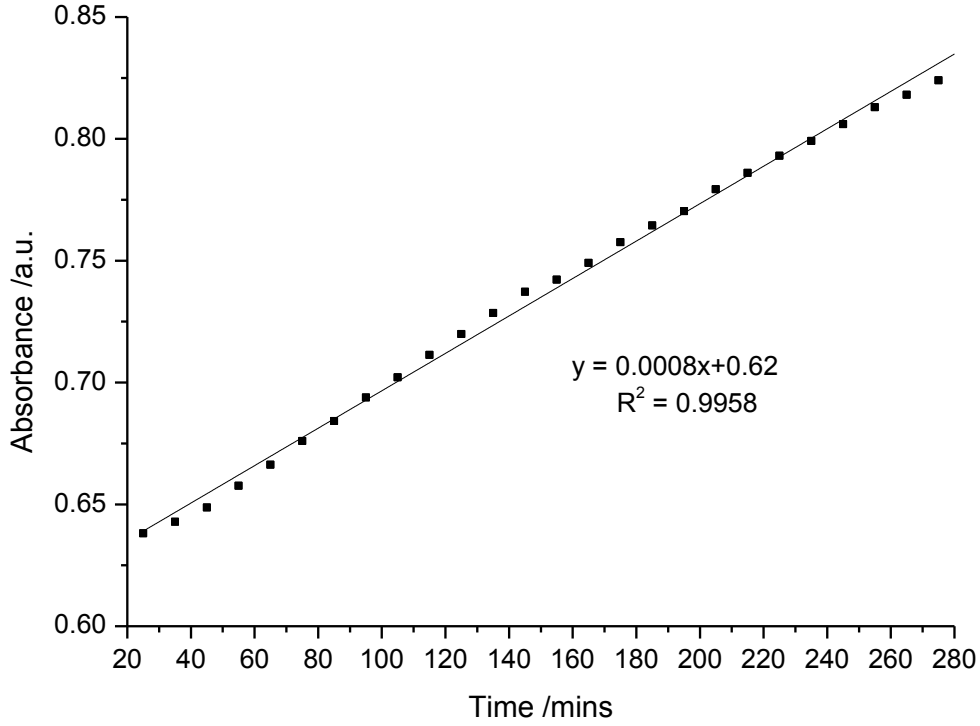

Figure A19: Change in absorbance *vs*. time plot for the 1787-1731 cm^{-1} vibrational mode. Reaction conditions: [**1e**] = 8.3 mM, $[CHO]_0$ = 8.24 M in DEC, 80 °C at 1 bar CO_2 pressure. For clarity 50 % of the data points have been omitted. The gradient value = initial rate.

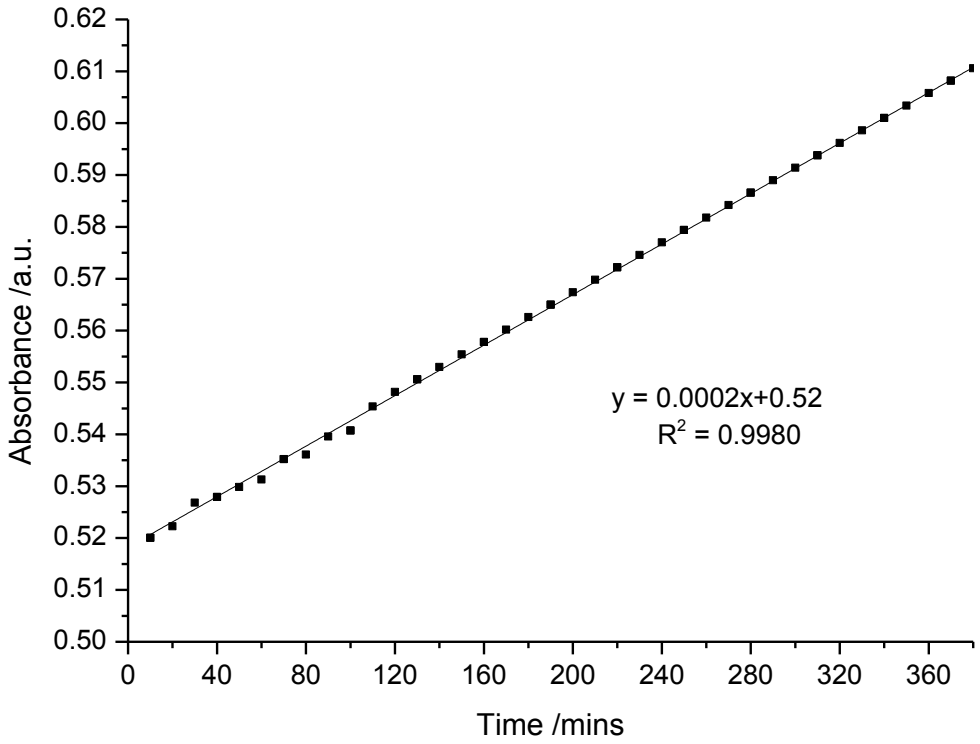

Figure A20: Change in absorbance *vs*. time plot for the 1787-1731 cm^{-1} vibrational mode. Reaction conditions: [**1f**] = 8.3 mM, $[CHO]_0$ = 8.24 M in DEC, 80 °C at 1 bar CO_2 pressure. For clarity 50 % of the data points have been omitted. The gradient value = initial rate.

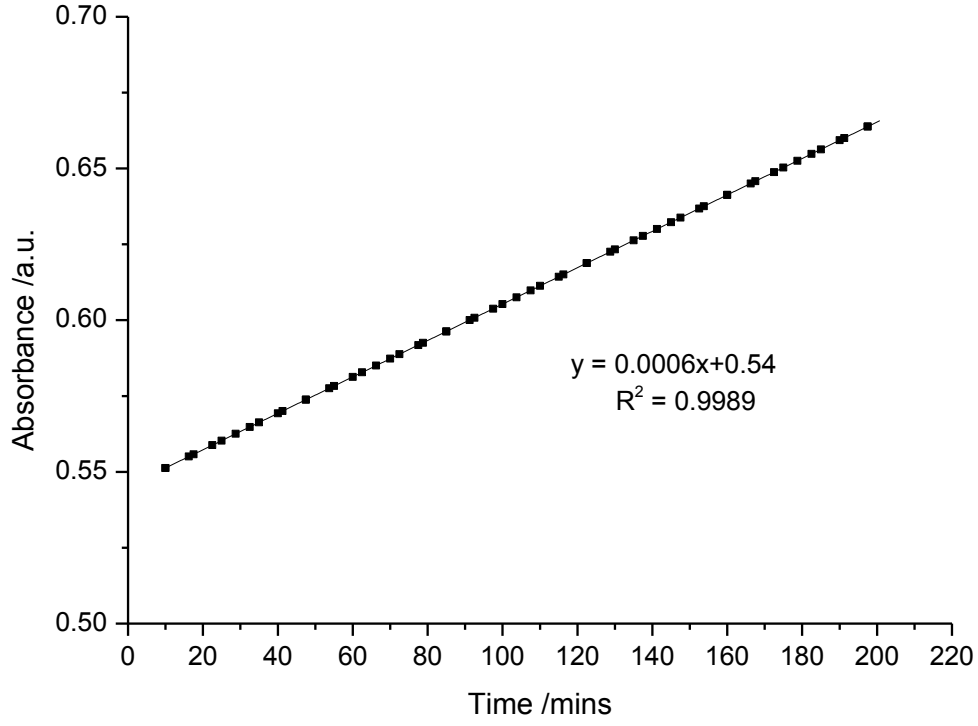

Figure A21: Change in absorbance *vs*. time plot for the 1787-1731 cm^{-1} vibrational mode. Reaction conditions: [**1g**] = 8.3 mM, $[CHO]_0$ = 8.24 M in DEC, 80 °C at 1 bar CO_2 pressure. For clarity 50 % of the data points have been omitted. The gradient value = initial rate.

Appendix B – Spectra for Chapter 3

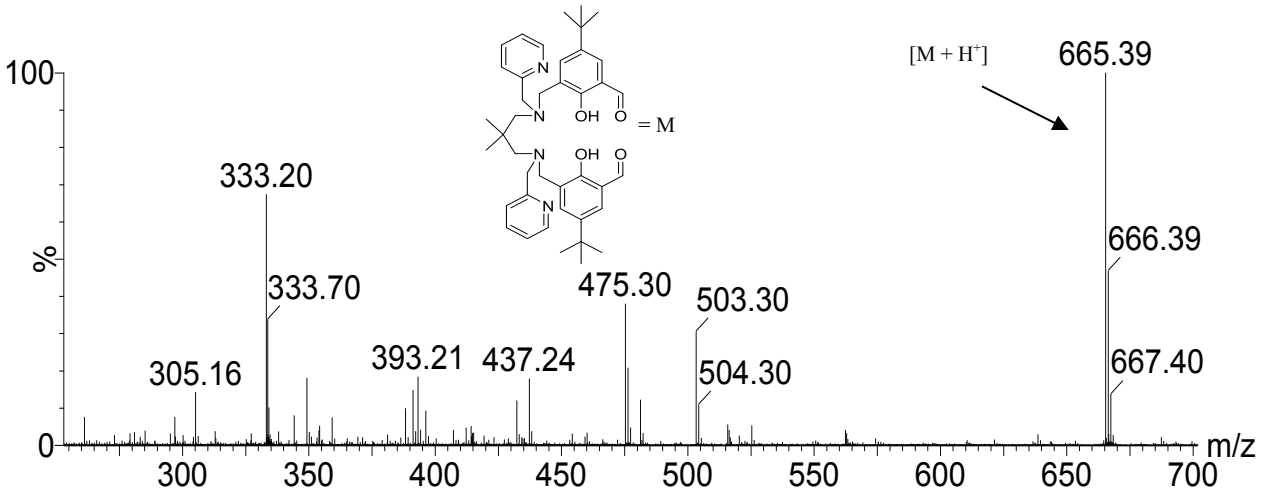

Figure B1: ESI mass spectrum of the half macrocyclic ligand.

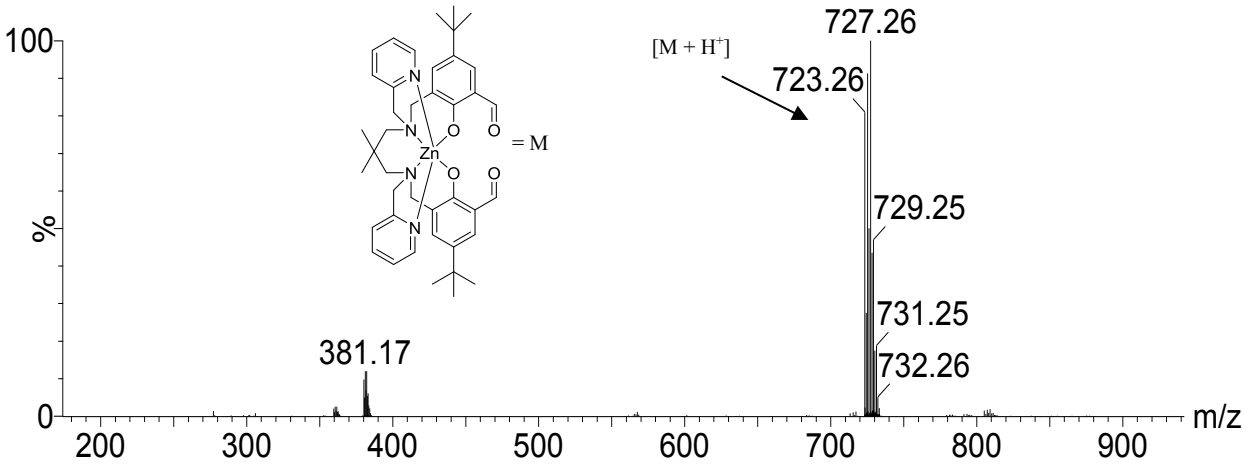

Figure B2: ESI mass spectrum of complex **3**.

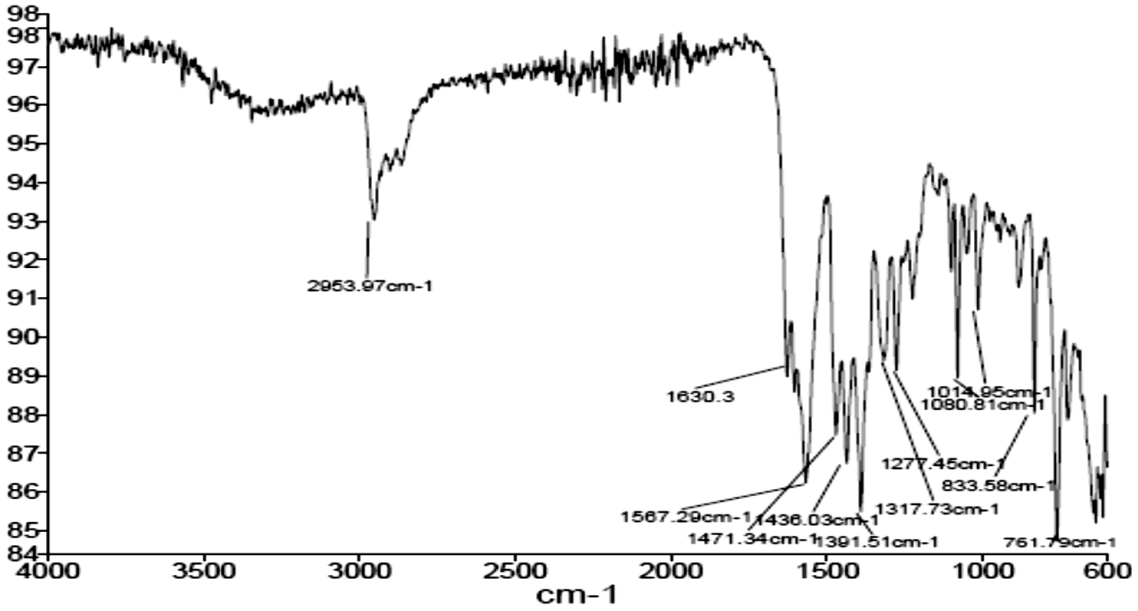

Figure B3: IR spectrum of complex **4**.

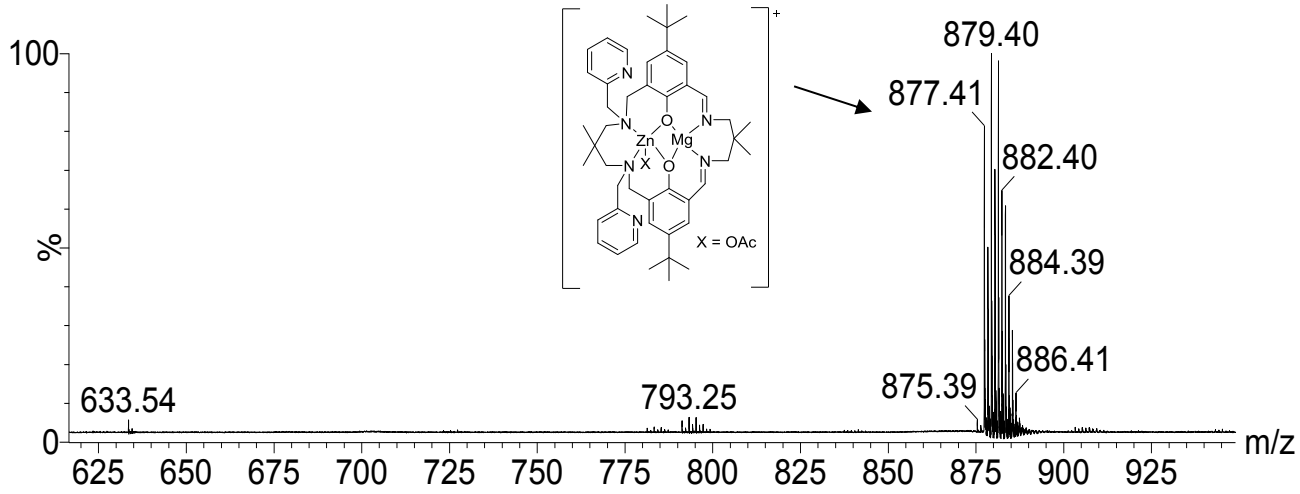

Figure B4: MALDI-ToF mass spectrum of complex **4**.

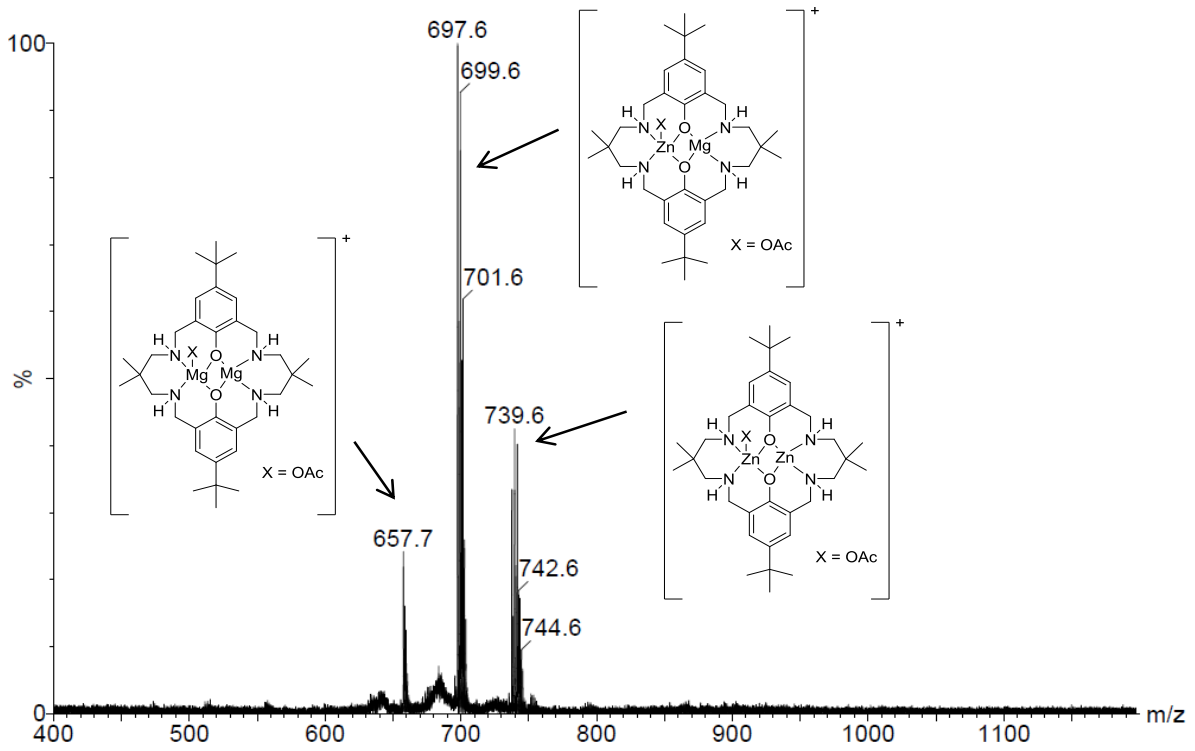

Figure B5: Full MALDI-ToF spectrum of catalyst system **7**, with the assignment of the signals due to the molecular ions.

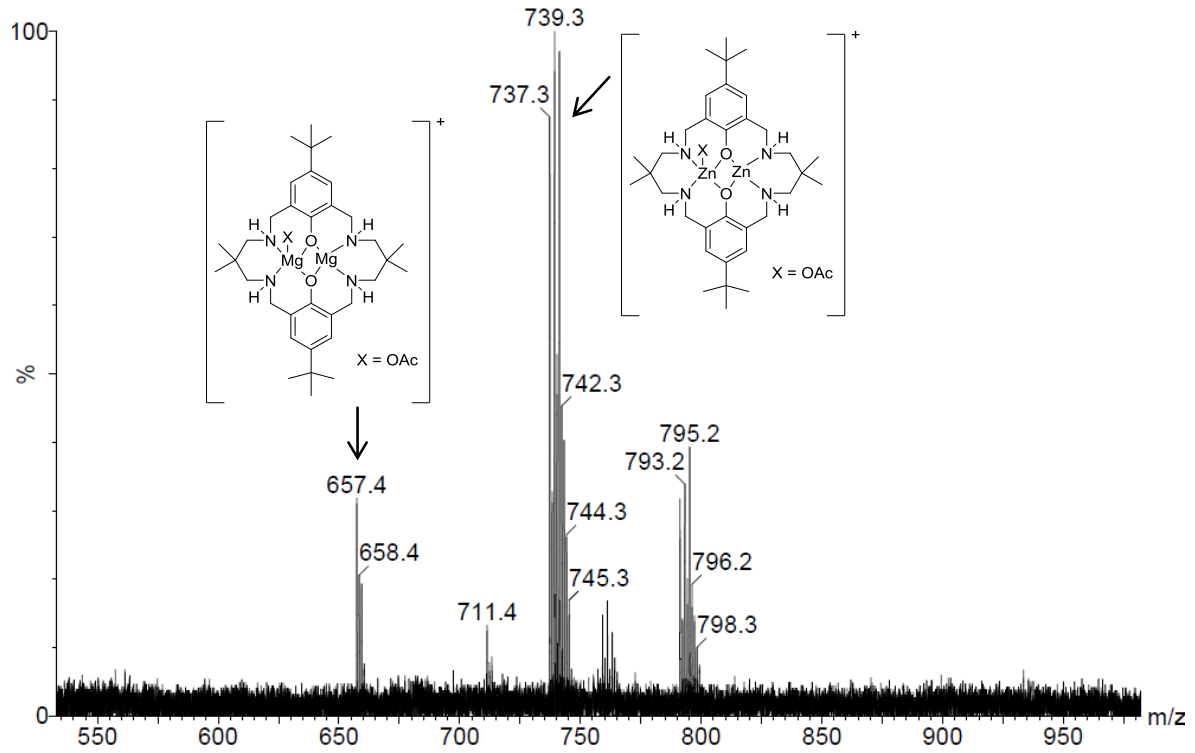

Figure B6: MALDI-ToF mass spectrum of 50:50 mixture of ($LZn_2(OAc)_2$) and ($LMg_2(OAc)_2$) after being heated in THF at 80 °C for 16 h. Peaks at 711 and 793 amu correspond to $LMg_2(O_2CCF_3)]^+$ and $LZn_2(O_2CCF_3)]^+$, respectively. These peaks arise due to the use of $K(O_2CCF_3)$ as a cationising agent in this analysis technique.

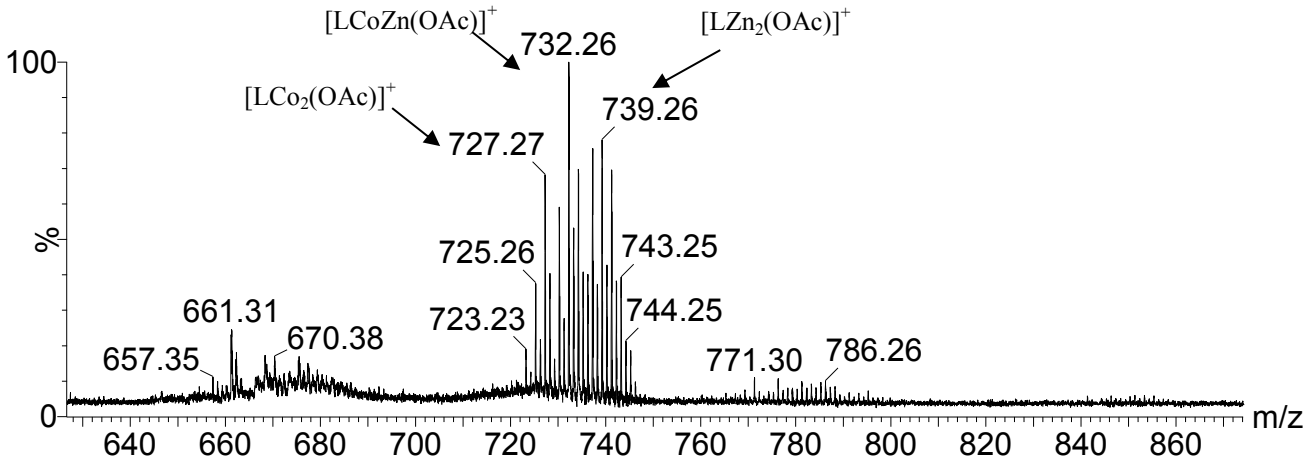

Figure B7: MALDI-ToF mass spectrum of catalyst system **8**. Peaks at 782, 787 and 794 represent $[LCo_2(OOCCF_3)]^+$, $[LCoZn(OOCCF_3)]^+$ and $[LZn_2(OOCCF_3)]^+$, respectively. These peaks arise due to the use of $K(O_2CCF_3)$ as a cationising agent in this analysis technique.

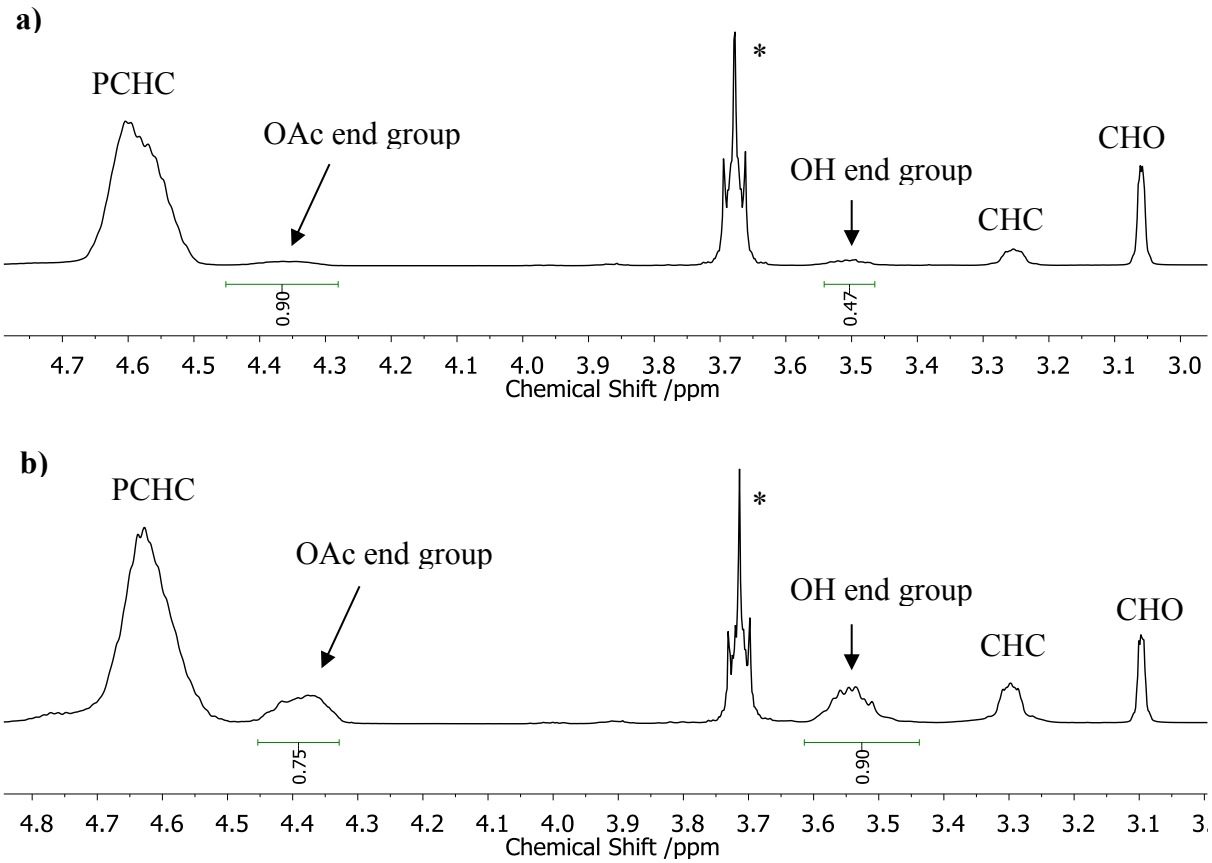

Figure B8: ^1H NMR spectra of PCHC and end groups in $CDCl_3$. Reaction conditions: a) 1:1000, catalyst **7**:CHO loading, 80 °C and 1 bar CO_2 pressure; b) 1:1000, catalyst **7**:CHO loading, 80 °C, 1 bar CO_2 pressure and 16 equivalents of H_2O relative to catalyst.

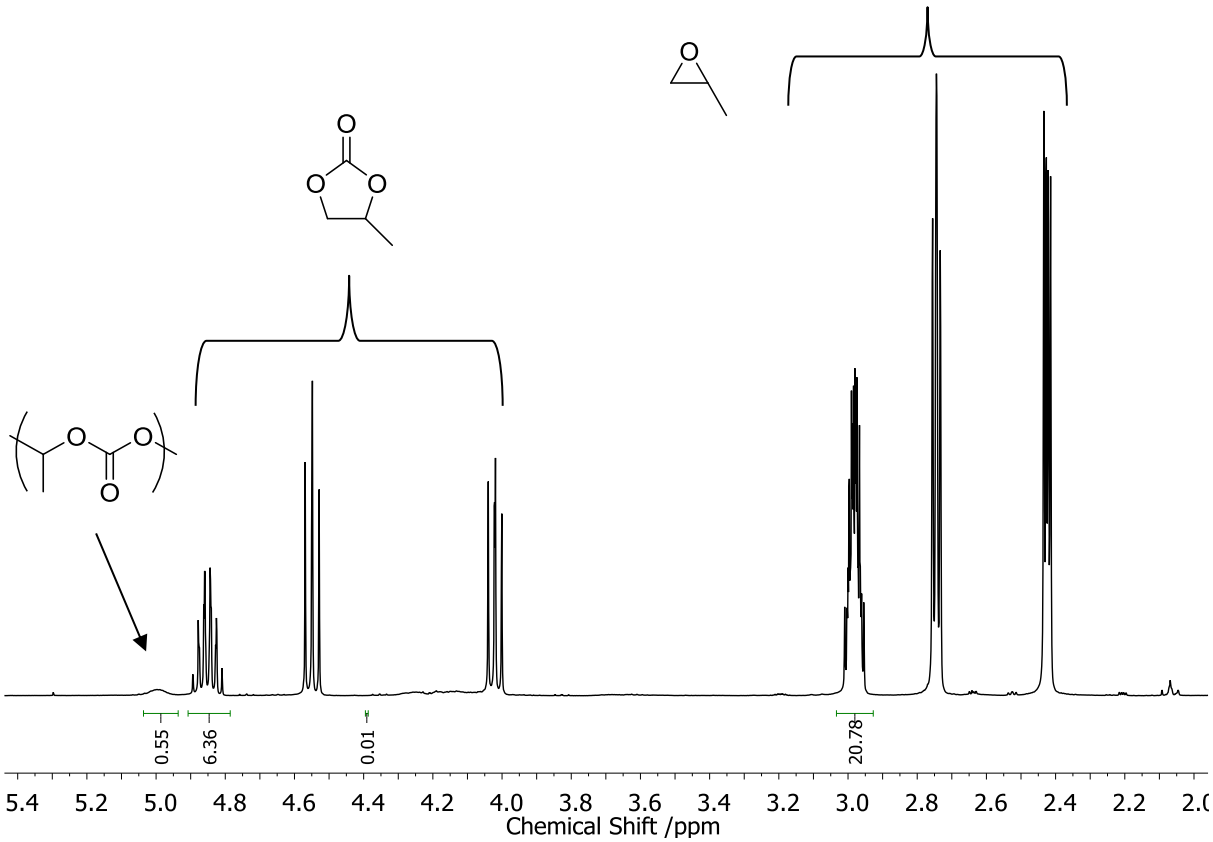

Figure B9: ^{1}H NMR spectrum of crude reaction mixture of PO/CO_2 copolymerisation reaction with a 1:1000, catalyst **7**:CHO loading, at 60 °C and 50 bar pressure.

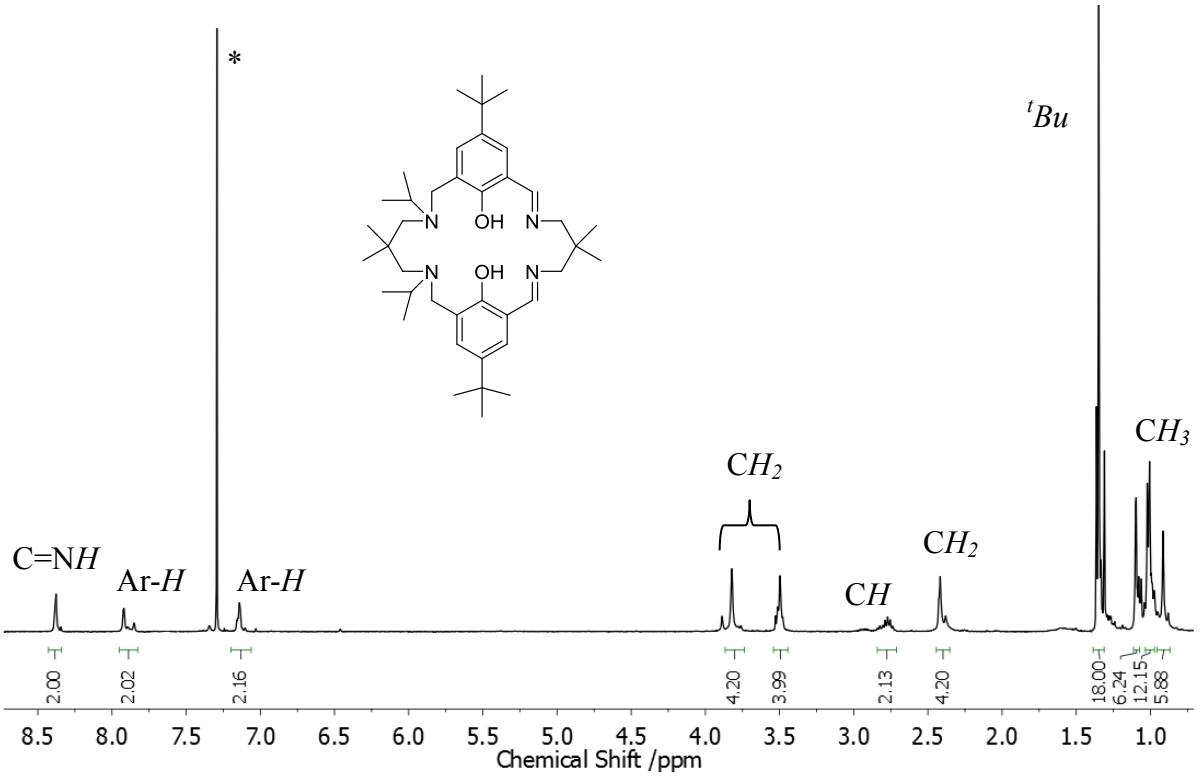

Figure B10: ^{1}H NMR spectrum of asymmetric macrocyclic pro-ligand **2** in $CDCl_3$.

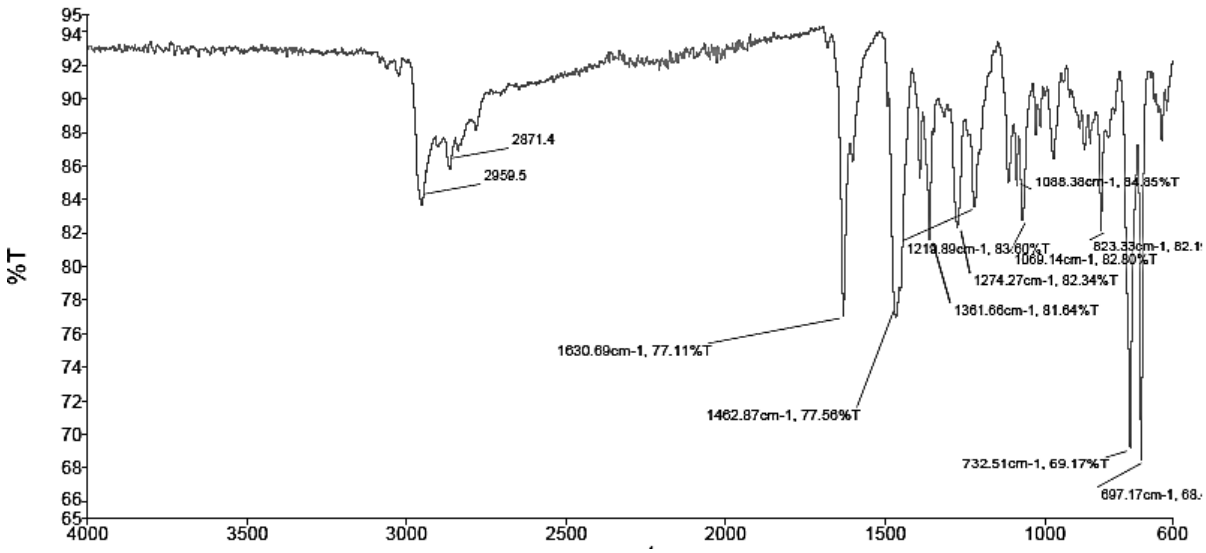

Figure B11: IR spectrum of asymmetric macrocyclic pro-ligand **1**.

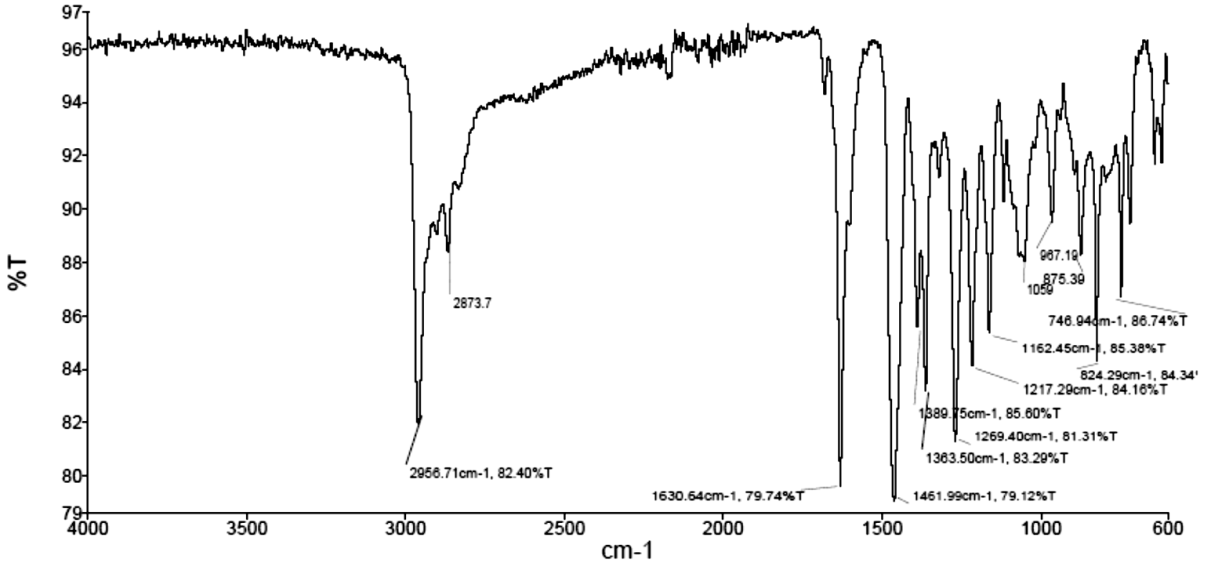

Figure B12: IR spectrum of asymmetric macrocyclic pro-ligand **2**.

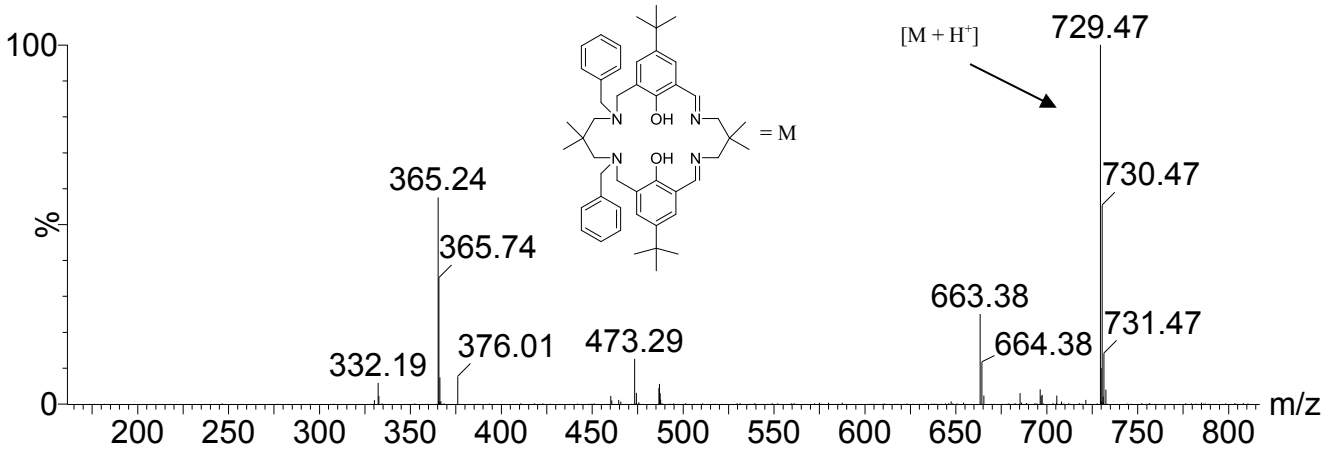

Figure B13: ESI mass spectrum of asymmetric macrocyclic pro-ligand **1**.

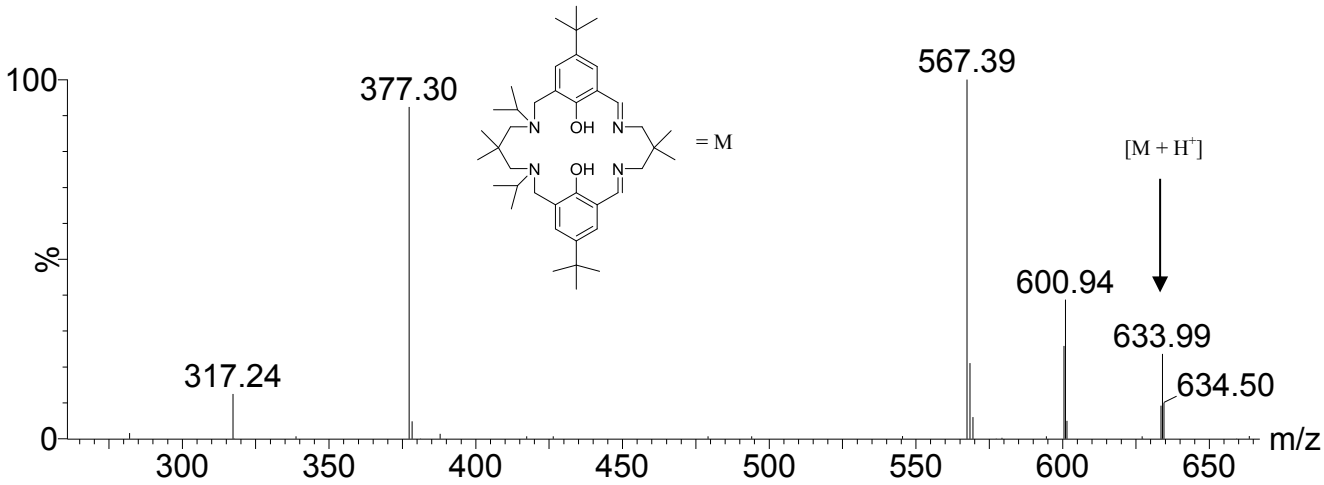

Figure B14: ESI mass spectrum of asymmetric macrocyclic pro-ligand **2**.

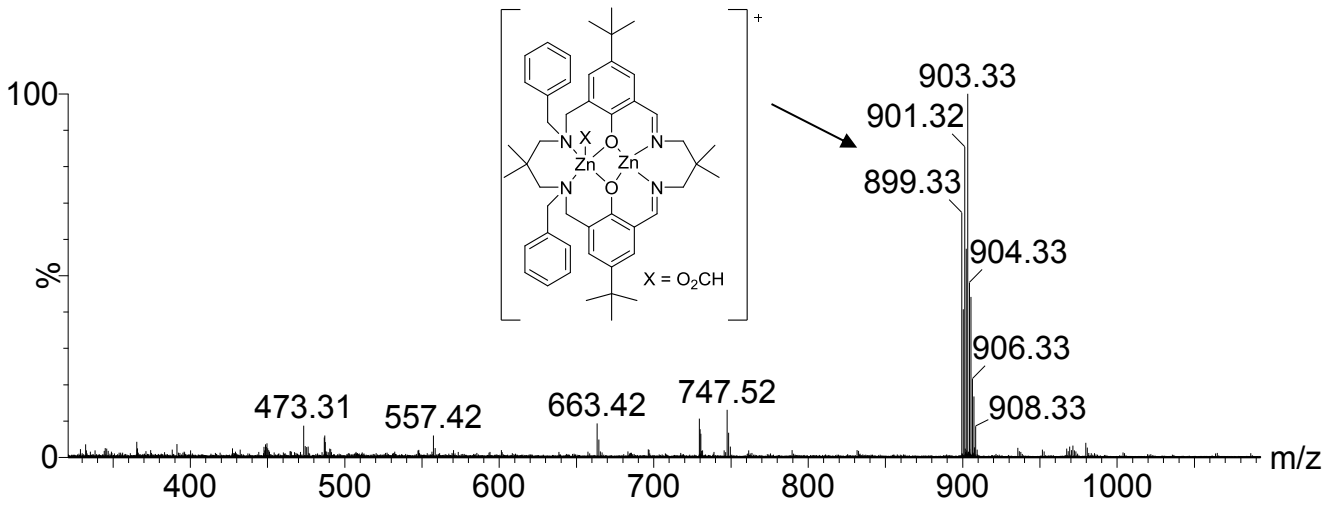

Figure B15: ESI mass spectrum of complex **9**.

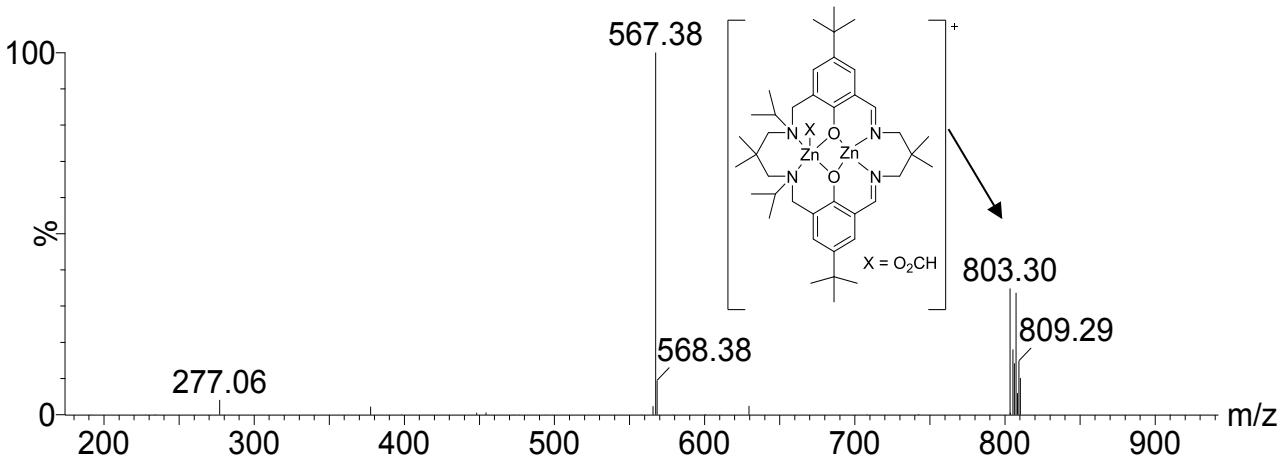

Figure B16: ESI mass spectrum of complex **10**.

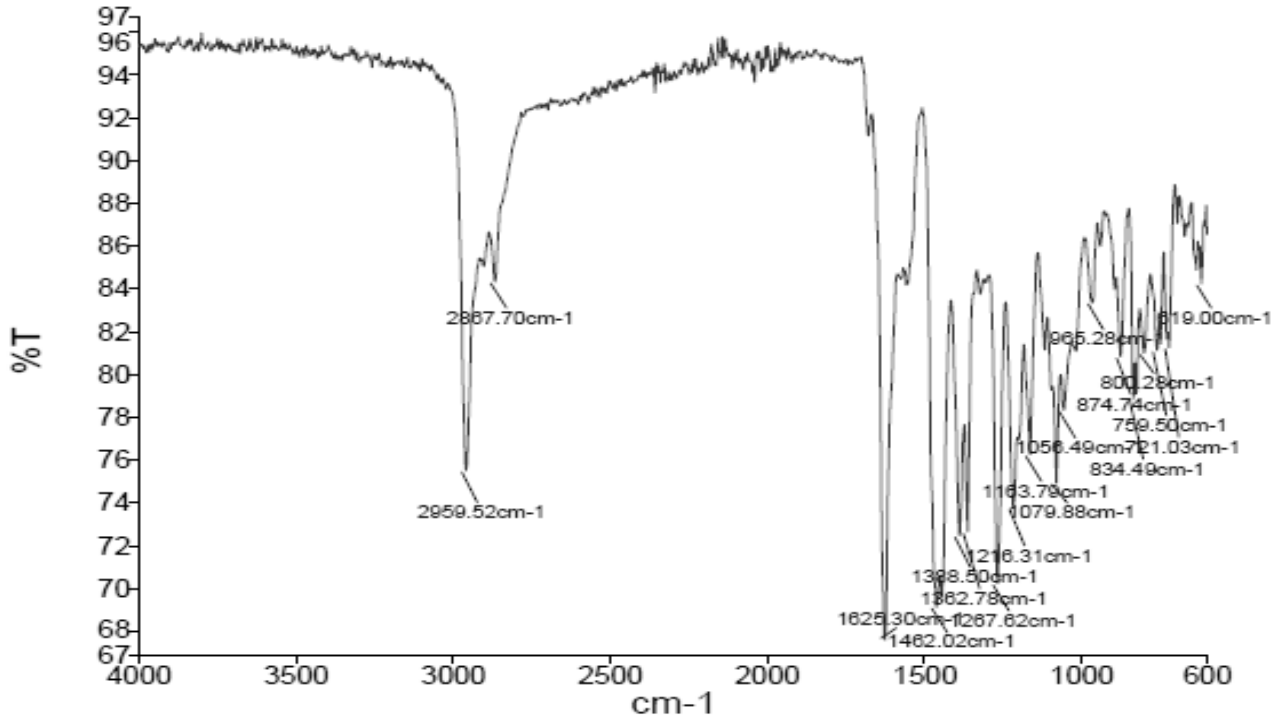

Figure B17: IR spectrum of complex **9**.

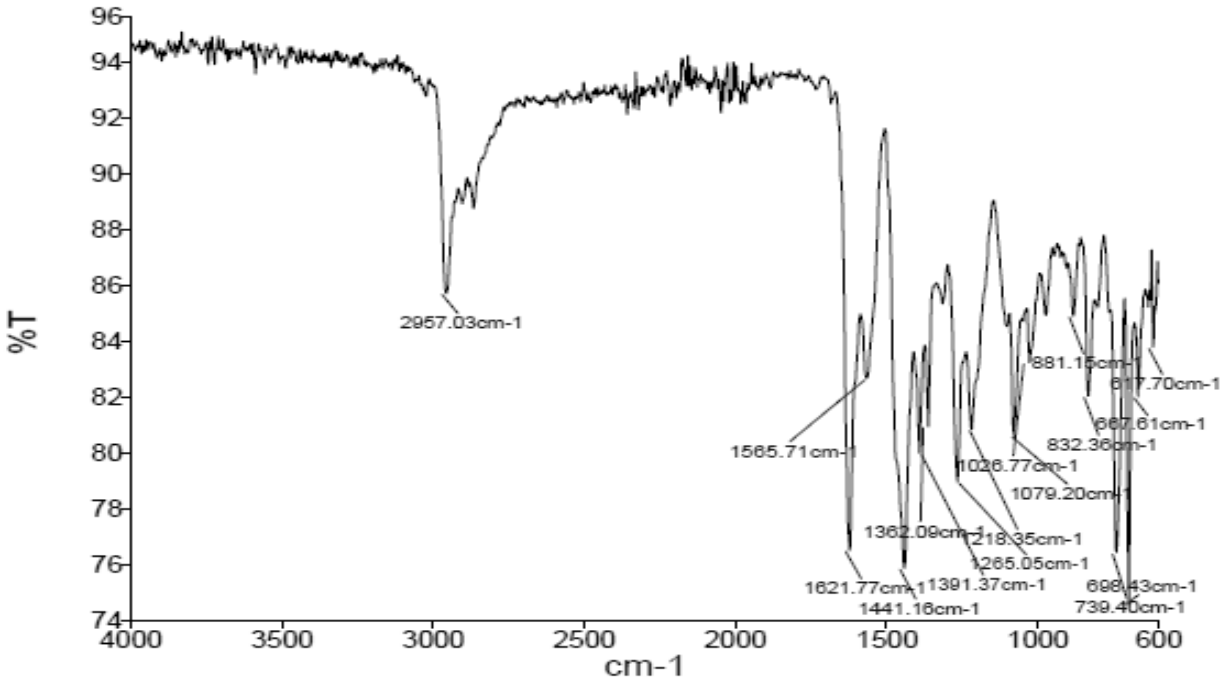

Figure B18: IR spectrum of complex **10**.

Appendix C – Spectra for Chapter 4

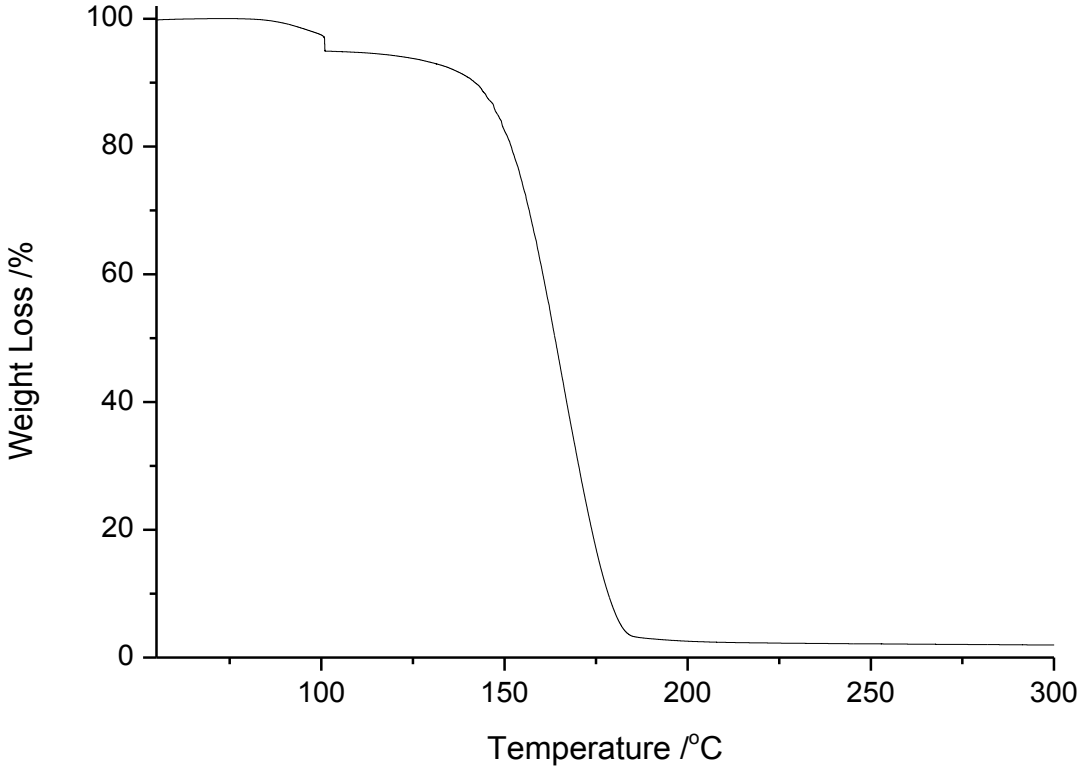

Figure C1: TGA graph for PCHC sample produced by **2**.

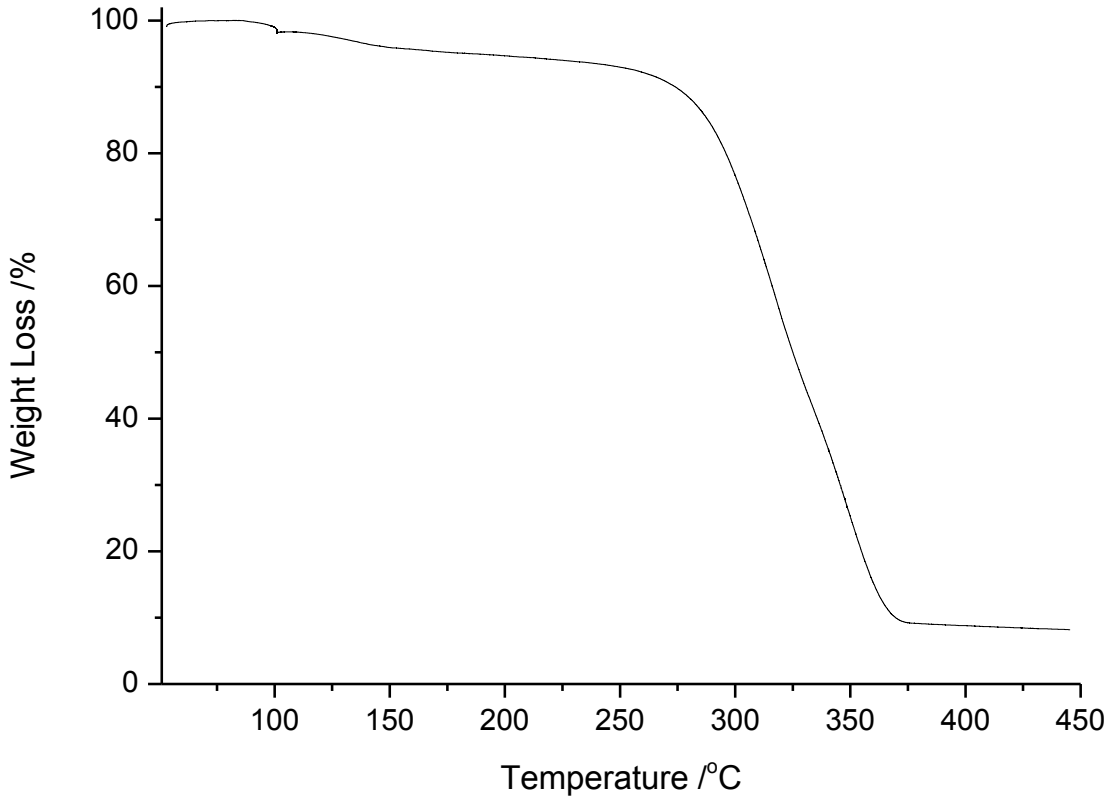

Figure C2: TGA graph for PE sample produced by **2**.

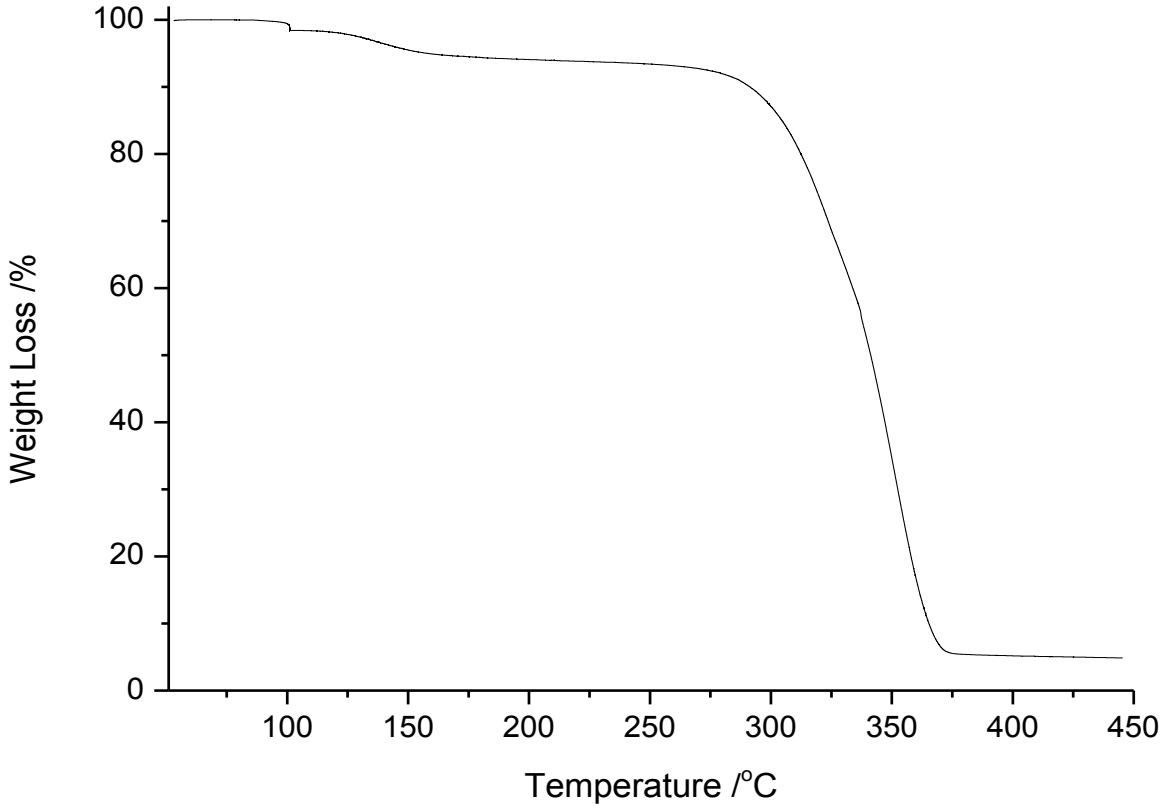

Figure C3: TGA graph for PE sample produced by **1a**.

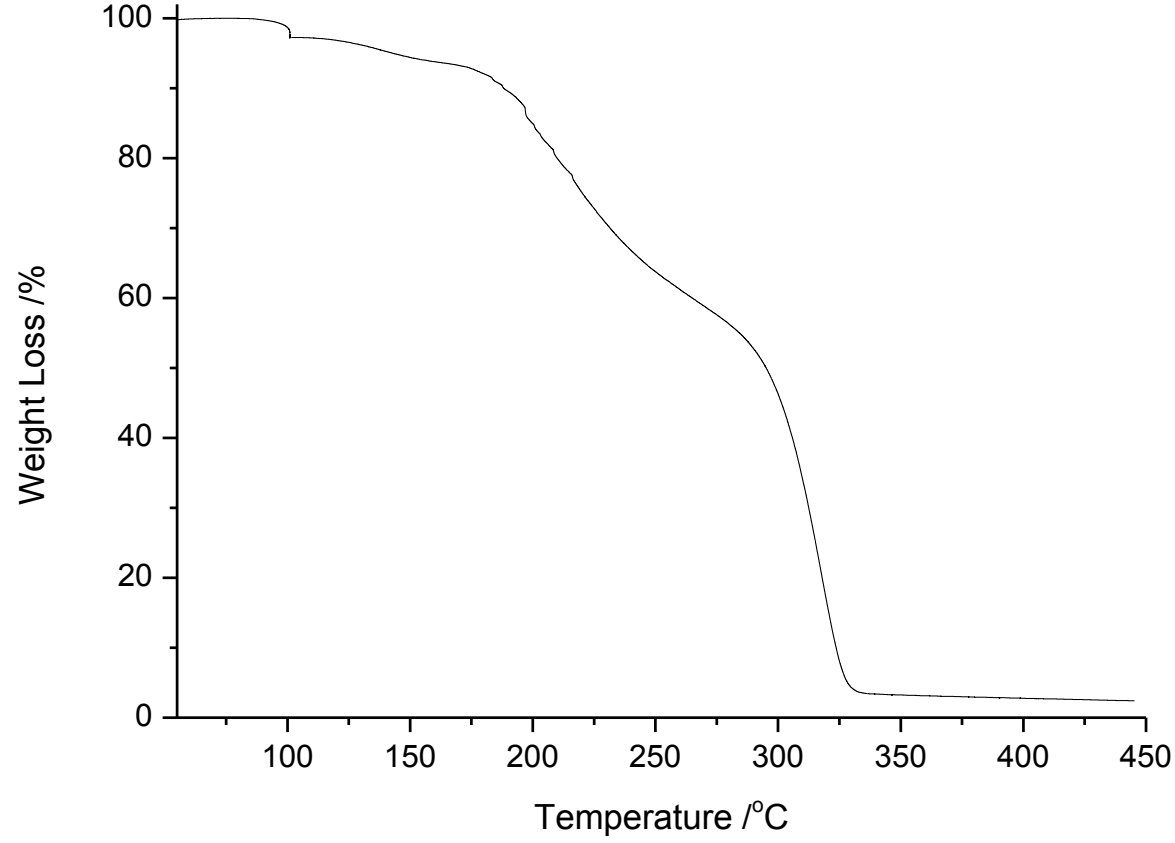

Figure C4: TGA graph for PE-PCHC sample produced by **2**.

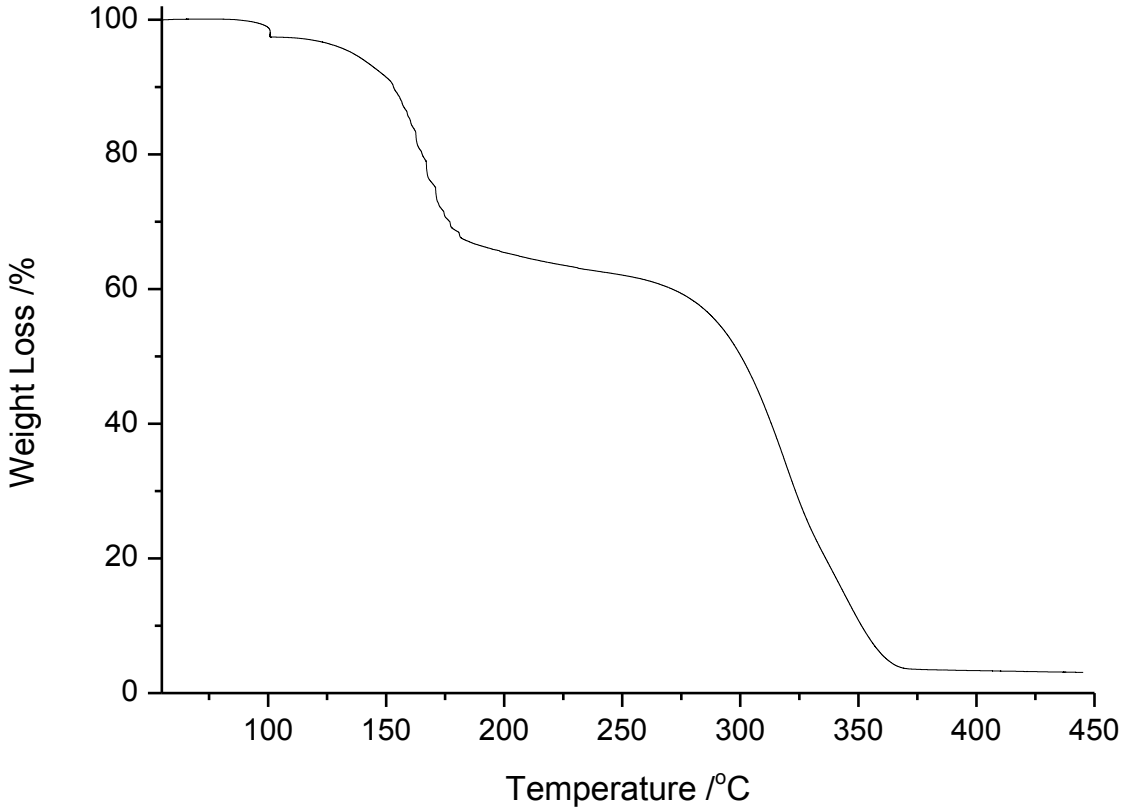

Figure C5: TGA graph for PE-PCHC sample produced by **1a**.

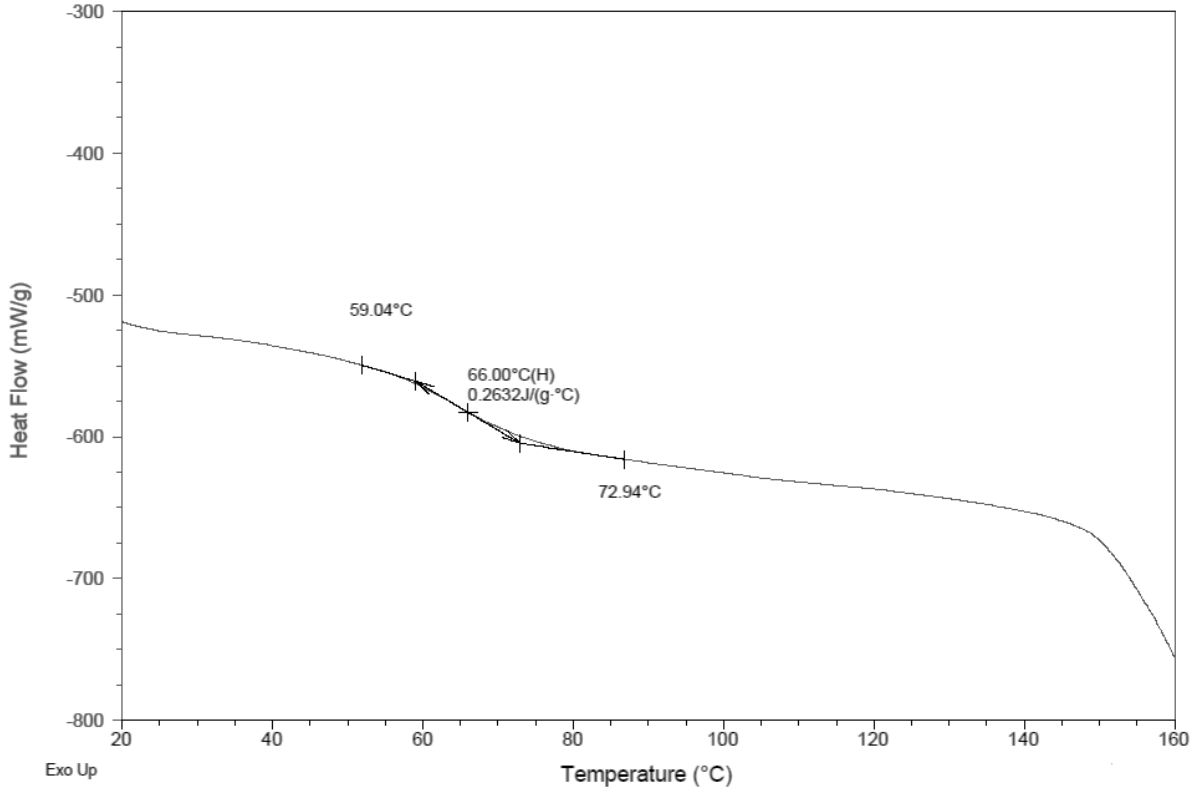

Figure C6: DSC graph for PCHC sample produced by **2**.

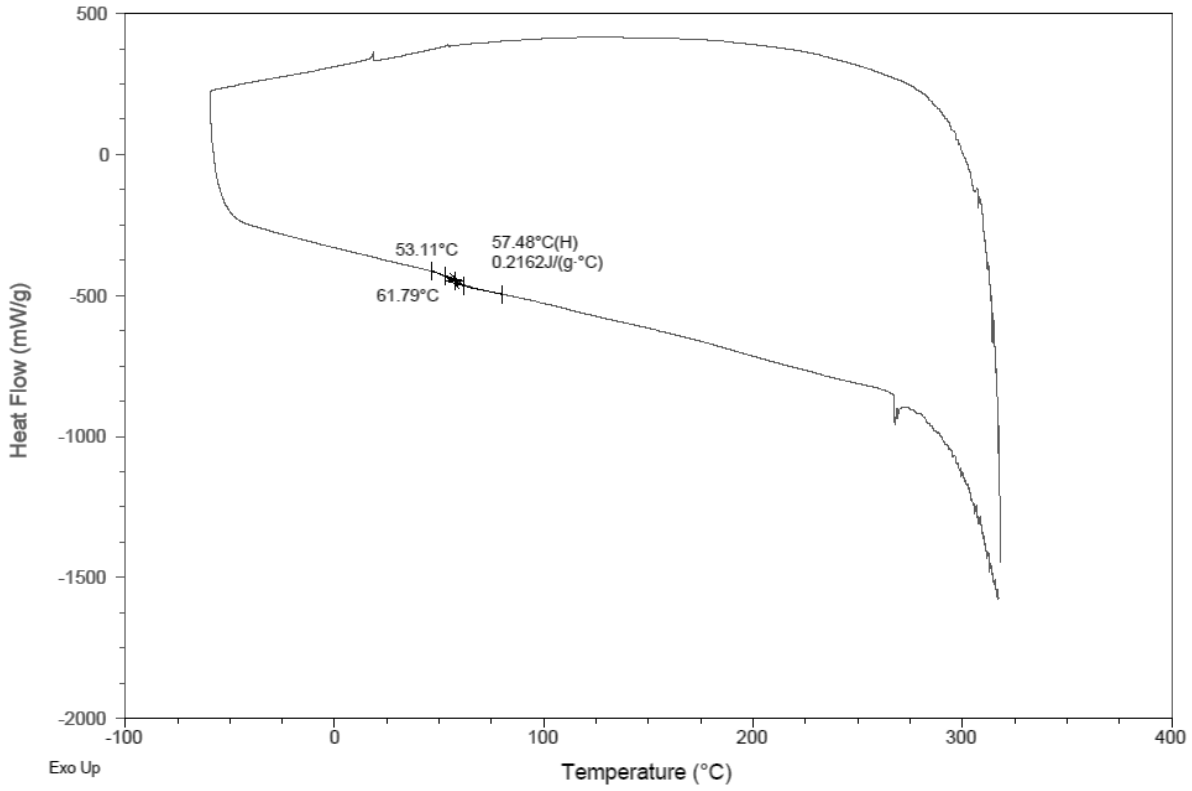

Figure C7: DSC graph for PE sample produced by **2**.

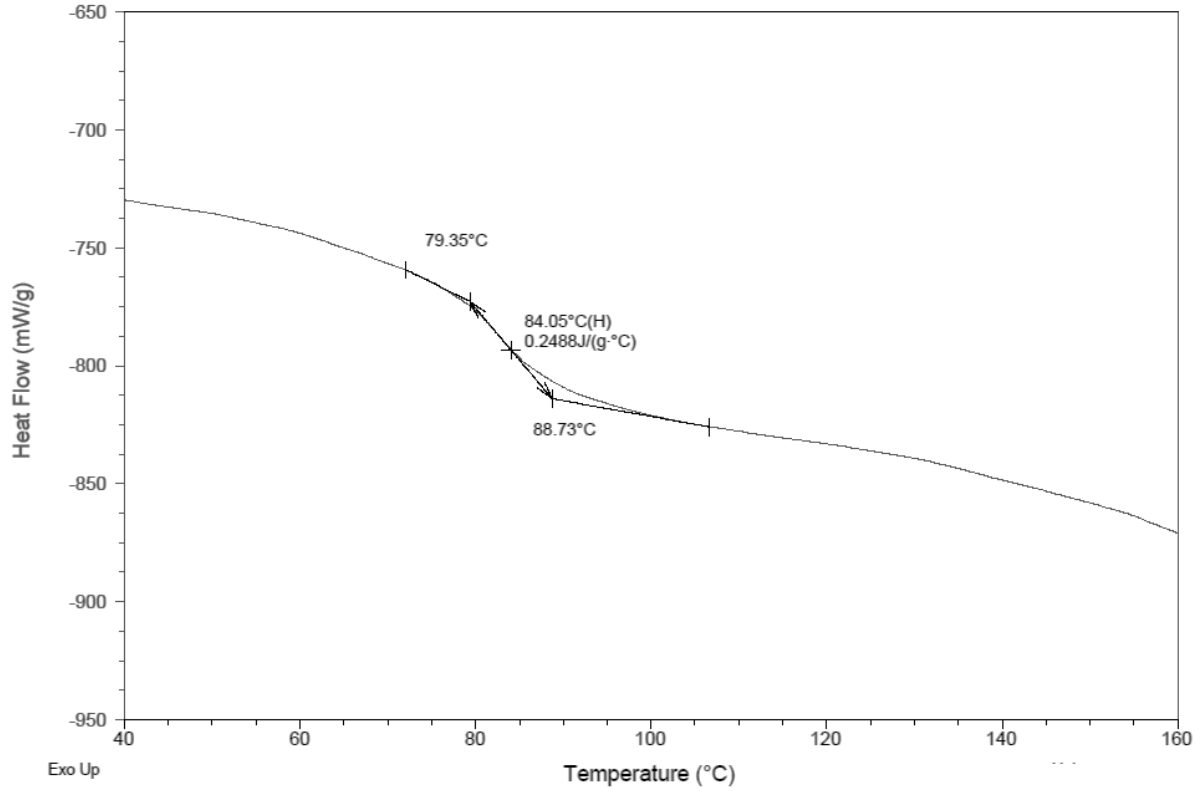

Figure C8: DSC graph for PE sample produced by **1a**.

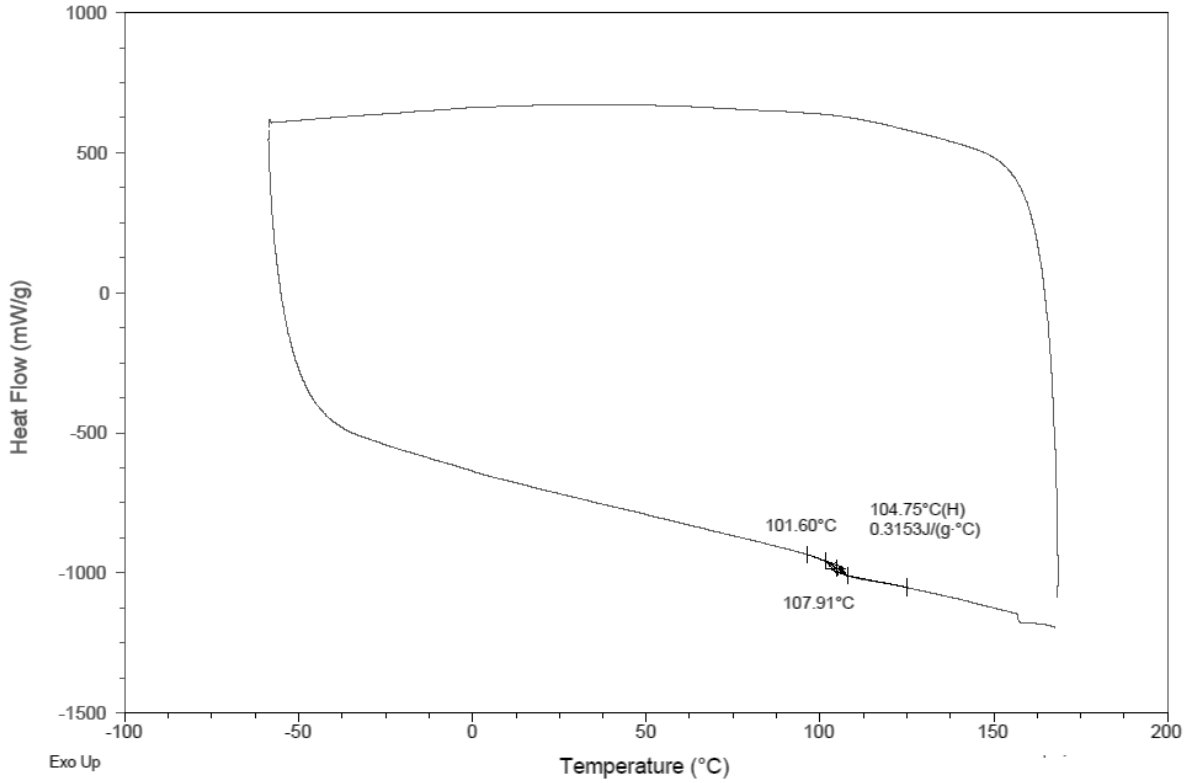

Figure C9: DSC graph for PE-PCHC sample produced by **2**.

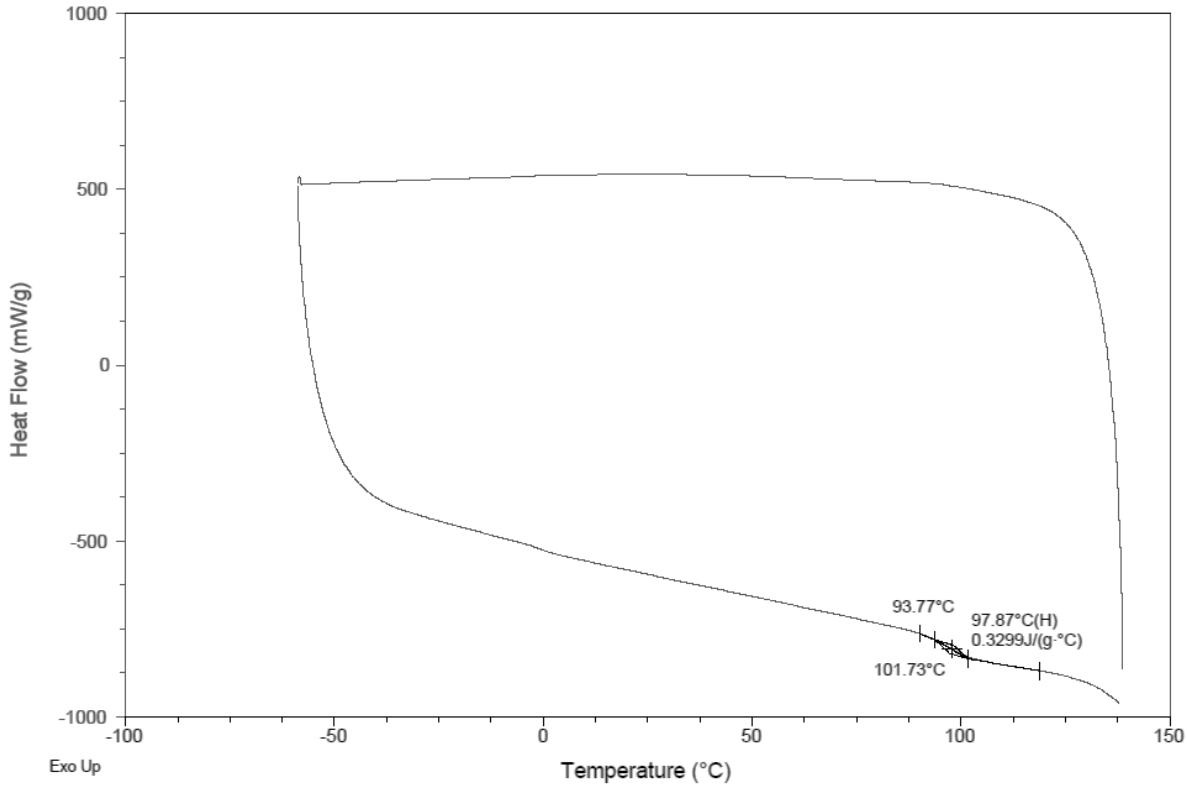

Figure C10: DSC graph for PE-PCHC sample produced by **1a**.

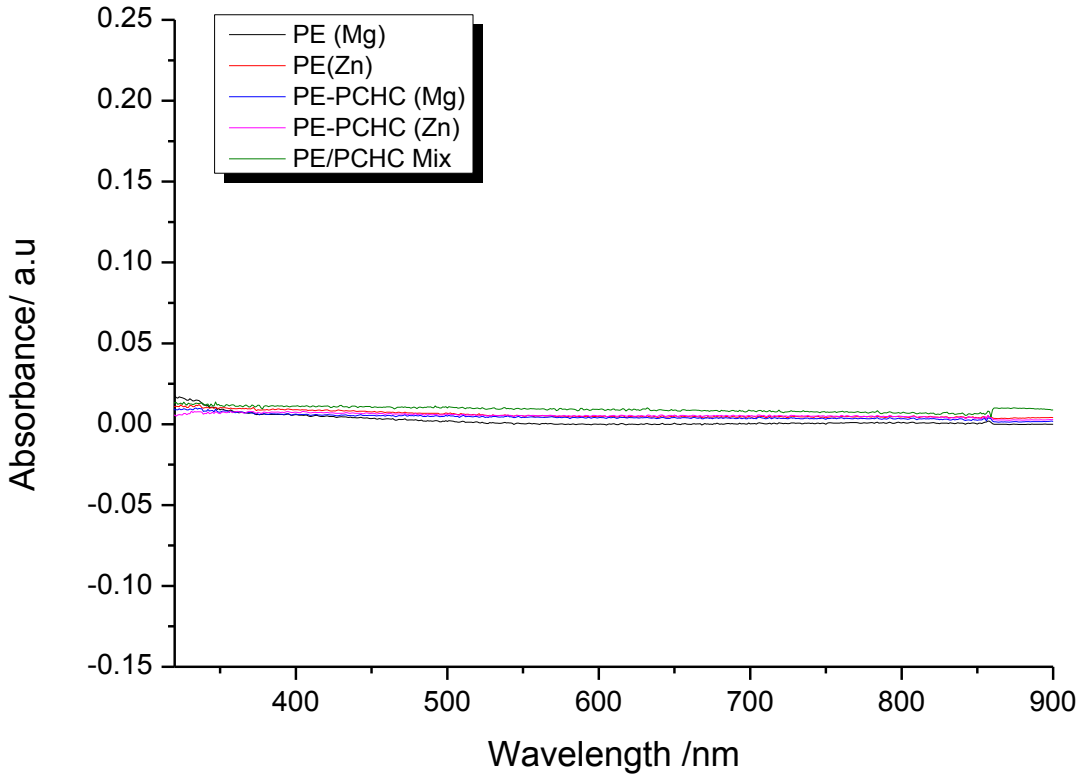

Figure C11: UV-Vis spectra obtained for the thin films of the PE, PCHC and block copolymer samples.